TWO CUT SLOPES IN FIBROUS ORGANIC SOILS BEHAVIOR AND ANALYSIS

Dissertation for the Degree of Ph. D.

MICHIGAN STATE UNIVERSITY

WAYNE A. CHARLIE

1975

This is to certify that the

thesis entitled

TWO CUT SLOPES IN FIBROUS ORGANIC SOILS
BEHAVIOR AND ANALYSIS

presented by

Wayne A. Charlie

has been accepted towards fulfillment
of the requirements for

Ph.D. degree in Civil Engineering

O. B. Andersland

Major professor

Date May 14, 1975

O-7639

ABSTRACT

TWO CUT SLOPES IN FIBROUS ORGANIC SOILS
BEHAVIOR AND ANALYSIS

By

Wayne A. Charlie

The behavior of two cut slopes in a consolidated fibrous organic soil (papermill sludge) landfill is analysed. Information presented includes site data, physical properties of the fibrous organic soil, in-situ and laboratory shear strengths, lateral movements near the cut slope, and a stability analysis for the observed slope failure. A 3:4 (β = 53.1 degrees) slope 16 feet (4.88m) in height was stable. Observed lateral movements were less than 1 inch (2.54cm) ten days after excavation. The slope was then trimmed to a 1:8 (β = 82.9 degrees) slope 16 feet (4.88m) in height which failed four days later. Immediately preceeding failure lateral movements were close to 3.75 inches (9.52cm).

Fresh sludge samples and field water contents were taken at the time of construction of the landfill. Undisturbed block samples of consolidated sludge and field water contents were taken at the time of slope excavation. Laboratory shear test results, using triaxial, plane strain, and unconfined compression tests, are presented. It is shown that soil mechanics theory can be used to predict the stability of slopes excavated in a sludge landfill. The significant increase

in shear strength of the papermill sludge as a direct consequence of consolidation resulted in a stable 3:4 slope with small observed lateral movements. This behavior was in contrast to the very soft, almost fluid behavior of the fresh sludge placed in the landfill during construction. For the 1:8 slope, Janbu's method for a composite failure surface gave excellent agreement between the actual factor of safety and the computed factor of safety. The field vane shear strength, corrected by Bjerrum's method for deformation rate and sludge anisotropy effects, appeared to give a good representation of the undrained field shear strength for the sludge. A finite element method (FEM) of analysis, using laboratory test results and a bilinear stress-strain model for sludge behavior, was in good agreement with observed field behavior for the 1:8 slope.

Triaxial test data show that the strength of pulp and papermill sludges appear to be frictional and in accordance with the principle of effective stress. Angles of internal friction (effective stress basis) ranged from about 45 degrees at low organic contents (28%) to about 70 degrees at higher organic contents (63%). The high values for $\bar{\phi}$ represent an exceedingly strong material but may be unrealistic in assessing the strength. Fibers extending across failure surfaces probably go into tension as the sample is deformed, thereby giving a pseudo value for the angle of internal friction. Large strains are required to fully mobilize available strength. For a given organic content, anisotropic consolidation increased the angle of internal friction when the direction of compression was normal to the plane in which the fibers would tend to be aligned. Unconfined

compressive strengths were also greatest for sample compression normal to the plane in which the fibers would tend to be aligned. Lower values for the angle of internal friction and the unconfined compressive strength were observed when the direction of compression was in the plane of maximum fiber alignment (horizontal). It is shown that the papermill sludge has properties in many respects similar to peat and other fibrous organic soils.

TWO CUT SLOPES IN FIBROUS ORGANIC SOILS

BEHAVIOR AND ANALYSIS

By

Wayne A. Charlie

A DISSERTATION

Submitted to
Michigan State University
in partial fulfillment of the requirements
of the degree of

DOCTOR OF PHILOSOPHY

Department of Civil Engineering

1975

ACKNOWLEDGMENTS

The writer wishes to express his appreciation to his major professor, Dr. O. B. Andersland, Professor of Civil Engineering, for his encouragement, initiative, and aid throughout the writer's doctoral studies and for his guidance during the preparation of this thesis. Thanks are also due the other members of the writer's doctoral committee: Dr. T. S. Vinson, Assistant Professor of Civil Engineering; Dr. W. A. Bradley, Professor of Metallurgy, Mechanics, and Materials Science; and Dr. R. Carmichael, Assistant Professor of Geology. The writer also owes his appreciation to: Dr. Robert P. Vallee for the construction of the landfill; Mr. Tom Danis Sr. of the B. G. Danis Co., Dayton, Ohio for his help and cooperation during the excavations in the landfill; Mr. Donald Kindred for his cooperation and suggestions during the field portion of the research; Mr. Rodney W. Lentz for his time and suggestions; Mr. Leo Szafranski for his help in preparation of required apparatus for experimentation; and to his friends who helped proofread the manuscript and gave encouragement throughout the writer's doctoral studies.

Special appreciation is also given to the writer's parents for their encouragement. Appreciation is also given to the Rohn family.

Thanks are also extended to the U.S. Environmental Protection Agency, the National Council of the Paper Industry for Air and Stream Improvement, and the Division of Engineering Research at Michigan State University for the financial assistance which made this research possible.

TABLE OF CONTENTS

Chapter | Page

LIST OF TABLES

LIST OF FIGURES

Figure | Page

Figure		Page

Figure		Page

LIST OF SYMBOLS

$\bar{a}$ = y intercept, effective stress basis

A = pore pressure parameter

b = slice width

c = cohesion

c_u = total stress strength parameter

c_v = coefficient of consolidation

$\bar{c}$ = cohesion, effective stress basis

e = void ratio

E = Young's modulus

E = normal force on slice sides

F = factor of safety

H = Henry's coefficient of solubility

H = thickness of sludge layer or sample

H_p = thickness of sludge layer or sample at the end of primary consolidation

I_p = plasticity index

k = coefficient of permeability

K = total stress earth pressure coefficient

K_f-line = line through $\bar{p}_f$ versus q_f

K_o = coefficient of earth pressure at rest

ℓ = length

L_w = liquid limit

N = normal force

O = center of failure circle

p = consolidation pressure

p_o = initial pressure; present overburden pressure

$\bar{p}$ = $\frac{1}{2}(\bar{\sigma}_1 + \bar{\sigma}_3)$

$\bar{p}_f$ = $\bar{p}$ at failure

P = force

q_o = applied surface load

$\bar{q}$ = $\frac{1}{2}(\bar{\sigma}_1 - \bar{\sigma}_3)$

$\bar{q}_f$ = $\bar{q}$ at failure

Q = line load

R = radius

s = shearing resistance

S = shear force

S_o = initial degree of saturation

t = time

T = temperature

T = shear force

u = pore water pressure

u_{a_o} = initial air pressure

u_{a_s} = pressure necessary for full saturation

w = water content

W = total weight

x = distance

X = shear force on slice sides

z = depth to a point in a soil layer

α = inclination angle of force

$\bar{\alpha}$ = slope of $\bar{p}_f$ versus $\bar{q}_f$

γ = unit weight

γ_w = unit weight of water

Δ = increment

ε = strain

σ = normal stress

$\bar{\sigma}$ = effective normal stress

$\bar{\sigma}_{ff}$ = normal stress on failure surface at failure

$\sigma_1, \sigma_2, \sigma_3$ = principal stresses

τ_{ff} = shear stress on failure surface at failure

μ = correction factor

$\bar{\phi}$ = friction angle based on effective stresses

ϕ_u = total stress strength parameter

The Greek Alphabet

α	Alpha	ν	Nu
β	Beta	π	Pi
γ	Gamma	ρ	Rho
δ	Delta	σ	Sigma
ε	Epsilon	τ	Tau
ξ	Xi	ϕ	Phi
η	Eta	χ	Chi
θ	Theta	ψ	Psi
λ	Lambda	ω	Omega
μ	Mu		

CHAPTER I

INTRODUCTION

A. Need for Study

In order to protect the nation's lakes and streams, the pulp and paper industry removes a large percentage of the suspended and dissolved matter from their effluent streams. In the United States, an estimated 2,500,000 dry tons ($2{,}300 \times 10^6$ kg) of waste solids, having a volume close to 200,000,000 cubic yards (150×10^6 m^3), are removed annually (Gillespie, Mazzola, and Gellman, 1970). As many times happens, one solution presents another problem. Today, disposal of these large volumes of pulp and papermill sludges in an economical and ecologically safe manner is a major problem for the paper industry. More than 1,100 acres (4,450,000 m^2) of land are in use as depositories for these man-made waste materials. These deposits, which may have water contents in excess of 300 percent (percent of dry weight), are very unstable and are subject to large settlements when any load is placed on the surface.

Mechanically dewatered papermill sludges can be described as a fibrous organic soil which have the physical appearance of clay interwoven with cellulose fibers. Their composition depends on the type of manufacturing process and the conservation steps at the mill, for both pulp and papermill wastes. In general, the solids include clay (used in paper as a coating and filler), fibers, and fine pulp which escape the pulp or paper making process. Fiber losses during production, generally averaging three percent or less, are significant because of the large quantities of fibers produced per day (Nemerow, 1971).

Land disposal of papermill sludge appears to be the most feasible approach currently available. Bacon (1967) has suggested the possibility of using sludge as an economical method for land reclamation, especially in marginal lands, coal mining areas, and abandoned gravel pits. A survey conducted by Gillespie (1969) indicated that landfills are in wide use for the disposal of papermill waste solids throughout the United States. However, landfills are not necessarily an inexpensive or trouble-free means of disposal. Many land disposal sites have experienced difficulties with the waste. Many of these difficulties are due to a lack of understanding of both the engineering properties and field behavior of these materials. Guidelines for the efficient and safe disposal of pulp and papermill solid wastes are incomplete (Mazzola, 1969). Landfill construction that is most suitable for efficient operations, for extending both the capacity and life of disposal sites, and designed for future uses requires an understanding of many variables. These include volume change and settlement, slope stability and bearing capacity, and changes in water content through drainage. Possible adverse environmental effects must be guarded against.

It is desirable that a completed landfill be stable and have the potential for a number of future uses, including recreation, agriculture or as a foundation for light construction. The size and slope of sludge embankments will be determined by the embankment stability. However, little information is available on field shear strengths and stability of cut slopes in these sludge deposits. Core sampling investigation of a few existing sludge deposits found that many of the pulp and papermill solid waste landfills were very unstable, of low shear strength (0.12 to 0.37 kg/sq cm), and contained high water contents (Mazzola, 1969). Previous studies (Vallee and Andersland, 1974) showed that large volume changes do occur under a small surcharge (surface loading). Results also showed that a significant increase in shear strength occurred as a result of consolidation. These results are the same as those expected for compressible soils such as clays, loose silts, and most organic soils (Terzaghi and Peck, 1967).

B. Objectives of Study

The general objective of this study was to contribute basic information on the stability of pulp and papermill solid wastes. This information was obtained through field observations, laboratory tests, and analysis of the data. This information is needed for developing guidelines and recommendations on the design, operation, and regulation of landfills containing pulp and papermill solid wastes. The specific objective of this study was to determine whether methods and theory used to estimate the stability of cut slopes in soft clay soils could also be used for excavations in consolidated sludges. A field stability study, involving two cut slopes in an experimental sludge landfill project, provided data which has been compared to predictions based on soil mechanics theory and experimental laboratory data.

The following is a summary of specific items of research and implications relative to the stability of the landfill which are discussed in this thesis:

1. Surcharge loads in combination with drainage blankets make possible a large reduction in water content of fresh papermill sludge in a landfill. This consolidation improves the shear strength of the sludge. The magnitude of this increased shear strength was demonstrated by both field and laboratory tests.

2. Undrained shear strength data obtained by the vane borer is compared with shear strength data from laboratory triaxial and plane-strain tests. Laboratory tests were conducted on both fresh sludge samples and undisturbed block samples obtained from the landfill. Suitability of the shear strength for the stability calculations is discussed.

3. An excavation was made to produce a 3:4 slope (β = 53.1 degrees). Two weeks later this stable slope was trimmed to a 1:8 slope (β = 82.9 degrees). Observed lateral and vertical movements within the sludge landfill, resulting from the excavation, are summarized and discussed.

4. Failure zones develop where the maximum shear stress approaches the shear strength. Although the overall factor of safety may be above unity for a given slope, local or small areas in the slope may be stressed beyond their shear strength. Development of these failure zones during the excavation of the 1:8 slope are studied using the finite element method of analysis and laboratory stress-strain data.

5. Slope failure occurred shortly after excavation of the 1:8 slope. By definition, the factor of safety against slope failure should be equal to unity. Using soil mechanics theory and both laboratory and field shear strength data, the slope stability was analyzed so as to compare the field behavior with predicted behavior.

6. Pore water pressures and total pressures were recorded at various points in the landfill before and during slope excavation, after slope failure, and during the following winter and spring. Implications relative to the slope behavior are discussed.

Specific items relative to the consolidation behavior and the leachate analysis and lysimeter study are covered elsewhere (Andersland, et al., 1973).

C. Nature and Scope of Study

Theories on soil strength and slope stability (Terzaghi and Peck, 1967; Lambe and Whitman, 1969; Janbu, 1954 & 1957) provided the theoretical basis for the research work. Test equipment and test techniques used were similar to those described in soil mechanics literature. Many similarities between papermill sludges and organic clay, peat or muck become evident when the experimental data is reviewed. The research program was a continuation of an earlier project which involved construction of the experimental landfill and monitoring of instrumentation during consolidation. Laboratory work for the determination of certain physical properties and one-dimensional consolidation characteristics of the fill material have been reported by Vallee (1973).

The stability study portion of the project was initiated in early September, 1972, to observe the behavior of cut slopes in consolidated sludge and to provide data needed to verify in situ vane and laboratory shear strengths used in stability calculations. The field work involved in situ vane shear strength tests, installation of slope indicator casings and additional piezometers, removal of the dike on the North side, excavation for the experimental slope in two increments, taking undisturbed block samples and field water contents at several levels in the exposed cut, and monitoring of field instrumentation as needed to provide a continuous record of the slope performance. Laboratory work included tests to determine the current physical properties of the sludge and the shear strength parameters and stress-strain properties based on both triaxial and plane strain type test methods. The ash content (organic content), taken on a number of samples, provided a check on sludge uniformity and helped show which samples were more representative of the sludge.

Failure zones which developed in those regions where the maximum shear stress values exceeded the undrained shear strength of the sludge were studied using a finite element method computer program (Dunlop, et al., 1968). Development of failure zones in the 1:8 slope were simulated as the excavation proceeded to greater depths and compared to actual field behavior.

CHAPTER II

LITERATURE REVIEW

Information on the design, operation and engineering characteristics of papermill sludge landfills is very limited. Sanitary landfill design and operation (Stoll, 1971) is oriented towards municipal wastes and provides little information on stability and strength characteristics of papermill wastes. Strength data for these sludges are essentially nonexistent except for laboratory work (Andersland and Laza, 1971). Literature related to pulp and papermill sludge is available in the areas of composition, methods for solids removal, improved dewatering techniques and conservation steps required to reduce fiber loss in production.

A. Physical Properties of Fiberous Organic Soils

Composition

Gillespie, Gellman and Janes (1970) defined "high ash sludges" as those which have a fixed solids content of 60 percent or greater. Andersland, *et al.* (1972) found that the organic content of the fresh papermill sludge from the West Carrollton, Ohio, landfill varied from 40.6 to 67.8 percent. The physical properties of these sludges show a wide variation due to the type of paper being produced and the internal methods being used to recover the fibers. Mazzola (1969) examined sludge deposits from eight different mills for physical properties including water content, ash content, Atterberg limits, vane shear strength, and a study to evaluate decomposition. Decomposition of the organic fiber in the sludge, if found to be significant, could lead to larger settlements, loss of shear strength, and possible gas production due to biological action. MacFarlane (1969) states that the gas content in peat deposits is of considerable theoretical and practical importance. Laboratory and field measurements of pore pressures, permeability, and rate of consolidation, etc. are affected by the presence of gas.

Samples from a sludge deposit taken at depths of 2 and 12 feet (0.61 and 3.66m) and representing ages of 1 and 12 years were examined using photomicrographs (Mazzola, 1969). No visual indication of degradation was observed. This lack of decomposition was attributed to four factors:

1. the inhibition to degradation of microbial substances bound to clay,
2. the absence of available nitrogen in papermill waste effluent,
3. the lignin content of the fiber, and
4. the hydrophilic nature of cellulose.

Both aerobic and anaerobic biological organisms responsible for the breakdown of organics require a minimal source of nitrogen for the synthesis of new cell tissue (Eckenfelder and O'Connor, 1961). Decomposition of cellulose becomes essentially inactive when the available nitrogen becomes less than 1.2 percent (Imshenetsky, 1968). Mazzola (1969) estimated the available nitrogen for the sludges examined at 0.0002 to 0.0005 percent. In recent years, to reduce the dissolved BOD of the wastewater, an accelerated aerobic biological treatment which requires the addition of nitrogen to increase biological activity, is used before the solids are settled out as sludges (Nemerow, 1971; Koch and Lugar, 1958; Eckenfelder and O'Connor, 1961). Therefore, the possibility exists that some newer deposits may have larger amounts of nitrogen than reported by Mazzola (1969).

Consistency Limits

The consistency limits (Atterberg limits), largely through the work of A. Atterberg and A. Casagrande (1948), have become very useful characteristics for classifying soils. The consistency limits indicate the range of water contents (in percent of dry weight) for which a disturbed soil or sludge may be considered as a fluid, plastic, or solid. The liquid limit (L_w) is the water content at which the soil will flow and close a groove of standard width when jarred in a specified manner (ASTM D 423). The fibrous nature of the sludge samples interferes with making the required groove cross section. The plastic limit (P_w) is the water content at which the soil begins to crumble when rolled into threads of a specified size (ASTM D 424).

Casagrande (1966) suggested that peat ranges from low plasticity for thoroughly weathered deposits to non-plastic for highly fibrous deposits. Organic soils fall below the "A" line on the plasticity chart as shown in Figure 2.1. Casagrande suggested that, with an

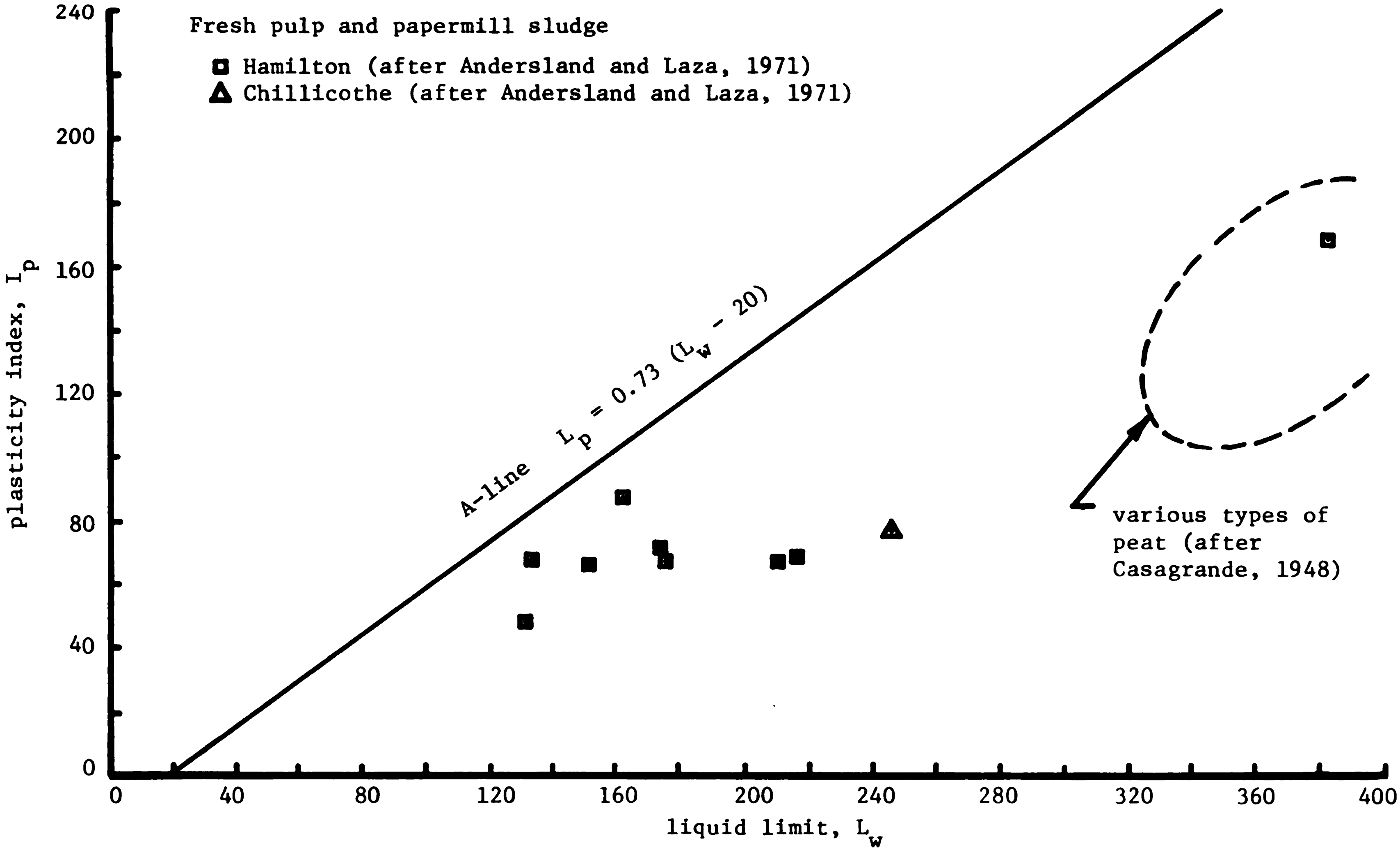

Figure 2.1.--Plasticity chart (Unified Soil Classification System) with data points for several fresh pulp and papermill sludges.

increase in fibrosity, the points on the chart move down and to the left.

Mazzola (1969) concluded that the plastic and liquid limits of papermill sludges were dependent on the ash content, which is indicative of the clay content of the sludge. An increase in fiber content reduces the influence of the clay, hence plasticity would be expected to be reduced. These findings are in agreement with those reported by Vallee and Andersland (1974) for fresh papermill sludge and by Bauer (1966) and MacFarlane (1969) for peat, muck, and similar highly organic soils. On Casagrande's (1948) plasticity index (L_w - P_w) vs. liquid limit chart, the fresh sludge samples tested by Andersland and Laza (1971) fall below the "A" line as shown in Figure 2.1.

Mazzola (1969) found that the field water contents (w), for the field sludge samples tested, were greater than there respective liquid limits. The liquidity index $(w-P_w)/(L_w-P_w)$ for field sludge samples tested ranged from one to over 1000, with most of the deposits in essentially a fluid state. The consolidation potential for deposits with a high index is large since a high index indicates an unconsolidated material, which, when loaded, will experience a large degree of consolidation. A high index also indicates that if the deposit is disturbed there will be a decrease in the shear strength, since remolding transforms the soil into a thick viscous slurry (Terzaghi and Peck, 1967). Consistency limits reported for the fresh papermill sludge by Vallee (1973) are summarized in Table 2.1.

TABLE 2.1 PHYSICAL PROPERTIES OF THE FRESH PAPERMILL SLUDGE (AFTER VALLEE, 1973).

Sludge sample No.	Elevation in layer, ft.	Consistency limits[1] L_w	P_w	Ash[2] content %	Solids[3] content % by wt.	Specific[4] gravity
L-0	5	325.4	141.6	35.7	28.5	2.01
L-1*	2.5	257.3	102.7	42.2	27.2	2.05
L-2*	7.5	247.7	105.6	43.3	28.2	2.07
U-1+	2.5	184.5	86.0	59.4	34.4	2.24
U-2+	4	218.5	101.6	46.5	31.9	2.07
U-3+	5	297.5	133.0	36.5	26.9	1.91
U-4+	7.5	287.4	122.1	34.2	29.0	1.87
U-5+	10	302.8	138.6	32.2	28.4	1.92

*Average of three samples. +Average of 3 tests per sample location.

[1] L_w--liquid limit. P_w--plastic limit. ASTM test methods D 423-66 and D 424-59.

[2] ASTM test method D 586-63.

[3] Solids content of fresh sludge. Water content by dry weight given by the equation

$$w\% = 100 \left[\frac{100}{\%\ \text{solids by wt.}} - 1 \right].$$

[4] ASTM test method D 854-48.

Laboratory test sample locations.

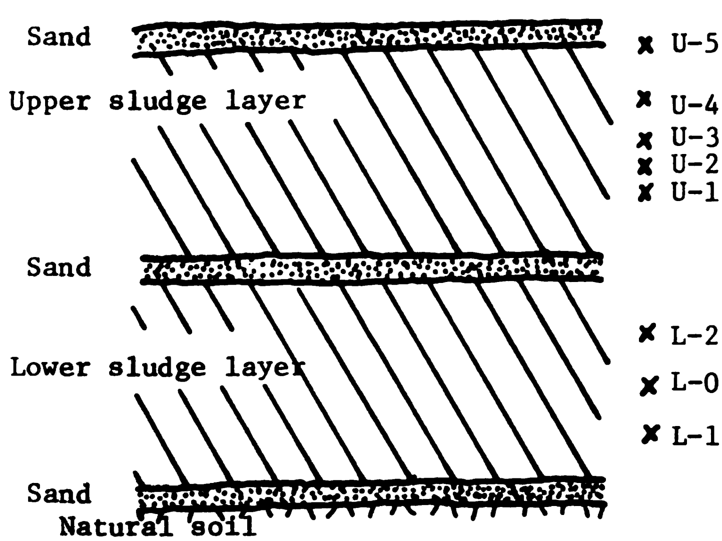

Water Content

The water found in pulp and papermill sludges exists in three different phases (Gehm, 1959): (1) free water, (2) adsorbed water and (3) absorbed water. The free water is not bonded to the sludge and is readily removed, while the adsorbed water molecules are firmly bound by the hydroxyl groups of cellulose and can only be removed with difficulty. The absorbed water in cellulose fibers is not removed by normal mechanical methods. Mazzola (1969) found that the water content for a single sludge deposit varied in both the horizontal and vertical direction. An inverse linear relationship was found to exist between water content and the amount of ash per sample. This appeared to explain the variation of water content observed in the horizontal direction. Water contents ranged from 46 to 740 percent with no samples taken from below the ground water table. Mazzola (1969) noted that the water content of the sludge deposits changes very little with time. Peat and muck deposits have also been reported (MacFarlane, 1969) to give similar results.

B. Stress-Strain Characteristics

The stress-strain behavior of fiberous organic soil or papermill sludge depends on the composite behavior of the material components. Papermill sludge consists primarily of pulp fiber debris and kaolinite clay.

Organic Fibers

The fiber debris includes portions of the elongated cell walls of the wood structural elements. Undamaged, the fibers are tapered, thick- or thin-walled tubes, closed at both ends. Their dimensions and overall structural properties vary within every plant species (spring or summer wood) and between different species. The average length ranges from about 1 mm (beech, straw) to 3 or 4 mm (spruce, pine) or even centimeters (cotton, hemp). The width varies from 10 to 40 microns. Mechanical treatment can alter the dimensions and shapes of the fibers considerably. In paper, thin-walled, long and flexible fibers are collapsed to ribons, where thick-walled, short and rigid fibers retain much of there tubular shape. Cellulose fibers swell in water, mainly in thickness, and shrink when being dried (Corte, 1966). Swelling of the cellulose fibers can result in a 200 to 300 percent weight increase, a one percent length increase, 15 to 20 percent diameter increase and up to a 35 percent volume increase (Mazzola, 1972).

Jayne (1959) reports Young's Moduli for softwood fibers to be 2.5 to 3.6 x 10^5 kg/sq cm (3.6 to 5.2 x 10^6 psi). Kallnes and Bernier (1962) reports Young's Moduli for spruce fibers to be 2.8 to 3.5 x 10^5 kg/sq cm (4.1 to 5.1 x 10^6 psi). Tensile strengths have been reported from 10 to 50 grams per fiber, which is a stress of 4 to 10 x 10^3 kg/sq cm (5.8 to 14.5 x 10^4 psi). Values are very dependent on the method of clamping, rate of straining or loading, relative humidity and plant species (Jayne, 1959; Leopold and McIntosh, 1961; and Harter, et al., 1963). Robertson, et al. (1961) have reported on the bending and shearing resistance of fibers.

There is little known of the bonds between fibers in paper. Corte (1966) reports experiments on a wet fiber mat deposited on a laboratory sheet-making machine that was treated with alcohol to extract the water without disturbing the geometrical structure of the mat. The alcohol was displaced in a similar way with carbon tetrachloride. The resulting sheet had virtually no mechanical strength. These experiments show that the coherence and strength of a sheet of paper are caused primarily by hydrogen bonds between the hydroxyl groups of cellulose on the surfaces of adjacent fibers, and not by the mechanical entanglement of the fibers. At and above about 20 percent solids content, according to experiments by Lyne and Gallay (1954), hydrogen bonds are formed. At high water contents (over 10 percent) the hydroxyl groups of water compete with those of cellulose and by mechanical stirring, the fibers can usually be completely separated (Brecht, 1962).

Studies for the purpose of evaluating the effect of fiber on sludge behavior, by examining both the relative amount of fiber and the length of the fiber present, have been conducted. The amount and length of fiber was found to have a strong influence on the effectiveness of removal of water by mechanical pressing methods (NCASI Tech. Bull. No. 174 and 136). Andersland and Laza (1971) reported that, for fresh papermill sludge samples, the organic content had a direct influence on the angle of internal friction.

Kaolinite Clay

The primary clay mineral added to the fiber suspension for paper making is kaolinite (5 to 10 percent, sometimes up to 25 percent by weight). It is added partly for economic reasons because it is cheaper than pulp, and partly because it improves the appearance of the paper, and because it makes the sheets lie flat and improves the printability of the paper (Corte, 1966). In recycling, the fibers are the economic portion recovered and the clay is the waste product along with some lost fibers. In paper production, some clay and fibers are lost during production. Paper sludge, therefore, is composed primarily of the lost or unwanted fibers and clay.

Kaolinite is an important and common two-layer mineral (layer of gibbsite on top of a layer of silicate). Olson (1974) has reported on more than 200 triaxial compression tests conducted on commercially available kaolinite. For this clay the liquid limit ranged from 40 to 50 percent, the plastic limit 27 to 31 percent, and the specific gravity was equal to 2.65. Olson observed that the angle of internal friction, $\bar{\phi}$, ranged from 25 to 30 degrees. Gibbs, et al. (1960) reported an angle of internal friction of 25 degrees. Lamb and Whitman (1969) report that the plastic limit of kaolinite ranges from 27 to 37 percent and the liquid limit ranges from 38 to 59 percent depending on the exchangeable ion.

Fibrous Organic Soils as a Composite Material

Papermill sludge consists primarily of fiber debris and kaolinite clay. This composite material should have mechanical properties dependent on the elastic behavior of the fibers imbedded in the plastic clay and the bond between these fibers and the clay matrix. The shear strength parameters for kaolinite clay with zero organic content has been reported by Gibbs, et al. (1960) and Olson (1974). Laza (1971) has reported on the shear strength parameters of papermill sludge with varying amounts of organic fibers and clay. However, little is known about the wet strength of the fibers, their stress-strain properties, both average and range of fiber length and shape, and the type of bonding between the fiber and the clay matrix. There is also little data on properties of random oriented discontinuous fiber reinforced composites. It is known that the size and shape of the fibers plays a very important role in determining their properties. Fibers with smaller diameters can, in general, take higher stresses than fibers with larger diameters (Sears, 1962). Paper fiber, when viewed under a microscope, shows a balloon swelling (bamboo-like) structure. Such fibers are generally lower in strength, but because of the bamboo grip, a substantial matrix reinforcement may be attainable through friction, even in the absence of good adhesion.

As generally accepted, the load is transfered from the matrix to the reinforcement through shear. The shear results from displacements of the reinforcing fibers by means of shear tractions at the fiber-matrix interface according to the stresses on the composite (Wohrer and Economy, 1966). The presence of the fibers should reinforce the sample and help retard the propagation of cracks. The relatively low modulus of the clay matrix should allow for the effective transfer of stress to the higher modulus fibers, provided the length of the fibers is sufficient. Biggs (1966) points out that, for an elastic fiber of length (L) and radius (r) embedded in a plastic matrix, there will be a tangential stress (τ) exerted on the fiber by the slipping matrix. The stress (σ_x) in the fiber at a point distance x from one end is

$$\sigma_{(x)} = \frac{2\tau x}{r} \tag{2.1}$$

and the elastic strain in the fiber is

$$\varepsilon_x = \frac{\sigma_x}{E} \tag{2.2}$$

The fiber stress increases approximately linearly from the ends. Wohrer and Economy (1966) and Kelly and Tyson (1964) state that the "rule of mixing" can be applied to calculate the potential strengthening attainable with random discontinuous fibers, as expressed by, the following equation:

$$\sigma_c = k\,\sigma_f\,V_f\,(1 - \frac{L_c}{2L}) + \sigma_m^*\,V_m \tag{2.3}$$

in which,

σ_c, σ_f, σ_m^* = break stress of composite, fiber, and matrix,

V_f, V_m = volume fraction of fiber, and matrix,

L_c, L = critical fiber length, fiber length

k = 0.2 for random fiber orientation

The critical fiber length (L_c) is defined as the maximum length at which the fiber will pull out of the matrix and not break.

The critical length (L_c), the average length (L), and the average breaking stress (σ_f) of the fibers, along with the deviations from the averages, are unknown for papermill sludges. If these were known, it would be theoretically possible to calculate the strength of the composite (σ_c) by considering the properties of both the fiber and the clay matrix using the "rule of mixing" equation. Further research is needed to explain the mechanism and effect of fiber reinforcement in papermill sludge and other fibrous organic soils.

Similarity to Organic Soils

Considerable work has been reported in the literature on consolidation properties of highly organic soils such as peat. Limited work has been reported regarding the shear strength since these soil types are generally avoided in engineering practice. Organic terrain has only come under serious scientific study within the last few years. The National Research Council of Canada, through its Associate Committee on Geotechnical Research (NRCC-ACGR), first gave serious consideration to the problem of organic terrain in 1947. MacFarlane's (1969) handbook on muskeg (peat) contains a review of the state of the art of organic terrain and the outcome of discussions at the annual meetings of the NRCC-ACGR.

Little research has been done on the correlation of different types of peat with the physical and strength properties. Peat is composed of organic material. When submerged beneath the groundwater table, peat is not entirely inert and undergoes a very slow anaerobic decomposition which produces methane gas. When the water table is lowered, oxidation of peat occurs releasing carbon dioxide. No widely recognized method is presently available to measure the gas content of peat (MacFarlane, 1969).

Low shear strengths and large settlements of organic soils, when loaded, are partly due to a low degree of consolidation found in the field (MacFarlane, 1969). This may be due to the low effective vertical pressure and the long drainage paths. The low effective vertical pressure is due to (1) the low specific gravity of the organics, (2) the lack of a surcharge, and (3) a high water table. Hanrahan (1954) pointed out that one of the difficulties in tests on peat is the anisotropic nature of the material. Obtaining representative undisturbed samples is very difficult. Hanrahan (1954) ran triaxial tests on undisturbed peat samples which were first consolidated and then allowed to swell. These tests were difficult to carry out due to the large and non uniform volume change associated with the peat. The friction angle $\bar{\phi}$ for the overconsolidated samples was only about 5 degrees leading Hanrahan (1954) to conclude that the strength of overconsolidated peat was exclusively cohesive in character.

Adams (1961 and 1965), using consolidated-undrained triaxial tests on peat, observed friction angles as large as 50 degrees. In each test the pore pressure buildup was rapid and at failure essentially equal to the cell pressure. Cohesion values were found to be negligible. The value of K_o was determined to be 0.3 from anisotropic consolidation with no lateral strain. Other investigations (Hanrahan, <u>et al.</u>, 1967) on remolded samples of an organic peat have shown similar results. The values for $\bar{c}$ varied from 0.7 to 1.0 psi and the friction angle $\bar{\phi}$ ranged from approximately 35 to 44 degrees. The pore pressure coefficient B was found to be unity for the soft saturated peat.

MacFarlane (1969) discusses the use of surcharges on peat and muck to increase shear strength and to reduce the long-term settlement. Preconsolidation has become widely accepted in Canada and has specific application where the depth of peat is in excess of 6 to 8 feet (1.83 to 2.44 meters). With surcharges on peat considerable settlements can be expected and the stability of the peat must be ascertained. Kovalenko (1969) reported a field test in which a surcharge (2 meter sand layer) was placed over a peat deposit to accelerate the consolidation. As the consolidation progressed the shear strength of the peat increased from about 0.1 to about 0.3 kg/sq cm. The organic content of the peat was not reported.

MacFarlane (1969) and others have suggested an approximate method (max error of 18 percent in extreme cases) for determining the specific gravity of peat. It assumes that the ash is composed of clay materials with a specific gravity of 2.7 and that the organic material has a specific gravity of 1.5. The average specific gravity of the peat solids is then given by the equation

$$G = (1 - A_c)\ 1.5 + 2.7\ (A_c) \qquad (2.4)$$

where A_c is the ash content.

Andersland and Laza (1971) used consolidated-undrained triaxial tests with pore pressure measurements on an integrated pulp and paper-mill sludge and a secondary fiber mill sludge. Cohesion values ($\bar{c}$)

ranged from zero to 0.3 kg/sq cm. The angle of internal friction ($\bar{\phi}$) ranged from about 45 degrees at low organic contents (28%) to about 64 degrees at a higher organic content (50%). Large strains were required to fully mobilize the available shear strength. Triaxial test data show that the strength of pulp and paper mill sludges to be essentially frictional and in accordance with the principal of effective stress. It was shown that both shear strength and permeability were influenced by the solids content of the sludge and the amount of organic matter. The pore pressure coefficient B was found to be unity for saturated sludge.

C. Vane Shear Strength vs. Field Shear Strength

In 1948 Cadling (Bjerrum, 1972) developed the vane test for in-situ measurements of the undrained shear strength. Most of the uncertainties due to disturbance of samples used for the laboratory determination of shear strength were thereby removed. Originally, shear strengths measured with the vane were assumed to be equal to the field undrained strength. However, an analysis of actual failures by Casagrande (1960) and Bjerrum (1972) shows that the undrained strength measured by an in-situ vane test is, in general, greater than the field strength. Bjerrum (1972) observed that the discrepancy between the vane and the field shear strength for 14 embankment failures was larger the more plastic the clay. He therefore developed a correlation between the ratio of the vane shear strength to the actual shear strength at failure and the plasticity indices of the clays (Figure 2.2). Hence

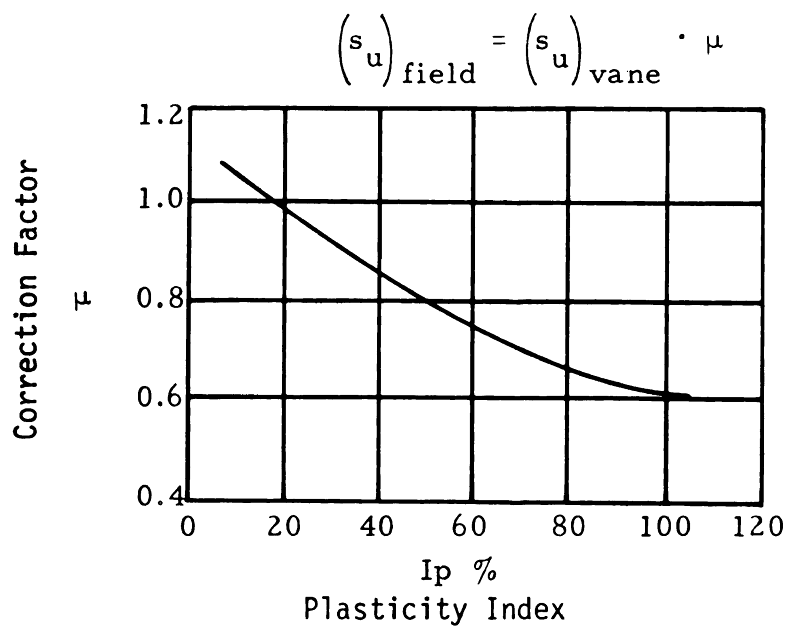

Figure 2.2.--Correction factor for converting vane shear strengths to field shear strengths (after Bjerrum, 1972).

$$(S_u)_{field} = (S_u)_{vane} \cdot \mu \qquad (2.5)$$

where μ equals the correction factor from Figure 2.2.

Three of the fourteen embankment failures cited by Bjerrum (1972) to define the correction factor where embankments of organic clays.

D. Movement and Stability of Cut Slopes

Dewatered high ash pulp and papermill sludges disposed of in landfills may have a solids content as high as 40 percent by weight (equivalent to 150 percent water content by dry weight). When pulp fibers are present in significant amounts (greater than 15 percent by weight) the sludge appears fibrous and will hold its shape in the dewatered condition. In the absence of fiber, the sludge is putty-like, and fluid at solids contents as high as 35 percent. The ash materials in these sludges are comprised mostly of kaolinite clay with small amounts of lime, titanium oxide and iron. The semi-liquid to liquid state of these dewatered sludges means that lateral confinement is needed during construction of a cell type of landfill.

The use of drainage blankets together with a small earth surcharge permits drainage of water from the sludge resulting in a significant decrease in volume and an increase in the strength of the sludge. The weight of overlying sludge helps consolidate material at lower levels. Information on shear strength is given in Section V-B. The vertical movement or settlement of the experimental landfill surface was produced entirely by the decrease in water content associated with consolidation. Photomicrographs of fibers from papermill waste deposits that have been in place for up to 12 years have shown that virtually no decomposition of the fiber had occurred (Gillespie, Mazzola, and Gellman, 1970). The presence of lignin (Umbreit, 1962) and clay (Lynch, 1956) and the absence of sufficient available nitrogen (Imshenetsky, 1968) are known to inhibit the biological breakdown of cellulose. All three of these conditions probably exist in a papermill sludge landfill. Prediction of the amount and rate of settlement observed in an experimental sludge landfill has been presented elsewhere (Vallee and Andersland, 1974).

Lateral movement may occur when an excavation is to be made in the sludge landfill or when the foundation for a structure is to be placed on the consolidated papermill sludge. Factors affecting the behavior of excavated slopes include slope height, slope angle, unit weights, pore pressures, initial stress conditions (prior to excavation), stress-strain and strength characteristics of the sludge, creep characteristics of the sludge, drainage conditions, time, and perhaps more. Information on initial stresses, based on the total pressure cell data taken towards the end of the consolidation period and data on other factors, are given later in this thesis. During excavation the stresses on the slope surface are reduced to zero. This reduction in stresses will induce strains and displacements in the exposed sludge slope. Numerical techniques for predicting slope deformations require information on the stress-strain behavior of the consolidated sludge. Experimental data are given later in this thesis on sludge samples tested under conditions closely simulating field conditions.

Soil or sludge located beneath a sloping surface has a tendency to move downward and outward under the influence of gravity. Material beneath foundations moves downward and outward as loads approach the bearing capacity of the material. When this tendency is counteracted by the shearing resistance of the soil or sludge, the slope or foundation is stable. Otherwise a failure occurs. For a slope this failure may take the form of a flow, a rotational movement along a circular slip surface, or a movement along a composite slip surface. Slides in soil or sludge may be caused by external disturbances such as excavation near the base of the slope or additional loading on or behind the slope from more fill or the placement of some other load. Failure in soils may also be caused by a temporary increase in pore water pressure or by a progressive deterioration of the strength of the material.

In principle an analysis of the distribution of displacements or stresses throughout a slope could be used to decide the question of its behavior. At present, however, there is generally insufficient knowledge of the in situ stresses and stress-deformation-time properties of soils to make this approach practicable. As a result it is general practice to use limit equilibrium methods to assess the stability of soil slopes (Lambe and Whitman, 1969). In all methods of limit equilibrium analysis, a condition of incipient failure is postulated along a continuous slip surface of known or assumed shape. A quantitative estimate of the factor of safety of the slope with respect to shear strength is then obtained by examining the equilibrium of the soil mass above this rupture surface. The problem is usually assumed to be one of plane strain. The two methods of analysis

summarized include rotational movement along a circular slip surface and movement along a composite (non-circular) slip surface. A summary of a recent approach for investigating the development of failure zones around slopes during excavation completes this chapter. Methods for evaluating the stability of slopes are summarized in the following sections.

Shear Strength Theory

Information on bearing capacity and slope stability of papermill sludges in landfills is not available. One must draw on methods available in the field of soil mechanics which require data on the shear strength of the sludge material in question. Shear failure starts at a point in a mass of soil when, on some surface passing through the mass, a critical combination of shear stress and normal stress is reached. Experience has shown that the Mohr-Coulomb theory of failure has been very successful for defining failure in soil materials (Terzaghi and Peck, 1967). This theory, represented in the form

$$\tau_{ff} = c + \sigma_{ff} \tan \phi \qquad (2.6)$$

states that the shear stress τ_{ff} on a failure surface at failure is a function of the normal stress σ_{ff} on that plane at failure and the material properties cohesion c and angle of internal friction ϕ. In this form the soil skeleton must carry all the normal stress, that is the soil must be free draining.

For cohesive soils or papermill sludges that are not free draining, the pore fluid will carry part of the normal stress. This portion cannot contribute to the frictional resistance and shear strength. Hence for these materials the stress carried by the pore fluid must be subtracted from the total normal stress and the shear strength will be based only on that portion of the normal stress carried by the soil skeleton. This is done by measuring the pore water pressure during triaxial testing and presenting the results in terms of effective stresses. Equation 2.6 now becomes

$$\tau_{ff} = \bar{c} + (\sigma_{ff} - u) \tan \bar{\phi} \tag{2.7}$$

where u is the pore water pressure, $\bar{c}$ is the cohesion intercept based on effective stresses, and $\bar{\phi}$ is the angle of internal friction based on effective stresses. Equation 2.7 represents a straight line with intercept on the shear stress axis equal to $\bar{c}$ and slope angle equal to $\bar{\phi}$ as shown in Figure 2.3. The shear strength, so defined, is the maximum shear stress that may be sustained on any plane in a given soil or sludge material. When information on the pore pressure u is not available or when total stresses are to be used in a stability analysis, the undrained shear strength τ_{ff}, defined as

$$\tau_{ff} = c_u + \sigma_{ff} \tan \phi_u \tag{2.8}$$

may be used. The total stress strength parameters c_u and ϕ_u denote the apparent cohesion and the angle of shearing resistance, respectively. When ϕ_u equals zero, c_u equals $1/2(\sigma_1 - \sigma_3)_f$ where σ_1 and σ_3 are the major and minor total principal stresses at failure. Relations between angle of internal friction ($\bar{\Phi}$), principal effective stresses, and shear strength at failure are shown in Figure 2.4.

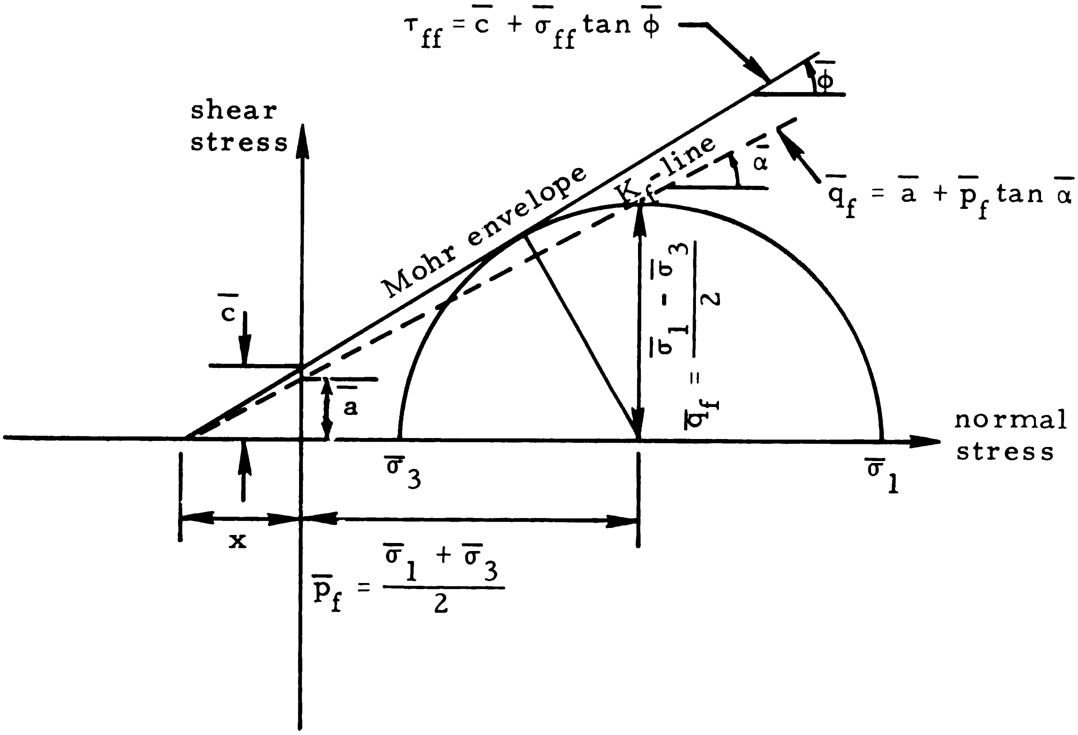

$$\tan \bar{\alpha} = \frac{\dfrac{\bar{\sigma}_1 - \bar{\sigma}_3}{2}}{\dfrac{\bar{\sigma}_1 + \bar{\sigma}_3}{2} + x}$$

$$\sin \bar{\phi} = \frac{\dfrac{\bar{\sigma}_1 - \bar{\sigma}_3}{2}}{\dfrac{\bar{\sigma}_1 + \bar{\sigma}_3}{2} + x}$$

$$\therefore \tan \bar{\alpha} = \sin \bar{\phi}$$

$$\tan \bar{\alpha} = \frac{\bar{a}}{x} \quad \text{or} \quad x = \frac{\bar{a}}{\tan \bar{\alpha}}$$

$$\tan \bar{\phi} = \frac{\bar{c}}{x} \quad \text{or} \quad x = \frac{\bar{c}}{\tan \bar{\phi}}$$

$$\therefore \frac{\bar{a}}{\tan \bar{\alpha}} = \frac{\bar{c}}{\tan \bar{\phi}}$$

$$\text{but } \tan \bar{\alpha} = \sin \bar{\phi}$$

$$\therefore \frac{\bar{c}}{\tan \bar{\phi}} = \frac{\bar{a}}{\sin \bar{\phi}}$$

$$\bar{c} = \frac{\bar{a}}{\cos \bar{\phi}}$$

Figure 2.3.--Equations and definitions for shear strength theory, effective stress basis.

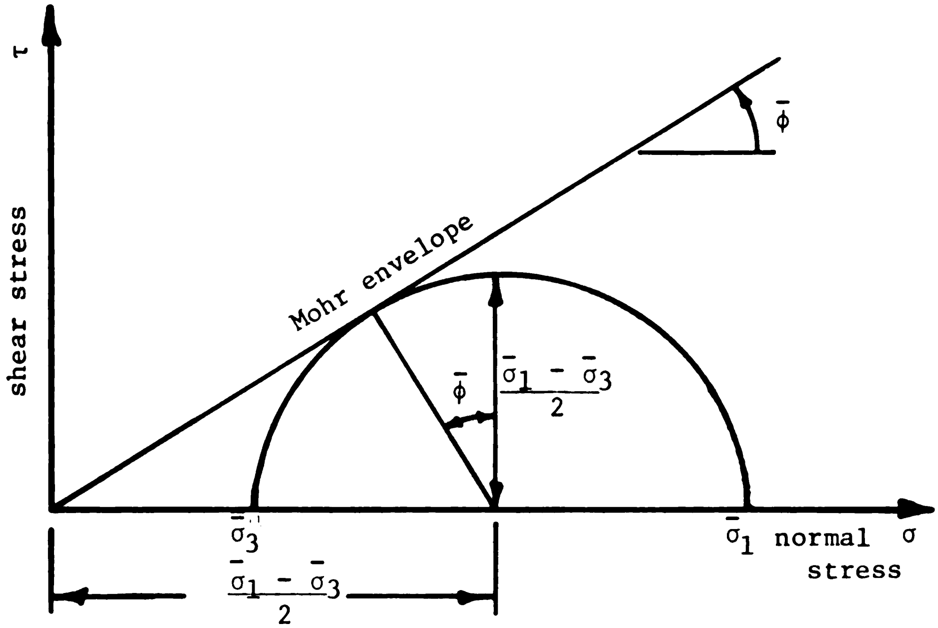

$$\frac{\bar{\sigma}_1}{\bar{\sigma}_3}\Big]_f = \tan^2\left[45^\circ + \frac{\bar{\phi}}{2}\right]$$

$$\text{Undrained shear strength} = \bar{q} = \frac{1}{2}(\bar{\sigma}_1 - \bar{\sigma}_3)_f$$

$$= \frac{\bar{\sigma}_{3f}}{2}\left[\tan^2\left(45^\circ + \frac{\bar{\phi}}{2}\right) - 1\right]$$

Figure 2.4.--Relations between angle of internal friction ($\bar{\phi}$), principal stresses, and undrained shear strength (Lambe and Whitman, 1969).

Experience has shown that the $\bar{c}$ and $\bar{\phi}$ values determined by consolidated-undrained triaxial tests on soils with pore pressure measurements (Bishop and Henkel, 1962) correlated well with field behavior. For these tests a soil sample, usually 1 1/2-in. in diameter by 3 in. high, is subjected to an all-around pressure σ_3 and allowed to consolidate under drained conditions. The vertical stress σ_1 is next increased under undrained conditions until the sample fails. Failure is taken to be the maximum deviator stress $(\sigma_1 - \sigma_3)$ or for some soils is taken at an arbitrary strain of 10 percent or 20 percent. During the loading period measurements are taken of pore water pressure, axial deformation, and axial load. Results from each test are represented by an effective stress circle at failure. If several triaxial tests are performed with different consolidation pressures and the measured stresses corresponding to failure plotted, the points representing failure are given by the envelope of stress circles. This envelope is known as the rupture line and, although it may not be perfectly straight, it can be represented by a straight line with sufficient accuracy so that the resulting material properties adequately reflect field behavior for soils. In normal laboratory evaluation three to five tests are made and the rupture line is drawn tangent to the observed failure circles. Since this method of evaluation depends on visual determination of the tangent points, it is desirable to adopt a method that uses the points of maximum shear stress at failure. Lambe and Whitman (1969) represented these points as

$$\bar{p}_f = \frac{\bar{\sigma}_1 + \bar{\sigma}_3}{2} \text{ and } \bar{q}_f = \frac{\bar{\sigma}_1 - \bar{\sigma}_3}{2} = \frac{\sigma_1 - \sigma_3}{2} \tag{2.9}$$

These points are unambiguous and precisely determined, allowing curve fitting methods to determine the line of best fit. This method gives the K_f failure line and results in a y intercept $\bar{a}$ and a slope angle $\bar{\alpha}$. The geometric transformations given in Figure 2.3 permit computation of the desired values of $\bar{c}$ and $\bar{\phi}$. Detailed information on triaxial tests used in this study are given in Chapter III.

<u>Rotational Movement</u>

The circular arc analysis which is sufficiently accurate for most purposes is that given by Bishop (1954) and generally termed the Bishop simplified method (Figure 2.5a). This method is derived by equating the moments about point O of the weight of soil within ABCD with the moment of the shear forces acting on the slip surface. For convenience the soil within ABCD is divided into a number of slices, one of which is shown in Figure 2.4a. The normal effective force $(P - u\ell)$ on the base of the slice considered, denoted by $\bar{P}$, is found by resolving forces vertically. Thence, assuming that $(X_n - X_{n+1}) = 0$, the following expression for the factor of safety F is obtained:

$$F = \frac{1}{\Sigma W \sin \alpha} \cdot \quad \Sigma\left[\{\bar{c}\ b + (W - u\ b) \tan \bar{\phi}\} \frac{1}{m_\alpha}\right] \qquad (2.10)$$

where

$$m_\alpha = \cos \alpha \left(1 + \frac{1}{F} \tan \alpha \cdot \tan \bar{\phi}\right) \qquad (2.11)$$

Symbols are defined in Figure 2.5a. The factor of safety F is defined as the ratio of the available shear strength of the soil to that required

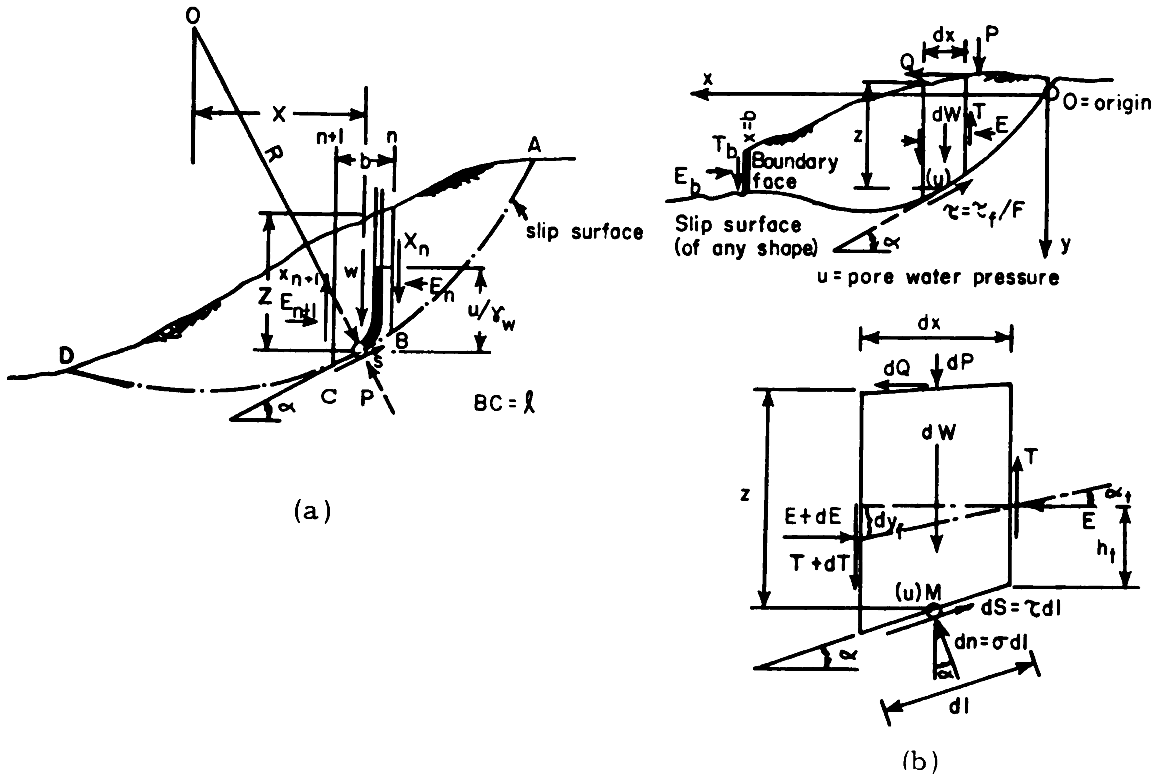

Legend

b = slice width

c = cohesion

E = normal force on slice sides

l = length of slip surface

O = center of failure circle

P = force normal to base

R = radius of failure circle

s = shearing resistance

u = pore water pressure

W = total weight of slice

x = distance

X = shear force on slice sides

Z = depth to a point

α = inclination of base

γ_w = unit weight of water

σ = normal stress

τ = shear strength

Figure 2.5.--(a) Forces in the circular arc analysis (after Bishop, 1954)
(b) Notation to Janbu's (1957) analytical procedure.

to maintain equilibrium. As the term F appears on both sides of equation 2.10 the solution has to be obtained by a process of successive approximation. Convergence is very rapid and the method can be carried out easily by hand or by computer (Bailey and Christian, 1969). Values of m_α can be read off a chart for any assumed value of F. In general the error resulting from use of the Bishop simplified method is 7 percent or less and is usually under 2 percent (Whitman and Bailey, 1967).

For the total stress ($\phi_u = 0$) analysis the shear strength mobilized equals c_u/F. Since this shear strength is independent of the normal stress on the slip surface, a simplification results. Equating moments, as before, yields the expression for the factor of safety F. If the method of slices is used this expression has the form:

$$F = \frac{\Sigma c_u \ell}{\Sigma W \sin \alpha} \tag{2.12}$$

This expression is exact, and is easily adaptable to irregular slope profiles and non-uniform shear strength conditions.

Composite Sliding Surface

A rather accurate method for analyzing noncircular slip surfaces is given by Janbu (1954, 1957). In order to render the problem statically determinate Janbu assumed that the reaction forces dN (Figure 2.5b) acted at the center of the base $d\ell$ of the slice and that the position of the resulting earth pressures E and E + dE at the interface between adjacent slices are known. Using the notation of Figure 2.5b, the equations of equilibrium for each slice are:

$$\text{Vertical:}\quad dW + dP + dT = dS \sin\alpha + dN \cos\alpha \tag{2.13}$$

$$\text{Horizontal:}\quad dE - dQ = - dS \cos\alpha + dN \sin\alpha \tag{2.14}$$

$$\text{Moment about M:}\quad Tdx + E\, dy_t - dEh_t + dQ\, z = 0 \tag{2.15}$$

For a stability analysis in terms of effective stresses, introduction of the appropriate expression for shear strength leads to the following working formula for finite differences:

$$F = \frac{\Sigma\, \tau_f \cos^{-2}\alpha \cdot \Delta x}{Q - E_b + \Sigma(p + t)\tan\alpha \cdot \Delta x} \tag{2.16}$$

where

$$\tau_f = \frac{\bar{c} + (p + t - u)\tan\bar{\phi}}{1 + (\tan\alpha \cdot \tan\bar{\phi})\frac{1}{F}}, \tag{2.17}$$

$$p = \frac{\Delta W}{\Delta x} + \frac{\Delta P}{\Delta x} = \gamma z + q, \text{ and } t = \frac{\Delta T}{\Delta x}.$$

By assuming a reasonable position for the line of thrust, accurate values for the internal forces, E and T, are obtained by means of successive approximation procedures. Initial values of E and T can be calculated for the condition $t = 0$. When τ_f is introduced into the moment equation for slip circle analyses, one obtains the formula derived by Bishop (1954). Total stress ($\phi_u = 0$) analysis for non-circular slip surfaces is provided by using the average undrained shear strength on the base of the slice in equation 2.17.

Failure Zone Around Slopes During Excavation

Failure zones develop in excavated slopes when the maximum shear stress values approach the shear strength of the papermill sludge or when tensile stresses exceed the very low tensile strength of the sludge. When idealized elastic properties are assumed for soil slopes, local overstress will occur when the factor of safety (by the slip circle method) lies below a value of about 1.8 (Bishop, 1954). Plans for the experimental papermill sludge landfill included slope failure (factor of safety close to unity), hence local overstress, such as tension cracks, was anticipated. It appeared desirable to determine in what portions of the experimental slope failure first occurred and how it progressed. In order to predict stresses within the slope, it was necessary to employ analytical procedures other than the equilibrium methods. The finite element method of analysis, as used by Dunlop, et al. (1968) in their analyses of slopes in soil, appeared suitable for investigating the development of failure zones in the sludge slope. The basic concepts of the finite element method are summarized in the following paragraphs and its application to the experimental papermill sludge slope is given in Chapter VI.

The finite element method may be thought of as an application of the displacement or stiffness method of structural analysis. The basic concept of the method is that a continuum with infinite degrees of freedom can be approximated as an assemblage of elements interconnected at a finite number of nodal points having a finite number of unknowns. The elements may be triangles, groups of triangles, or rectangles for two-dimensional plane strain analyses. Within each element, displacements are assumed to vary in such a way that compatibility within the element and along its boundaries is maintained. Displacement continuity between adjacent elements is satisfied at common nodal points. For triangular elements with three nodal points this may be accomplished by specifying displacements which vary linearly in two mutually perpendicular directions within the element. For elements with more nodal points, higher order displacement variations are employed.

The finite element analysis of an elastic continuum consists of five basic steps:

1. Idealization of the continuum so that the finite element assemblage simulates the continuum,

2. Determination of the stiffness properties of each element to obtain a total stiffness matrix,

3. Prescribe boundary conditions,

4. Analysis by standard structural methods to determine the nodal point displacements, and

5. Determination of the element stresses from the nodal point displacements, since forces acting at the nodes are uniquely defined by there displacements (Zienkiewicz, 1971).

Because each element in the assemblage may have a different modulus value from its neighbors, the method is well-suited to soil problems involving heterogeneity. Approximate analyses of nonlinear earth structures are possible by incremental loading or iterative procedures. The finite element method is also capable of handling virtually any boundary conditions specified in terms of forces, stresses (resolved into nodal forces) and displacements. Mixed boundary value problems may be handled as easily as problems involving only force or displacement boundary conditions.

Dunlop, et al. (1968) performed a detailed finite element analysis of excavated soil slopes. In their analysis the basic finite element consisted of a quadrilateral composed of four constant strain triangles. The study provided computations of displacements, strains, and stress distributions, and it enabled the location of failure zones. The effect of such factors as in situ stresses, anisotropy, variation of strength within the soil deposit, pore pressure distributions, and sequential construction were studied. Various constitutive laws, such as linear, bilinear, and multilinear (piecewise linear) were compared. Requirements for boundary conditions for plane-strain, element sizes and element shapes, and a finite element computer program for excavated slopes are given by Dunlop, et al. (1968).

CHAPTER III

ENGINEERING PROPERTIES OF PAPERMILL SLUDGE

The physical properties and stress-deformation behavior of the papermill sludge are needed for making slope stability predictions, based on theory, for comparison with observed field behavior of the experimental cut slopes. Methods and equipment for measurement of these engineering characteristics are described below. Reference is made to standard test procedures where possible.

A. Physical Properties

Physical properties of papermill sludge characterize, to some extent, the quality of the sludge relative to engineering purposes. The fibers in the sludge are shown in Figure 3.1a. Information on measurement of water content, unit weight, specific gravity of the solids, ash (or organic) content, and consistency limits are included later in this thesis and have been reported by Vallee and Andersland (1974). The water content and unit weight are used in describing changes in the sludge as a result of consolidation. Specific gravity was required for computations involving solids-water-air relationships. Ash contents from block samples provided more information on sludge uniformity. Consistency limits were reported for the fresh papermill sludge by Vallee and Andersland (1974) and are summarized in Table 2.1.

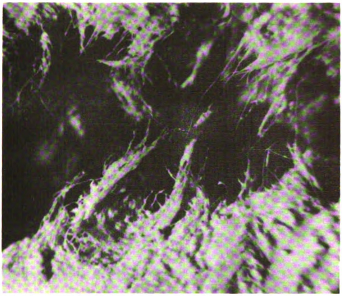

(a)

(b)

Figure 3.1.--(a) Fibers in papermill sludge (Magnification x 30)
(b) Undisturbed block sample of consolidated sludge.

B. Strength Characteristics

Undisturbed block samples were obtained from the landfill when the north dike was removed for the stability study. Each block was cut from the exposed slope as shown in Figure 3.1b. The sides and top were wrapped in saran wrap and aluminum foil. Elevations were taken to properly describe the block location. Next a wooden box with the bottom removed was placed over the wrapped sludge. The block bottom was cut loose and the entire block turned over. After additional trimming, saran wrap and aluminum foil were folded over the bottom of the block. Warm paraffin was poured into the open spaces around the block and the box bottom was attached. These block samples of sludge were easily transported to the laboratory with a minimum of disturbance. Sludge blocks were protected against possible moisture loss during storage by placing each unopened box in a sealed plastic bag. Temperature during storage did not exceed about 24°C.

Fresh sludge samples, reported by Vallee (1973) during construction of the landfill, are identified and described in Table 2.1.

Triaxial Shear Tests

The triaxial test requires that the cylindrical specimen (Figure 3.2a) be sealed in a water-tight membrane and be enclosed in a cell (Figure 3.2b) in which the specimen can be subjected to a fluid pressure. A load applied axially, through a ram acting on the top sample cap, was used to control the deviator stress. Under these conditions the axial stress was the major principal stress, σ_1, and the intermediate and minor principal stresses (σ_2 and σ_3, respectively)

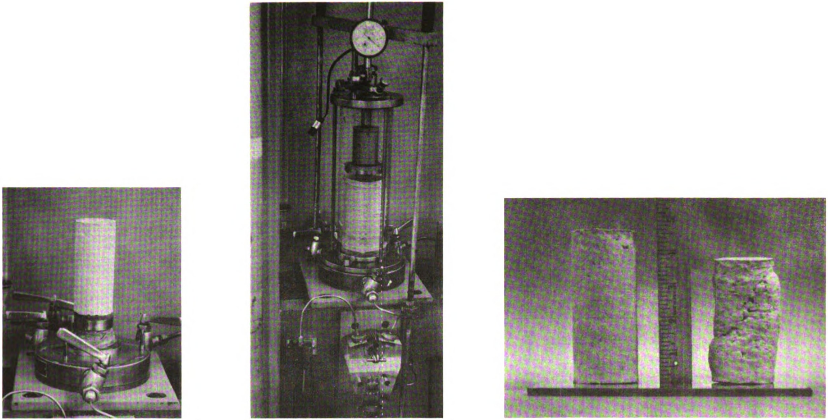

(a) (b) (c)

Figure 3. 2. Triaxial tests. (a) Mounting the cylindrical sample. (b) Anistropic consolidation in the triaxial cell. (c) Newly prepared sample left, failed and oven dry sample right.

were both equal to the cell pressure. Connections to the ends of the sample permitted either drainage of water and air from the voids in the sludge, or alternatively, the measurement of the pore pressure under conditions of no drainage. Generally the application of the all-around pressure and of the deviator stress form two separate stages of the test. Therefore triaxial tests are classified according to the conditions of drainage developed during each stage and any special conditions imposed on the sample to simulate field conditions. Sample preparation, undrained tests, and consolidated-undrained tests are described below. All triaxial tests were run at room temperature, close to 23°C.

Sample Preparation.--Two types of samples were prepared: remolded (laboratory consolidated) and undisturbed (field consolidated). For the fresh sludge obtained during construction of the landfill, sample preparation involved placement into a cylindrical mold 7.13 cm high by 3.56 cm in diameter. Care was taken to work the sludge into the mold so as to minimize layering and the formation of any cavities. Fibers were not oriented in any preferred direction. With the mold filled, the ends were carefully trimmed until they were perpendicular to the sample axis. Next the mold was disassembled by pulling the sides directly away from the specimen. The sample was then weighed, placed in an air tight container, and stored in a high humidity compartment until just prior to mounting in the triaxial cell. Different organic content test specimens were obtained by the appropriate selection of sludge from the available field samples.

Undisturbed test specimens were obtained from block samples C and G. Specimen preparation involved cutting, by means of a hand saw, a 4 in. by 4 in. by 6 in. (10 cm by 10 cm by 15 cm) chunk from the block of sludge. For additional strength during handling, each end of the sample was wrapped with tape and encased in wax. This sample of sludge was then placed in a motorized soil lathe. Since wire trimming devices were not suitable, a hobby tool with a high speed rotating 3/4 in. (1.9 cm) diameter circular saw was used for trimming the sludge into cylindrical specimens 2 in. (5.08 cm) in diameter by 4 in. (10.16 cm) high (Figure 3.2c). The low sensitivity of the consolidated sludge helped minimize sample disturbance. Specimens were prepared with the cylindrical axis vertical, horizontal, or at 45 degrees to the horizontal as needed for the test program. After trimming, sample dimensions and weight were recorded. Sample specimens were stored in a sealed plastic bag and placed in a high humidity compartment until just prior to testing.

Undrained Test.--The undrained strength of the sludge was determined by tests in which no overall water content change was permitted to occur during application of the deviator stress. When a saturated sludge is subjected to a change in magnitude of an all-around total pressure without change in water content, the undrained strength in a given direction remains unaltered. Thus the sludge for these conditions behaves, in respect to changes in total stress, as a material with zero angle of shearing resistance, i.e., $\phi_u = 0$ and $c_u = 1/2(\sigma_1 - \sigma_3)$. This result is a consequence of the fact that a change in all-around pressure causes a precisely equal change in pore pressure, provided the sludge is fully saturated; and the effective stresses therefore remain unaltered. For partly saturated sludges there will be some increase in effective stresses as air in the voids is compressed and passes into solution. When stresses are large enough to cause full saturation the sludge again behaves as a material with zero angle of shearing resistance. Bishop and Henkel (1962) have shown that the increase in pore pressure Δu_{as} necessary to lead to full saturation is given by the expression

$$\Delta u_{as} = u_{ao} \frac{(1 - S_o)}{S_o H} \tag{3.1}$$

where u_{ao} is the initial air pressure (abs.), S_o is the initial degree of saturation, and H is Henry's coefficient of solubility (approximately 0.02 at 20°C). A back pressure of 20 psi (0.703 kg/cm^2) was used for fresh sludge samples and 40 psi (1.406 kg/cm^2) was used for undisturbed sludge samples to ensure full saturation. No back pressure or lateral pressure was used for the unconfined compression tests. The effect of sludge anisotropy on undrained strength was determined by testing samples with their axis oriented at zero, 45 degrees, and 90 degrees to the horizontal. More details for the undrained test are given by Bishop and Henkel (1962).

Consolidated-Undrained Test.--Consolidation and application of the deviator stress form two separate stages of the test. For isotropic consolidation of the fresh sludge, samples were allowed to consolidate under a cell pressure of known magnitude, the three principal stresses thus being equal. Side drains consisting of filter paper strips (Bishop and Henkel, 1962) were used to accelerate consolidation. Then the sample was sheared under undrained conditions by increasing the deviator stress. A back pressure of 40 psi (1.406 kg/cm^2) was used for the undrained stage of the test to ensure full saturation of the undisturbed samples. The test result, in terms of total stresses, was expressed as the value of the undrained strength, c_u, plotted against consolidation pressure, p. As before, $c_u = 1/2(\sigma_1 - \sigma_3)_f$, since $\phi_u = 0$ with respect to changes in total stress during undrained shear. When pore pressures were measured during the undrained stage of the test, the results were expressed in terms of effective stress. This permitted evaluation of the strength parameters $\bar{c}$ and $\bar{\phi}$ as outlined in Chapter II. Side drains helped equalize pore pressures within the undrained specimen more rapidly when the deviator stress was increased.

The stress conditions under which consolidation occurs in most practical problems does not approximate equal all-around pressure. The consolidation of natural strata under their own weight occurs under conditions of no lateral yield, for which the stress ratio $\bar{\sigma}_3/\bar{\sigma}_1$ is equal to the coefficient of earth pressure at rest, K_o. Therefore, anisotropic consolidation with $K_o = 0.3$ was used on most of the undisturbed sludge samples. The K_o value selected was based on total pressure cell and piezometer data for the landfill. For selected specimens this test procedure was further modified by holding σ_1 constant and permitting σ_3 to decrease. This modified test procedure was intended to more closely reproduce field conditions existing during excavation.

For example, excavation for the experimental sludge landfill slope involved primarily a decrease in lateral stresses while the vertical stresses remained constant. Both the method of consolidation and any special loading conditions are given with the experimental data reported in Chapter V. Details on test procedures may be found in the Measurement of Soil Properties in the Triaxial Test by Bishop and Henkel (1962). Certain abbreviations describing most of the above test conditions which have come into general usage include:

$\overline{\text{CIU}}$ -- consolidated undrained triaxial test with isotropic consolidation and pore pressure measurements,

$\overline{\text{CAU}}$ -- consolidated undrained triaxial test with anisotropic consolidation and pore pressure measurements.

Plane-Strain Shear Tests

Since the distance normal to the slope section was about 5 times the thickness of the sludge plus sand blankets, it was reasonable to assume that plane-strain was approximated in the cut slopes (Dunlop, et al., 1968). Hence it was decided to include plane-strain shear tests which would more closely simulate the slope unloading during excavation. The plane-strain device used in the test program is shown in Figure 3.3a. This device is a replica of the plane-strain device used by Duncan (1965) in his testing of clays. The essential feature of the device is a pair of end plates which force the sample to undergo plane-strain deformation during consolidation and testing. It is small enough to fit inside a six inch diameter triaxial pressure cell. The device utilizes polished lucite and a layer of silicone grease to reduce friction.

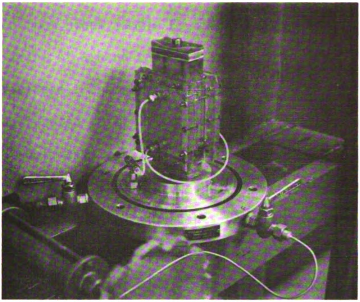

(a)

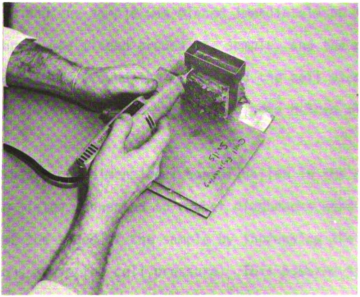

(b)

Figure 3.3.--(a) Plane-strain apparatus mounted on base of triaxial cell.
(b) Sample preparation using a high speed rotary saw.

For the plane-strain test program, undisturbed test specimens were obtained from block sample E. Specimen preparation involved cutting, by means of a hand saw, a 4 in. by 4 in. by 6 in. chunk from the block of sludge. The sample of sludge was then trimmed using a specially constructed metal mitre box (Figure 3.3b). All samples were trimmed with their axis vertical. A hobby tool with a high speed rotating 3/4 in. diameter circular saw cut the pulp fibers giving a smooth trimmed sample. Since Duncan's plane-strain device required that the samples be rectangular, use of the mitre box gave samples with dimensions of 2.80 in. wide, 2.80 in. high and 1.00 in. thick. The cross sectional area before and after consolidation was 3.08 sq. in., very close to the average area for the triaxial samples of approximately 3.14 sq. in. After trimming, the sample dimensions and weight were recorded and the sample was placed immediately on the base of the cell; a membrane was placed around the sample, and the plane-strain device was assembled around the sample and the cell placed in position. The low sensitivity of the consolidated sludge helped minimize sample disturbance.

To insure one-dimensional consolidation in the plane-strain device, side plates connected to rubber diaphragms were pushed into place against the sides of the sample by increasing the pressure in the diaphragms above the cell pressure. This assured that the cross-section of the sample during consolidation maintained the shape and area of the cap and base. The stress conditions were anisotropic, with K_o equal to 0.33.

When consolidation was complete, the side plates were moved away from the sample, by reducing the pressure on the diaphragms, leaving the sample standing free on two sides. A load applied axially through the triaxial pressure cell ram, acting on the top sample cap, was used to control the deviator stress. Connections to the ends of the sample permitted either drainage of water and air from the voids in the sludge, or alternatively, the measurement of the pore pressure under conditions of no drainage. The shearing part of the plane-strain test was run undrained in the same manner as the triaxial shear tests described in the previous section.

Field Vane Shear Test

Because of the extreme difficulty of obtaining representative undisturbed samples of peat and other organic soils, the vane shear test has frequently been used to evaluate in situ shear strength. In-place measurements of the undrained sludge shear strength provided the undrained strength data for comparing the predicted slope stability with the actual stability. Increase in undrained strength due to consolidation was observed by comparing test data taken shortly after construction of the landfill with data taken at later intervals of time prior to the stability study (Vallee and Andersland, 1974).

The vane shear test was performed by inserting a four bladed vane (two inch diameter Acker Vane) thru the hollow core auger stem and pushed the final 6 inches to test depth. The vane was then slowly rotated until the sludge failed along a cylindrical surface with conical surfaces at the top and bottom. The maximum torque was a function of the sludge shear-strength. Using the maximum torque reading and vane dimensions (Figure 3.4), the shear strength τ_f was calculated as follows:

$$\tau_f = \frac{3T}{2\pi R^2(2\ell + 3L)} \tag{3.2}$$

where τ_f equals the shear strength, T equals the torque reading, R equals the radius of the vane, and L and ℓ equals the vane dimensions shown in Figure 3.4.

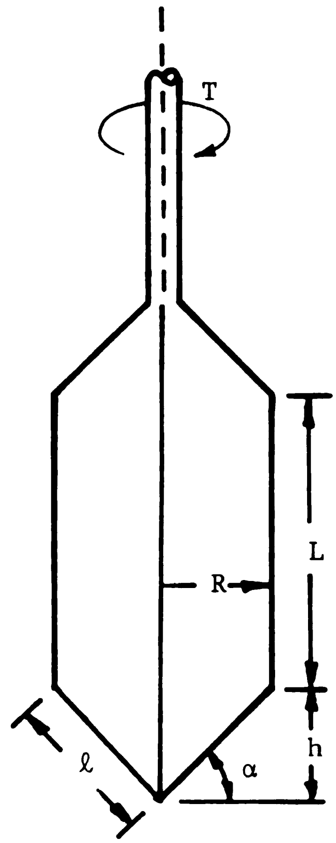

Note: Rod resistance has been ignored since holes were augured to within 6 inches of test depth.

α = 45 degrees
R = 1 inch
L = 3.49 inches
T = Torque

$$T = (2\pi R L \tau_f)R + 2\tau_f \int_0^h 2\pi h^2 \csc \alpha \, dh$$

$$T = 2\pi R^2 \tau_f (L + \frac{2}{3}\ell)$$

Solving for shear strength, τ_f

$$\tau_f = \frac{3T}{2\pi R^2 (2\ell + 3L)}$$

Solving for τ_f in lbs/sq ft,

$$\tau_f = 5.17\ T$$

where T is in inch-lbs.

Figure 3.4.--Acker Vane dimensions and equation for computation of the in-situ shear strength.

CHAPTER IV

FIELD SITE, INSTRUMENTATION, MONITORING AND EXCAVATION

A. Field Site

The experimental sludge landfill was constructed in an old gravel pit located close to West Carrollton, Ohio, and within sludge hauling distance of the papermill. Construction of the landfill was part of an earlier project and details of construction have been reported by Vallee and Andersland (1974). The experimental papermill sludge landfill consisted of two sludge layers, each initially 10 feet (3.05 m) thick, with horizontal sand blankets at the top, bottom, and between the upper and lower sludge layers. An earth dike provided lateral confinement for the soft sludge during and after construction. The surface load consisted of 3 feet (0.915 m) of earth fill material. Instrumentation included piezometers and settlement plates duplicated at a number of locations in the landfill (Figures 4.1 and 4.2).

To obtain information on slope stability, the experimental papermill sludge landfill was altered by removal of the North dike and excavation of a 3:4 slope followed two weeks later by a 1:8 slope. The B.G. Danis Company, Inc., Dayton, Ohio, provided equipment and operators. Coordination of excavation operations was handled by the author working with Mr. Tom Danis, Sr. The Bowser-Morner Testing Laboratories, Inc., Dayton, Ohio, installed both the slope indicator

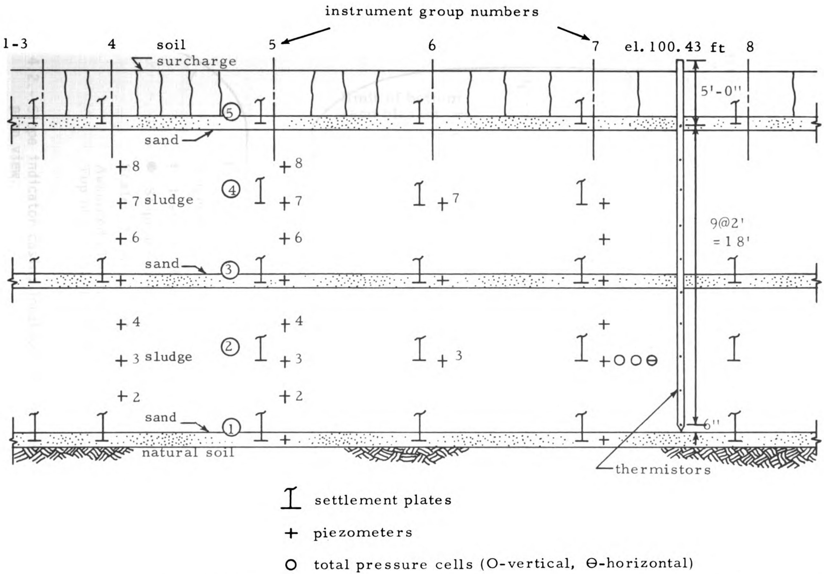

Figure 4.1.--Distribution of settlement plates, piezometers, and total pressure cells in the instrument groups.

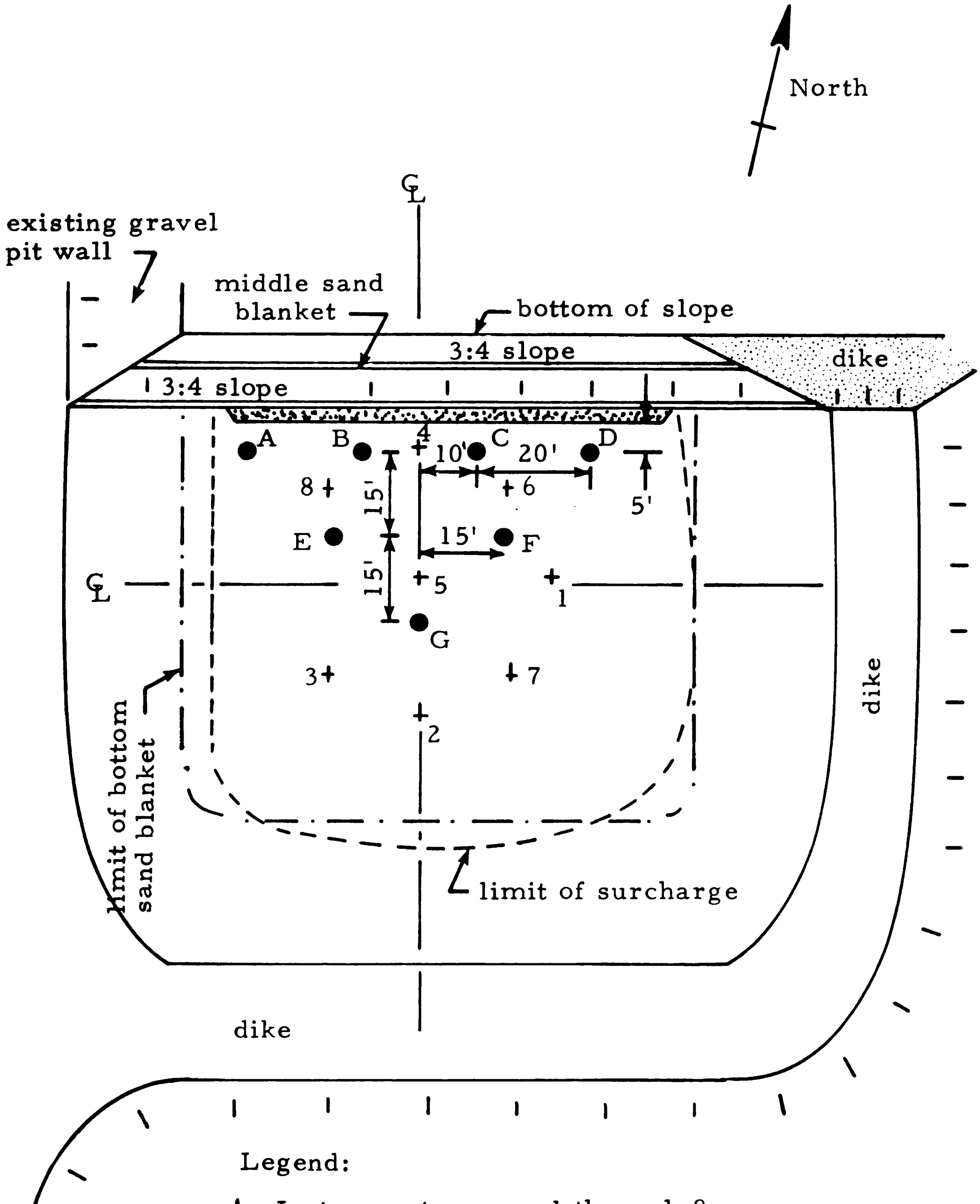

Legend:

+ Instrument groups 1 through 8

● Slope indicator casings A through G

Scale: 1-in. = 30-ft

Assumed elevation datum
Top of gas line marker = 100. 00 ft

Figure 4.2.--Slope indicator casing locations, A through G, and 3:4 slope, plan view.

casings and additional piezometers, and carried out the vane shear and Dutch cone tests prior to the excavation. A plan view of the field site after excavation of the 3:4 slope (β = 53.1 degrees) is shown in Figure 4.2 and the experimental slope cross-sections are shown in Figure 4.3.

B. Instrumentation and Monitoring

Instrumentation placed during construction of the experimental landfill continued to serve the monitoring needs during the stability phase of the project. Additional instrumentation placed September 7-11, 1972, included seven slope indicator casings, six more piezometers, and horizontal control stakes. These were located so as to provide information on the slope behavior. All instruments were monitored before, during excavation of the experimental slope, and as needed during the remainder of the second year of the project. The following sections describe instrumentation for horizontal and vertical movement, piezometers, total pressure cells and temperature sensors.

Horizontal Movement

Removal of the north dike and excavation of the experimental slope reduced lateral stresses and pore pressures on the exposed sludge surface to zero. Unloading the slope permits lateral deformations to occur which may be stress related and/or creep dependent. The magnitude of movement may vary with depth and with the location of any failure zones. Slope indicator casings and surface measurements provided information on these horizontal movements.

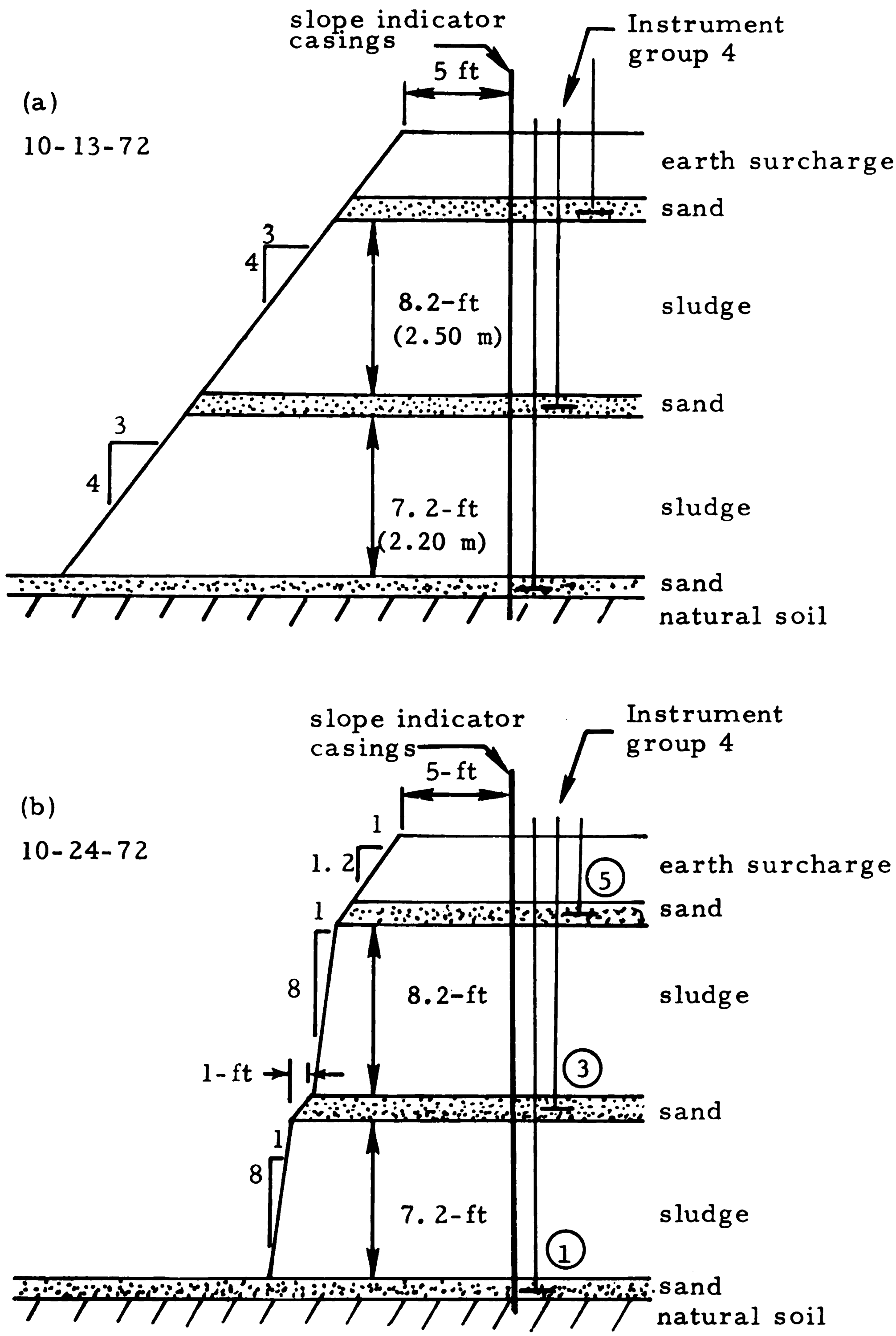

Figure 4.3.--Experimental slope cross-sections. (a) 3:4 slope. (b) 1:8 slope.

Slope Indicator Casings.--Flexible vertical casings were installed through the earth surcharge, sand drainage blankets, and both sludge layers, to about one foot into the natural soil below the experimental landfill at locations A through G, shown on Figure 4.2. Installation involved drilling a 6 inch hole using a hollow core auger, placement of the 3.19 in. OD aluminum casing (0.093 in. wall), and pumping a bentonite clay-water mixture into the opening outside the casing. Lateral movement in the sludge was transferred by the clay to the flexible casing. A precision Slope Inclinometer (Slope Indicator Company Series 200B) was lowered down the casing with the orientation of the instrument governed by the direction of the Slope Indicator's fixed pair of wheels. These fixed wheels track in one of the four grooves in the casing. During installation, the grooves in the casings were oriented so two grooves were parallel (East-West) and the two other grooves were normal (North-South) to the experimental slope. Reference readings were taken after the slope indicator casings were installed and before excavation for the slope was initiated. Inclination readings taken at 2 foot intervals of depth were subsequently converted to lateral displacements. Sensitivity of the inclinometer permits displacement measurements in thin shear zones of less than 1/16 inch. Consecutive readings at the same orientations and depths, taken at periodic intervals of time, were used to determine the amount and rate of ground movement.

Surface Measurements.--Wood control stakes, 2-in. by 2-in. by 1 1/2-ft. long, were placed in the earth surcharge and dike opposite to the slope as shown in Figure 4.4. Movements of the sludge embankment toward the slope were noted by an increase in measured distance from the three reference stakes placed in the dike. Consecutive readings taken at periodic intervals of time were used to determine rate of surface movement. Damage to the stakes from external sources was minimal.

Vertical Movement

Vertical movement results from consolidation of the sludge and downward movement at and near the face of the experimental slope during and following excavation. This movement was monitored using settlement plates placed during construction of the experimental landfill. Settlement plate locations are given by instrument group (Figure 4.2) and plate number (Figure 4.1). Each settlement plate consisted of a 2-ft. by 2-ft. by 1/8-in. thick aluminum plate with a 3/8-in. diameter steel rod of known length attached to the center. A 1 1/2-in. O.D. aluminum tube placed around the steel rod eliminated any adhesion between the sludge and the rod. The lower plate was located at the center of the group with each higher plate offset by 1 1/2-ft. Elevations taken with a surveyor's level (or transit) on the top of each steel rod were referenced to a bench mark outside the fill area. Duplicate plate locations also served as insurance in case of accidental loss and the additional data served as a check on adjacent groups.

Piezometers

Piezometers measure the static pressure or head (elevation to which water will rise in an open standpipe) of the fluid in the pore

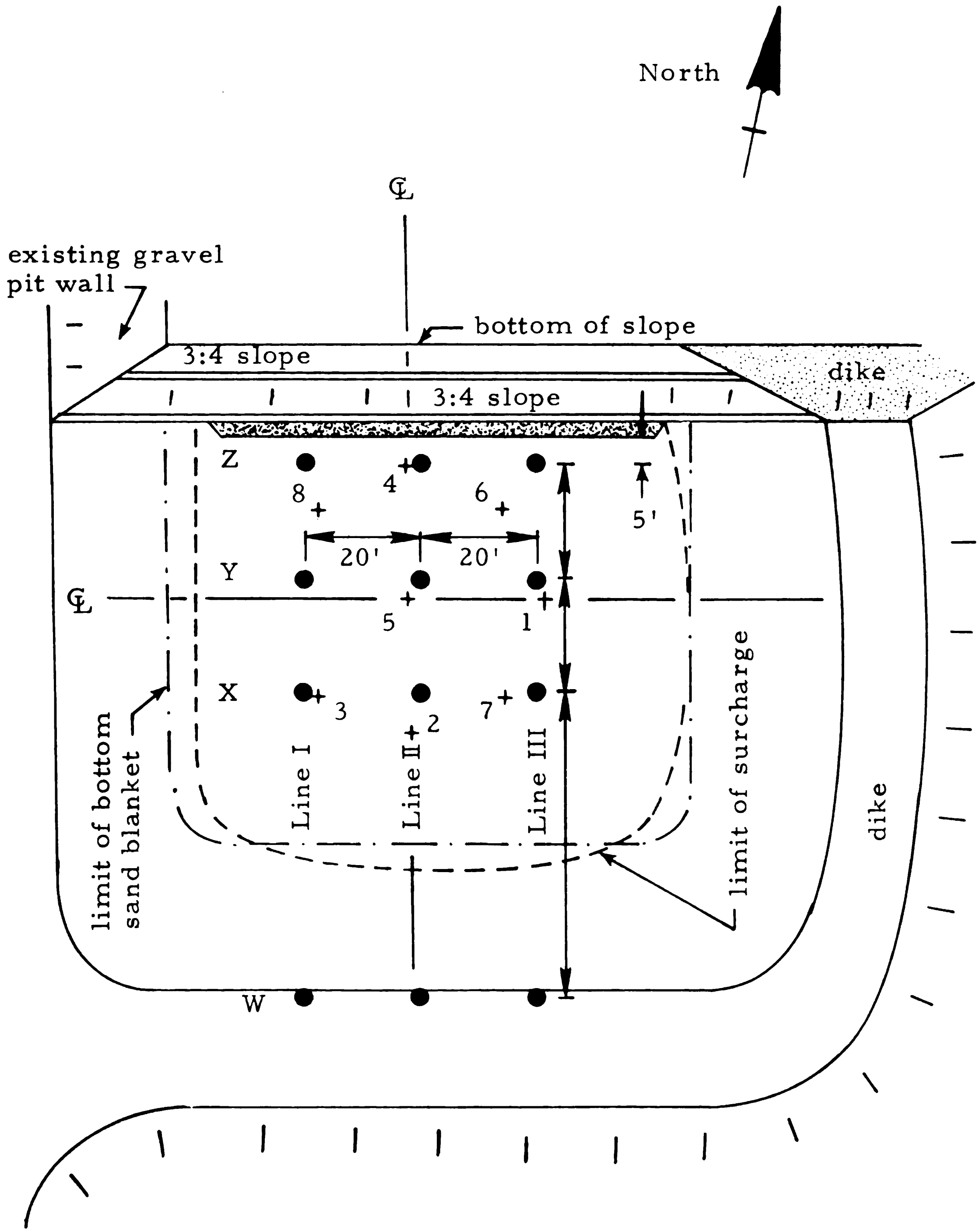

+ Instrument groups 1 through 8

● Horizontal control stakes

Scale: 1-in. = 30-ft.

Assumed elevation datum
Top of gas line marker = 100.00 ft.

Figure 4.4.--Horizontal control stake locations, plan view.

space between the solid sludge particles. Stress reduction to zero at the exposed experimental slope will reduce pore water pressures. Measurement of these pore pressure changes involved installation of six additional units as part of instrument group 4, near the experimental slope. Piezometer locations are given by instrument group (Figure 4.2) and piezometer number (Figure 4.1).

The pneumatic type piezometer (Slope Indicator Company Model 51401) used on the project did not require in-place calibration and was not subject to changes in sensitivity. The sensitivity of the unit approaches 0.5 in. of water. The sensitivity to pore pressure changes was high because the water displacement during reading of the piezometers was small (0.03 cu inches), thus requiring practically no flow of water. The standard Norton Casagrande type filter with large pore size and low air entry pressure was used because the sludge has a high degree of saturation. All piezometers were separated from direct contact with the sludge by about 3-in. of sand so as to minimize any influence sludge decomposition might have on the piezometer operation. The transducer converts water pressure into pneumatic pressure which is relayed to the surface reading station by means of twin nylon tubing. Pore pressure readings were taken with the Model 51421 (Slope Indicator Company) portable pore pressure indicator from terminal boxes which were housed in two wooden boxes located on the landfill.

Total Pressure Cells

Total pressure cells helped in determining the state of stress in the sludge mass. Cell description and installation have been reported by Andersland, et al. (1972). Locations of the two vertical cells and one horizontal cell, part of instrument group 7, are given on Figure 4.1.

Temperature Sensors

Temperature sensors, small YSI precision thermistors (Part #44033), provided temperature data at 2 ft. depth intervals for a given location in the experimental landfill. Thermistors and the method of installation have been reported by Andersland, et al. (1972). Thermistor elevations are given in Figure 4.1.

Vane Shear

Vane shear tests were carried out at one foot depth intervals in the sludge. The vane used was a four-bladed 2 inch O.D. Acker Vane. Details on computation of the vane shear strength have been given in Chapter III.

The vane shear test was used to determine the in situ field undrained shearing strength of the sludge deposit just prior to excavation for the slope stability study. The tests consisted of boring with a hollow stem auger to within 6 inches of the test depth, then inserting the vane through the hollow stem auger and forcing the vane vertically the last 6 inches to the test depth. This method was followed to keep disturbance to a minimum and reduce the vane's rod resistance to a value near zero. The vane's extension rod was then slowly rotated clockwise until the maximum torque was obtained. The vane was then rotated 25 times clockwise to remold the sludge adjacent to the vane. After which the remolded shear strength was determined by slowly rotating the vane until the maximum torque was obtained. The shear strength (undisturbed and remolded) was computed from Equation 3.2. This procedure was repeated for each test at one foot intervals of depth.

Dutch Cone Tests

The Dutch Cone Penetrometer tests were carried out at one foot depth intervals. The Dutch Cone used had a 60 degree cone of base area equal to 10 sq cm. The Dutch Cone test consisted of boring with a hollow stem auger to within 6 inches of the test depth, then inserting the Dutch Cone through the hollow stem auger and slowly forcing the cone vertically the last 6 inches to the test depth. The resistance of the cone at the test depth was recorded. This procedure was repeated at one foot intervals of depth for each test.

C. Excavation for the Experimental Slope

Preparation of the experimental slope involved removal of the North dike and sludge excavation so as to give the slopes shown on Figure 4.3. Preliminary information on the sludge stability was obtained by excavating a vertical trench about 40 ft. long and 8 ft. deep, down to the middle sand drainage layer, using the dragline bucket on September 21, 1972. The trench face was about 20 ft. forward from slope indicator casings B and C. The following day surface cracks had appeared about 2 ft. back from the exposed sludge face. The trench excavation was continued to a depth close to 15 ft. The next day (Sept. 23, 1972) the trench remained open but with new surface cracks about 4 ft. back from the exposed face. Sand falling from the middle drainage blanket removed support for the upper sludge layer to about 1 1/2 ft. back from the cut face. Dike removal was started on September 24, 1972. Heavy rain during the night softened the dike surface and adjacent area to an extent which prevented effective equipment operation. More rain delayed work until September 29, 1972. Dike material and sludge was removed, weather permitting, until completion of the 3:4 slope on October 13, 1972. Excavation work and the completed slope are shown in Figure 4.5.

Excavation for the 1:8 slope was initiated at noon on October 24, 1972. The dozer removed sludge seven feet back from the toe of the 3:4 slope giving a vertical face to the lower sludge layer. Next the backhoe removed sludge (Figure 4.6a) so as to give the 1:8 slope. Sludge was removed from in front of the slope using the dozer (Figure 4.6b). Work was completed by noon on October 25, 1972.

(a)

(b)

Figure 4.5. 3:4 slope preparation. (a) Sludge removal by dragline. (b) Slope cross-section, October 13, 1972.

(a)

(b)

Figure 4.6. 1:8 slope preparation. (a) Trimming the upper sludge layer. (b) Sludge removal using a dozer, October 25, 1972.

CHAPTER V

FIELD AND LABORATORY EXPERIMENTAL RESULTS

The experimental results for this project are presented under three headings: physical properties of the papermill sludge, stress-deformation behavior of the sludge, and slope behavior. Each section may include laboratory test data and/or field observations.

A. Physical Properties of the Papermill Sludge

Physical properties of the papermill sludge, tabulated in Tables 5.1 and 5.2, include field water contents, ash contents, and unit weights. Water contents were taken at selected elevations immediately after excavation of the 3:4 slope (October 12, 1972) and 1:8 slope (October 30, 1972). A plot of this data in Figure 5.1 shows a decrease in water content with a greater depth. The scatter of points on Figure 5.1 is apparently due to the non-homogenous nature of the sludge. Small variations in ash (or organic) content appear to significantly alter the water content based on oven dry (105°C) weights. Water contents from 1 ft. cube block samples B, C, F, and G tabulated in Table 5.1, show the range in variability. Ash contents and unit weights given in Table 5.2 refer to block samples B, C, F, and G on which extensive laboratory tests were conducted. Unit weights were determined from weight and volume measurements of carefully trimmed sludge samples. Greater consolidation of the lower sludge layer significantly increased the unit weight.

TABLE 5.1. VARIATION IN WATER CONTENTS FOR ONE CUBIC FOOT BLOCK SAMPLES

	Block B	Block C	Block F	Block G
	213 %	162 %	149 %	159.1 %
	206	157	162	157.7
	218	163	165	153.7
	222	169	154	157.2
	212	169	150	158.6
	209	170	164	158.6
	193	169		157.2
	212	178		157.0
	218			160.0
	211			158.6
	204			
	212			
	206			
	214			
	202			
	200			
Avg.	209.5%	167.1%	157.3%	157.8%
Block Elev.	88.8 ft	87.5 ft	80.9 ft	80.7 ft

TABLE 5.2. PHYSICAL PROPERTIES OF THE PAPERMILL SLUDGE, OCTOBER 1972

Sludge sample No.	Elevation (ft)	Water content (% dry wt)	Ash[1] content (%)
Block A	91.8	196	
		202	
		212	
Block B	88.8	214	38.6
		209	
		200	
Block C	87.5	183	49.1
		165	
		173	
Block D	85.5	191*	
		187*	
Block E	81.9	161*	
		164*	
		162*	
Block F	80.9	154*	39.3
		156*	
		156*	
Block G	80.7	157*	39.0
		159*	
		161*	
moisture content samples	92.8	199	
	92.6	178*	
	92.4	179*	
	92.3	200	
	92.2	187	

Sludge sample No.	Elevation (ft)	Water content (% dry wt)
moisture content samples	91.7	199
	91.6	177
	91.4	182*
	91.2	200
	90.6	193
	90.5	187
	90.4	188*
	89.9	194
	89.4	189
	89.4	201*
	89.1	144
	88.7	149
	88.4	161
	88.4	172*
	88.0	177
	87.7	173
	87.4	164*
	85.4	207
	84.4	175
	84.4	211*
	83.4	204
	83.4	175*
	82.4	153*
	81.4	163*
	81.4	158*

Field water contents correspond to 3:4 slope, October 12, 1972, except * which correspond to 1:8 slope, October 30, 1972.

Unit weight: block B γ = 72.6 lb per cu ft.
block C γ = 74.0 lb per cu ft.
block F γ = 76.5 lb per cu ft.

[1]ASTM test method D586-63.

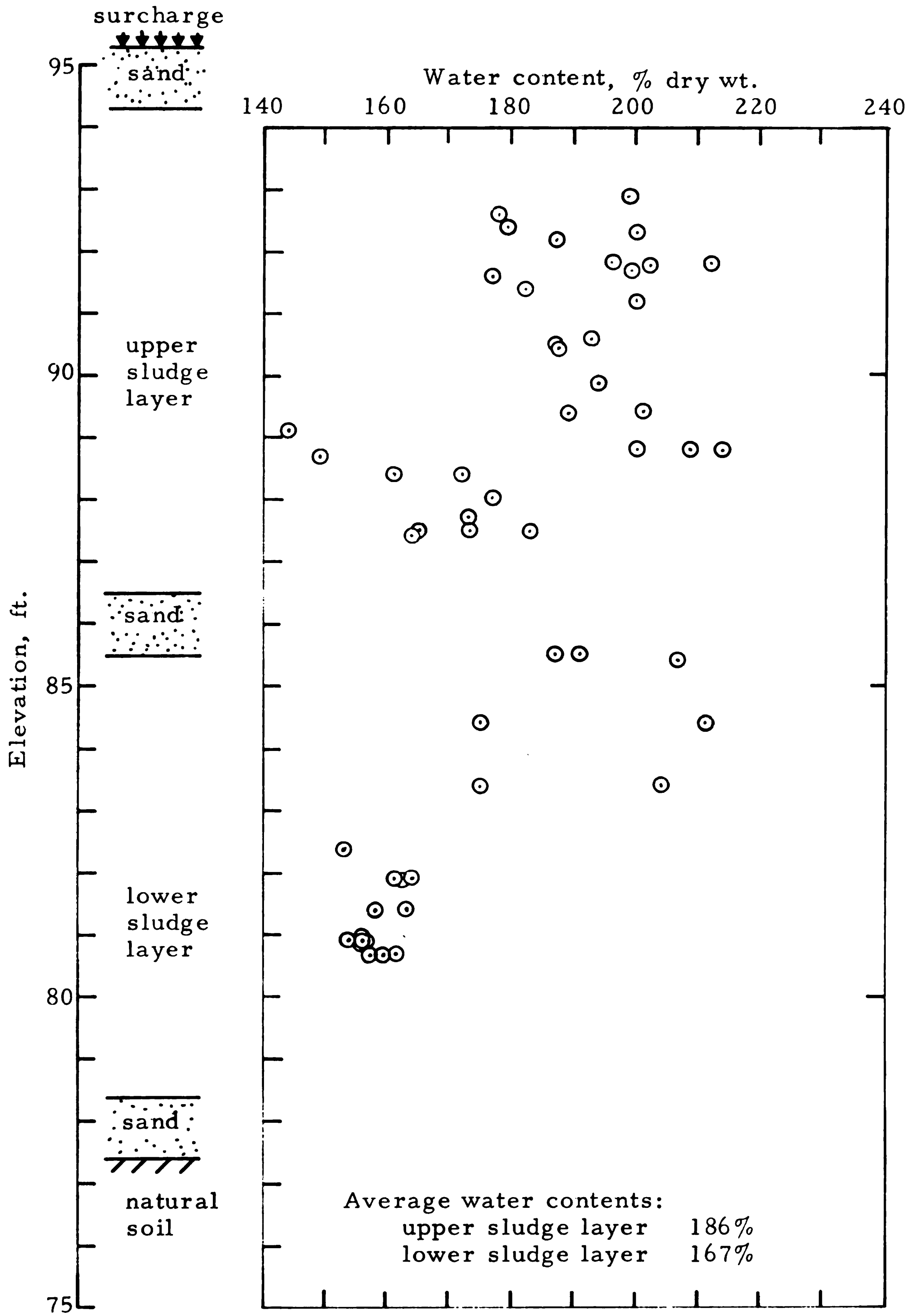

Figure 5.1.--Field water contents of the sludge in the landfill, October 1972.

B. Strength Characteristics of the Papermill Sludge

The shear strength of the papermill sludge has been measured using triaxial and plane strain tests in the laboratory and the vane shear test in the field. Results from the triaxial tests are presented for fresh sludge samples obtained during construction of the landfill and undisturbed block samples taken after field consolidation. Only normally consolidated sludges are considered under strength characteristics.

Triaxial Shear Tests

Fresh Sludge Samples.--Samples taken during construction of the landfill have been identified and described in Table 2.1 (after Andersland, et al., 1972). Portions of fresh sludge samples U-1, U-2, and U-3 were molded into triaxial test specimens. A summary of these test results are given in Table 5.4 Laboratory data are given in Appendix I, Tables I-1 through I-12. A back pressure of 0.703 kg/sq cm was used on all the fresh sludge samples to ensure full saturation and to de-air the space between the membrane and the sample. With this back pressure, the pore-pressure parameter B was equal to one.

Typical stress-strain behavior of the fresh sludge in undrained shear is given in Figure 5.2. The obliquity $\bar{\sigma}_1/\bar{\sigma}_3$, deviator stress $(\sigma_1 - \sigma_3)$, pore pressure change Δu, and pore pressure parameter A are all plotted against axial strain. The obliquity becomes very large at larger axial strains because of the very small effective minor principal stress $\bar{\sigma}_3$. The A pore pressure parameter increases to about 0.75 at failure, which appears to be typical for the fresh sludge. Triaxial strength data for sludge sample U-3 is summarized in Figure 5.3. The $\bar{p}_f$ - $\bar{q}_f$ plot has been used to obtain an angle of internal friction

TABLE 5.3.--Summary of $\bar{\phi}$ Values for the Triaxial and Plane-Strain Tests.

Sample No.	Organic Content (100 - % ash)	Test Procedure	$\bar{\phi}$ (degrees)	Remarks
U - 1[a]	40.6	$\overline{\text{CIU}}$	61.5	Fresh sludge
U - 2[a]	53.5	$\overline{\text{CIU}}$	66.2	Fresh sludge
U - 3[a]	63.5	$\overline{\text{CIU}}$	70.5	Fresh sludge
Block G	61.0	$\overline{\text{CAU}}$	76.5	Field sample
Block G	61.0	$\overline{\text{CIU}}$[b]	45.5	Field sample
H - 2[c]	28.6	$\overline{\text{CIU}}$	45.7	Fresh sludge
	34.7	$\overline{\text{CIU}}$	51.4	Fresh sludge
	43.6	$\overline{\text{CIU}}$	58.5	Fresh sludge
	50.1	$\overline{\text{CIU}}$	64.2	Fresh sludge
Block E	59.3	$\overline{\text{CAU}}$	74.9	Field sample
Block E	59.3	$\overline{\text{CAUPS}}$	74.9	Field sample

[a]Sample information given by Andersland et al. (1972).

[b]Sample axis horizontal.

[c]Data after Andersland and Laza (1971).

$\overline{\text{CIU}}$ - Consolidated undrained triaxial test with isotropic consolidation and pore pressure measurements.

$\overline{\text{CAU}}$ - Consolidated undrained triaxial test with anisotropic consolidation and pore pressure measurements.

$\overline{\text{CAUPS}}$ - Consolidated undrained plane-strain test with anisotropic consolidation and pore pressure measurements.

$\bar{\phi}$ - angle of intenal friction, effective stress basis.

TABLE 5.4. SUMMARY OF TRIAXIAL TEST RESULTS

Sludge sample	Consolidation pressure		Water content		Initial dry density	Undrained strength c_u	$\bar{\sigma}_{1_f}$ [a]	$\bar{\sigma}_{3_f}$ [a]	A_f
	p (kg/cm^2)	K_o	Initial (%)	Final (%)	(pcf)	(kg/cm^2)	(kg/cm^2)	(kg/cm^2)	
U-1-10	0.703	1.0	182.9	116.2	25.86	0.52	1.02	0	0.69
U-1-11	1.41	1.0	200.0	101.2	26.60	0.83	1.76	0.10	0.78
U-1-12	2.11	1.0	194.4	94.3	25.78	1.17	2.44	0.09	0.85
U-1-13	3.52	1.0	180.2	84.2	27.50	1.90	4.08	0.28	0.85
U-2-21	3.52	1.0	215.0		23.88	2.07	4.36	0.23	0.79
U-3-1	0.703	1.0	310.0	150.9	18.96	0.45	0.91	0	0.77
U-3-2	0.703	1.0	306.0	147.4	18.41	0.62	1.20	0	0.60
U-3-3	1.40	1.0	276.2	118.8	19.25	1.48	3.05	0.056	0.45
U-3-4	2.11	1.0	258.0	111.2	20.39	sample tilted during test			
U-3-5	3.51	1.0	255.0		20.34	1.52	3.27	0.22	1.08
U-3-6	2.11	1.0	285.8	122.8	18.65	1.18	2.31	0	0.90
U-3-7	1.41	1.0	289.6	127	18.32	0.94	1.91	0.04	0.73
U-3-8	3.52	1.0	293.6	111	18.23	2.10	4.27	0.08	0.82
G-3	1.17	0.3	159.1	142	26.56	0.70	1.44	0.04	0.45
G-4	1.17	0.3	157.7	134	26.63	0.91	1.83	0.009	0.30
G-5	1.17	0.3	153.7	130	27.65	0.954	1.92	0.015	0.30
G-6	2.34	0.3	157.2	115	27.79	2.05	4.15	0.046	0.24
G-7	Unconfined compression		158.6	158.6	28.63	0.318	0.637	0	--
G-8	Unconfined compression		158.6	158.6	28.12	0.322	0.644	0	--
G-9	0.696	0.3	157.2	153	28.17	0.484	0.99	0.021	0.40
G-10[b]	0.703	1.0	157.0	145	29.00	0.449	1.08	0.18	0.57

TABLE 5.4. SUMMARY OF TRIAXIAL TEST RESULTS (CONTINUED)

Sludge sample	Consolidation pressure p (kg/cm^2)	Consolidation pressure K_o	Water content Initial (%)	Water content Final (%)	Initial dry density (pcf)	Undrained strength c_u (kg/cm^2)	$\bar{\sigma}_{1_f}$ [a] (kg/cm^2)	$\bar{\sigma}_{3_f}$ [a] (kg/cm^2)	A_f
G-11[b]	2.11	1.0	160.0	114	28.71	1.12	2.66	0.43	0.75
G-12[b]	Unconfined compression		158.6	158.6	27.78	0.202	0.404	0	--
G-20[c]	2.34	0.3	159.0	122	27.78	--	--	--	--
G-21[c]	0.703	0.3		135	31.26	--	--	--	--
C-2	Unconfined compression		162	162	28.17	0.134	0.268	0	--
C-3	Unconfined compression		157	157	28.83	0.156	0.311	0	--
C-4	Unconfined compression		163	163	27.64	0.102	0.204	0	--
C-5[b]	Unconfined compression		169	169	27.73	0.094	0.189	0	--
C-6[b]	Unconfined compression		169	169	27.75	0.076	0.152	0	--
C-7[d]	Unconfined compression		170	170	28.35	0.104	0.208	0	--
C-8[d]	Unconfined compression		169	169	27.75	0.124	0.248	0	--
C-9	Unconfined compression		178	178	25.72	0.132	0.265	0	--
C-10[c]	0.703	0.3	177	150	26.94	--	--	--	--
C-11[c]	0.935	0.3	174.5	133.5	27.30	--	--	--	--
C-14[c]	2.343	0.3	174.3	104.3	27.26	--	--	--	--

[a] Total stress basis for unconfined compression. [b] Sample axis horizontal.

[c] Undrained shear with σ_1 constant and σ_3 decreasing. [d] Sample axis 45 degrees from the horizontal.

$\bar{\sigma}_{1_f}$ and $\bar{\sigma}_{3_f}$ equal the major and minor principal effective stresses at failure, respectively.

A_f equals the pore pressure parameter at failure.

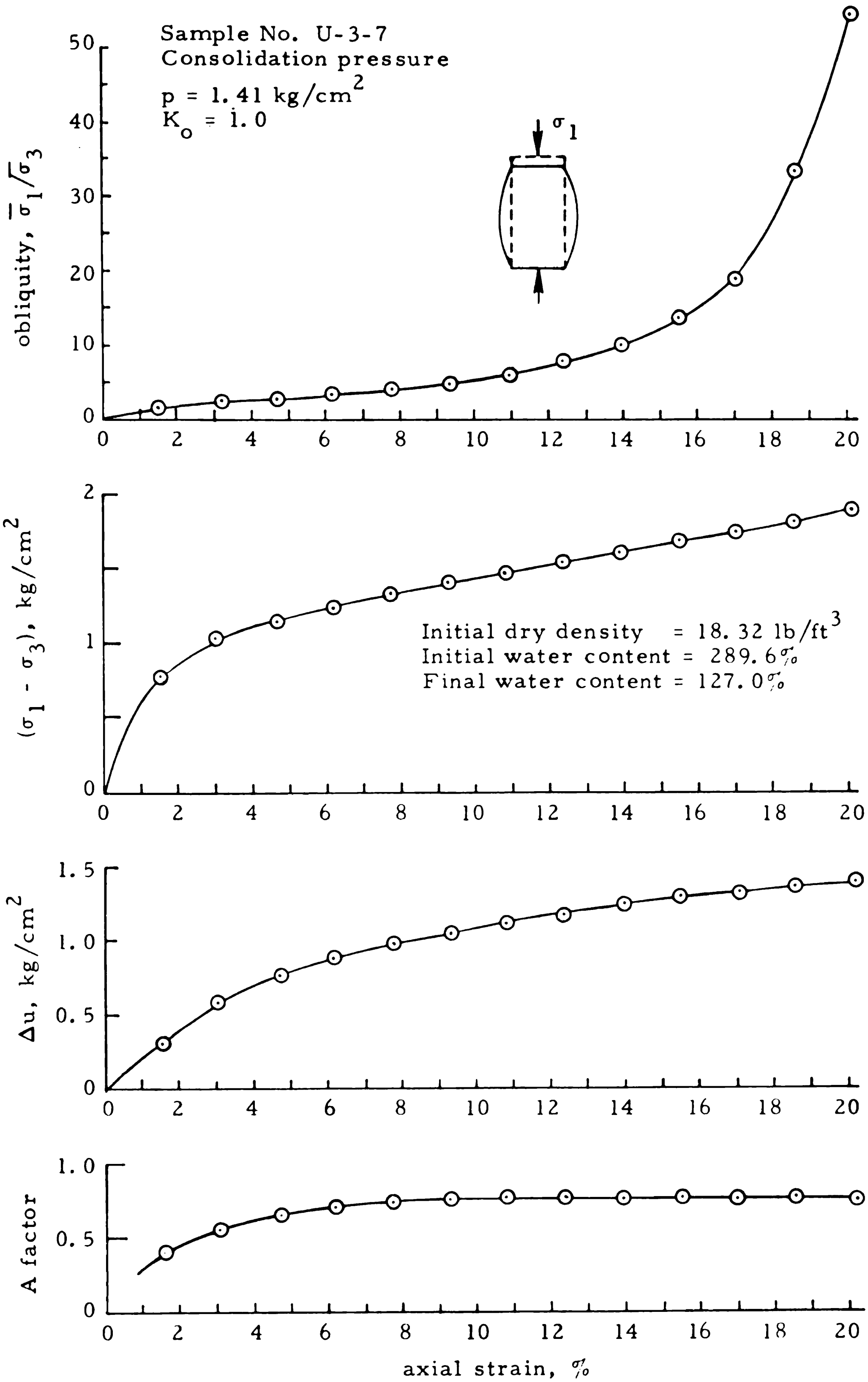

Figure 5.2.--Stress-strain behavior of fresh sludge in undrained shear, sample U-3-7.

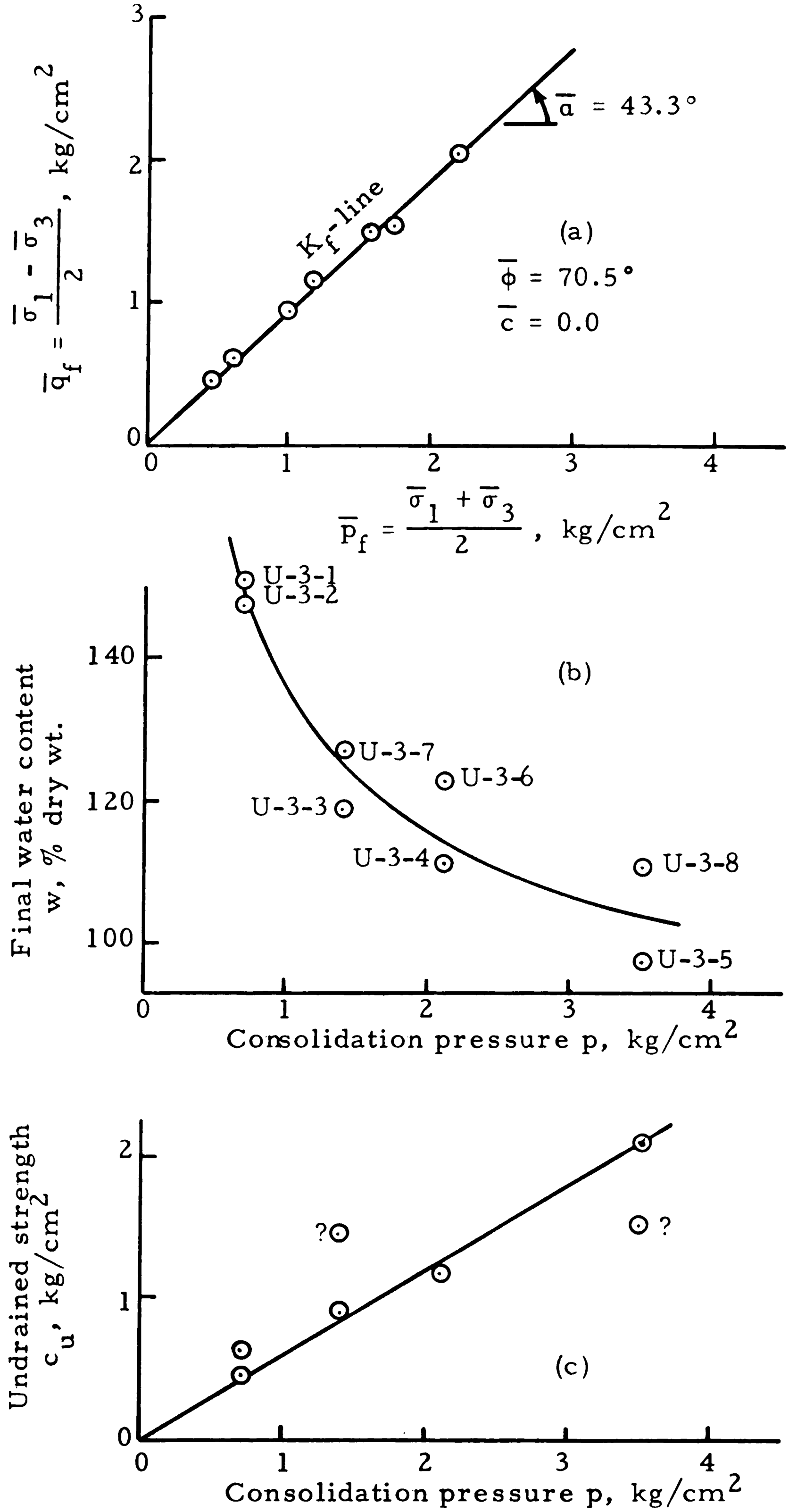

Figure 5.3.--Consolidated undrained triaxial test results for sludge sample U-3. (a) K_f-line. (b) Water content. (c) Undrained strength.

equal to 70.5 degrees. Next is shown the change in water content for several levels of all-around consolidation pressure. Part c of Figure 5.3 shows the increase in undrained strength versus consolidation pressure. Similar results are shown for sludge sample U-1 in Figure 5.4. The smaller angle of internal friction, 61.5 degrees, appears related to the lower organic content of sample U-1, 40.6 percent versus 63.5 percent for sample U-3.

Undisturbed Sludge Samples.--Triaxial test specimens were cut from undisturbed block samples C and G which were obtained during excavation of the slope for the stability study. A summary of the triaxial test results is given in Table 5.4. Laboratory data are given in Appendix I, Tables I-13 through I-35. Except for the unconfined compression tests, a back pressure of 1.41 kg/sq cm was used on all undisturbed sludge samples to ensure full saturation of the sludge and to de-air the space between the membrane and the sample. With this back pressure, the pore-pressure parameter B was equal to one. Special test conditions include anistropic consolidation and applying the major principle stress (σ_1) at different sample orientations. Unless otherwise noted, the samples were trimmed so that their cylindrical axis was the same as in the field with the major principle stress vertical. The stress-strain behavior of sample G-5, shown in Figure 5.5, corresponds to anisotropic consolidation. The coefficient of earth pressure at rest, K_0, equal to 0.3, was selected on the basis of field total pressure cell and piezometer data. Figure 5.5 includes the obliquity ratio, deviator stress, change in pore pressure, and the A pore pressure parameter all plotted against axial

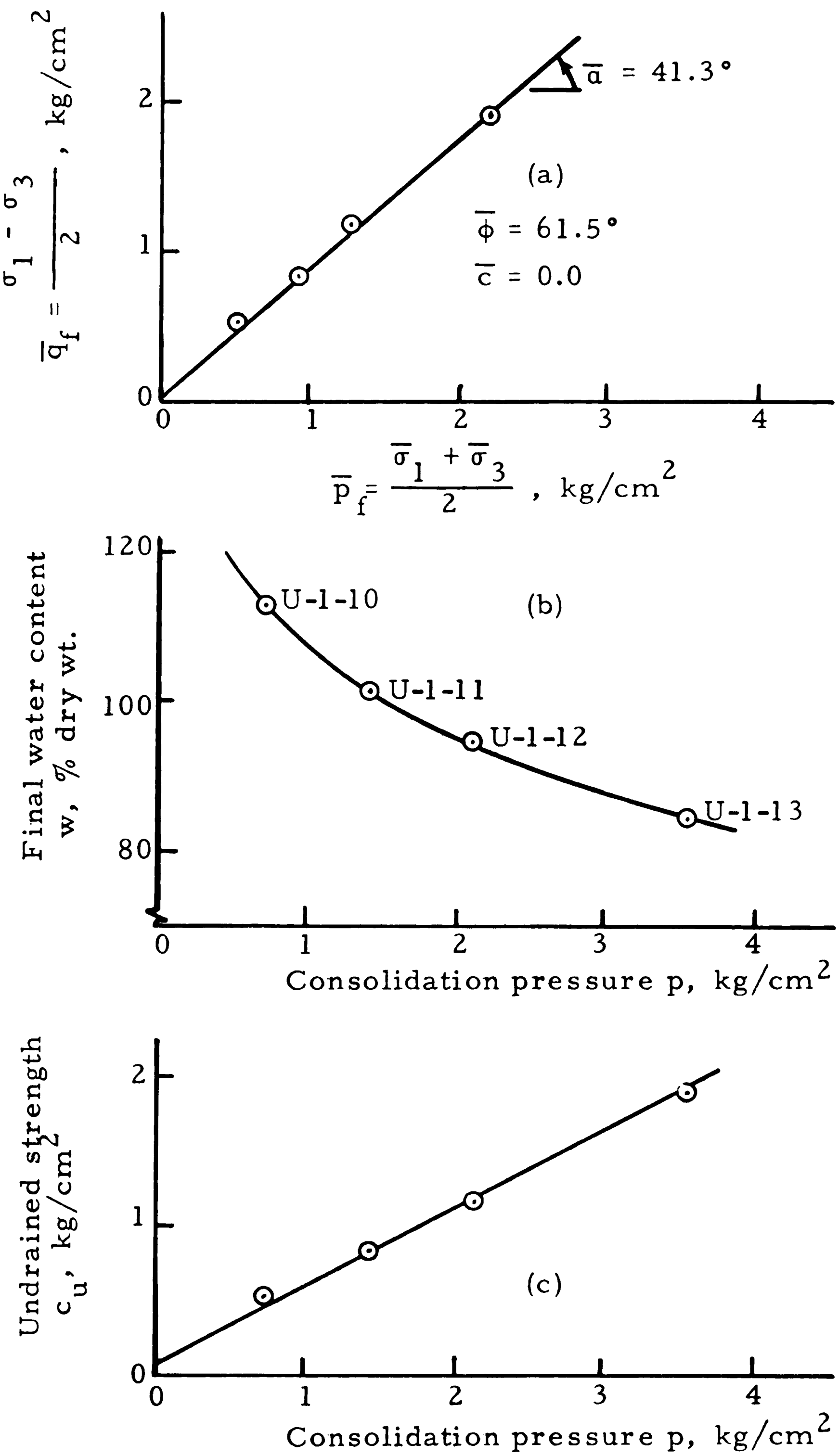

Figure 5.4.--Consolidated undrained triaxial test results for sludge sample U-1. (a) K_f-line. (b) Water content. (c) Undrained strength.

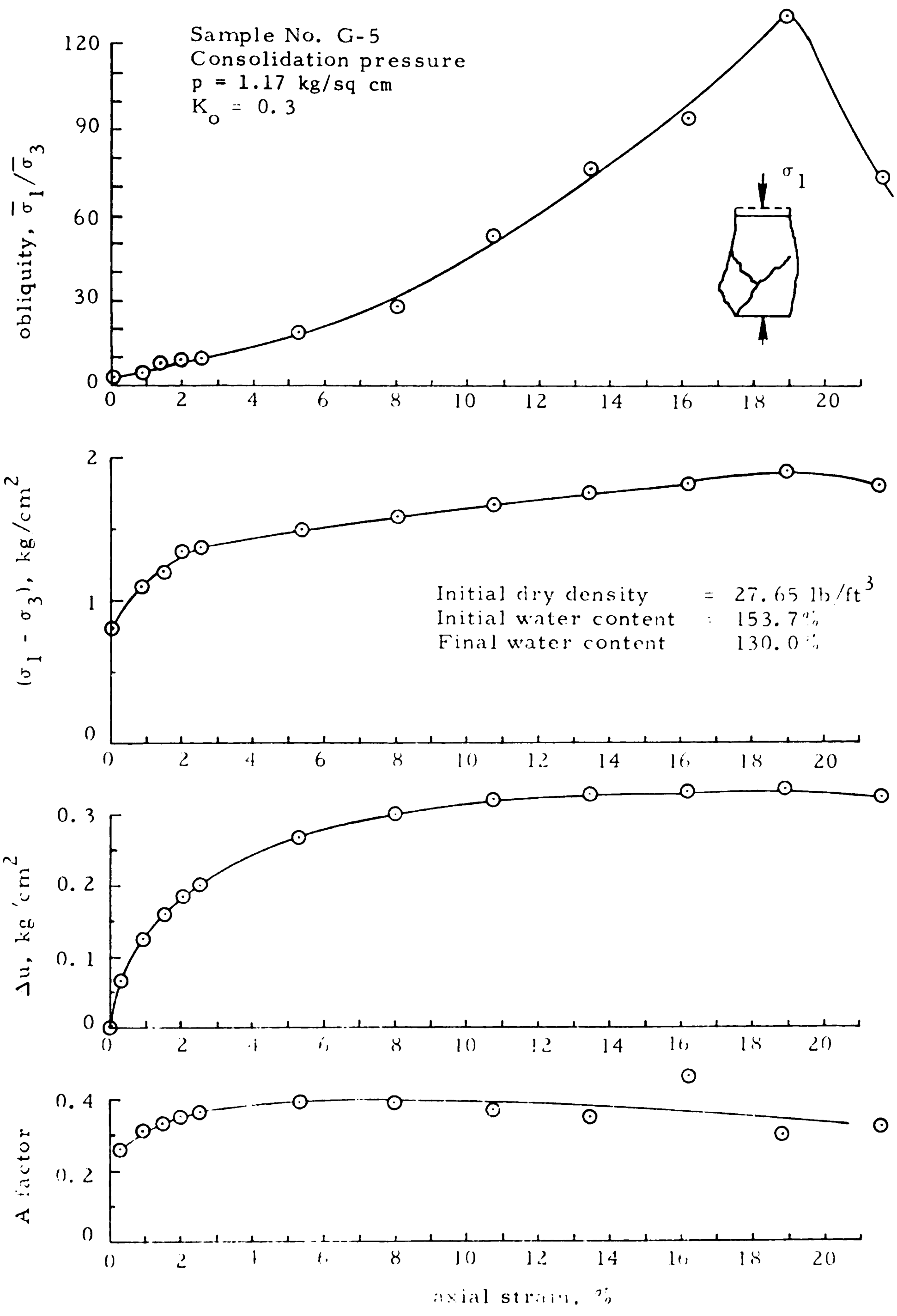

Figure 5.5.--Stress-strain behavior of consolidated sludge in undrained shear, sample G-5.

strain. The break in the obliquity curve corresponds to failure at about 19 percent axial strain. The deviator stress starts at a value greater than zero because of anisotropic consolidation. The A pore pressure parameter has decreased, in comparison to results for the fresh sludge, with the value at failure a little below 0.4. A summary of data from similar tests at other consolidation pressures is shown in Figure 5.6. The angle of internal friction obtained from the $\bar{p}_f$ - $\bar{q}_f$ plot is very large, close to 76.5 degrees. This suggests that some relationship exists between the angle of internal friction and the anisotropic nature of the sludge for this group of specimens. At greater consolidation pressures, the water content decreases while the undrained strength increases. These relationships are shown in Figure 5.6.

The stress-strain behavior for sample G-10, shown in Figure 5.7, corresponds to all-around consolidation with the major principle stress (σ_1) applied horizontally. This was accomplished by trimming the sample so that its cylindrical axis was at a 90 degree orientation to that in the field. Lower obliquity ratios are noted and the A pore pressure parameter has increased in comparison to sample G-5 shown in Figure 5.5. The summary of data for specimens G-10 and G-11 is given in Figure 5.8. The angle of internal friction is much lower, about 45.5 degrees, and the undrained strengths are lower as compared to data given in Figure 5.6 for the sample trimmed with the cylindrical axis vertical.

The stress change prior to slope failure involved a decrease in lateral pressure as the sludge was excavated. To reproduce this

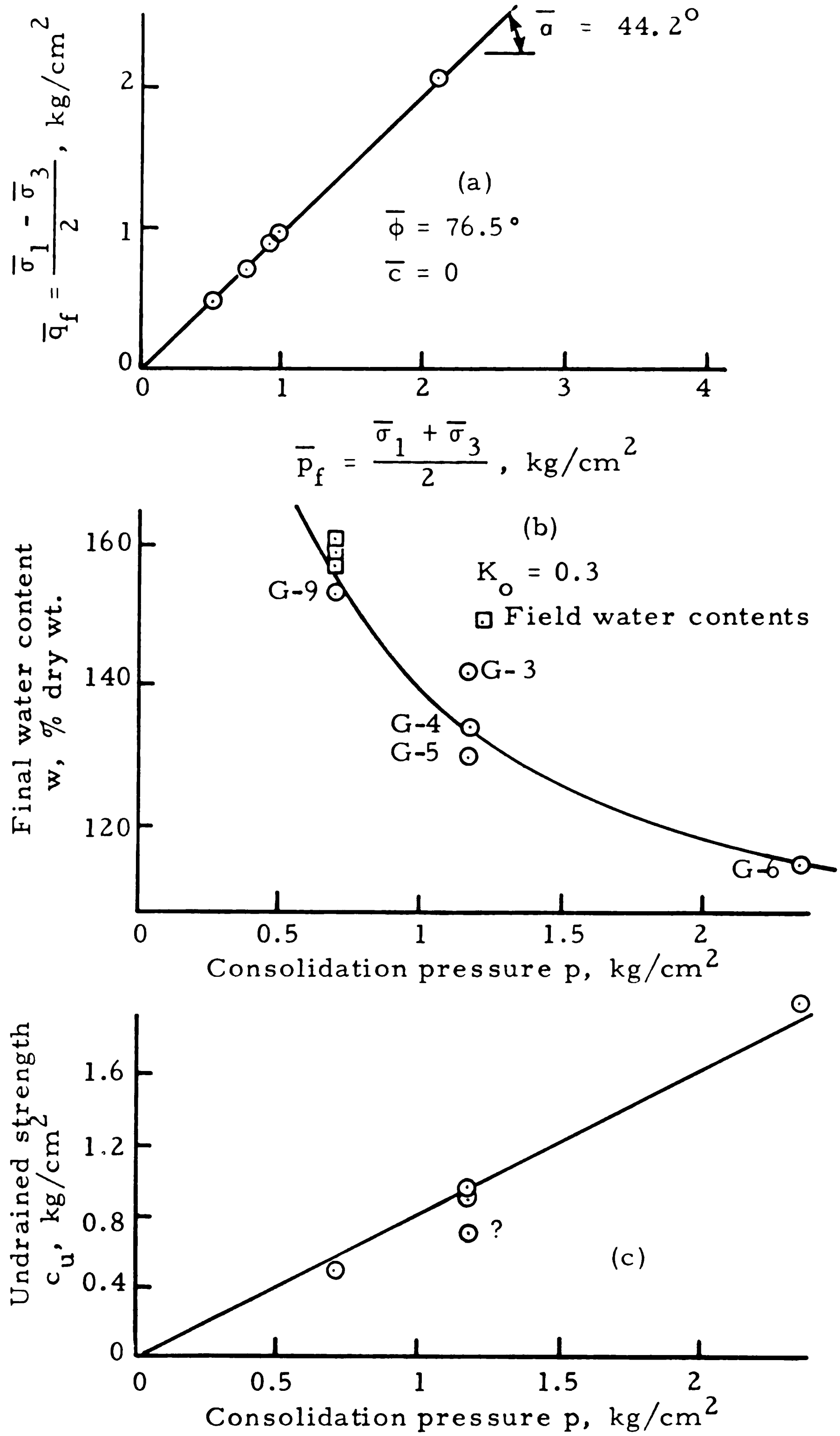

Figure 5.6.--Consolidated undrained triaxial test results for block G, anisotropic consolidation and vertical axis. (a) K_f-line. (b) Water content. (c) Undrained strength.

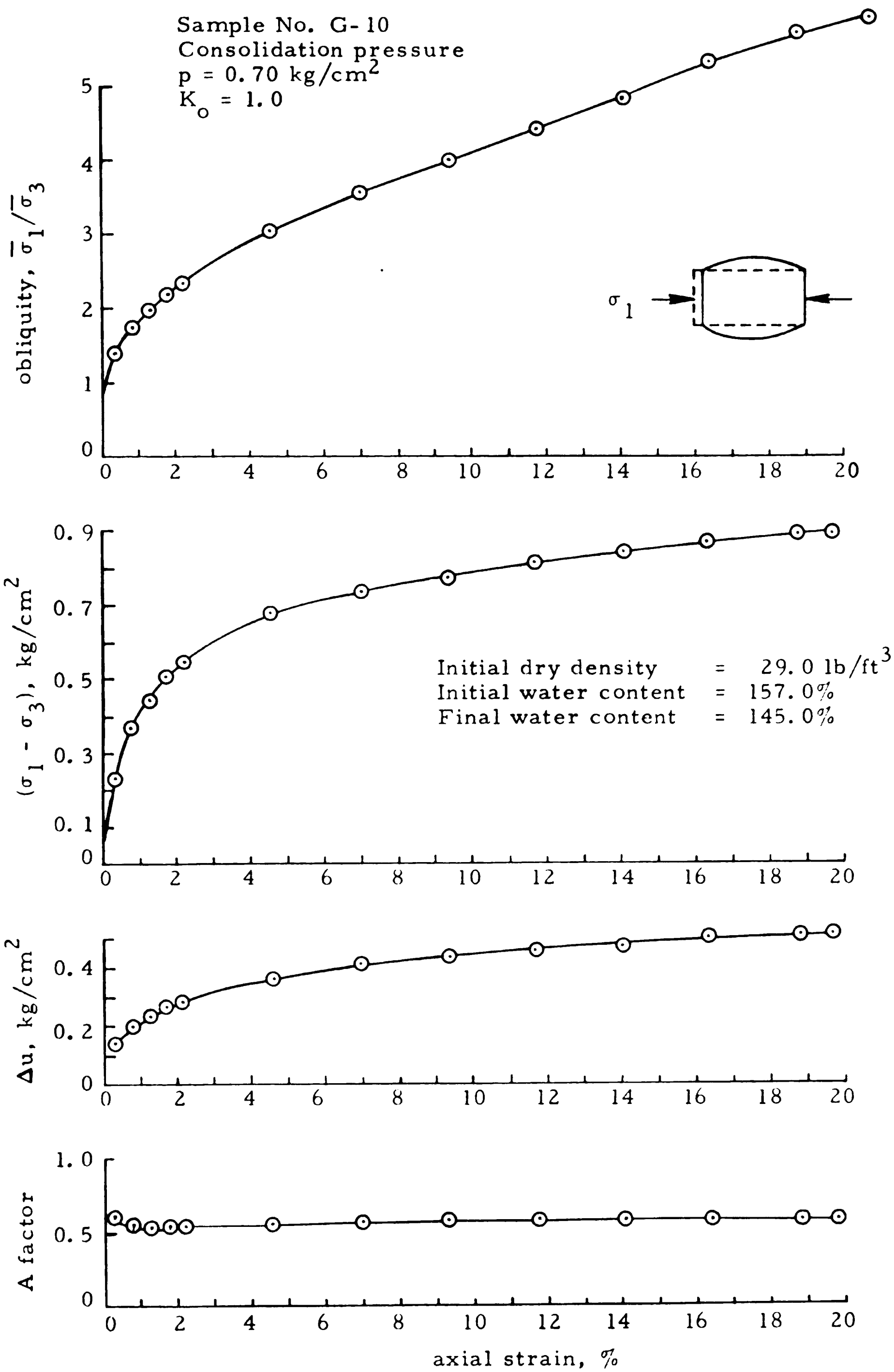

Figure 5.7.--Stress-strain behavior of consolidated sludge in undrained shear, sample G-10 with the major principal axis horizontal.

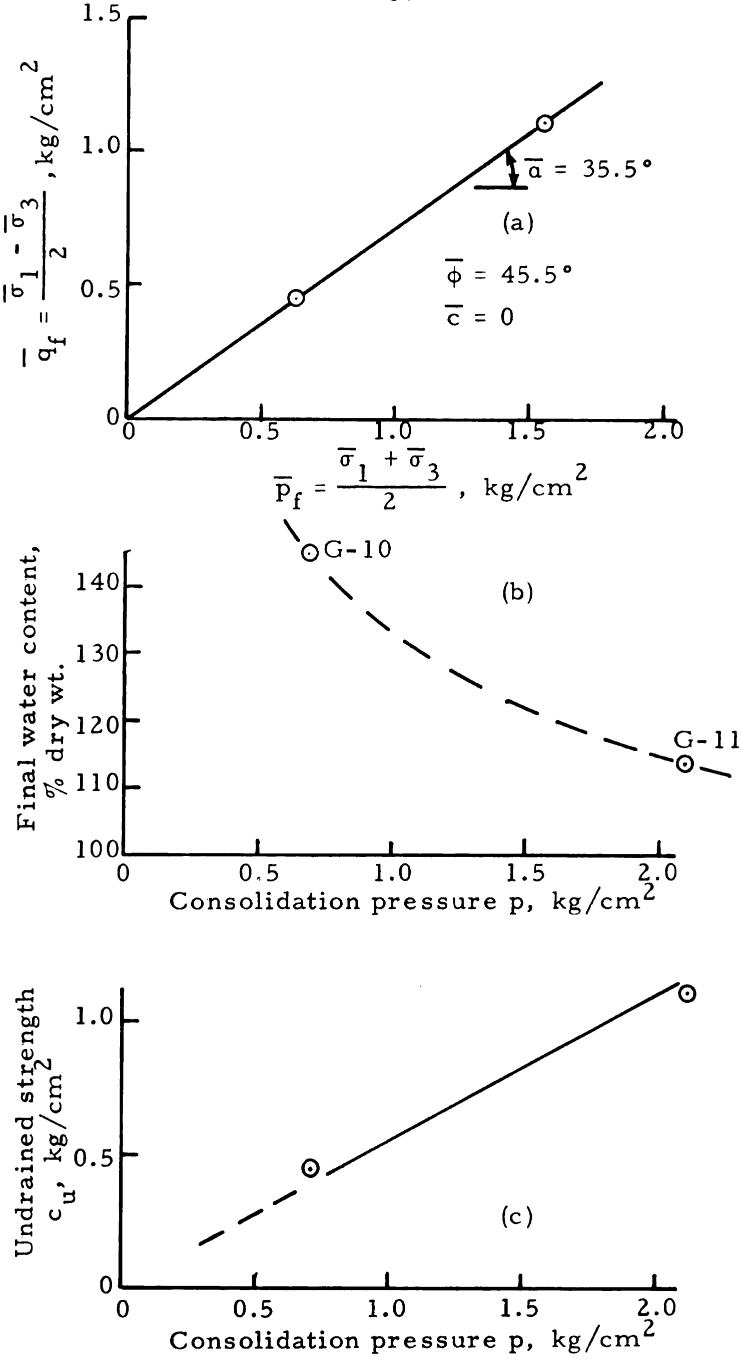

Figure 5.8.--Consolidated undrained triaxial test results for block G, isotropic consolidation, and horizontal axis. (a) K_f-line. (b) Water content. (c) Undrained strength.

field stress condition in the laboratory a series of tests were run in which the axial stress, σ_1, was held constant and deformation was brought about by reducing the lateral stress, σ_3. Prior to the test, samples were consolidated anisotropically to approximately field conditions based on data from the total pressure cells and a piezometer buried in the landfill. This test procedure perhaps best approximates the loading conditions for a sludge element adjacent to the excavated slope. Data shown in Figure 5.9 for sample C-11 represents an undrained test with σ_1 held constant and failed by decreasing σ_3. Negative pore pressures result for the unloading condition. The higher initial tangent modulus, obtained from the deviator stress versus axial strain curve, perhaps gives the best estimate of the field behavior. The A pore pressure parameter was again close to 0.53. The angle of internal friction was not fully mobilized since complete failure had not occurred. The strain was very small (less than 5 percent) when σ_3 was decreased to zero.

Plane-Strain Shear Tests

Plane-strain test specimens were cut from undisturbed block sample E which was obtained during excavation of the slope for the stability study. The plane-strain test results are summarized in Table 5.5. Laboratory data are given in Appendix I, Tables I-36 through I-40. Samples were consolidated anisotropically (K_o = 0.333) to approximate field conditions and then failed in undrained compression with pore pressure measurements. A back pressure of 1.41 kg/sq cm was used to ensure full saturation of the sludge and to de-air the space between the membrane and the sample. With this back pressure,

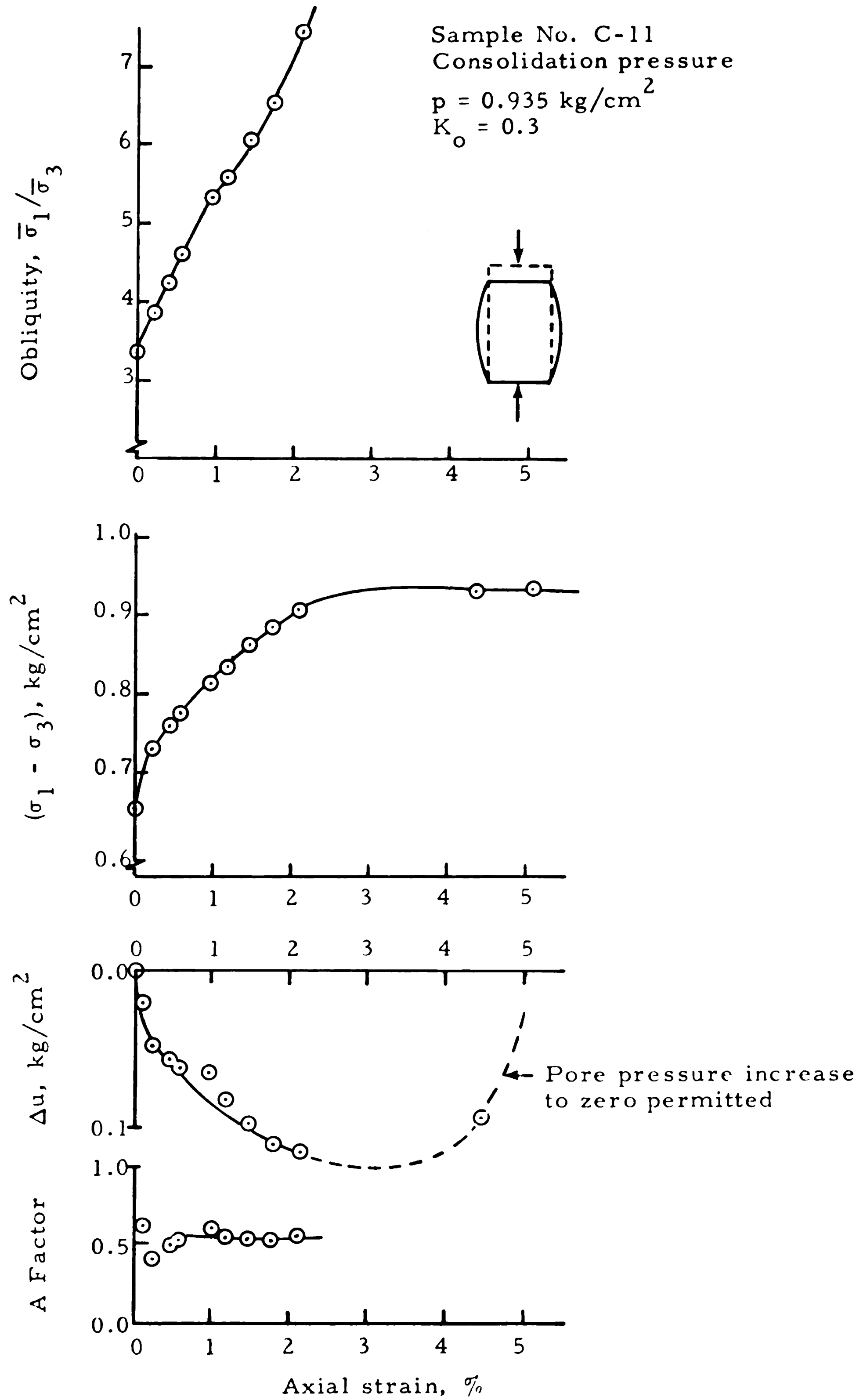

Figure 5.9.--Stress-strain behavior of consolidated sludge in undrained shear, sample C-11 with σ_3 constant and σ_1 decreasing.

TABLE 5.5.--Summary of Triaxial and Plane-Strain Test Results on Block E.

Sludge Sample	Consolidation p (Kg/cm^2)	K_o	Water Content Initial (%)	Water Content Final (%)	Initial Dry Density (pcf)	Undrained Strength c_u (Kg/cm^2)	$\bar{\sigma}_{1f}$ (Kg/cm^2)	$\bar{\sigma}_{3f}$ (Kg/cm^2)	A_f
E-1[a]	0.70	0.333	174.1	153.1	26.3	0.808	1.62	0.00	0.20
E-2[a]	1.41	0.333	170.3	131.6	26.2	1.54	3.19	0.10	0.17
E-3[a]	2.11	0.333	170.0	122	26.5	2.65	5.30	0.00	0.18
E-4[a]	2.11	0.333	167.4	119.6	27.5	2.04	4.09	0.01	0.26
E-5[a]	1.41	0.333	161.9	132.4	27.0	1.57	3.16	0.02	0.20
E-10[b]	2.29	0.333	174.8	117.1	26.6	2.19	4.41	0.28	0.24
E-11[b]	1.37	0.333	172.1	130	27.5	1.13	2.27	0.01	0.34
E-12[b]	0.67	0.333	173.4	154.4	26.9	0.59	1.17	0.00	0.31

a = Plane-strain test

b = Triaxial test

the pore-pressure parameter B was equal to one. The plane-strain tests are compared to triaxial tests run under the same test conditions on Figures 5.10 and 5.11. The stress-strain behavior of plane-strain sample E-5 and triaxial sample E-11, shown in Figure 5.10, corresponds to anisotropic consolidation and a consolidation pressure equal to 1.4 kg/sq cm. For failure in plane-strain, the obliquity ratio was smaller, the deviator stress was greater, the change in pore pressure was smaller, and the A pore pressure parameter was smaller than for the corresponding triaxial test. A summary of data from similar triaxial and plane-strain tests at other consolidation pressures is shown in Figure 5.11. The angle of internal friction and the final water content were approximately the same for both the triaxial and plane strain-tests, however, the undrained strength was approximately 25 percent greater for the corresponding plane strain test.

Unconfined Compression Tests

The unconfined compressive strength for undisturbed block samples of sludge are summarized in Figure 5.12 and Table 5.4 with the laboratory data given in Appendix I. Based on these strengths the sludge would be classified as soft to very soft (Terzaghi and Peck, 1967). The increase in strength with depth, due to greater consolidation, is observed in Figure 5.12 based on data for blocks C and G. The effect of sludge anisotropy on the unconfined compressive strength is shown in Figure 5.12 using data for sample orientations of zero, 45, and 90 degrees from the horizontal. Test specimens from the softer block C were more difficult to work with. The larger scatter in these

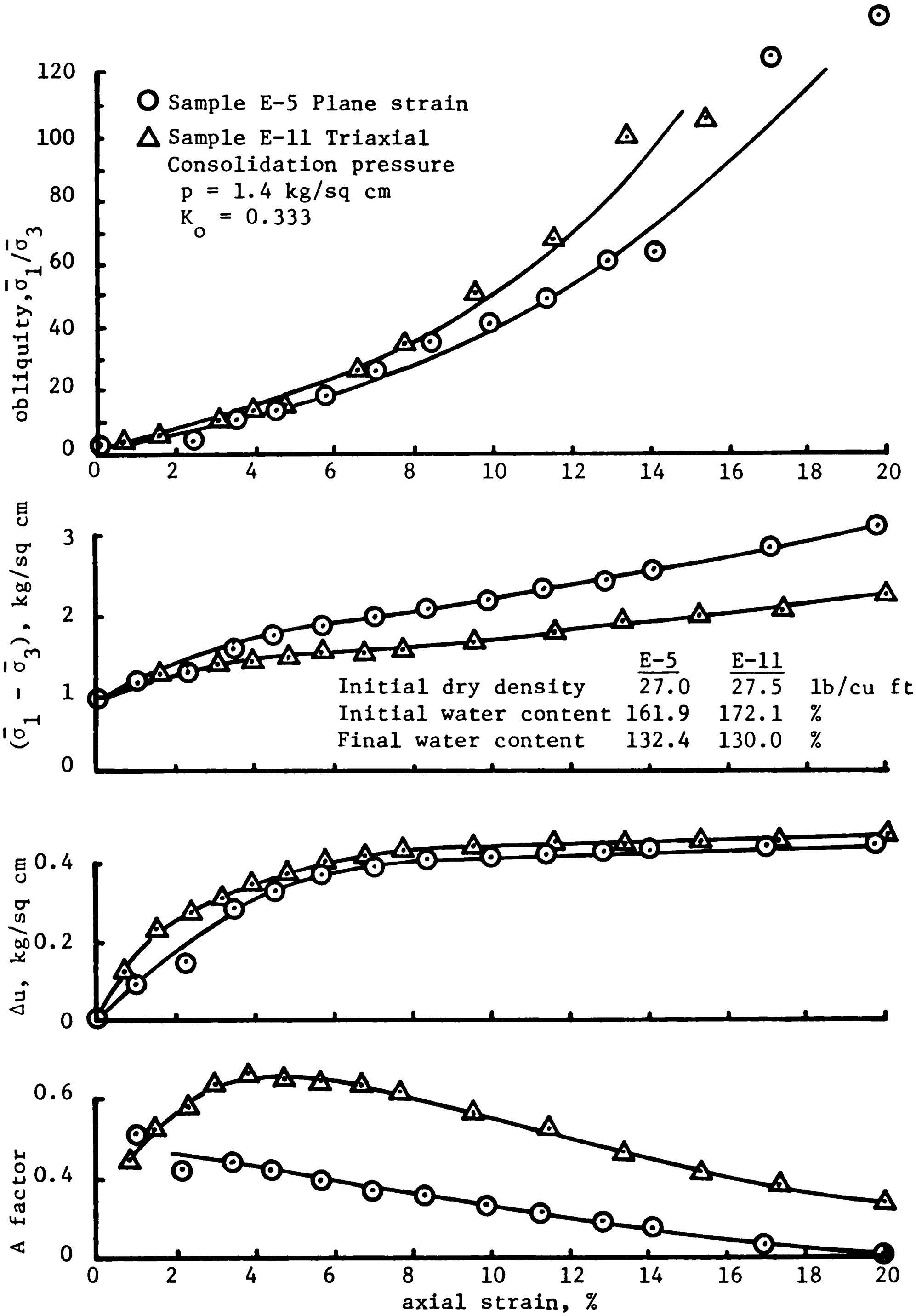

Figure 5.10.--Stress-strain behavior of consolidated sludge in undrained plane strain and triaxial shear, samples E-5 and E-11.

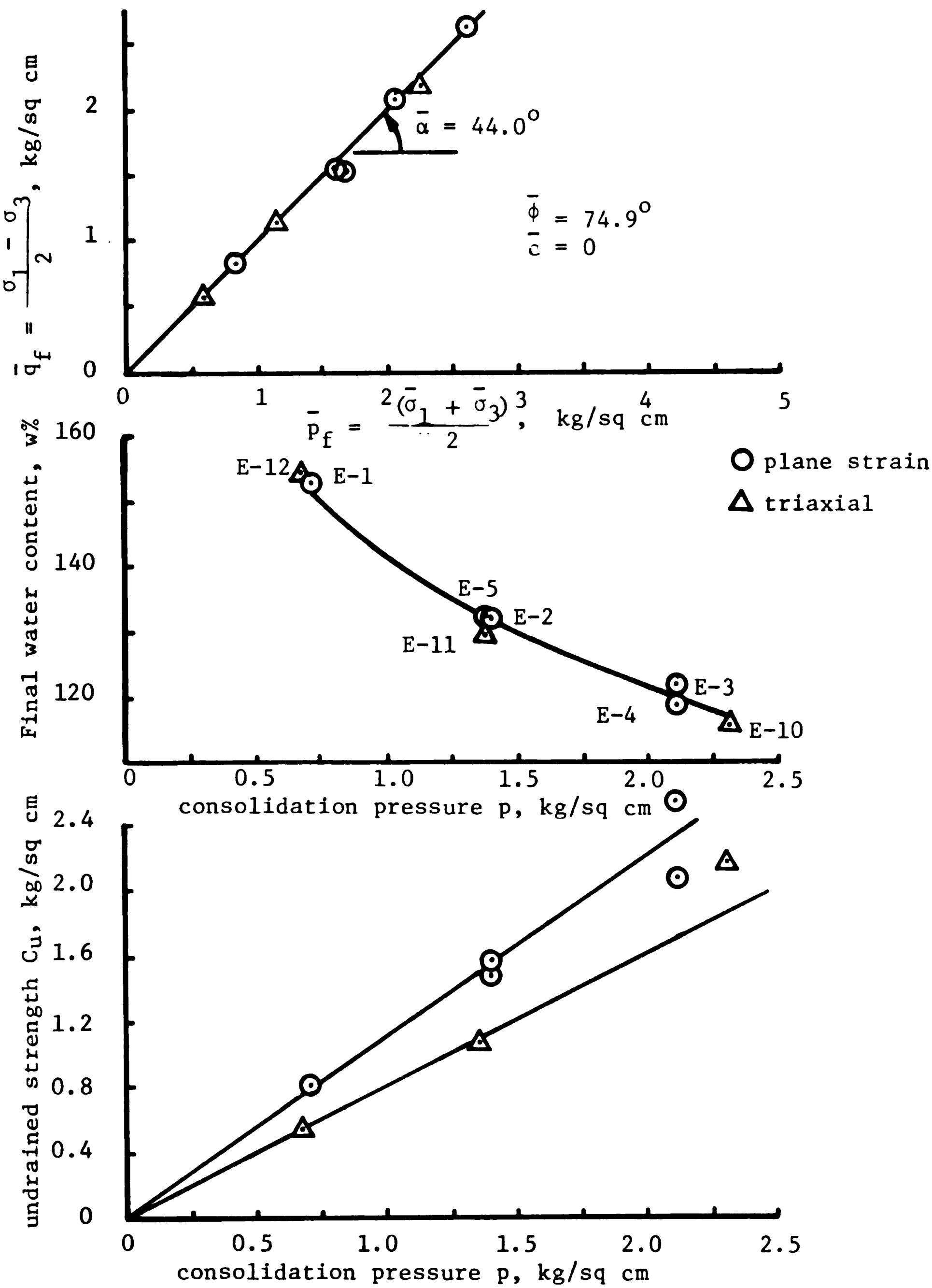

Figure 5.11.--Consolidated undrained plane strain and triaxial test results for Block E, anisotropic consolidation and axis vertical.

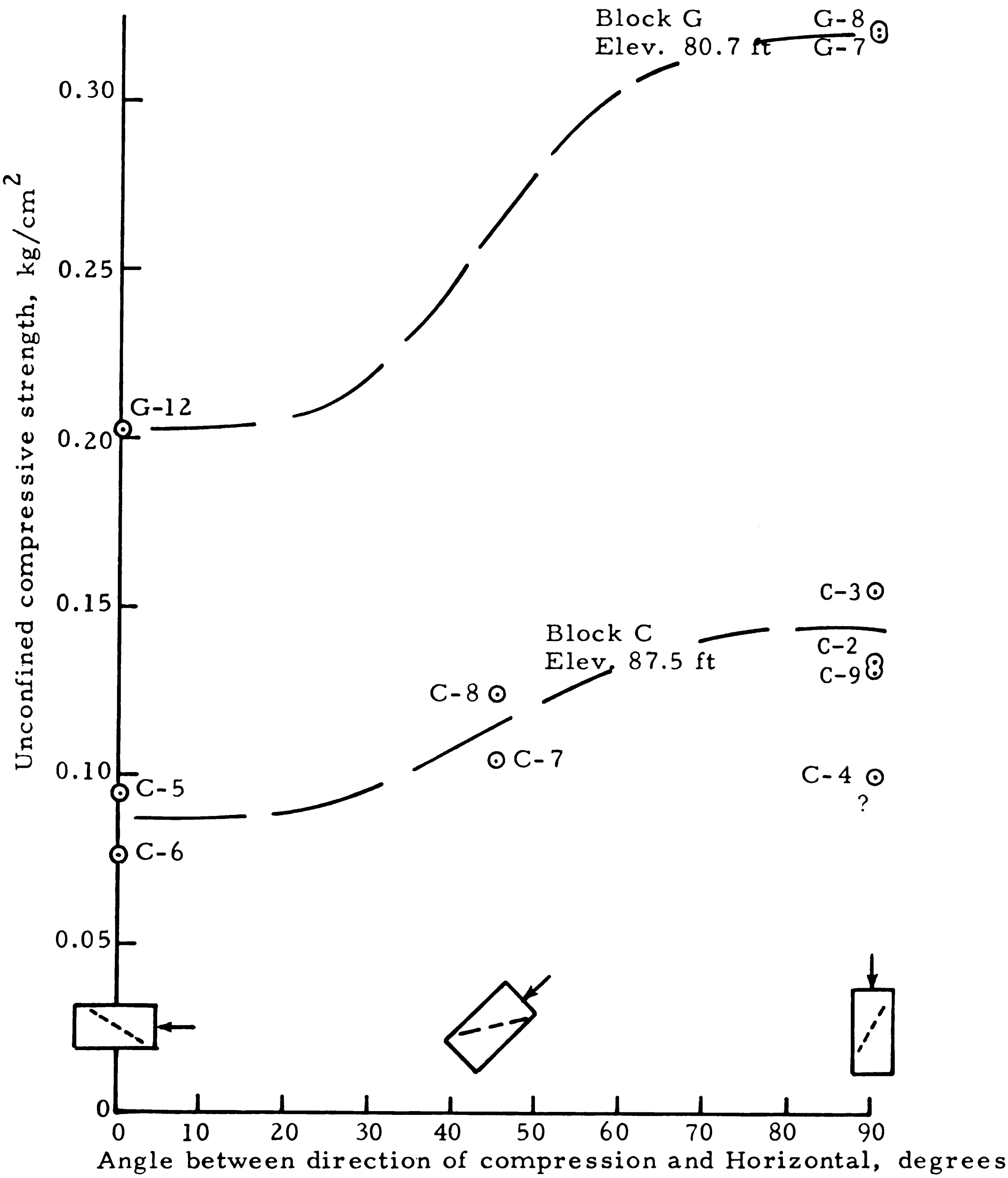

Figure 5.12.--Variation of unconfined compressive strength with sample orientation.

test results indicates more sample disturbance for some specimens during sample preparation.

In-Place Vane Shear Tests

Field data on the in-place vane shear strength of the sludge are summarized in Figure 5.13 and Appendix F. Additional test details are included as footnotes to Tables F-1 and F-2 in Appendix F. A gradual increase in undrained shear strength with depth is observed for the normally consolidated sludge. The ratio c_u/p is large, close to 2.5, when compared to normally consolidated clays, which are generally less than 1. Unconfined compression data, shown for two block samples in Figure 5.13a, are much less than the vane shear strength. This appears to be due to physical disturbance of the sludge during sampling and sample preparation for laboratory testing. Stress reduction during sampling permits small gas bubbles to expand which may cause additional disturbance. Shear strength data taken near the exposed slope shortly after excavation has been summarized in Table F-2, Appendix F. Comparisons for the same elevations show smaller undrained vane shear strengths, indicating that unloading of the slope appears to have had some influence. Also included in Table F-2 are data for the horizontal orientation of the vane. These values are larger as compared to the vertical vane orientation.

Dutch Cone Penetration Tests

Dutch cone penetration data given in Table F-3, Appendix F, has been summarized in Figure 5.13b. For the softer upper sludge layer no increase in cone resistance with depth was observed until the middle

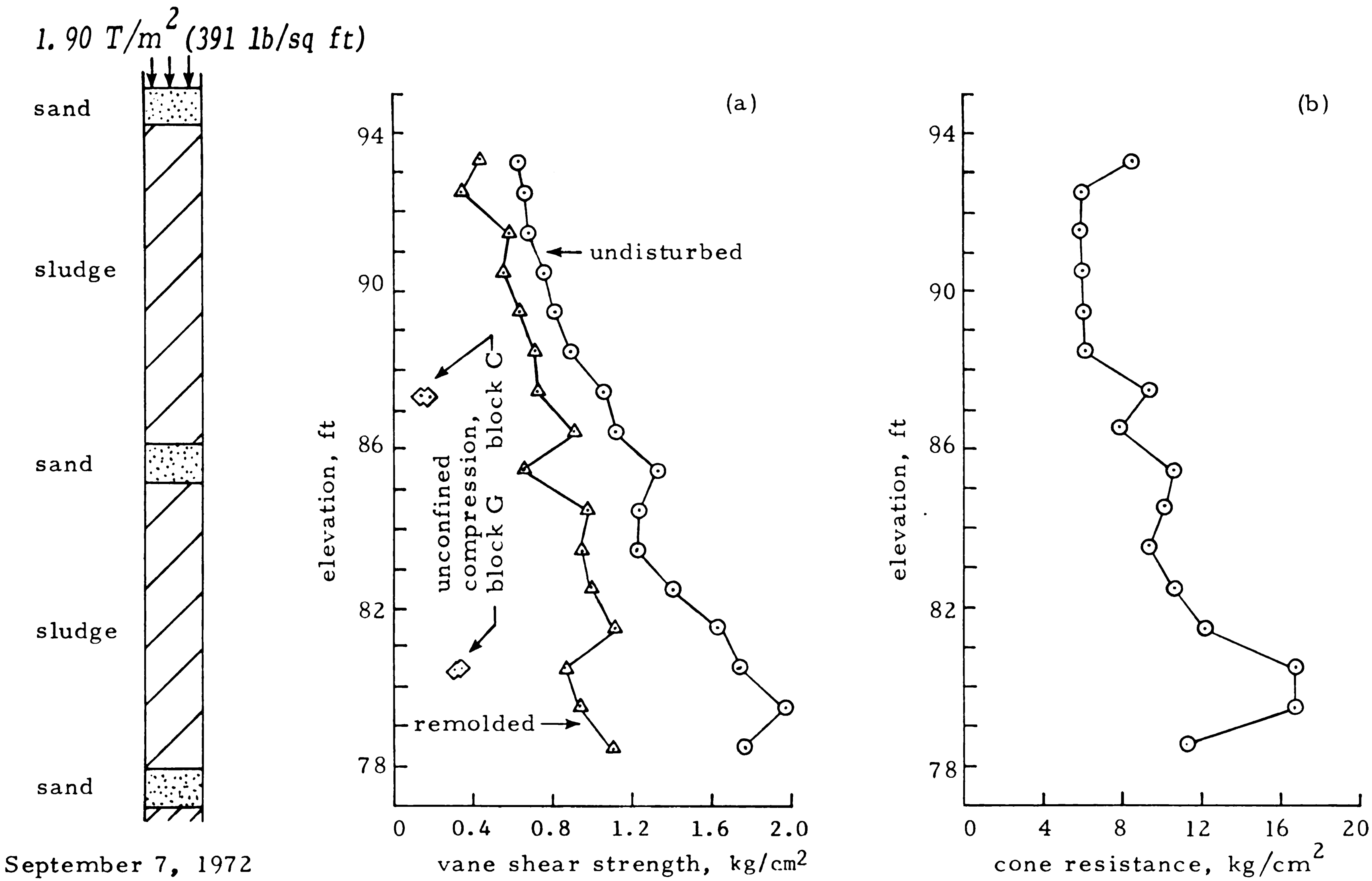

Figure 5.13.--Experimental landfill, immediately before slope excavation. (a) Vane sheer strength. (b) Dutch cone resistance.

sand blanket was approached. Directly below the middle sand blanket the cone resistance increased with larger values observed for the more highly consolidated bottom half of the lower sludge layer.

C. Slope Behavior

Slope behavior was monitored in terms of lateral movement, vertical movement, change in pore water pressures, temperature, and total pressure cell readings. Tables, figures and graphs are used to summarize the tabulated data which are given in the Appendices.

Lateral Movement

Lateral slope movements were monitored using both surface measurements on stakes (Appendix A) and slope indicator data (Appendix B) obtained using flexible vertical casings and an inclinometer instrument. Surface movements along three lines labeled I, II, and III, are given in Table A-1, Appendix A. Locations of the WX, WY, and WZ positions are given in Figure 4.2 with reference to instrument group locations and the plan view of the experimental slope. Movements in the experimental slope became more evident as the actual slope failure was approached. Tension cracks appeared in the earth surcharge very shortly after completion of the 1:8 slope. Their appearance and location relative to the slope indicator casings are shown in Figure 5.14. The stake for line II-WZ was lost after the October 28, 1972, reading at which time a total surface movement of 3.72 inches (9.45 cm) had been observed. The initial slope failure (Figure 5.15a) did not occur until four days after the 1:8 slope had been excavated. Shortly thereafter additional failures occurred in the top sludge layer along

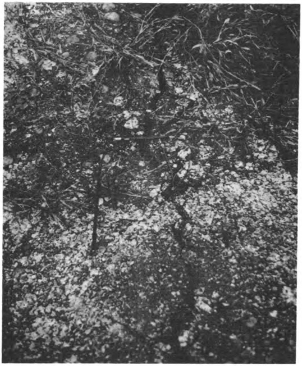

(a)

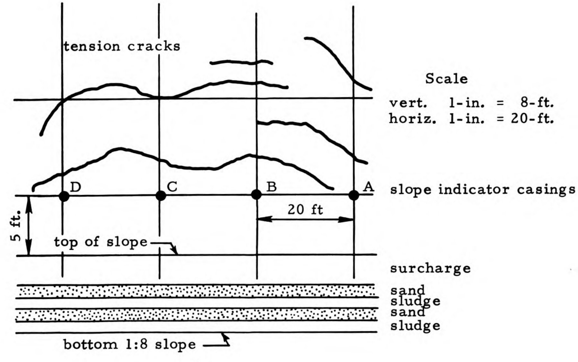

(b)

Figure 5.14 Tension cracks. (a) Photo. (b) Crack locations on October 25, 1972.

(a)

(b)

Figure 5.15 (a) Initial slope failure, October 29, 1972.
(b) Slope condition on November 11, 1972.

the slope as shown in Figure 5.15b. The surface extent of these slope failure areas for three different dates is given in Figure A-1, Appendix A for the 1:8 slope. Examination of these slope failures suggest that the typical cross-section can be approximated as shown in Figure 5.16. The tension cracks appeared to extend through the earth surcharge down to the upper sand drainage blanket. The failure surface in the sludge approximated a 1:1.64 slope (about 58.6 degrees from the horizontal). The failure surface in the sand drainage blankets were approximately as shown in Figure 5.16. Approximately five months after the excavation (April 7, 1973), line III-WZ recorded a total of 7.08 inches (17.98 cm) of movement for the 1:8 slope. The trench was then filled with fresh sludge and surface measurements taken approximately two months later (June 14, 1973) showed that the slope had moved back a small amount as shown in Table A-1.

Lateral movement at various levels in the landfill is shown very clearly by the slope indicator data summarized in Figure 5.17a through 5.17g. Field data are given in Tables B-1 through B-13, Appendix B. Locations of slope indicator casings A through G were given in Figure 4.1. All movements are referred to the base of each casing which was embedded about 1 ft. into the natural soil beneath the landfill and to the initial readings taken on September 19, 1972. Most of the movement toward the exposed slope occurred in the top sludge layer, reaching a maximum at the landfill surface. Each curve in Figure 5.17 is identified by the date on which readings were taken. Slope indicator casings A and D also moved significant amounts parallel to the slope as shown by the data summarized in Figure 5.17e. For

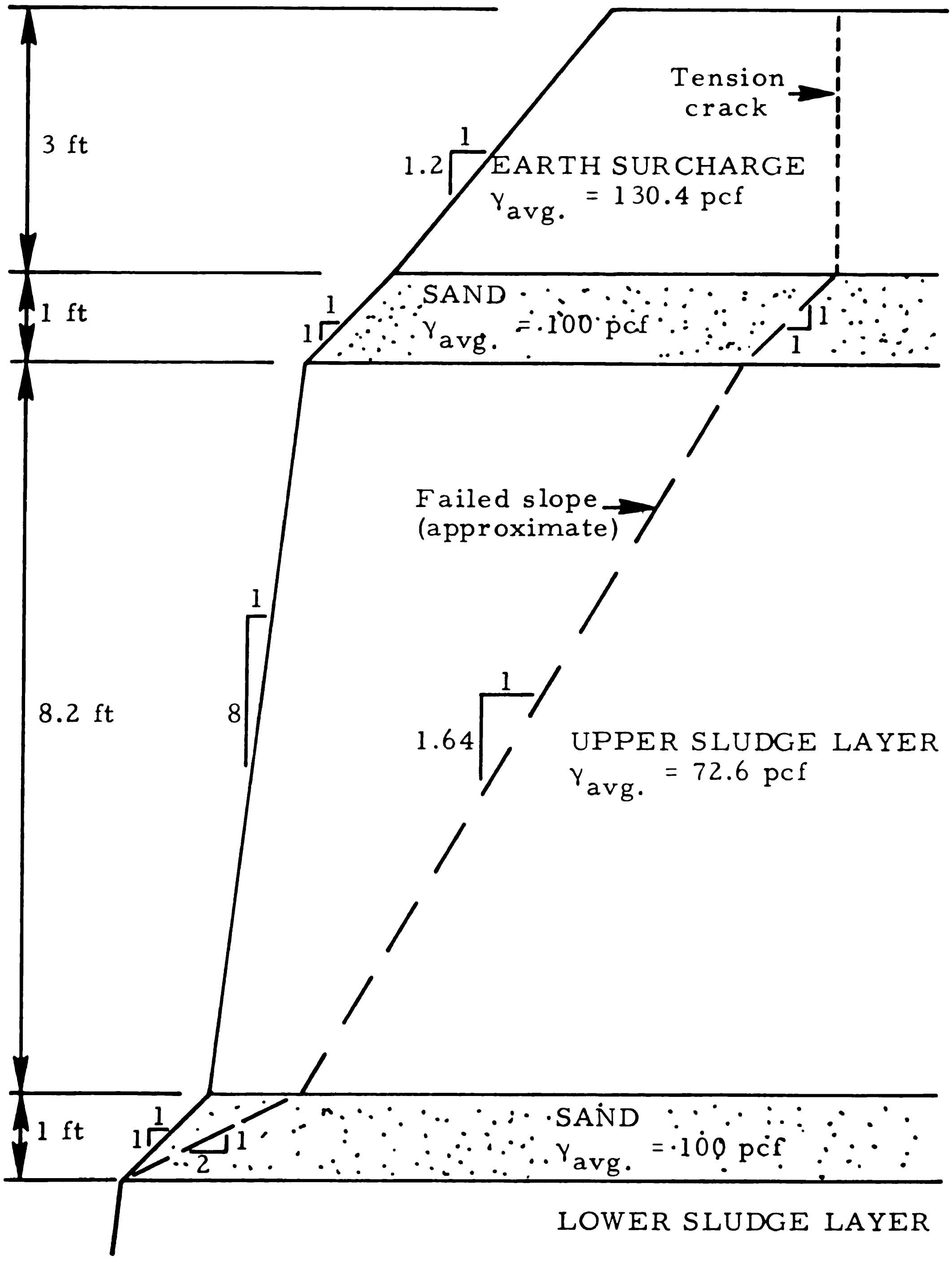

Figure 5.16.--Cross section of 1:8 slope, before and after failure.

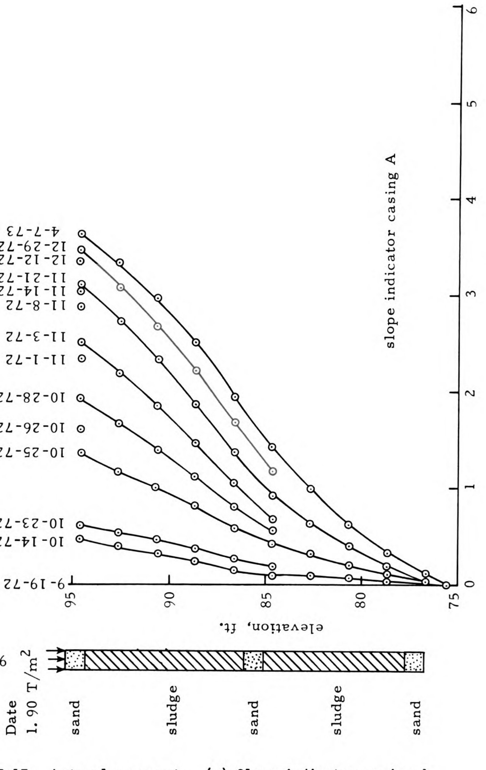

Figure 5.17.--Lateral movement. (a) Slope indicator casing A.

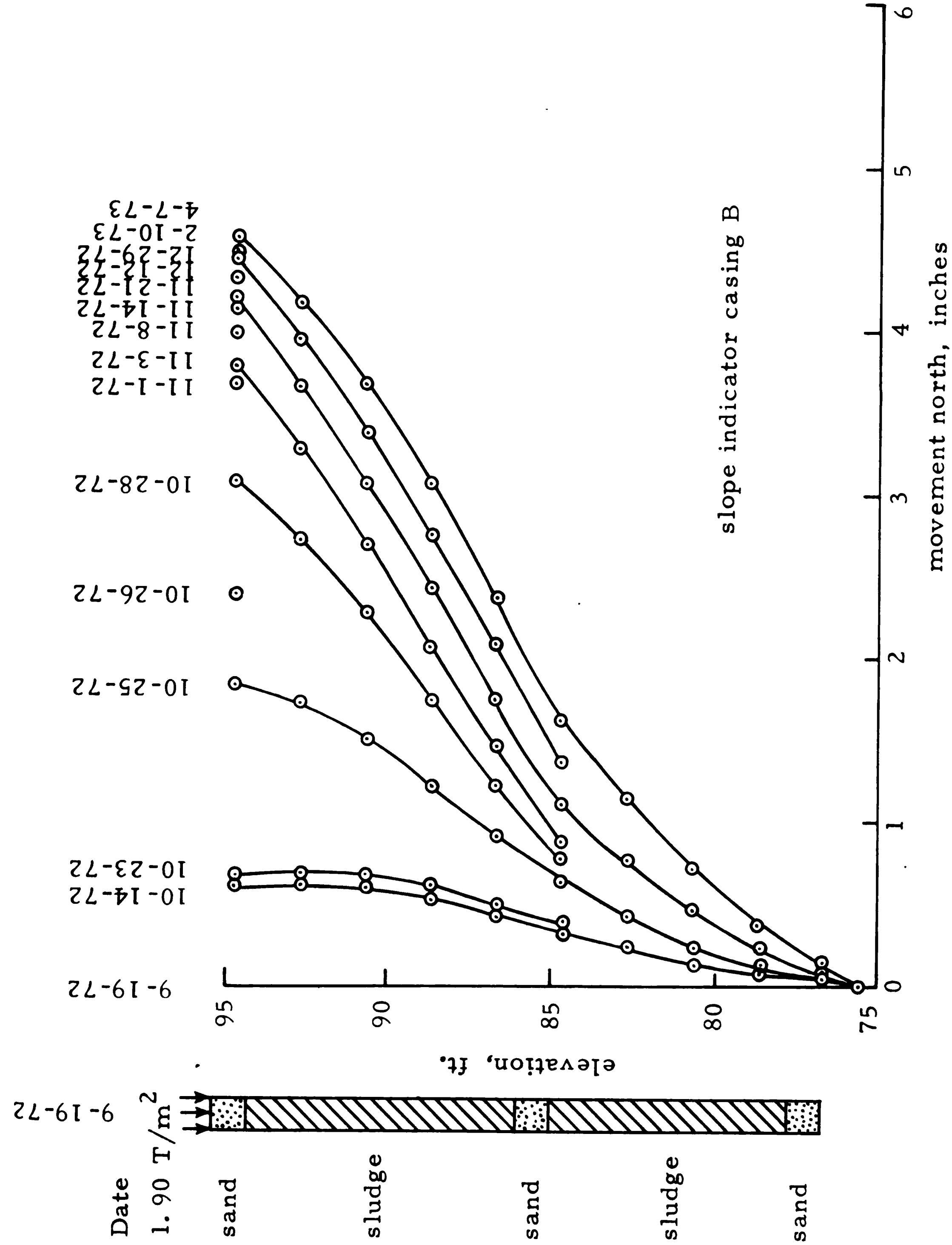

Figure 5.17.--Lateral movement. (b) Slope indicator casing B.

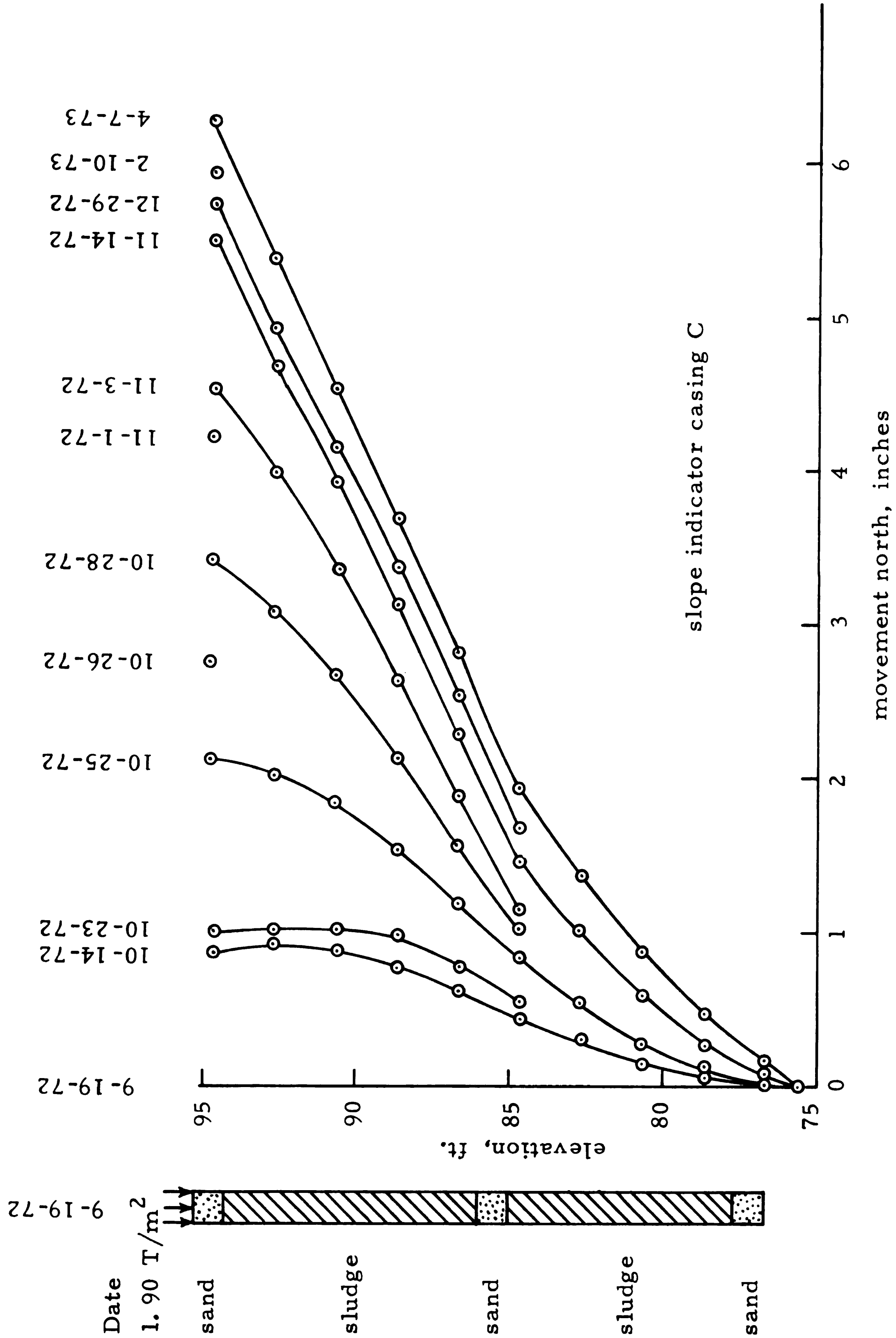

Figure 5.17.--Lateral movement. (c) Slope indicator casing C.

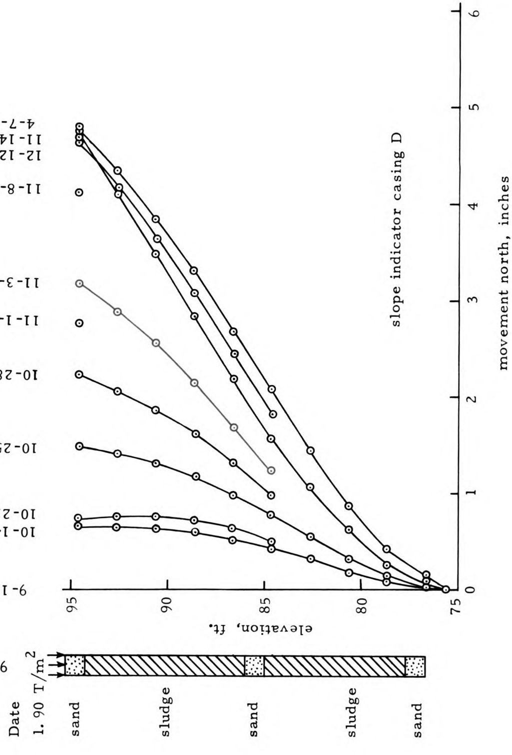

Figure 5.17.--Lateral movement. (d) Slope indicator casing D.

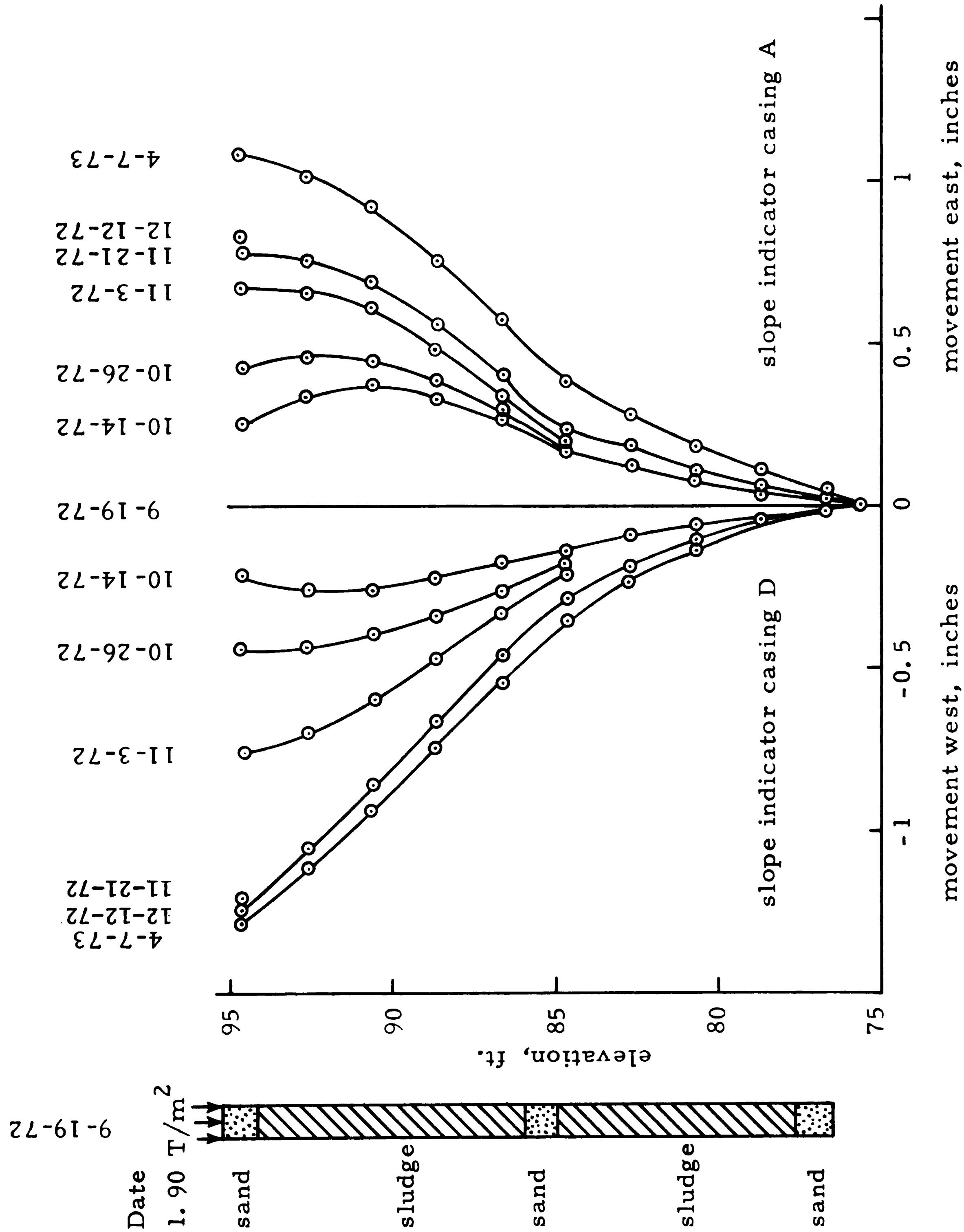

Figure 5.17.--Lateral movement. (e) Slope indicator casings A and D.

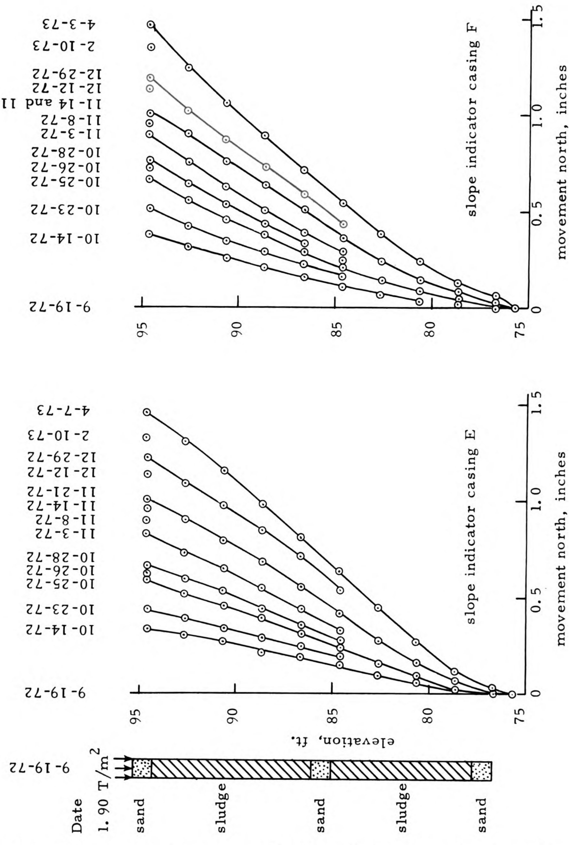

Figure 5.17.--Lateral movement. (f) Slope indicator casings E and F.

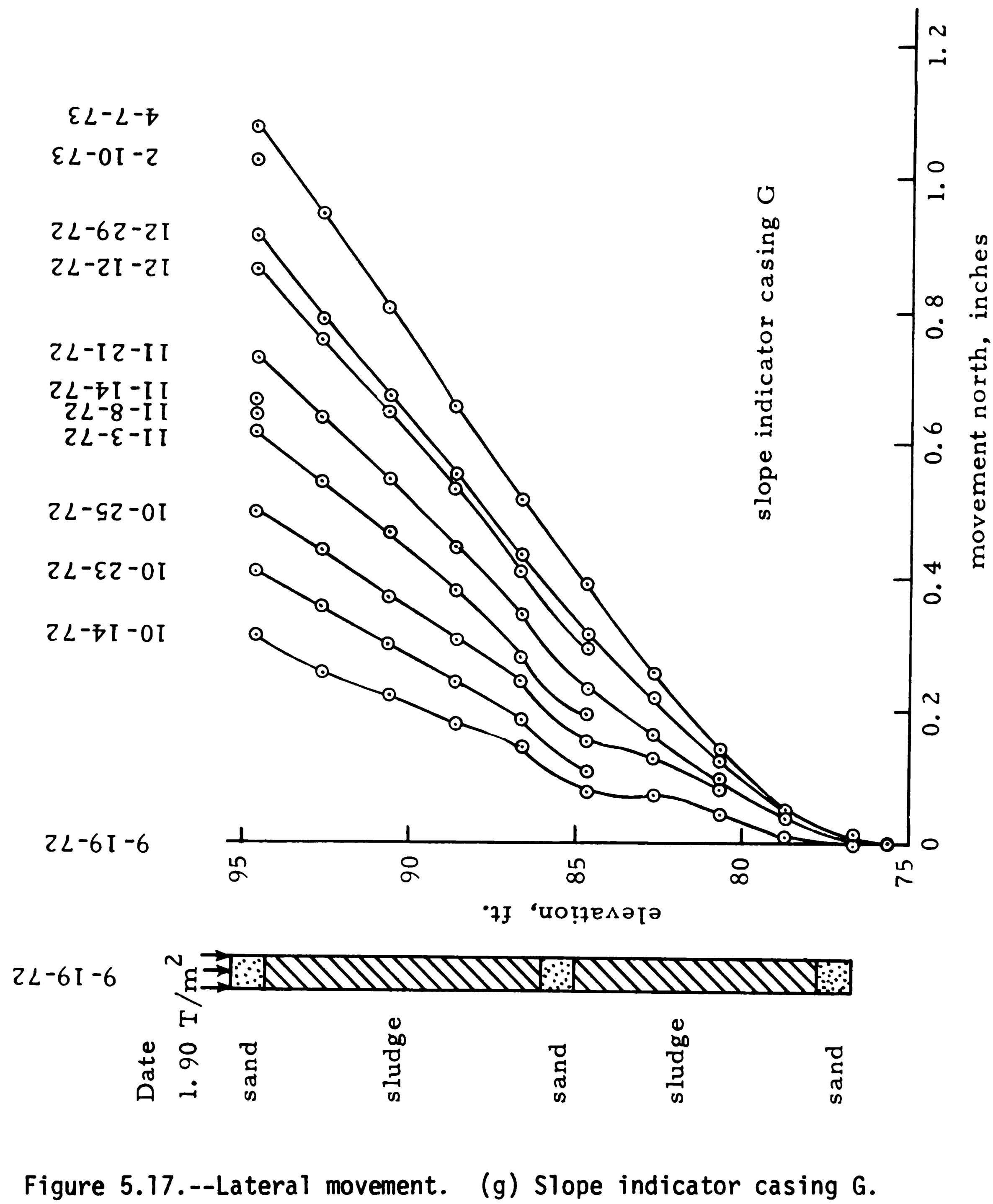

Figure 5.17.--Lateral movement. (g) Slope indicator casing G.

convenient reference the elevations for each sludge layer and sand drainage blanket have been included in Figure 5.17.

Vertical Movement

Downward movement of the sludge near the exposed slope and any settlement due to consolidation are summarized by elevation readings for the settlement plates given in Tables C-1 through C-4, Appendix C. Location and identification of the settlement plates have been given in Figures 4.1 and 4.3. In Figure 5.18 the movement in the upper and lower sludge layers is shown by curves labeled 5 - 3 and 3 - 1, respectively. The quantity 5 - 3 equals the elevation of plate 5 minus the elevation of plate 3. The numbers 1, 3, and 5 refer to settlement plates located in the bottom, middle, and top sand drainage blankets, respectively. The largest movement occurred in the softer top sludge layer near the slope as shown by data for instrument group 5. Part of the settlement appears to have been initiated when the middle sand blanket became fully drained due to slope excavation about September 29, 1972.

Pore Water Pressures

Piezometers, identified as to location and number in Figures 4.1 and 4.3, gave the data summarized in Figure 5.19. Field data are given in Tables D-1 through D-4, Appendix D. Instrument group 4, closest to the slope, and instrument group 5, about 29 ft. (8.84 m) back from the slope, gave pore water pressures which appear to be directly related to the reduction of load at the excavated slope. The 3:4 slope was completed on October 13, 1972. This unloading of the

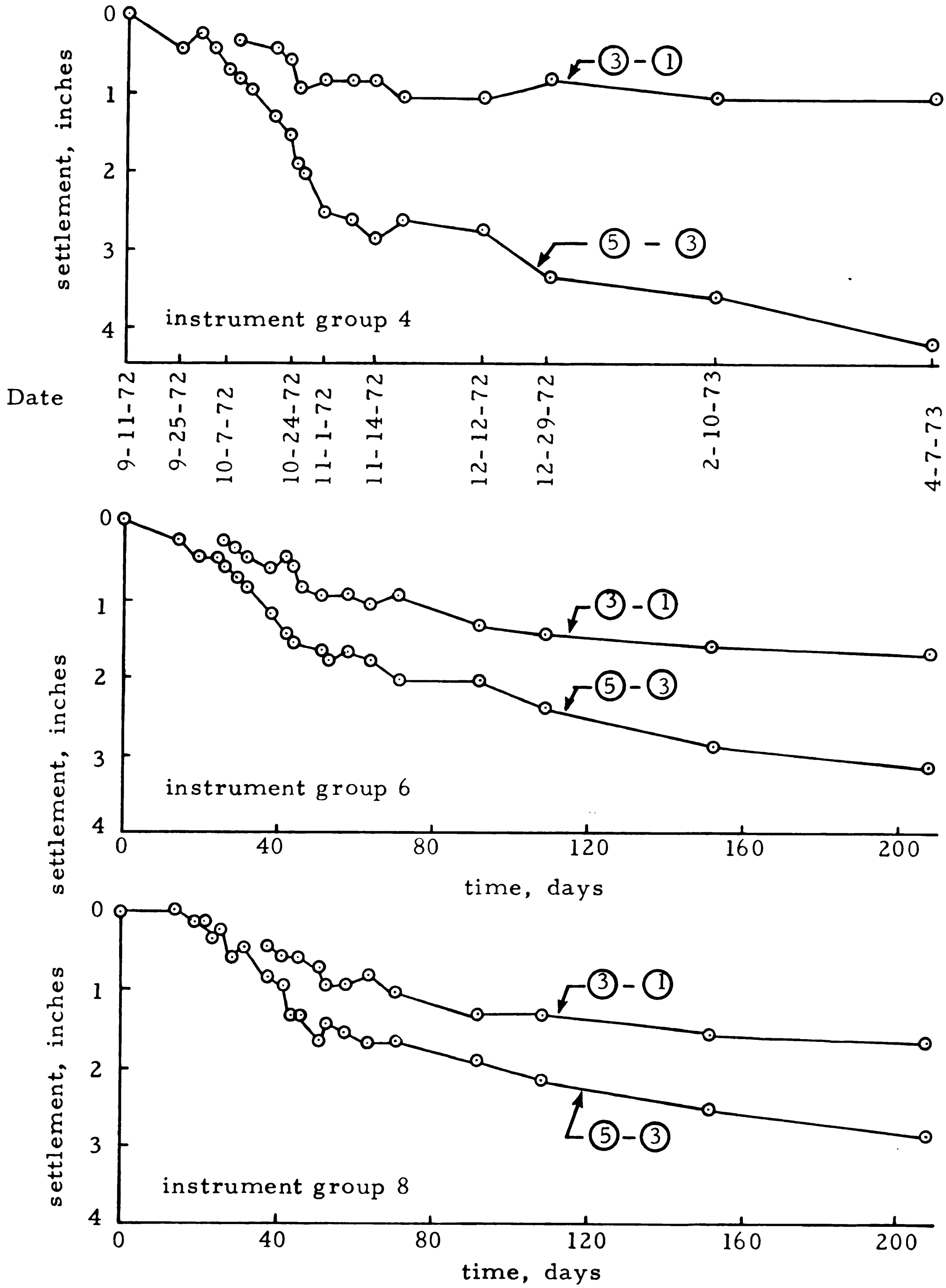

Figure 5.18.--Settlement in the top, ⑤-③, and bottom, ③-①, sludge layers.
(a) Instrument groups 4, 6, and 8.

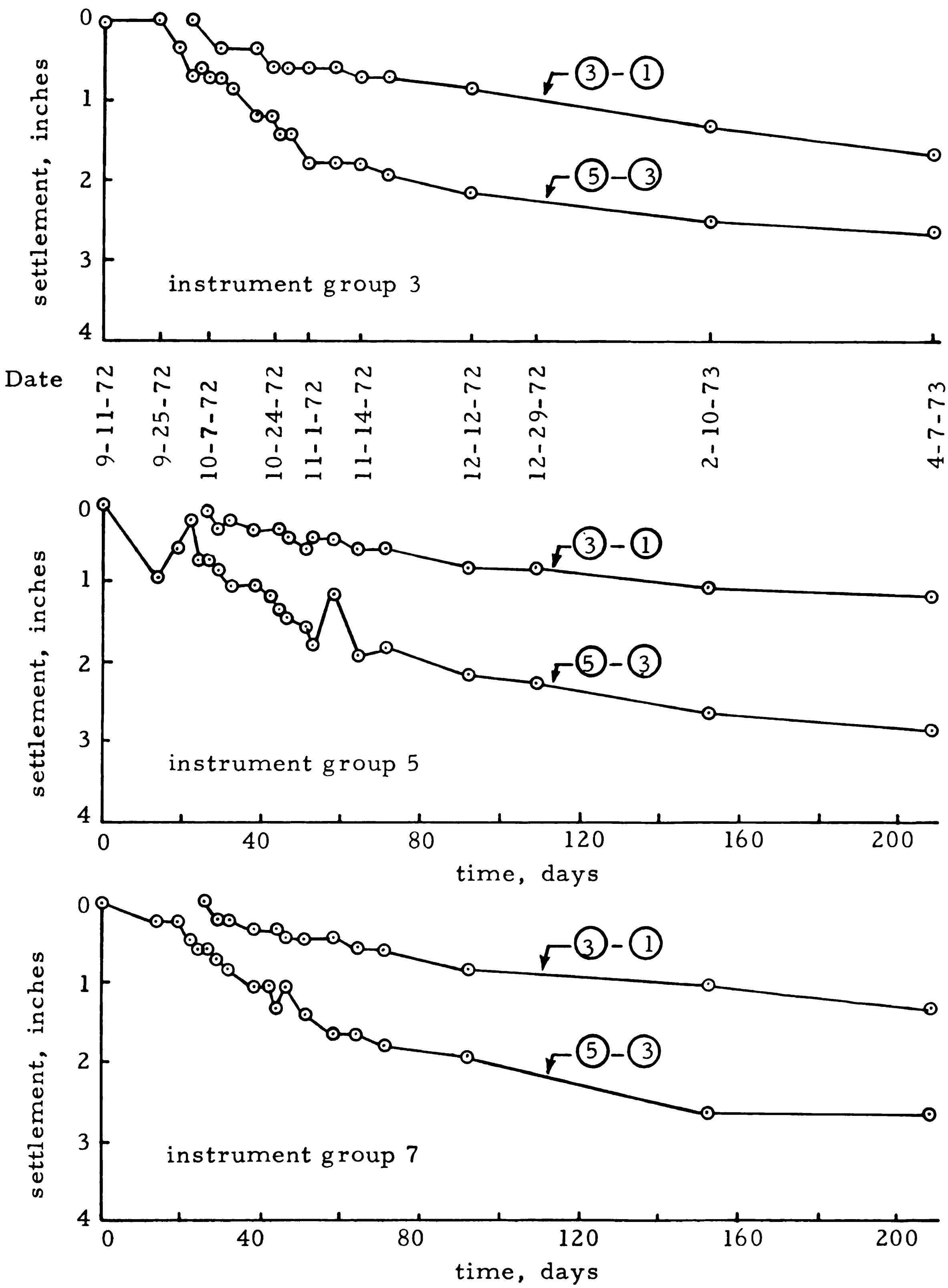

Figure 5.18.--Settlement in the top, 5-3, and bottom, 3-1, sludge layers. (b) Instrument groups 3, 5, and 7.

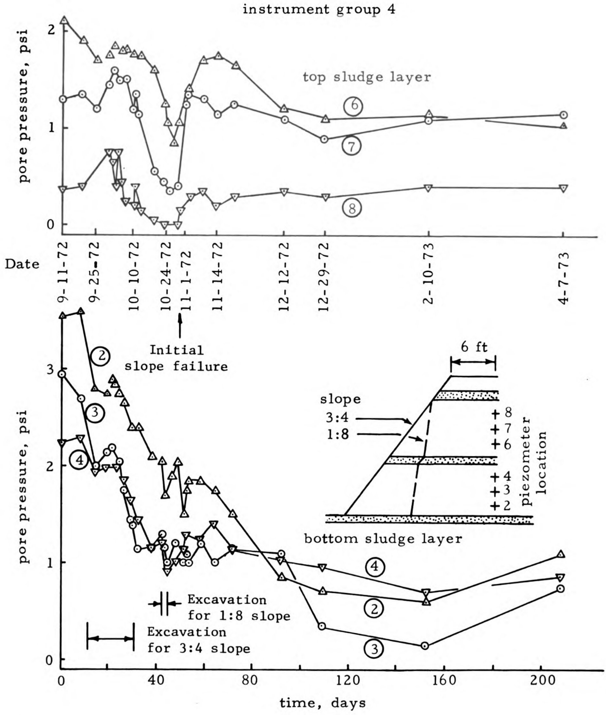

Figure 5.19.--Pore pressure versus time curves. (a) Instrument group 4.

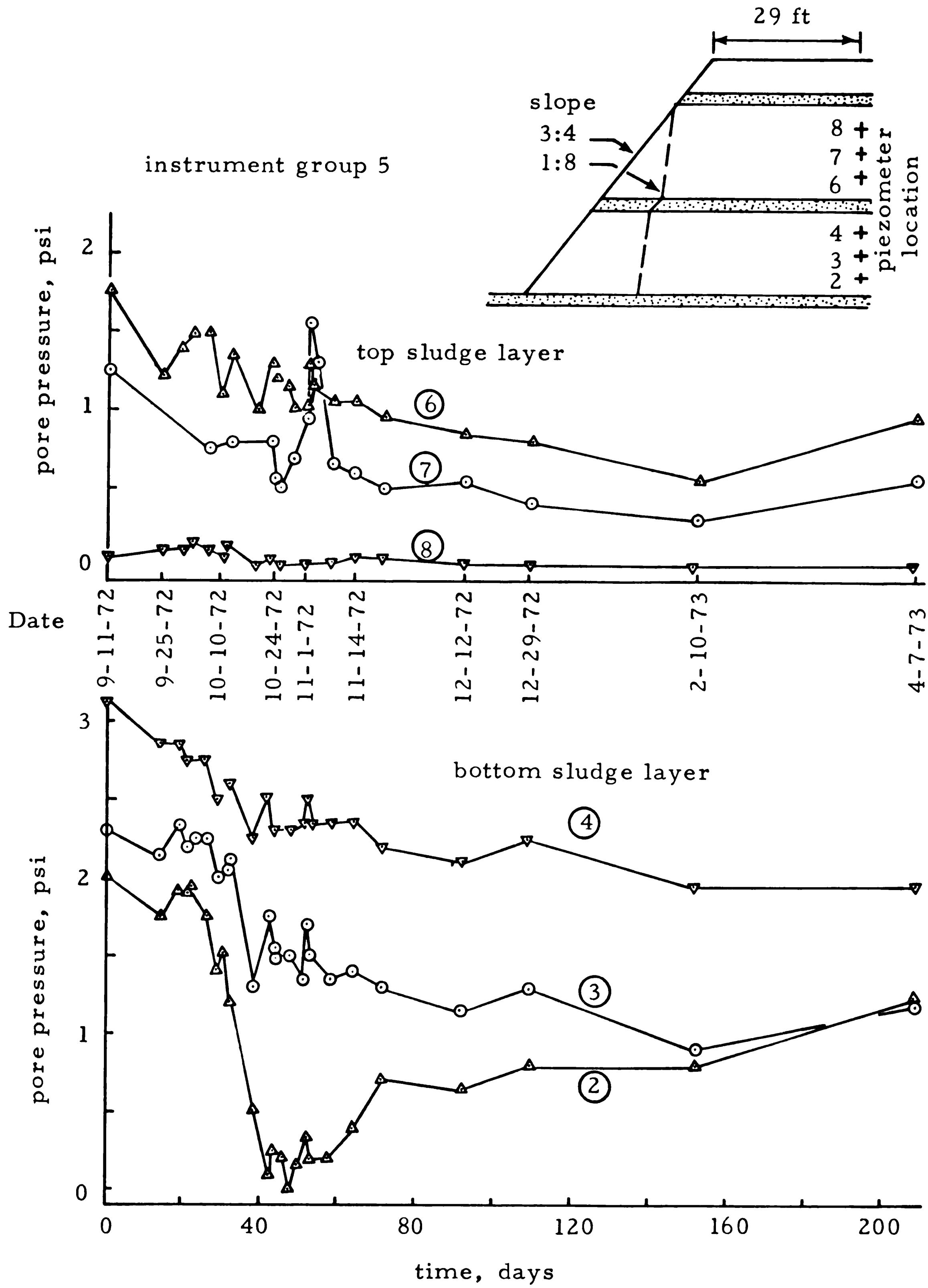

Figure 5.19.--Pore pressure versus time curves. (b) Instrument group 5.

slope is reflected by the decrease in pore pressures in both sludge layers at instrument group 4 and in the bottom sludge layer at instrument group 5. The reduction in pore pressure prior to this date was gradual as the excavation progressed. After October 13, 1972, lateral movements toward the slope (Figure 5.17) appear to be the cause of the decrease in observed pore water pressure. The rate of pore water pressure decrease accelerated with excavation for the 1:8 slope. The initial decrease in pore water pressure sharply reversed itself after the initial slope failure.

Temperature

The field data from the thermistors used for temperature measurement are tabulated in Table E-1, Appendix E, and are plotted against time in Figure 5.20. The observed temperatures show a pattern indicating that the sludge is responding to air and ground temperatures. Average daily air temperatures and precipitation during the entire project are given in Appendix H.

Total Pressure Cells

Total sludge pressures measured in the vertical and horizontal directions are tabulated in Table G-1, Appendix G, and plotted against time in Figure 5.21. The two working cells and adjacent piezometer G7-3 were located in the middle of the lower sludge layer as part of instrument group 7. Original plans had intended that the cell be parallel to the excavated slope, however, the vertical cell was oriented normal to the excavated slope due to the contractor's change in plans. The data in Figure 5.21 show a decrease in total horizontal

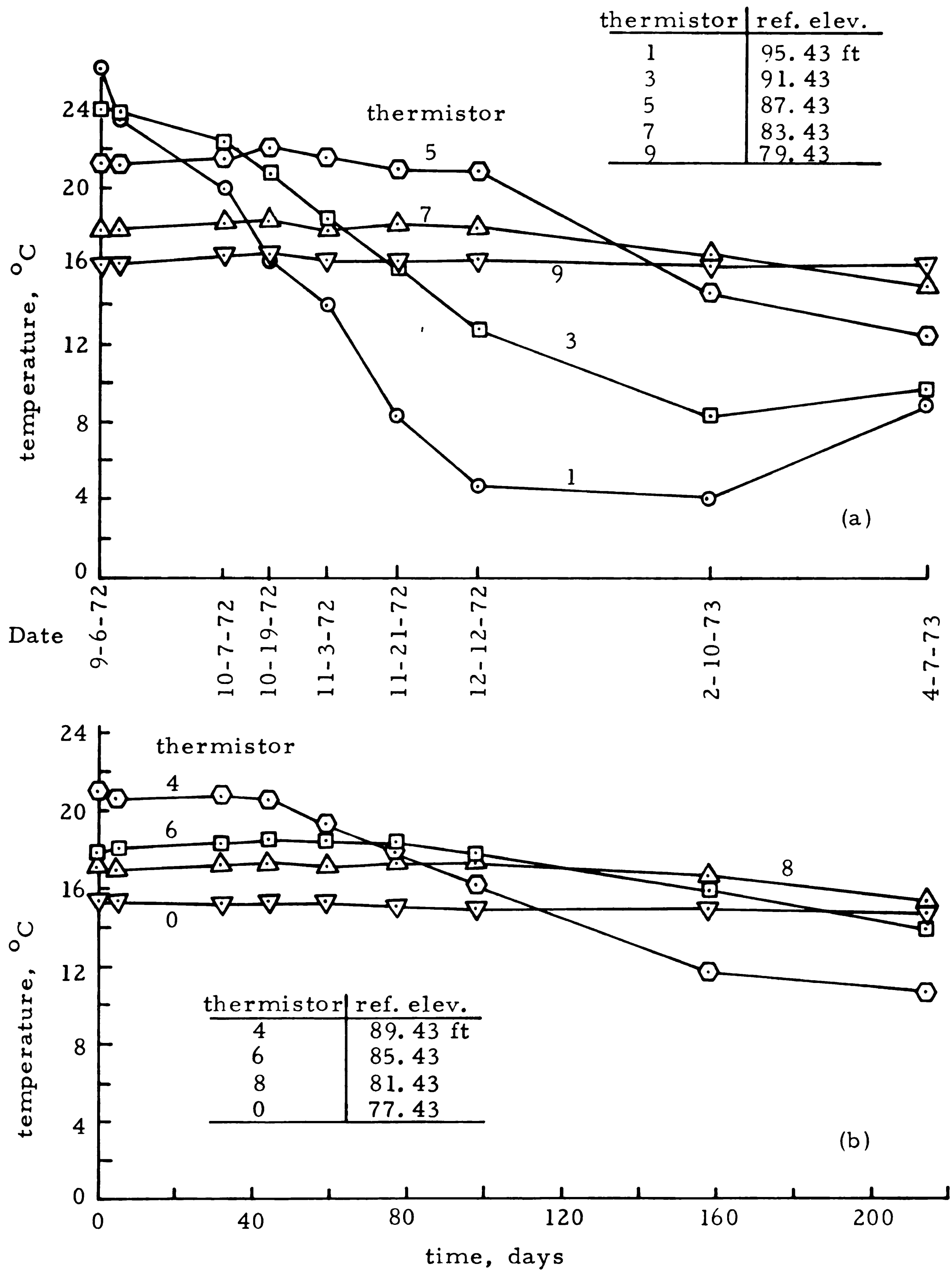

Figure 5.20.--Temperature versus time. (a) Thermistors 1,3,5,7 and 9. (b) Thermistors 4,6,8, and 0.

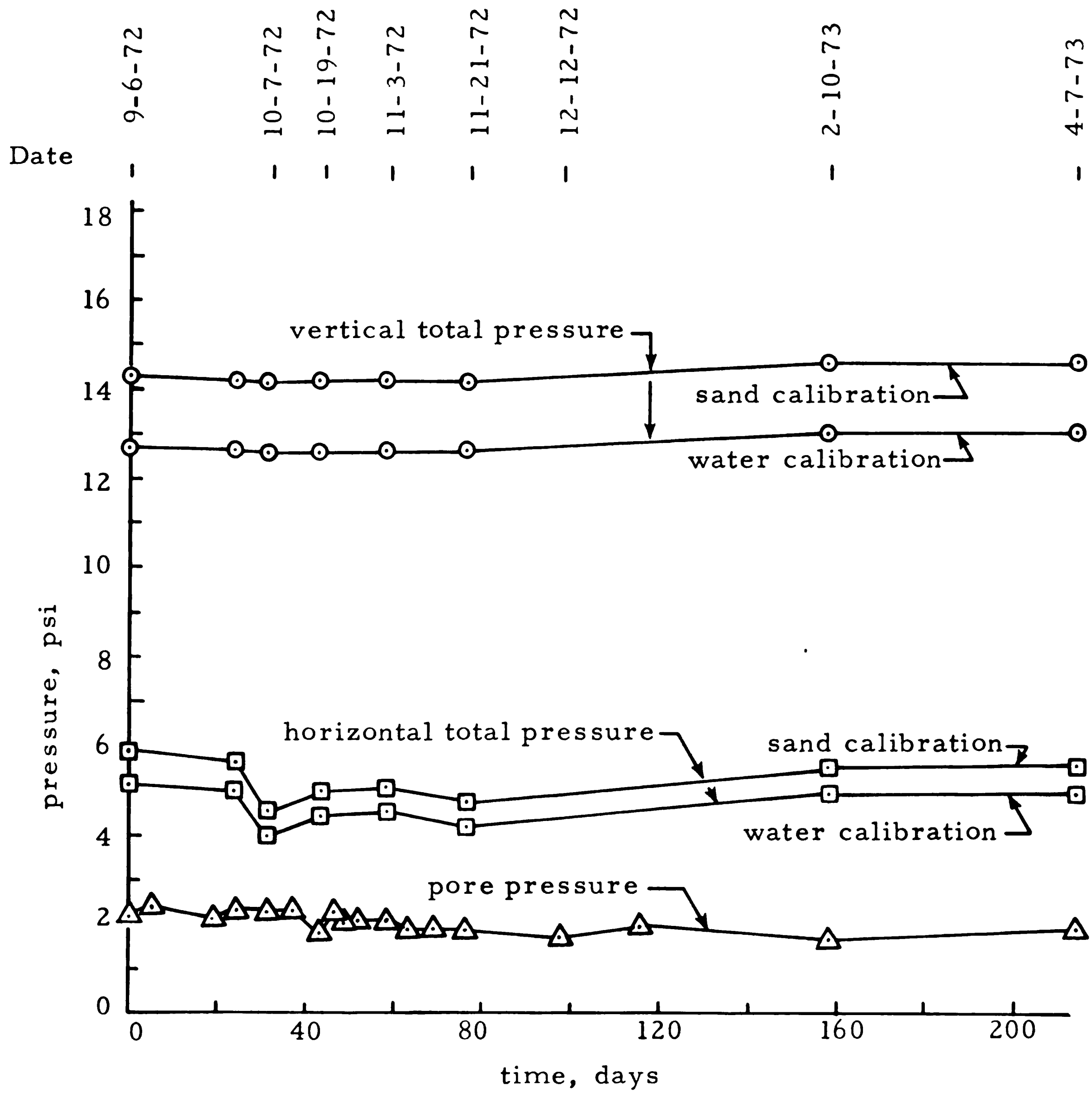

Figure 5.21.--Horizontal and Vertical total stresses, bottom sludge layer.

stress of about 1.4 psi (0.0984 kg/sq cm) during the period that the slope was being excavated. Over a period of time the stress again increased, perhaps due to internal stress adjustments related to creep. Pore pressures in the vicinity of the total pressure cells remained relatively constant during the period of slope excavation.

CHAPTER VI

ANALYSIS AND DISCUSSION OF PROJECT RESULTS

This discussion and interpretation of project data covers laboratory and field results for the stability study on consolidated papermill sludge. The material is presented in three sections: physical properties, strength characteristics, and slope movements and stability of the fibrous organic soil.

A. Physical Properties of the Fibrous Organic Soil

Physical properties of organic soils and papermill sludges characterize, to some extent, the quality of the material relative to engineering purposes. The properties discussed below include ash content, consistency limits, water content, and unit weights.

Ash (or Organic) Content

Representative ash contents for undisturbed block samples, given in Table 5.2, are very close to the average reported by Andersland, *et al.* (1972), for fresh sludge samples taken during construction of the papermill sludge landfill, approximately one year earlier. These data show that ash contents for the sludge in the landfill range from about 32 percent to about 60 percent. Earlier work (Andersland and Laza, 1971) has shown that organic contents for papermill sludges, based on ash contents determined by ASTM test method D586-63, agree reasonably well with organic contents determined on the basis of the test method given in Agronomy No. 9, section 92-3.3 (Black, 1965). For information, weight loss for papermill sludge samples from blocks C and G, which were first dried to 105°C, have been plotted against temperature in Figure 6.1. The small samples, 6.7861 grams for block C and 5.0706 grams for block G, reached essentially a constant weight after one hour at each temperature. These data show no drastic weight loss for temperatures above 300°C. The small weight loss above 400°C may be partly caused by dehydration. Dehydration involves the loss of any water held by the clay mineral. Dehydration curves, given by Grim (1968) for kaolinite clay, show little or no dehydration up to about 400°C. Most of the dehydration takes place between approximately 400 and 525°C with the rest taking place up to approximately 750°C where dehydration is complete. However, part of the weight loss for temperatures above 300°C may also be caused by incomplete burning of the organic material at lower temperatures. The ash (or organic) content of the sludge is shown in the following sections to have some relationship to the consistency limits, water contents, unit weights, and to the shear strength parameter, $\bar{\phi}$.

Consistency Limits

Organic content of the sludge also influences the consistency limits. Ash content has been plotted against the liquid and plastic limits giving the relationships shown in Figure 6.2. Specifically, as the ash content increased, both the liquid limit and plastic

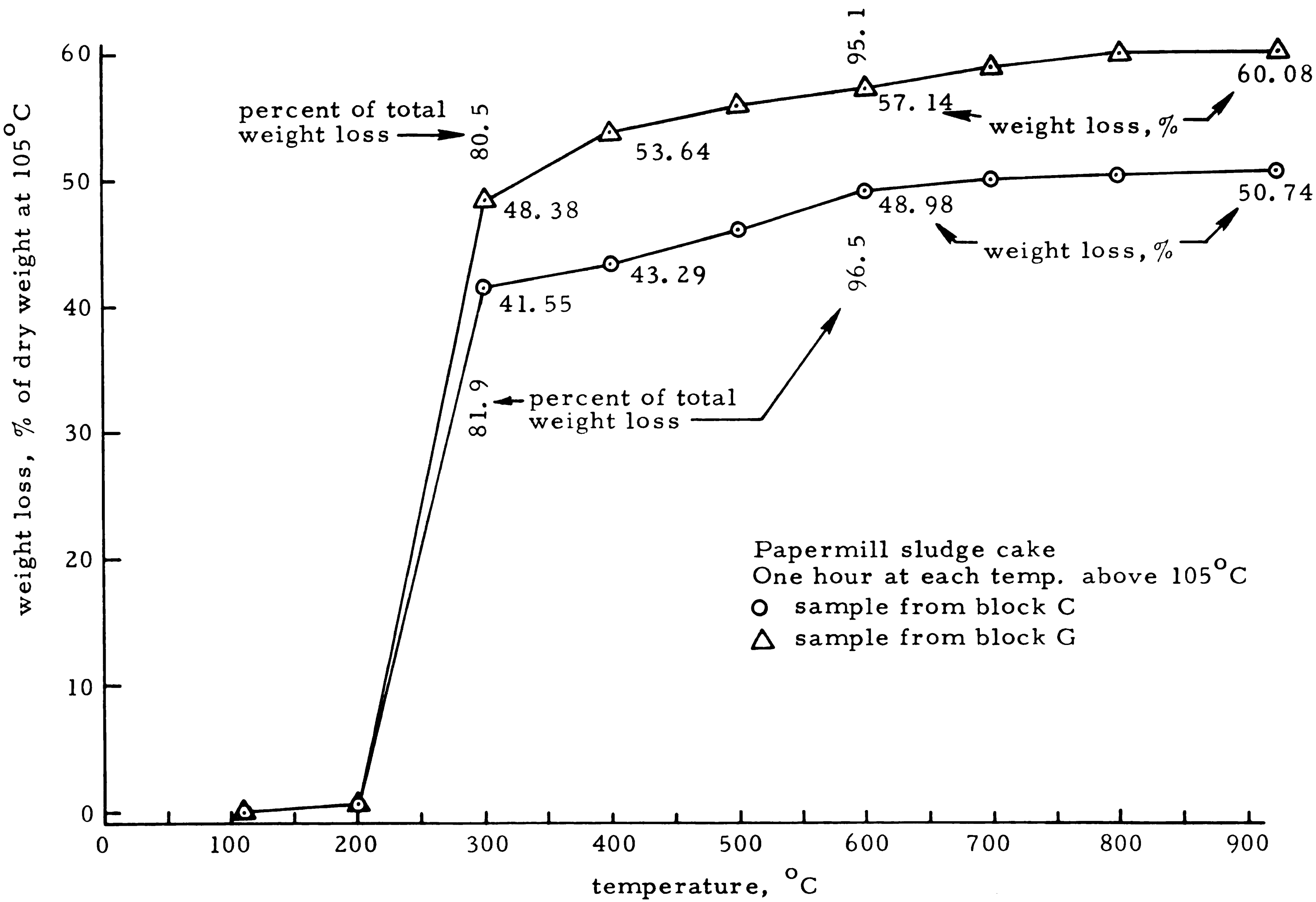

Figure 6.1.--Weight loss versus temperature for papermill sludge samples from blocks C and G.

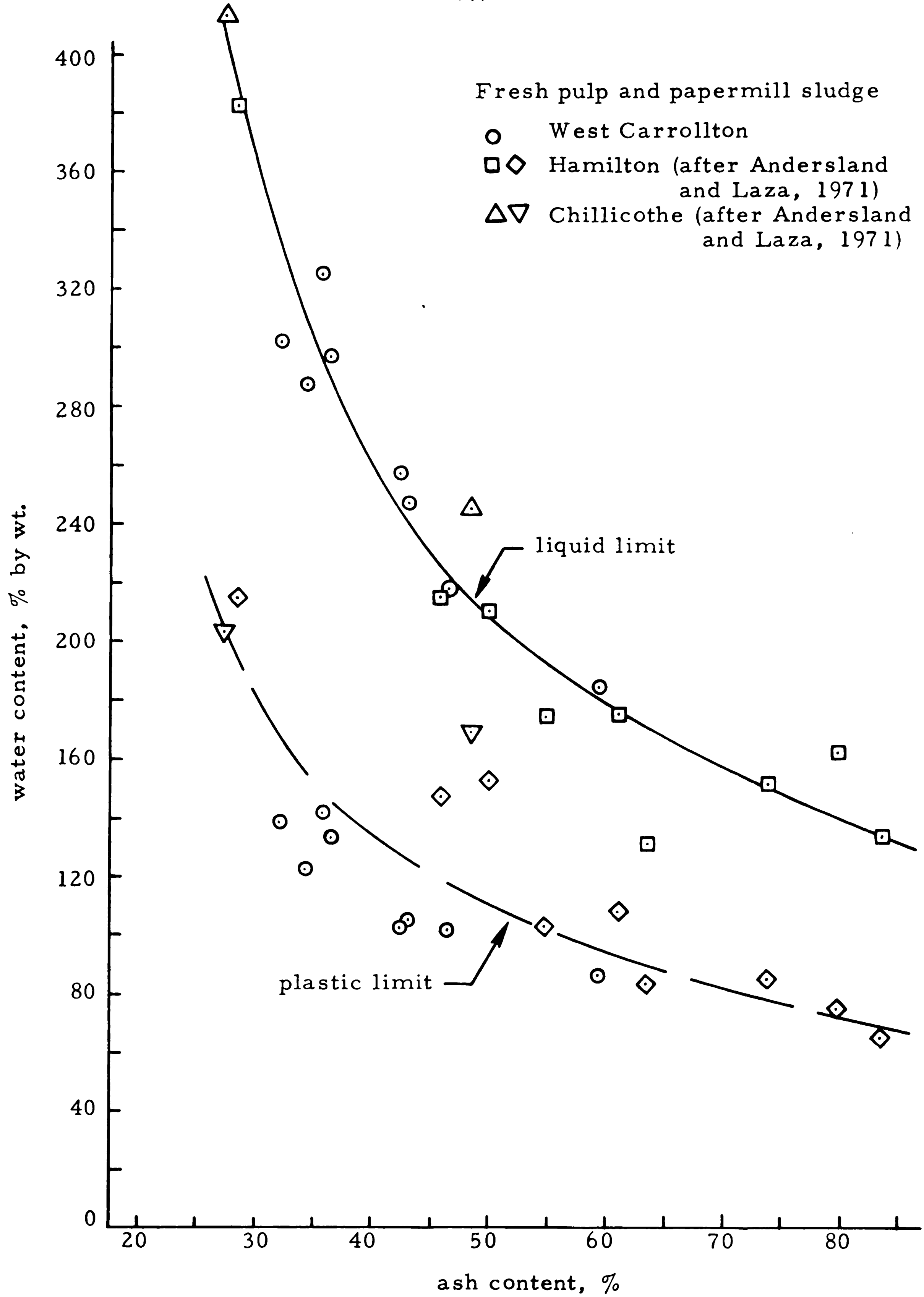

Figure 6.2.--Relationships between ash content and consistency limits.

limits decreased. The greater water retention of the organic material appears to be responsible for the higher liquid and plastic limits at high organic contents (low ash content). The liquid limit data for the three sludges appear to give a consistent relationship with a continuous curve. Plastic limits are more difficult to measure at high organic contents since fibers interfere with crumbling of the thread at the appropriate water contents. It appears that the dashed curve shown in Figure 6.2 approximates the plastic limit data. The liquid limit and plasticity index have been plotted on the plasticity chart in Figure 6.3. All data points fall in the region designated organic clay with some of the sludge perhaps more closely related to peat (Casagrande, 1948, 1966).

Water Contents

The water content of organic soils and dewatered sludges is unusually high in comparison with inorganic soils. Water contents of the sludge in the landfill after consolidation are summarized in Figure 5.1. The scatter in values appears to be related to variations in organic content of the sludge. Water retention of the sludge is greater for higher organic contents. Also, a small change in organic content will alter the dry weight because of large differences in specific gravity of the ash (clay) as compared to the organic material. Hence, two samples with the same volume of water may show significant differences in percent water content on an oven dry weight basis. Despite the scatter in observed water contents the value for the upper sludge layer dropped from an average of 257 percent for the fresh sludge to a value close to 186 percent for the consolidated sludge. For the lower

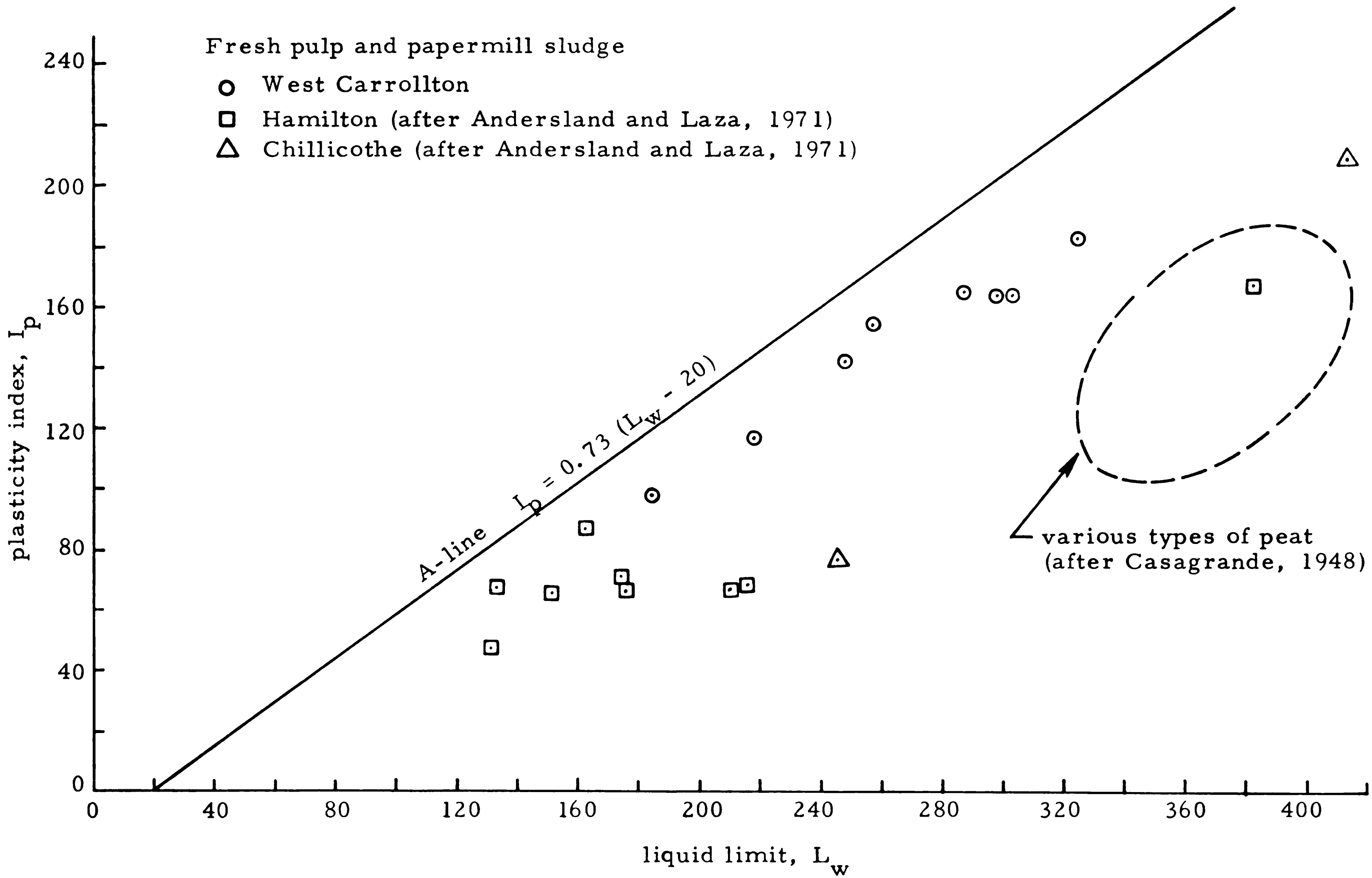

Figure 6.3.--Plasticity chart (Unified Soil Classification System) with data points for several fresh pulp and papermill sludges.

sludge layer the average water content dropped from an average of 265 percent for the fresh sludge to a value close to 167 percent. These overall changes in water contents agree with settlements reported by Vallee and Andersland (1974).

As shown in Figure 6.4, the undrained shear strength increases as the water content is decreased. This relationship is similar to that for inorganic soils (Lambe and Whitman, 1969) where failure water content varies linearly with the logarithm of undrained shear strength. Vertical displacement of the straight lines in Figure 6.4 is dependent on organic content as it relates to equilibrium water contents.

Unit Weights

During consolidation, the sludge unit weights increased as water drained from the material. Compared to the initial fresh sludge unit weight of 69.7 lb/cu ft. (1116 kg/cu m), the unit weight at elevation 88.8 ft. (27.07 m) increased to 72.6 lb/cu ft. (1162 kg/cu m) for Block B and at elevation 80.9 ft. (24.66 m) increased to 76.5 lb/cu ft. (1225 kg/cu m) for Block F. Block C, taken only 1.3 ft. (0.40m) below Block B, shows a higher unit weight of 74.6 lb/cu ft (1195 kg/cu m) partly because of its greater depth and partly because of more clay (higher ash content) which has a higher specific gravity. For the West Carrollton sludge, the specific gravity can be approximated with a straight line as shown in Figure 6.5. Assuming that the ash is composed of clay minerals having a specific gravity of 2.7 and that the organic material has a specific gravity of 1.54, the average specific gravity of the sludge solids (G) is approximated by the equation

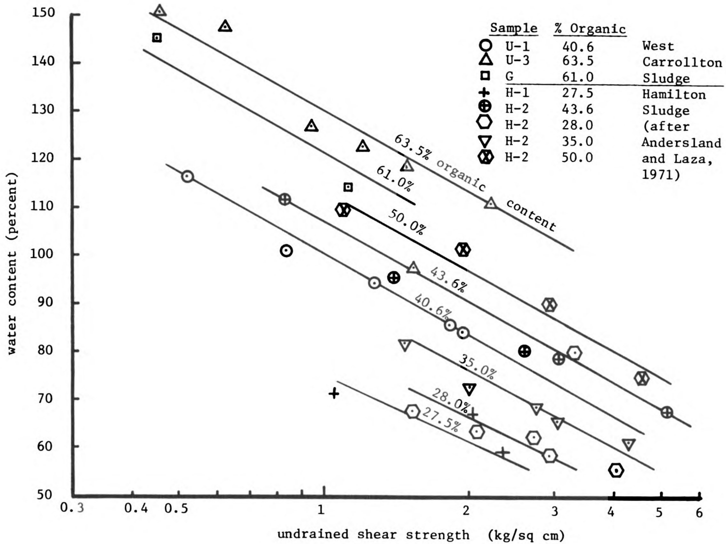

Figure 6.4.--Relationships between water content and undrained shear strength.

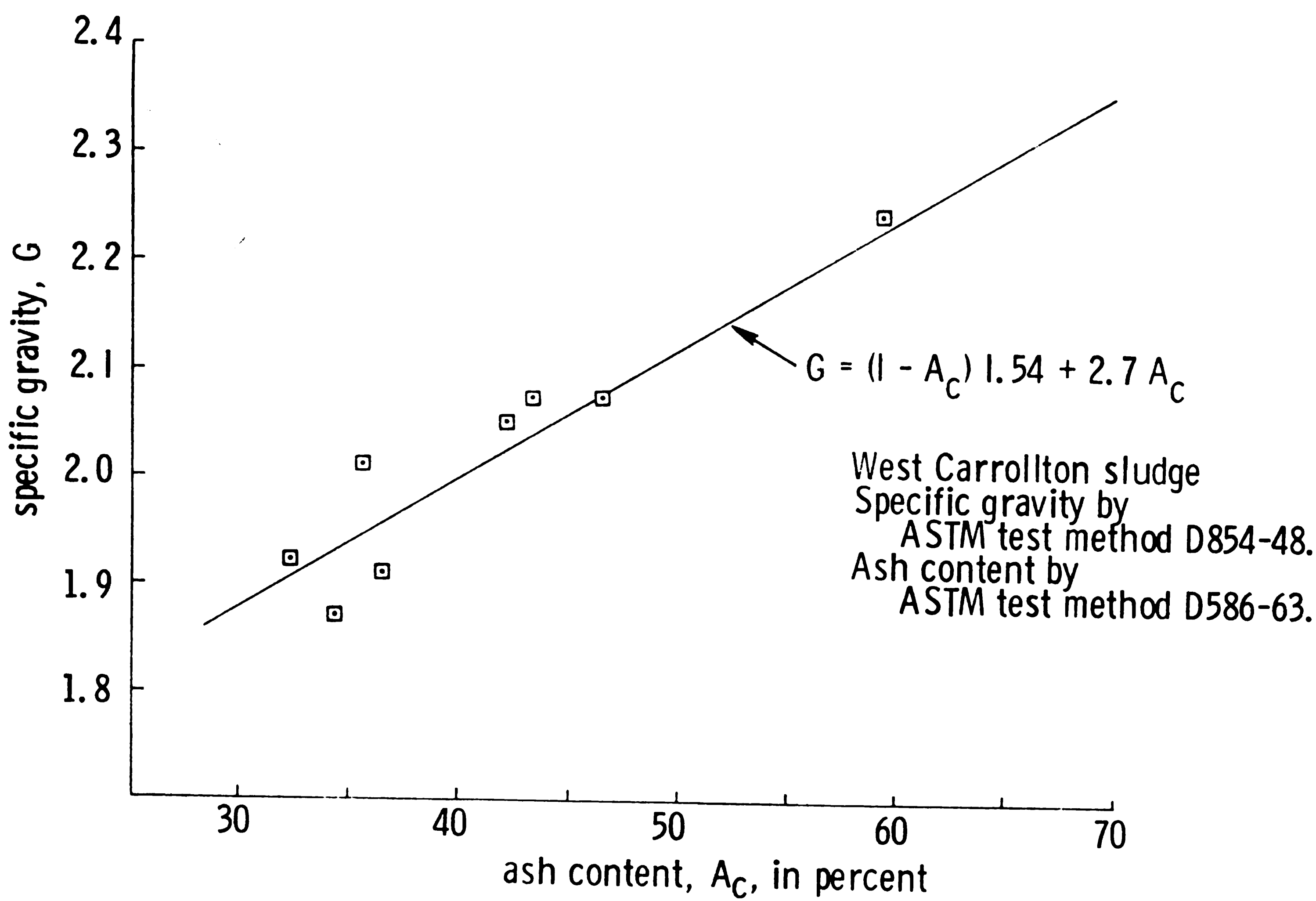

Figure 6.5.--Specific gravity - ash content relationship for the West Carrollton sludge.

$$G = (1 - A_c)\ 1.54 + 2.7(A_c) \qquad (6.1)$$

in which A_c is the ash content and $(1 - A_c)$ is the organic content.

B. Strength Characteristics of the Fibrous Organic Soil

Strength characteristics of the papermill sludge are discussed under two headings: stress-strain behavior, and strength parameters. Only normally consolidated sludges are considered under strength characteristics.

Stress-Strain Behavior

Typical triaxial stress-strain curves for fresh sludge with isotropic consolidation and axial stress increasing to failure show a relatively rapid increase in stress at low strains followed by a slower increase for larger strains (Figure 5.2). Usually no peak strength value was reached for axial strains up to 20 percent. Pore water pressures at failure tend to approach the confining pressure.

Typical triaxial stress-strain curves for axial stress increasing to failure and anisotropic consolidation (K_o equal to 0.3, sample G-5) also show a relatively rapid increase in stress at low strains followed by a slower increase at high strains. In this case the peak strength was reached at approximately 18 percent strain. For other samples with anisotropic consolidation, peak strength was not observed for strains up to 20 percent strain for some tests and for others peak strength was observed between 16 and 20 percent strain.

Plane-strain shear tests on undisturbed samples generally provide stress-strain characteristics which more accurately model the two dimensional field situation for the experimental cut slopes.

Tests were conducted on samples from Block E to investigate the possible differences between plane strain and triaxial test results. The samples were subjected to anisotropic consolidation (K_0 = 0.333) and failed by increasing the axial stress. Data summarized in Table 5.5 and plotted in Figure 5.10 for field sample E-5 show that the sludge was stiffer when failed in plane strain as compared to the triaxial test. However, the results from the more standard and easier run triaxial test's stress-strain results can be used as a first approximation to plane strain behavior.

The stress change, prior to failure of the experimental slope, involved primarily a decrease in lateral pressure as sludge material was excavated. To reproduce this field stress condition in the laboratory a series of tests were run in which the axial stress was held constant and deformation was brought about by reducing cell pressure. The sludge response to this loading, illustrated in Figure 5.9 for sample C-11, shows little sample deformation (less than 5%) until the decrease in pore pressure was permitted to dissipate. Since the minor principal effective stress approached zero in tests C-10, C-11, and C-14, one obtains an angle of internal friction equal to 90 degrees. Tensile stresses carried with fibers appear to be responsible for this unusual material behavior. With c_u equal to $[1/2(\sigma_1 - \sigma_3)]_{\varepsilon=5\%}$, the ratio of c_u/p has increased to greater than 3 in contrast to values less than one for the other tests. Different levels of anisotropic consolidation, representing different elevations in the sludge landfill, give the stress-strain curves shown in Figure 6.6. The data show an increase in modulus for higher consolidation pressures (greater depth).

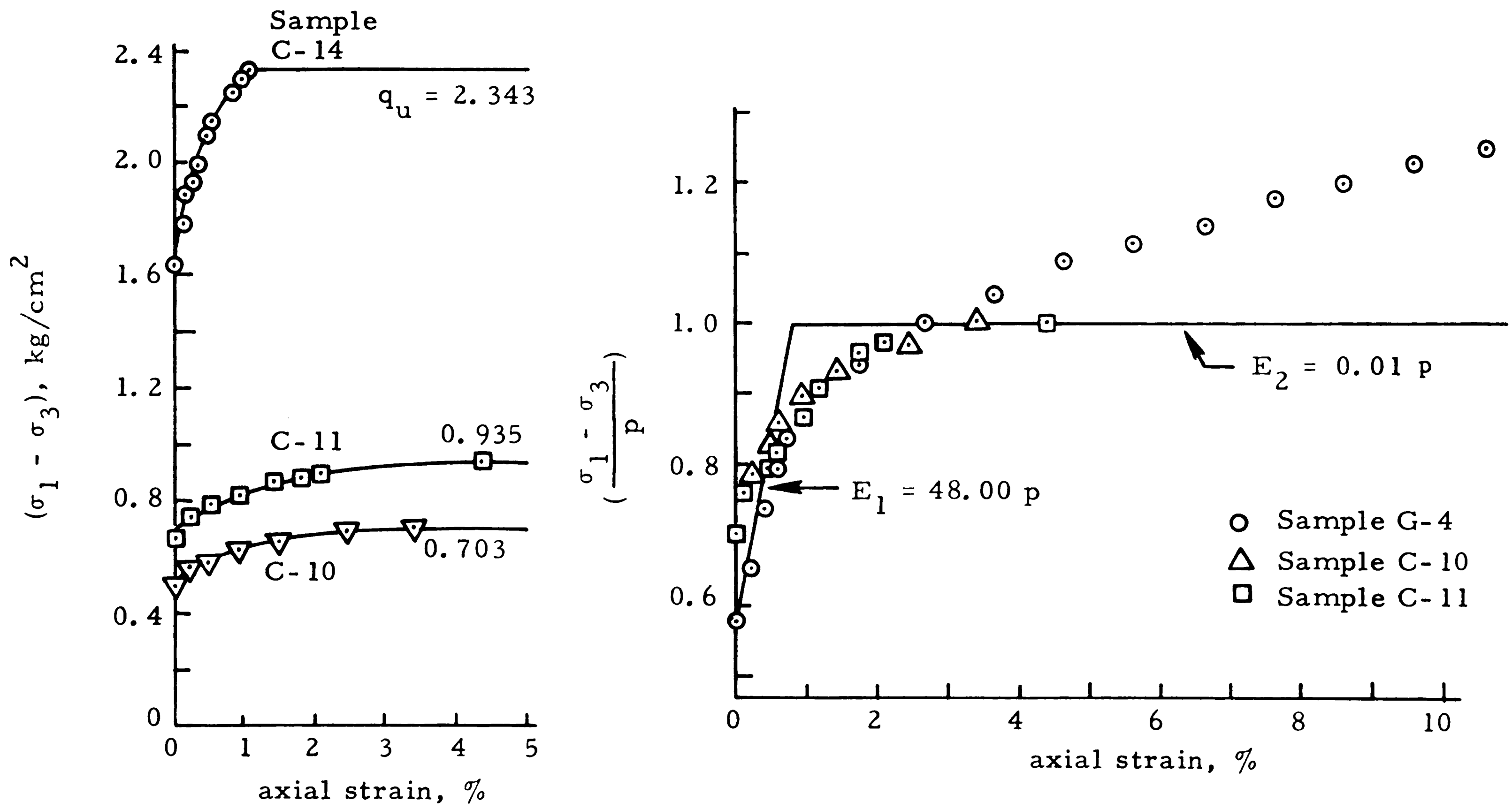

Figure 6.6.--Undrained stress-strain behavior of normally consolidated papermill sludge; samples C-10, 11, and 14, failure with σ_3 decreasing; sample G-4, failure with σ_1 increasing.

For the two levels of consolidation pressure which are representative of the upper sludge layer (samples C-10 and C-11) normalization gives essentially one curve. Here the ordinate is the stress difference, $(\sigma_1 - \sigma_3)$, divided by the consolidation pressure, p. For comparison, data from sample G-4 has been included to show the different behavior for failure with σ_1 increasing. The nonlinear behavior shown for samples C-10 and C-11 has been approximated with a bilinear relationship with elastic modulus values of 48.00p and 0.01p. Elastic modulus values take on the same units as the consolidation pressure p.

Strength Parameters

Shear strength parameters are discussed on both the total and effective stress basis.

Total Stress Basis.--For saturated samples the diameter of the failure stress circle for a given test is the same whether it is plotted in terms of total or effective stresses. This leads to a useful concept, called the $\bar{\phi} = 0$ condition, which is valid for conditions associated with complete lack of drainage (Terzaghi and Peck, 1968). This condition was approximated in the sludge landfill immediately after excavation since the low permeability of the sludge retarded drainage; as a consequence the decrease in pore pressures due to unloading required several days to dissipate. Samples C-10, 11, and 14 in Figure 6.8 and C-11 in Figure 5.9 showed little deformation until the negative pore pressure change was permitted to dissipate.

The undrained shear strength may be evaluated on the basis of triaxial tests (effective or total stress basis), unconfined compression tests, and vane shear tests. The results of triaxial tests on isotropically consolidated fresh sludge samples U-3 and U-1, in terms of total stresses, are expressed as the value of undrained strength c_u plotted against consolidation pressure p in Figures 5.3c and 5.4c. For the normally consolidated samples the ratio c_u/p appears to be constant, its value dependent to some extent on the sludge organic content. The results of triaxial tests on anisotropically consolidated (K_o = 0.3) undisturbed sludge samples G and E, in terms of total stresses, are expressed as the value of undrained strength c_u plotted against consolidation pressure p in Figures 5.6c and 5.11c. For the same vertical consolidation pressure, larger undrained strengths were obtained for the anisotropically consolidated sludge in comparison to samples consolidated with isotropic consolidation. The ratio c_u/p has increased over the values obtained for the fresh sludge with isotropic consolidation. These differences appear to be related to structural anisotropy of the sludge.

Unconfined compression tests on undisturbed samples generally provide shear strengths for use in the total stress analysis for slope stability and provide information on the anisotropy of the consolidated sludge. Data summarized in Table 5.4 and plotted in Figure 5.12 show that the sludge was significantly weaker when failed in the horizontal direction as compared to the vertical. The natural alignment of fibers in the horizontal direction form a plane of weakness which may be the reason for the lower strength. The two curves in Figure 5.12 can be normalized when the respective unconfined compression strengths are divided by the effective overburden pressure p_o. For example, taking the vertical unconfined compression strengths, c_u/p equals 0.49 for sample Blocks G and C. The unconfined compressive strengths are significantly lower than the undrained vane shear strengths shown by data plotted in Figure 5.13a. This lower strength is due partly to physical disturbance in sampling and sample preparation for laboratory testing. For soft clays with low to medium sensitivity Parry (1971) states that the physical disturbance and stress change are sufficient to reduce the laboratory shear strength below field values. Sensitivity of the sludge, equal to the undisturbed vane strength divided by the remolded vane strength, was very low (about 1.40) as shown by the data in Figure 5.13a. The vane shear strength to overburden pressure is reasonably constant. Some variation would be expected since ash contents, given in Table 5.2 for Blocks B, C, F, and G were not completely uniform. Blocks B and C at close to the same elevation and different ash contents contain significantly different water contents due primarily to different organic contents. The Dutch cone penetration test was less sensitive to increase in shear strength with depth than the vane shear test (Figure 5.13b).

Effective Stress Basis.--Since pore pressures were measured during triaxial and plane strain testing, the effective strength parameters can be determined using the Mohr-Coulomb failure theory. The maximum stress circles will be tangent to the rupture line defined by Coulomb's equation (Equation 2.7).

Consider first the triaxial test results on fresh sludge samples U-1, U-2, and &-3, summarized in Table 5.4. These samples were consolidated with an all-around pressure and failed by increasing the deviator stress for conditions of no drainage. The data plotted in Figures 5.3a and 5.4a give the K_f lines from which the angle of internal friction and the cohesion were obtained on an effective stress basis. These $\bar{\phi}$ values along with sample organic contents are summarized in Table 5.3. Additional data from Andersland and Laza (1971) for fresh sludge sample H-2 has been included. A plot of $\bar{\phi}$ versus organic content, Figure 6.7, suggests a linear relationship when comparisons are made using data obtained by a given test procedure. This agreement is quite good considering the accuracy of the organic content determinations. At lower organic contents the angle of internal friction appears to approach a value representative of the non-organic constuents in the papermill sludge. Extrapolation to zero organic content for the Hamilton sludge gives an angle of internal friction equal to about 24 degrees, close to a value of 25 degrees reported for kaolin clay by Gibbs, et al. (1960) and Olson (1974). Differences in fiber size and fiber orientation between the two sludges, represented in Figure 6.7, appear to be responsible for the different slopes and intercepts. If sludge decomposition is represented by a decrease in organic content, then for the same effective normal stress there will be a reduction in shear strength in a sludge landfill.

Water content has been plotted against all-around consolidation pressure in Figures 5.3b and 5.4b. With the higher organic content, sample U-3, a greater reduction in water content is observed for the same consolidation pressure. At the same time the higher organic

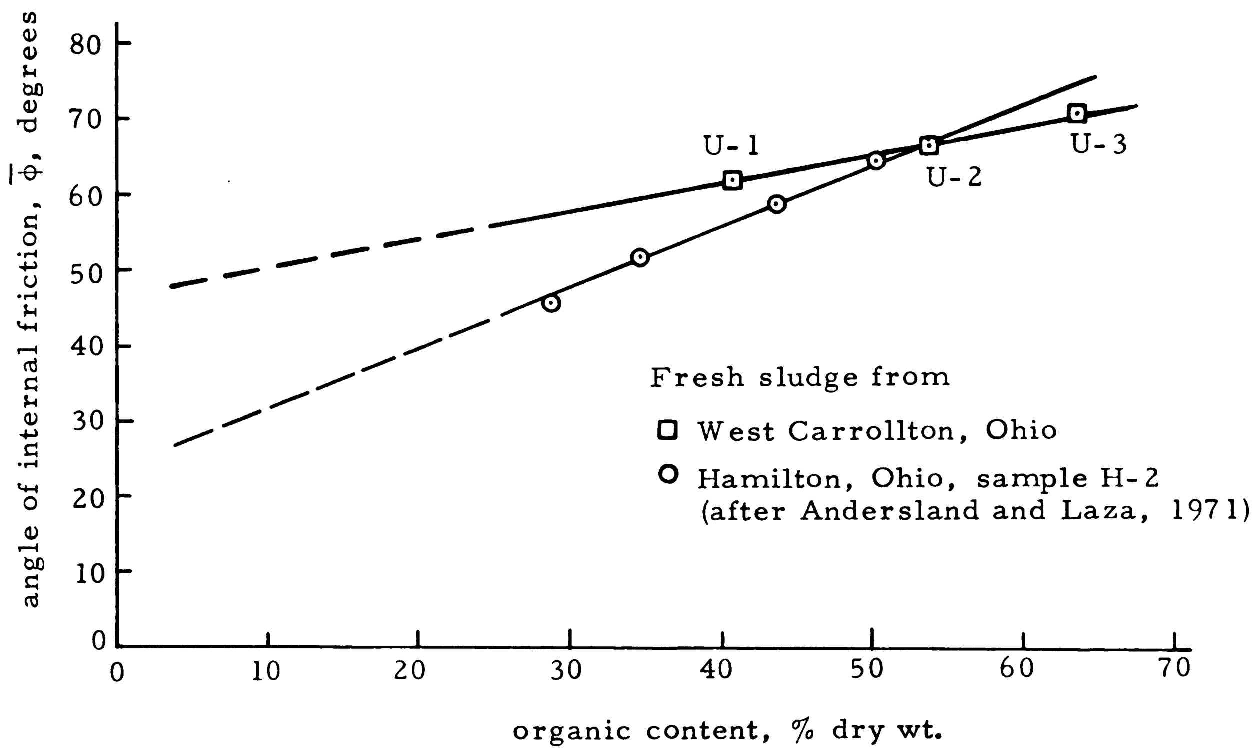

Figure 6.7.--Influence of organic content on the angle of internal friction, effective stress basis.

content is responsible for a greater water retention at a given consolidation pressure.

For the undisturbed sludge samples, anisotropic consolidation was used to approximate the field stress condition of no lateral yield. Data from the total pressure cells, buried in the landfill (Figure 5.21), gave a ratio of horizontal to vertical effective stress ($\bar{\sigma}_h/\bar{\sigma}_v = K_o$) close to 0.3. Consolidation under this stress ratio followed by increasing the deviator stress to failure gave the data summarized in Figure 5.8. For the same organic content, an apparent increase in the angle of internal friction is noted for the anisotropically consolidated sludge. A reduced angle of internal friction (Figure 5.8) was obtained when the sample axis was changed to the horizontal. These differences appear to be related to structural anisotropy of the sludge. A form of structural anisotropy tends to develop in sludge when fibers align themselves at right angles to the direction of the major principal stress during field consolidation.

To more closely approximate the field strain condition during excavation, anisotropically consolidated plane strain shear tests were also run on the undisturbed sludge samples. Triaxial results are correlated with plane-strain results for Block E in Table 5.5 and in Figure 5.11. The angle of internal friction, $\bar{\phi}$, was found to be 74.9 degrees for both types of tests on Block E. However, the plane strain tests indicated undrained strengths approximately 25 percent greater than those shown by triaxial tests consolidated under similar conditions.

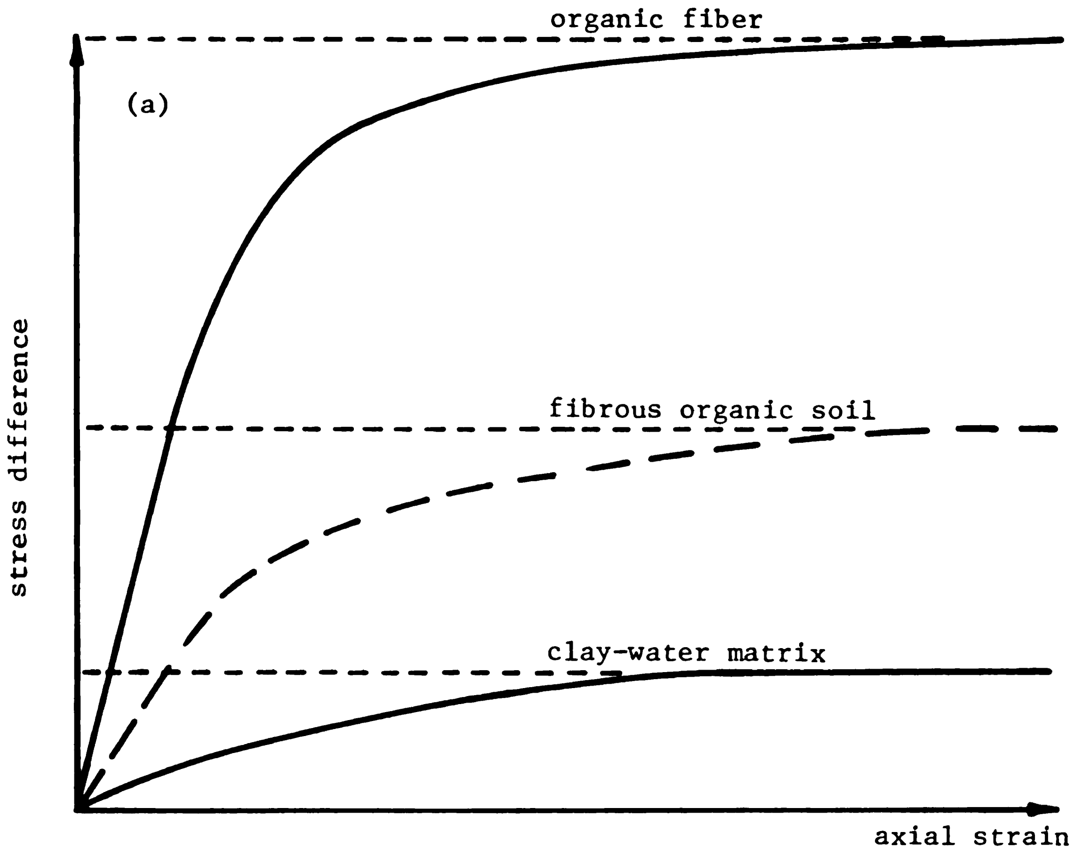

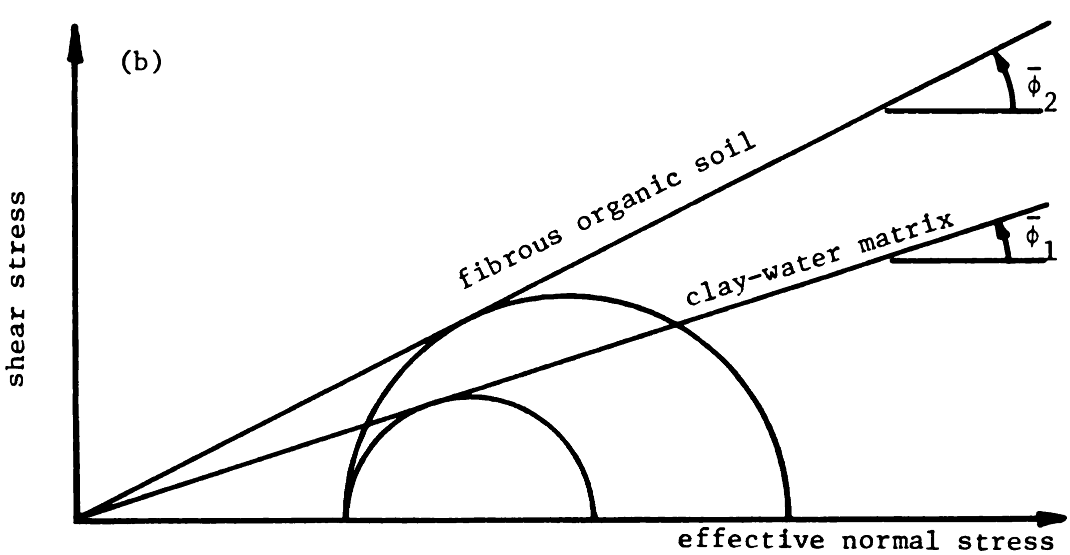

Figure 6.8.--Composite action of a clay-water matrix with organic fibers. (a) stress-strain curves. (b) failure envelope.

Figure 6.8 shows the concept behind a fiber reinforced material composed of a clay-water matrix interwoven with organic fibers. Figure 6.8a shows the probable stress strain behavior of the clay-water matrix, the organic fiber, and the composite action of the clay-water matrix reinforced with organic fibers. The higher modulus of elasticity of the fibers provides the primary stiffening action to the matrix as the composite deforms. Figure 6.8a also shows the effect on the failure envelope (or strength) by adding organic fibers to the clay-water matrix and Figure 6.8b helps explain the large $\bar{\phi}$ values of the papermill sludge. More research is needed to define the influence of fiber size and fiber orientation on the shear strength parameters and whether these parameters (effective stress basis) correctly model field shear strengths of a fibrous organic soil (sludge).

C. Movement and Stability of the Experimental Cut Slopes

Movement and stability of the experimental cut slopes in the papermill sludge are discussed under four headings: slope movements, development of failure zones, slope failure, and stability analysis for the failure surface.

Slope Movements

Field monitoring provided data on both lateral and vertical movements at a number of locations adjacent to the excavated slope. The lateral movements were measured by using surface stakes (Table A-1) and slope indicator casings (Figure 5.17). The surface measurements provided data which were in agreement with the upper level of the slope indicator casings. In addition to movement towards the slope all casings showed some movement away from the east or west dikes (Figure 5.17e). The resultant movements close to the landfill surface (elevation 94.6 ft. = 28.83m) for casings A through D are shown in Figure 6.9. The rate of movement was very much dependent on the stress release or excavation for the slope. The rate of movement for each casing is shown in Figure 6.10 by plotting lateral movement versus time. The low movement rate after completion of the 3:4 slope suggests that the sludge was relatively stable for this slope configuration. The highest movement rate occurred immediately after excavating the 1:8 slope. Rates decreased when partial slope failures occurred and reversed direction when fresh sludge was placed adjacent to the slope at the end of the field portion of the study.

Vertical movement (Figure 5.18) monitored by settlement plates was largest in the upper sludge layer adjacent to the excavated slope. A large part of this settlement appears to have been caused by consolidation related to complete drainage of the middle sand blanket when the slope was excavated on September 29, 1972. Increased settlement rates are observed for the top sludge layer at all instrument groups after this date.

Development of Failure Zones

Sludge movement occurred as the excavation progressed and as stresses were reduced to zero on this slope. Stress conditions within the slope change during excavation. Failure zones develop in those

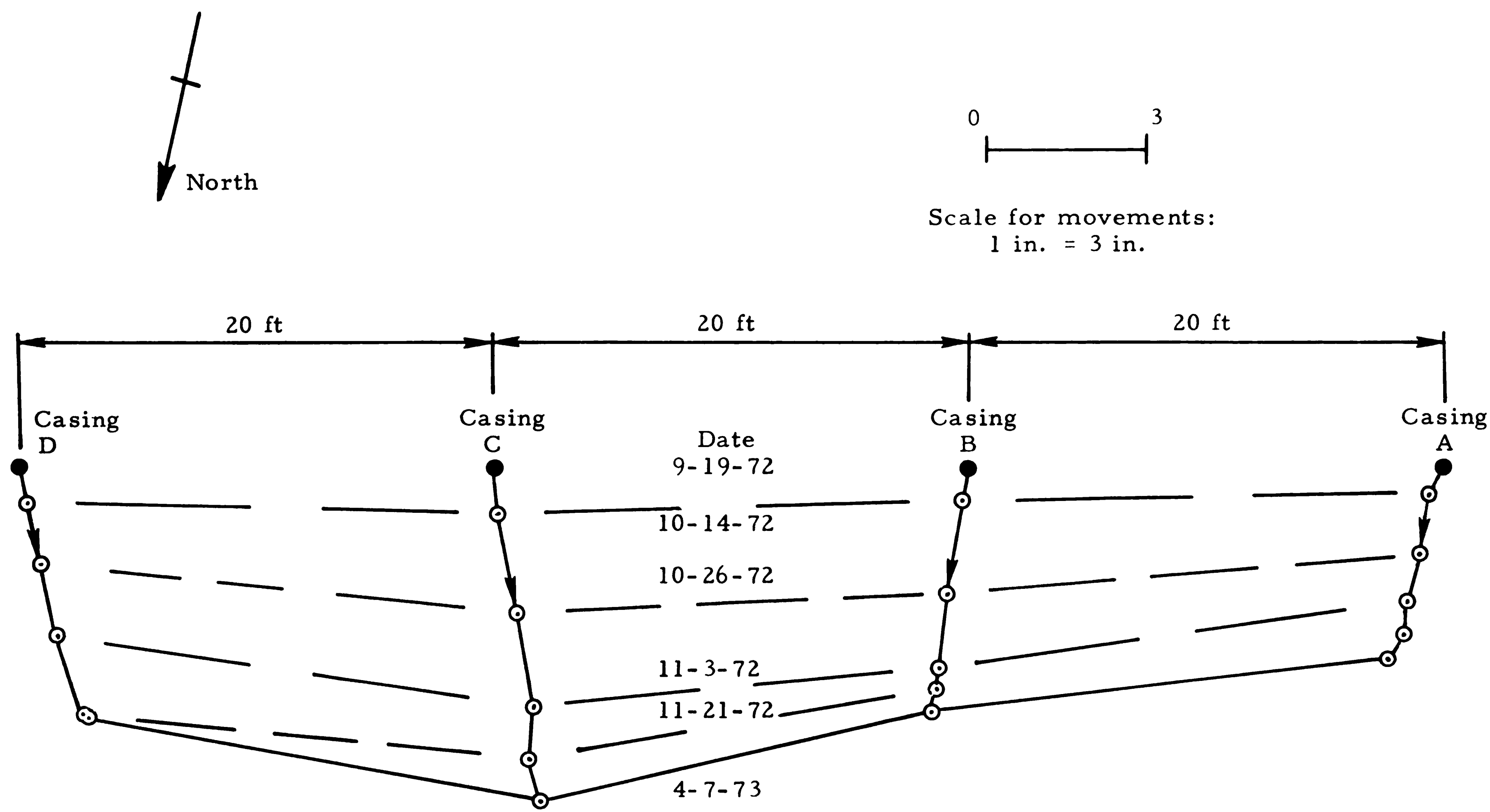

Figure 6.9.--Casing movements at elevation 94.6 ft. during and after excavation for the experimental slope.

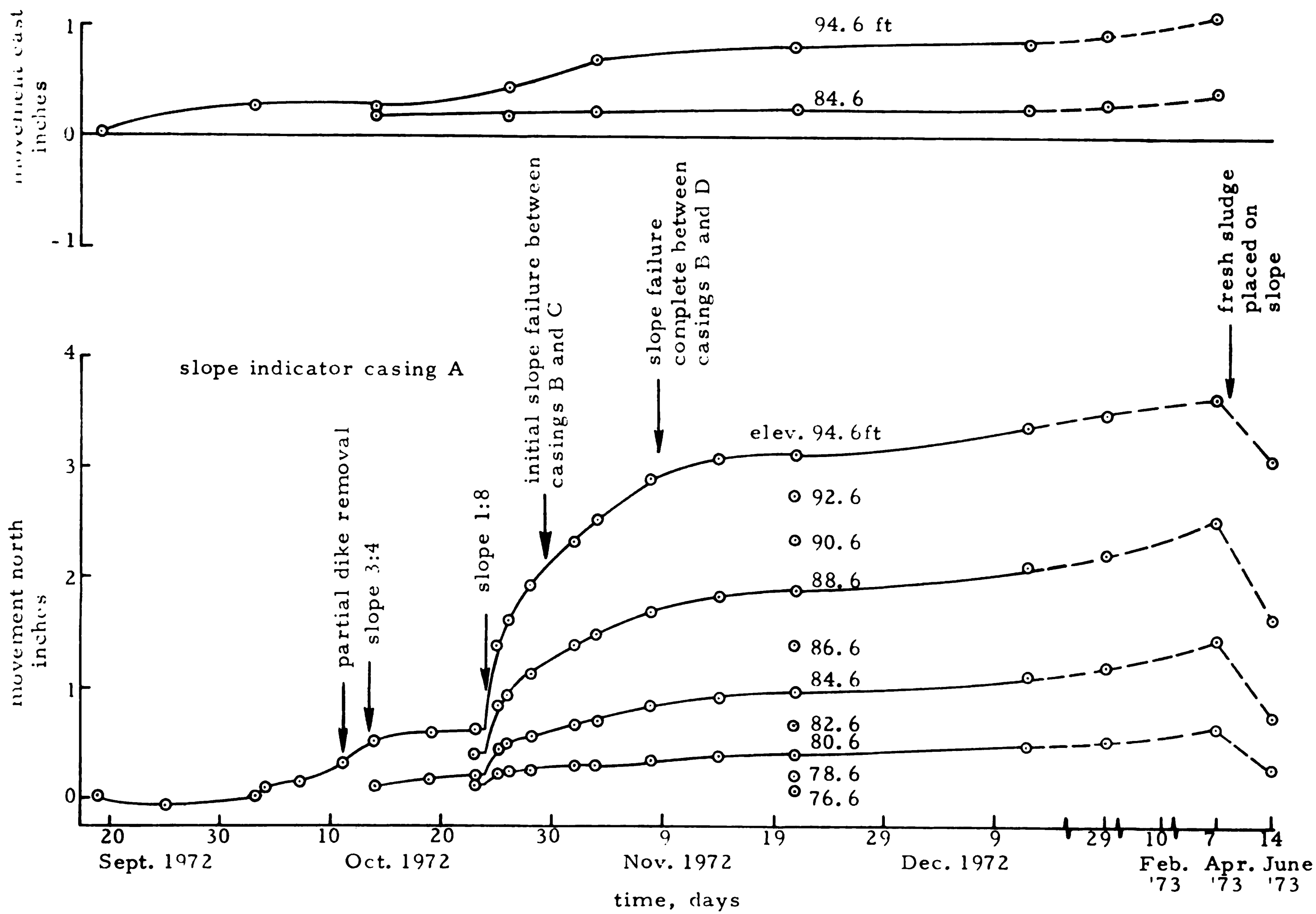

Figure 6.10.--Time-rate of lateral movement. (a) Slope indicator A.

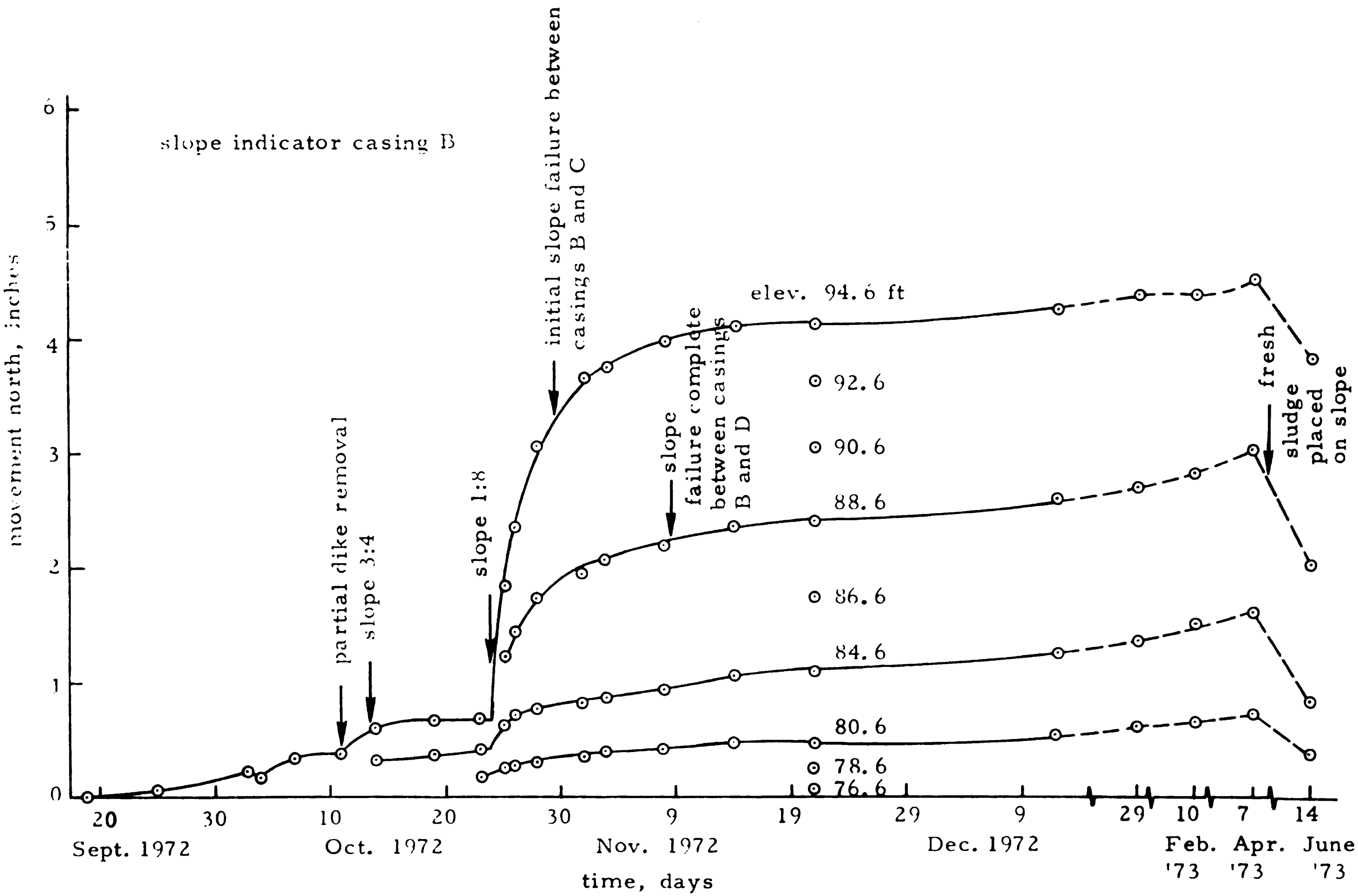

Figure 6.10.--Time-rate of lateral movement. (b) Slope indicator B.

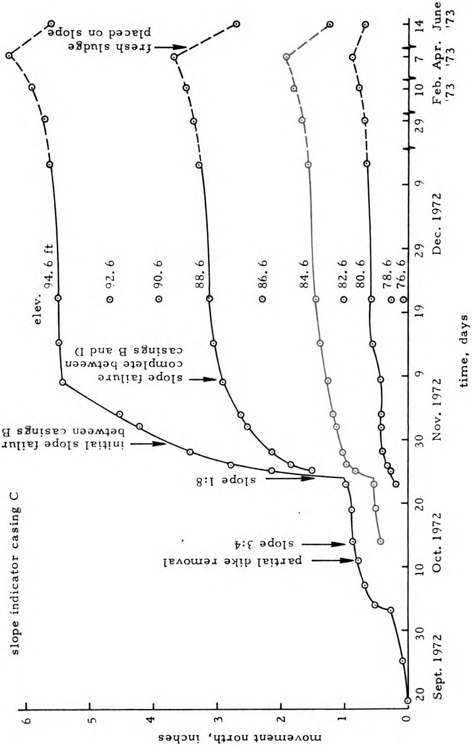

Figure 6.10.--Time-rate of lateral movement. (c) Slope indicator C.

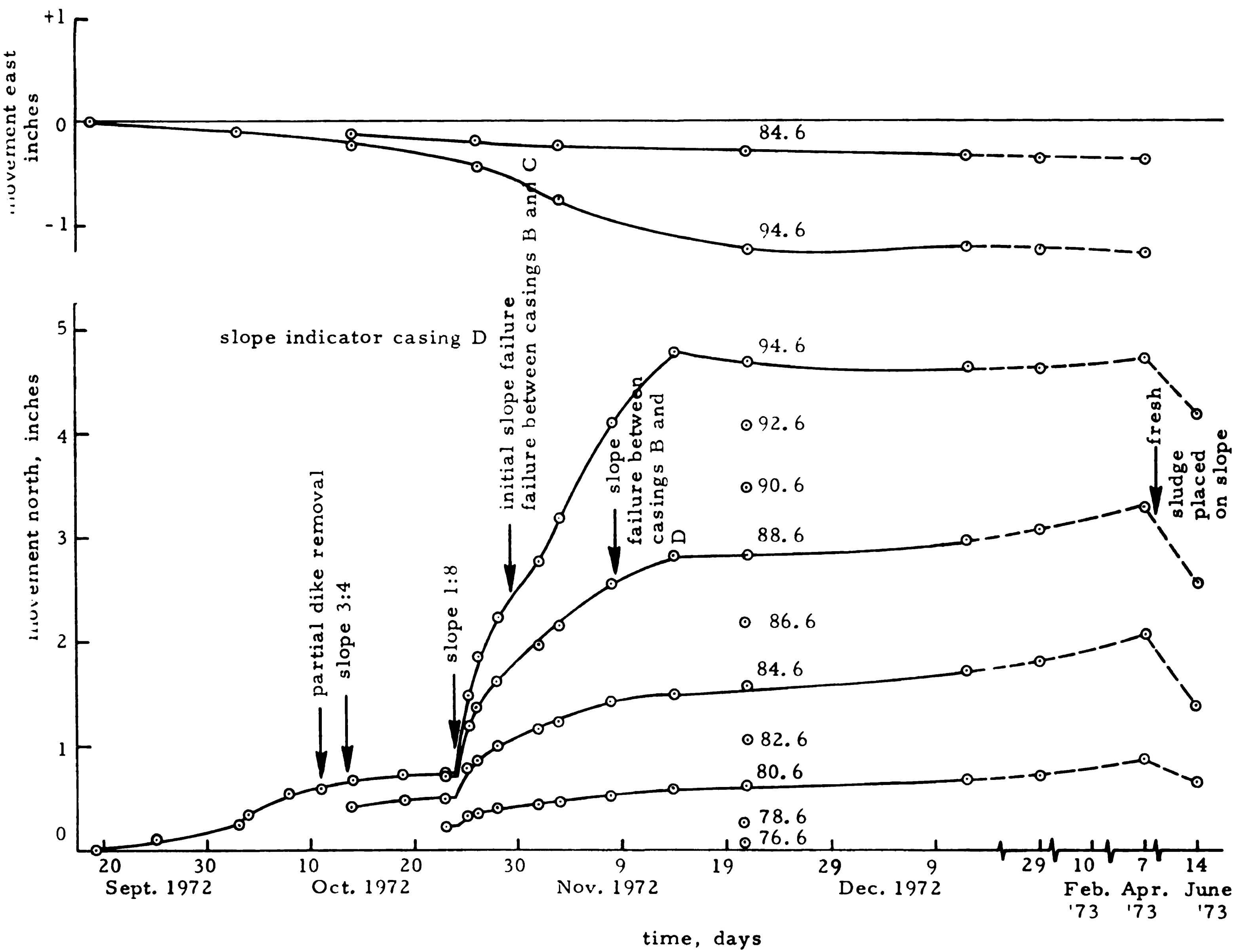

Figure 6.10.--Time-rate of lateral movement. (d) Slope indicator D.

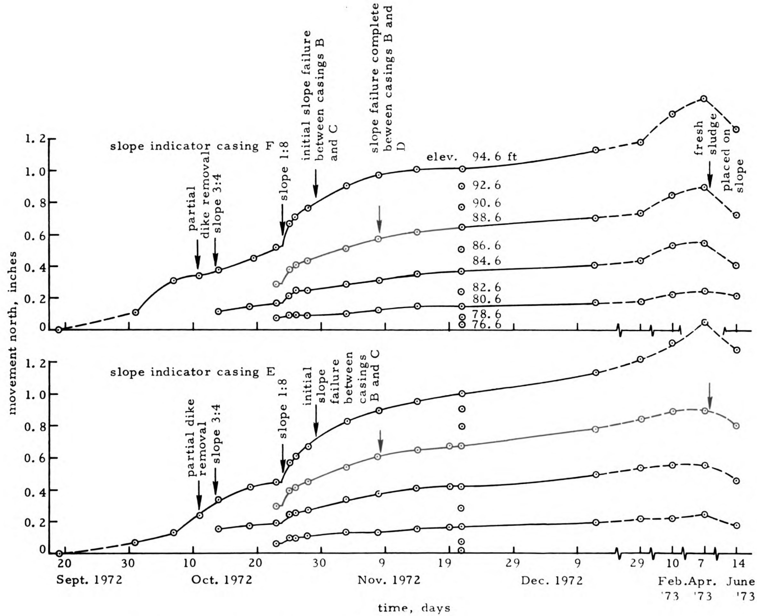

Figure 6.10.--Time rate of lateral movement. (e) Slope indicator casings E and F.

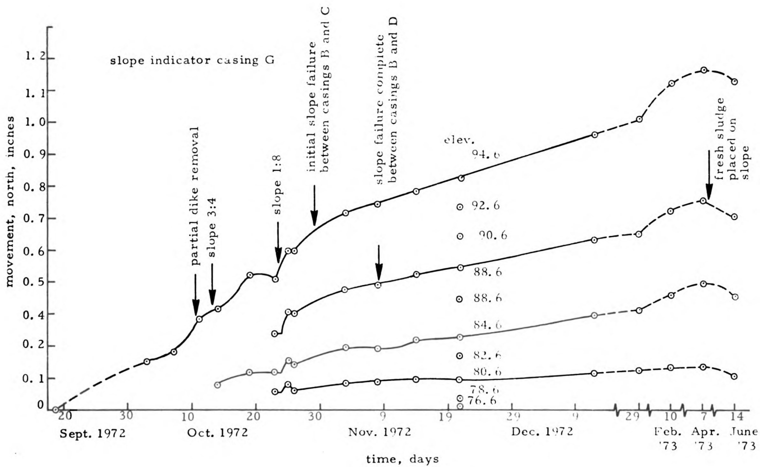

Figure 6.10.--Time-rate of lateral movement. (f) Slope indicator G.

regions where the maximum shear stress values exceed the undrained shear strength of the sludge. It is helpful to show these zones in a graphic manner. These zones can be determined by use of the finite element method of analysis (Dunlop, Duncan, and Seed, 1968).

For a slope excavated in the dry, both the earth and water pressures would be reduced to zero on the excavated slope. For analysis of these slopes, it was necessary to consider both the changes in earth and water pressures during excavation. This may be done by working with total stresses. At a depth y below the surface of a horizontal deposit with unit weight γ, the initial total stresses may be expressed as

$$\sigma_y = \gamma \cdot y \tag{6.2}$$

$$\sigma_x = K \cdot \sigma_y \tag{6.3}$$

where σ_y and σ_x are the total vertical and horizontal stresses and K is a total stress earth pressure coefficient. Field data (Figure 5.18) has shown that K was close to 0.4 just prior to excavation. It was convenient to consider the initial strains and displacements, before excavation, as being zero but with non-zero stresses. The stress-strain relationships for the sludge (Figures 5.9 and 6.6) were obtained from consolidated-undrained triaxial tests using test procedures which simulated field stress conditions existing before and during excavation of the slope.

Plane strain deformation has been assumed for the excavated slope since the distance normal to the section analyzed (Figure 6.11a)

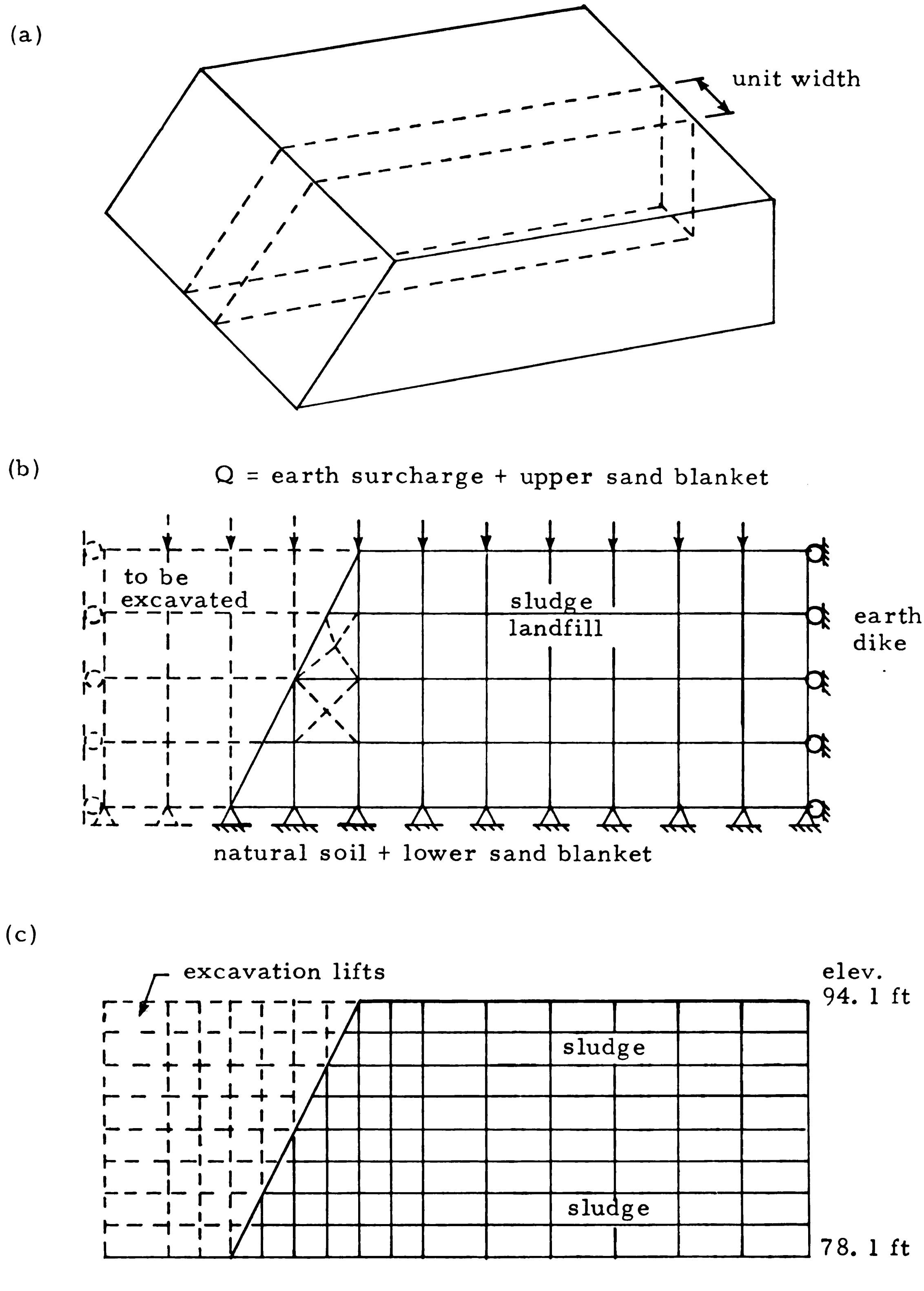

Figure 6.11.--(a) Excavated slope showing the section to be analyzed.
(b) Finite element idealization of slope cross-section.
(c) Typical finite element configuration of the slope showing the excavation sequence.

was about five times the thickness of the sludge plus sand blankets (Dunlop, et al., 1968). Field measurements of slope movement, given in Appendix B and summarized in Figure 6.9 for elevation 94.6 ft. (28.83m), close to the excavation indicated that the assumption of plane strain deformation was reasonable near the center line of the slope. Along this line the movements were perpendicular to the slope. A finite element idealization of the slope cross-section in Figure 6.11b includes boundaries representative of field conditions. The top and slope surfaces are free surfaces. Loads applied to the top surface nodes simulate the earth surcharge. Points along these boundaries are free to move in the vertical and horizontal directions. Since the sludge was very soft in comparison with the dike material and the natural soil below the landfill, it was assumed that these boundaries were fixed as shown in Figure 6.11b. The dike was far enough from the slope so that shear stresses could be assumed equal to zero. Field data showed that there was no vertical movement of the bottom surface and that there was no reason to suspect any horizontal movement of the firm base of the landfill.

The finite element configuration of the slope with simulation of the excavation by removal of elements has been illustrated in Figure 6.11c. The slope cross-section was represented by 252 rectangular elements with a total of 279 nodes. The basic element used was a quadrilateral composed of four constant strain triangles. Rectangles were used throughout with the exception of the region immediately adjacent to the sloping face, where triangles and trapezoids (Figure 6.11b) were employed alternately. This scheme of elements was well-suited to simulation of slope excavation by the removal of elements outside the slope and it was convenient for automatic mesh generation within the computer. The analyses were conducted in a series of steps. Eight steps were used to represent slope excavation. The stress-strain curve for any particular element was approximated by a bilinear curve (Figure 6.6), consisting of two straight line portions corresponding to the two values of modulus. Material numbers and properties for each row of elements are given in Table 6.1. Material 9 is the number assigned to elements after failure, and material 10 is the number assigned to elements which are being or have been removed.

The computer program given by Dunlop, et al. (1968) was used to obtain the results summarized in Figure 6.12 showing the development of failure zones in the experimental slope for simulated excavation depths of 6, 10, and 14 feet. Failure has been defined by the bilinear curve in Figure 6.6, and a total horizontal strain of 10 percent. A simulated excavation depth to 6 ft., Figure 6.12, shows that a small failure zone has developed behind the slope. A small tension zone now exists behind the crest of the slope. Additional excavation to 10 ft. alters stress conditions sufficiently so that the failure zone now extends farther behind the slope and to a greater depth. The tension zone has increased in size. At this stage the overall factor of safety against slope failure would be approaching unity. Excavation to 14 ft. shows the failure zone extending to the slope surface and behind the crest. Failure along the unsupported slope could be predicted and did occur. Line A-A in Figure 6.12 shows the location

TABLE 6.1. MATERIAL NUMBERS AND PROPERTIES FOR THE FINITE ELEMENT ANALYSIS

Material	Unit weight (pcf)	Elastic* modulus (psf)	Poisson's ratio	Undrained strength (psf)	Coeff. of total pressure
1	69.75	26900.	0.475	280	0.4
2	70.75	33600.	0.475	350.5	0.4
3	71.75	40500.	0.475	422	0.4
4	72.75	47500.	0.475	494.5	0.4
5	87.00	55200.	0.475	574.5	0.4
6	74.75	62900.	0.475	655.5	0.4
7	75.75	70200.	0.475	731	0.4
8	76.75	77500.	0.475	807.5	0.4
9	71.91	0.01	0.475	--	--
10	0	0.01	0.475	--	--

*Bilinear approximation to the stress-strain behavior shown in Figure 6.6.

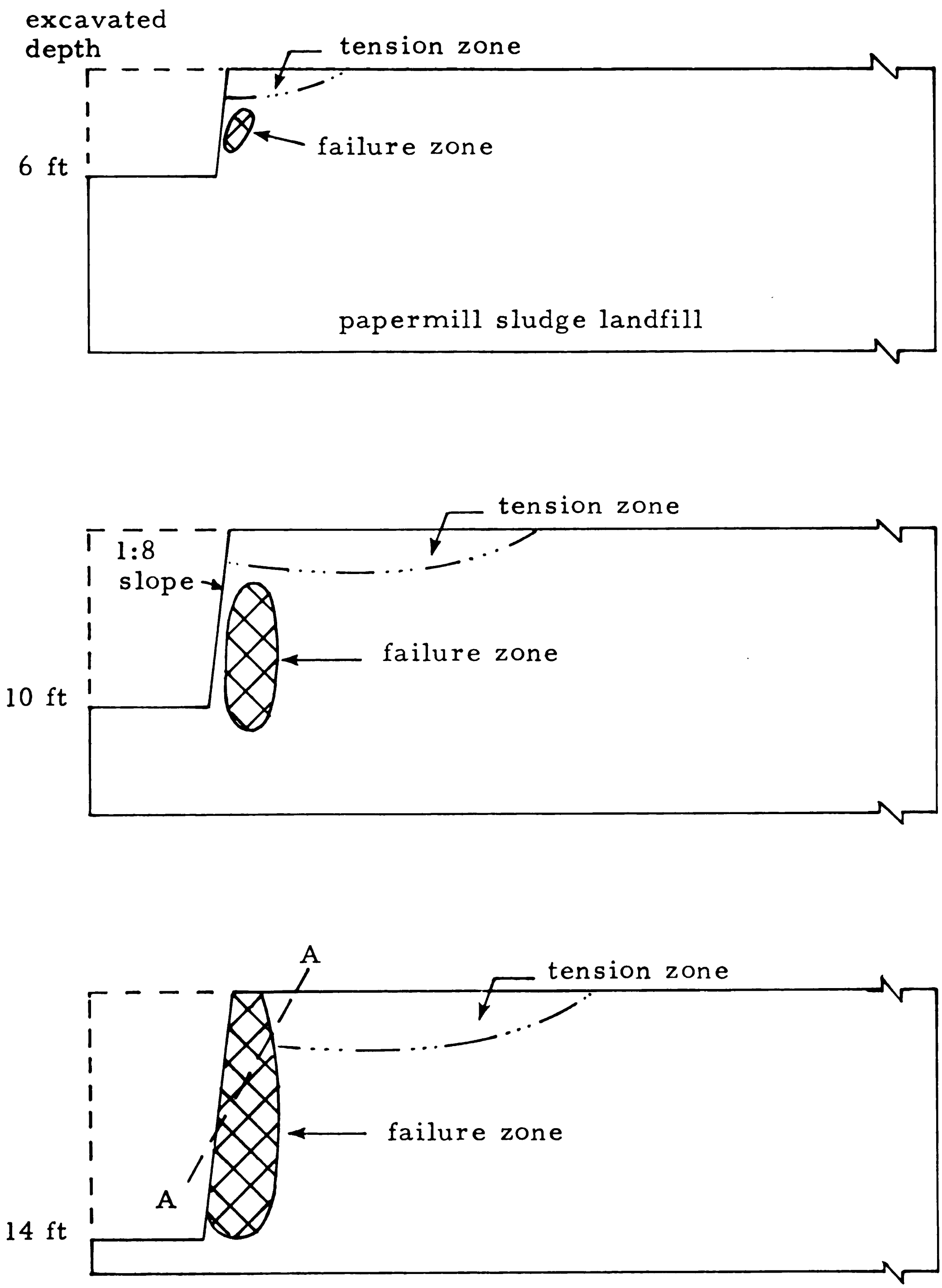

Figure 6.12.--Development of failure zones for the 1:8 slope, s_u/p = 1.00 and K = 0.4.

of the observed field failure (Figure 5.15a) which occurred four days after completing the excavation. Temporary tensile stresses, related to fibers in the sludge, may have contributed to the delay in failure. Increase in pore pressures, shown by piezometers in the upper sludge layer (Figure 5.19), would explain a lower shear strength several days after completing the excavation. Failure zones shown in Figure 6.12 may be over estimated because a bilinear stress-strain representation of the sludge was used in the finite element analyses. Dunlop, et al. (1968) have shown this to be the case for slopes in soil.

Slope Failure

The initial excavation produced a trial slope of 53.1 degrees (Figures 4.4a and 4.5) which was stable and showed less than 1 inch (2.54 cm) lateral movement at its 16 foot (4.88 m) height ten days after excavation. A second trial slope of 82.9 degrees (Figures 4.4b and 4.6) failed in the top sludge layer 4 days after excavation as shown in Figure 5.15. Tension cracks (Figure 5.14), which extended vertically down through the earth surcharge, indicated that the factor of safety with regard to slope stability was approaching unity. The rate of lateral movement shown by the slope indicator casings (Figure 6.10) was initially very high but did decrease somewhat before the initial slope failure occurred on October 29, 1972 (Figure 5.15a). Within the next three weeks additional failures occurred along the entire slope length as shown in Figure 5.15b. Surface measurements of the slope failure areas on three different dates (Figure A-1) show areal limits of failure. Based on field measurements a typical failed cross-section has been prepared in Figure 5.16. Failure in the sludge occurred on essentially a plane surface at a slope angle close to 58.6 degrees. The tension cracks appeared to extend down through the earth surcharge to the upper sand blanket. Slopes in the two sand blankets were close to those shown in Figure 5.16. Some variation to this average failed cross-section can be seen in Figure 5.15.

It is interesting to note that the angle of slope failure was very close to the failure surface observed for a number of undisturbed triaxial test specimens. Test specimen G-9, consolidated anisotropically with K_0 equal to 0.3, is shown in Figure 3.2c after failure in compression and oven drying. The critical plane in both cases rises at an angle close to 58.6 degrees from the horizontal. If the Mohr-Coulomb failure theory were applicable, the failure plane should rise at an angle of $(45 + \frac{\bar{\phi}}{2})$ degrees and $\bar{\phi}$ would equal 27.2 degrees. Olson (1974) reports that $\bar{\phi}$ for kaolinite ranges from 25 to 30 degrees. This field behavior suggests that a frictional mechanism determines the location of the failure surface. A cohesive mechanism would have required that the angle be 45 degrees.

Stability Analysis for the Failure Surface

The failure surface shown in Figure 5.16 involves a composite sliding surface which can best be analyzed using Janbu's (1954, 1957) method. At failure the factor of safety against sliding equals one. A computed factor of safety should also equal one when the method of analysis is appropriate to the field problem. Shear strengths used in the analysis must be representative of the consolidated sludge in the landfill. Difficulty in determining the actual pore pressures in the sludge at the sliding surface require that a total stress basis be used in the analysis. Piezometers in instrument group 4 were located several feet behind the failure surface. The top and middle sand blankets were fully drained so that total stresses equal effective stresses in the sand. Undisturbed vane shear strengths (Figure 5.13a) cannot be used directly in Janbu's (1954, 1957) method. Bjerrum (1972) has suggested that the discrepancy between the vane shear strength and the field shear strength can be attributed to differences in rate of loading and to the anisotropic nature of shear strength. He has recommended a correction factor μ (Figure 2.2) which is correlated to the plasticity index of soft clays. The average plasticity index for the sludge (Table 2.1) was close to 148 giving a correction factor for the vane shear strengths equal to about 0.6. Therefore

$$(s_u)_{field} = (s_u)_{vane} \times 0.6 \tag{6.4}$$

Application of Janbu's (1954, 1957) method requires that the sliding mass of sludge be divided into an appropriate number of slices. This has been done in Figure 6.13 where slice boundaries, for convenience, have been taken at points separating zones with different material properties or at points where a break occurs in the upper or lower boundary of the sliding mass. Janbu's (1954, 1957) method involves the use of successive approximations, hence a tabular computation form is convenient. Part of this tabular computation is given in Figure 6.13. Values from the cross-section including slice

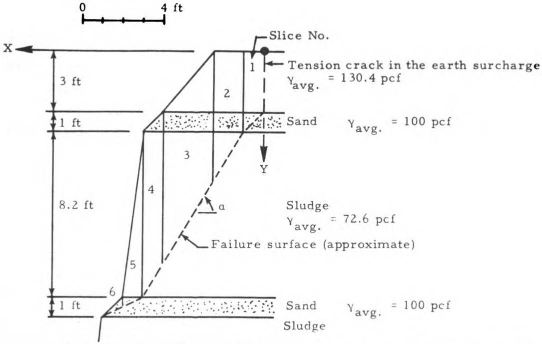

Slice No.	Values from the cross-section					Computations			
	$\tan\alpha$	Δx (ft)	p (psf)	s_u (psf)	$\bar{\phi}$ (deg.)	B_o	A'_o	n_α	A_o
1	1.00	1.0	441.2	--	39.0	441.2	357.3	0.9029	395.7
2	1.64	1.5	580.5	768.1	0	1428.0	1152.2	1.0	1152.2
3	1.64	2.5	623.0	983.2	0	2554.3	2458.0	1.0	2458.0
4	1.64	1.0	585.8	1339.6	0	960.7	1339.6	1.0	1339.6
5	0.50	1.0	322.7	--	39.0	161.4	261.3	1.1416	228.9
6	0.50	1.0	25.0	--	39.0	12.5	20.2	1.1416	17.7
					$\Sigma =$	5558.1	5588.6		5592.1

Δx = slice width,

p = average stress on slice base,

s_u = $(s_u)_{vane}$ · μ = undrained shear strength, $\bar{\phi}$ = angle of internal friction,

B_o = $p \tan\alpha \cdot \Delta x$, A'_o = $s_u \cdot \Delta x$ or $p \tan\bar{\phi} \cdot \Delta x$, $A_o = A'_o / n_\alpha$,

n_α = $\cos^2\alpha \left(1 + \frac{\tan\alpha \tan\bar{\phi}}{F}\right)$

Table complete only for $F_o = \frac{\Sigma A_o}{\Sigma B_o} = \frac{5592.1}{5558.1} = 1.006$

Additional calculations give $F_2 = \frac{\Sigma A_2}{\Sigma B_2} = 1.004$ for a line of thrust for side forces on each slice thru the lower 1/3 points.

Figure 6.13.--Stability calculations using Janbu's method (1954, 1957), total stress basis.

number, tan α, Δx, and p are given in the first four columns. For the sludge A_0' equals $s_u \cdot \Delta x$ and for the sand A_0' equals $p \cdot (\tan \bar{\phi}) \cdot \Delta x$. The table is complete only for the initial calculation ($t = {}^{\Delta T}/_{\Delta x} = 0$) for which F_0 equals 1.006. Two additional approximations give a more accurate value of F_2 equal to 1.004. The line of thrust for side forces on each slice was taken at the 1/3 points. Janbu (1954, 1957) states that the inclusion of the second step in calculation leads to an F-value that is usually within 1 to 1.5 percent of a rigorous F-value. In this case the agreement between the actual and computed factor of safety was excellent, the difference equal to about 0.4 percent. Larger variations in F are likely if inaccuracies exist in the measured sludge shear strength.

Use of the vane shear strength corrected to the field value (Bjerrum, 1972) in the stability analysis has avoided uncertainties with regard to probable sludge disturbance during sampling and sample preparation for laboratory testing. These disturbances may be caused by physical disruption and also by stress change associated with unloading. Small gas pockets, observed in block samples which had been stored for some time, would reduce unit weights and contribute to lower unconfined compressive strengths. Comparisons between vane shear strengths corrected to $(s_u)_{field}$ values and unconfined compressive strengths in the vertical direction (Figure 5.12) show that the latter values are much smaller. For these reasons use of unconfined compressive strengths in place of the corrected vane strengths in the stability analysis would have given an erroneously low factor of safety.

CHAPTER VII

SUMMARY AND CONCLUSIONS

The summary and conclusions are presented under three headings: engineering properties of the fibrous organic soil, behavior of a cut slope in fibrous organic soil, and practical implications of the investigation.

A. Engineering Properties of the Fibrous Organic Soil

Both physical properties and stress-strain characteristics of the papermill sludge were determined relative to evaluating the slope stability of the experimental sludge landfill. Physical properties included water content, unit weight, specific gravity of the sludge solids, ash (or organic) content, and consistency limits. Stress-strain characteristics refer to shear strength parameters of both fresh sludge and undisturbed samples from the consolidated landfill. The following conclusions refer to the engineering properties of the papermill sludge.

1. Physical properties of the papermill sludge are dependent on composition which may vary with production changes at the mill. An increase in organic content gives the sludge a higher water retention and lower unit weights for the same consolidation pressure. Liquid limits and plastic limits both increase with higher organic contents.

2. Relatively small consolidation loads produce a significant decrease in water content and increase in shearing strength of the

papermill sludge. Vane strengths increased from less than 0.1 kg/cm^2 for the fresh sludge to almost 2 kg/cm^2 at the bottom of the consolidated lower sludge layer.

3. The undrained strength was directly related to consolidation pressure for papermill sludges having essentially the same composition. Hence the undrained strength of a fairly uniform normally consolidated sludge may be characterized by the ratio of undrained strength to effective overburden pressure, c_u/p.

4. Triaxial test data suggest that the strength of papermill sludge is essentially frictional and in accordance with the principle of effective stress. The angle of internal friction appears to vary linearly with organic content for a given sludge when comparisons are made using data obtained by a given test procedure. The presence of the fibers may unduly influence the magnitude of the friction angle such that it is not representative of the field shear strength of the sludge.

5. For a given organic content, anisotropic consolidation increased the angle of internal friction when the direction of compression was normal to the plane in which fibers would tend to be aligned. Unconfined compressive strengths were also greatest for sample compression in the vertical direction. Lower values for the angle of internal friction and the unconfined compressive strength were observed when the direction of compression was in the plane of maximum fiber alignment (horizontal).

6. A comparison of test results for plane-strain versus triaxial test results on vertical anisotropically consolidated sludge

samples indicate little or no difference in the measured angle of internal friction, effective stress basis.

7. Plane-strain tests gave a higher initial tangent modulus and a greater ratio of undrained strength to effective overburden pressure C_u/p, for the anisotropically consolidated sludge in comparison to test results from triaxial tests with similar consolidation.

B. Behavior of a Cut Slope in Fibrous Organic Soil

The experimental papermill sludge landfill consisted of 2 sludge layers, initially 10 ft. thick, with sand drainage blankets at the top, middle, and bottom. An earth dike provided lateral confinement for the soft sludge during and after construction, and the surface load consisted of 3 ft. of earth fill material. Instrumentation included settlement plates and piezometers placed at a number of locations in the landfill.

After consolidation of the sludge under the 3 ft. earth surcharge, seven slope indicator casings and additional piezometers were installed in preparation for the slope stability study. Earlier instrumentation remained operative and monitoring was continued. At this stage the north dike was removed and the sludge was excavated to a 3:4 slope. After about 10 days it was apparent that the slope was stable since little lateral movement had occurred. Next the 1:8 slope was excavated with subsequent events leading to an initial slope failure in the top sludge layer about four days later. Relatively large lateral movements were recorded prior to failure causing tension cracks to form in the earth surcharge. The following conclusions refer to lateral movements, slope stability, and methods of analysis.

1. The significant increase in shear strength of the papermill sludge as a direct consequence of consolidation resulted in a stable 3:4 slope with small observed lateral movements, less than one inch at the surface. This behavior was in contrast to the very soft, almost fluid behavior of the fresh sludge placed in the landfill during construction.

2. Lateral movements in the sludge landfill increased rapidly after excavation of the 1:8 slope. Rate of movement decreased with time suggesting that creep behavior of the sludge was responsible for a large portion of the final 6 inches of movement at the surface. The amount of movement decreased with depth.

3. Computed stresses, based on measured sludge properties and a simulated excavation to 6, 10, and 14 ft., show a failure zone developing behind the 1:8 slope. A tension zone behind the slope crest increased in size with more excavation. Failure along the unsupported slope would have been predicted and did occur.

4. The vane shear test appears to be appropriate for in situ measurements of the undrained shear strength of the soft papermill sludge. Uncertainties with regard to sludge disturbance during sampling and preparation for laboratory testing were avoided. This vane strength must be corrected for deformation rate and sludge anisotropy effects before being used in a stability analysis.

5. Stability analysis of the 1:8 slope, using Janbu's method for a composite failure surface, gave excellent agreement between the actual factor of safety and the computed factor of safety when vane shear strengths were corrected to field strengths. The correction

factor (Bjerrum, 1972) was selected on the basis of experience with soft clays and the measured plasticity index of the papermill sludge.

6. Some lateral movement, less than 0.9 inch at the upper sludge surface, was measured during the five months of observation after the planned slope failure. The slope remained intact with only local surface changes due to snow or ice development.

C. Practical Implications of the Investigation

The following comments are made with reference to the entire experimental sludge landfill project. Soil mechanics theory was effective in predicting the settlement of the papermill sludge on the basis of laboratory data (Andersland, et al., 1972). This settlement or reduction in volume of the sludge, when properly accounted for, will permit significantly larger volumes of sludge to be placed in a landfill designed for a particular use, whether it be a green area, or for recreational, agricultural, or for light construction purposes.

The magnitude of the preload may be limited by stability considerations which are largely governed by the rate of porewater pressure dissipation. A method for estimating the magnitude and duration of a preload on highly organic soils has been given by MacFarlane (1969).

Sludge unit weights increased from 69.7 pcf for the fresh dewatered sludge to about 88 pcf at the bottom of the lower sludge layer. This fact combined with the relatively high stability of the consolidated sludge landfill suggests its use as a lightweight fill material for earth embankments and other special needs such as sound deflecting barriers. The fresh dewatered sludge from a mill could be deposited in a landfill which includes drainage blankets and a surcharge load. After sufficient time for primary consolidation the surcharge could be removed and the consolidated sludge removed for use as a lightweight fill material in another location.

The considerable increase in shear strength of the papermill sludge resulting from consolidation combined with the observed stability of the experimental 3:4 slope suggests that a landfill could be contoured so as to provide a golf course or coasting ramp during the summer and a toboggan run or ski hill during the winter. A soil cover capable of growing vegetation would serve to make the area suitable both as a recreational area as well as a green area.

Sand or gravel blankets and/or tile drains used in connection with a papermill sludge landfill can serve a dual purpose. With proper placement they will shorten the drainage path within the sludge thereby reducing the time needed for primary consolidation and drainage. Hence, much of the settlement under an earth surcharge could be accelerated permitting more options for operation and final use of a papermill sludge landfill. These drains could also be utilized to collect leachate for subsequent treatment by conventional means, should that alternative represent the optimum or most suitable method for protection of groundwater quality.

REFERENCES

REFERENCES

Adams, J. I., "The Engineering Behavior of a Canadian Muskeg," Proc. 6th Int. Conf. Mech. Found. Engr. I, 1965.

Adams, J. I., "Laboratory Compression Tests on Peat," Proceedings 7th Muskeg Research Conf., National Research Council of Canada, ACSSM, 1961.

American Society for Testing and Materials, Book of ASTM Standards, Part 15, Philadelphia, Penn.

Andersland, O. B., Charlie, W. A., Vallee, R. P., and Marshall, D. W., "An Experimental High Ash Papermill Sludge Landfill," Second Annual Report to the U.S. Environmental Protection Agency, Division of Engineering Research, Mich. State Univ., E. Lansing, Mich., 1971.

Andersland, O. B., and Laza, Robert W., "Shear Strength and Permeability of high Ash Pulp and Papermill Sludges," Tech. Rpt. 1 for the National Council of the Paper Industry for Air and Stream Improvement, Inc., Div. of Engineering Research, Mich. State Univ., E. Lansing, Mich., 1971.

Andersland, O. B., Vallee, R. P., and Armstrong, T. A., "An Experimental High Ash Papermill Sludge Landfill," First Annual Report to the U.S. Environmental Protection Agency, Div. of Engineering Research, Mich. State Univ., E. Lansing, Mich., 1972.

Bacon, V. W., "Sludge Disposal," Industrial Water Eng. 4, 27, 1967.

Bailey, W. A., and Christian, John T., "ICES LEASE-1, A Problem Oriented Language for Slope Stability Analysis," Soil Mechanics Publ. No. 235, Mass. Inst. of Technology, Cambridge, Mass., April, 1969.

Baver, L. D., Soil Physics, 3rd ed., John Wiley and Sons, New York, 1966.

Biggs, W. D., "Theoretical Background," Composite Materials, ed. by L. Holliday, Elsevier Publishing Co., New York, 1966.

Bishop, A. W., "The Use of the Slip Circle in the Stability Analysis of Slopes," Geotechnique, London, 5:7-17, 1954.

Bishop, Alan W., and Henkel, D. J., The Measurement of Soil Properties in the Triaxial Test, Edward Arnold (Publishers) Ltd., London, 1962.

Bjerrum, Laurits, "Embankments on Soft Ground," Proc. of the Specialty Conf. on Performance of Earth and Earth-Supported Structures, American Society of Civil Engineers, II:1-54, June 11-14, 1972.

Brecht, W., Trans. of the Symposium on the Formation and Structure of Paper, Oxford, 1961, ed. by F. Bolan, Technical Section of the British Paper and Board Makers' Association, Kenley, 1962.

Casagrande, A., "Research on the Atterberg Limits of Soils," Public Roads, Vol. 13, 1932.

Casagrande, A., "Classification and Identification of Soils," Trans. Am. Soc. of Civil Engineers, 113:901-930, 1948.

Casagrande, A., "An Unsolved Problem of Embankment Stability on Soft Ground," Panamerican Conference on Soil Mechanics and Foundation Engineering, 1, Mexico, 1960.

Casagrande, A., "Construction of Embankments Across Peaty Soils," Journ. of the Boston Soc. of Civil Engineers, 53:3:272-317, 1966.

Corte, H., "Paper and Board," Composite Materials, ed. by L. Holliday, Elsevier Publishing Co., New York, 1966.

Duncan, J., "The Effect of Anisotropy and Reorientation of Principal Stresses on the Shear Strength of Saturated Clay," Ph.D. Dissertation, University of California, Berkeley, 1965.

Dunlop, Peter, Duncan, J. M., and Seed, H. Bolton, "Finite Element Analyses of Slopes in Soil," Rpt. No. TE-68-3, Soil Mech. and Bituminous Materials Research Lab., Dept. of Civil Engineering, Univ. of Calif., Berkeley, 1968.

Eckenfelder, W. W., and O'Connor, D. J., Biological Waste Treatment, Pergamon Press, Oxford, 1961.

Engineering-Science, Inc., and the County of Los Angeles, "Development of Construction and use Criteria for Sanitary Landfills," County of Los Angeles, Dept. of County Engineer, California, 1968.

Gehm, H. W., "Current Developments in the Dewatering of Papermill Sludges," National Council for Stream Improvement, Tech. Bull. No. 113, March 1959.

Gibbs, H. J., Hilf, J. W., Holtz, W. G., and Walker, F. C., "Shear Strength of Cohesive Soils," Proc. Research Con. on Shear Strength of Cohesive Soils, American Society of Civil Engineers, 1960.

Gillespie, W. J., "Summary Report--Questionnaire Survey--Sludge Cake Disposal on Land," National Council of the Paper Industry for Air and Stream Improvement, Inc., Unpublished, September 1969.

Gillespie, W. J., Gellman, I., and Janes, R. L., "Utilization of High Ash Papermill Waste Solids," Proc. 2nd Mineral Waste Utilization Symposium, IITRI, Chicago, March 1970.

Gillespie, W. J., Mazzola, C. A., and Gellman, I., "Landfill Disposal of Papermill Waste Solids," Presented at the 7th Technical Association of the Pulp and Paper Industry Air and Water Conference, Minneapolis, Minn., June 7-10, 1970.

Grim, R., Clay Mineralogy, 2nd ed., McGraw Hill, New York, 1968.

Hanrahan, E. T., "An Investigation of some Physical Properties of Peat," Geotechnique, IV:108-123, 1954.

Hanrahan, E. T., Dunne, J. M., and Sodha, V. G., "Shear Strength of Peat," Proc. Geotechnical Conf. Oslo, I:193-198, 1967.

Hartler, N., Kull, G., and Stockmen, L., Svensk Papperstid, 66, 1963.

Imshenetsky, A. A., "Decomposition of Cellulose in the Soil," The Ecology of Soil Bacteria, University of Toronto Press, Canada, 1968.

Janbu, N., Discussion on "Application of Composite Slip Surfaces for Stability Analyses," European Conf. on Stability of Slopes, Stockholm, III:43-49, 1954.

Janbu, N., "Earth Pressures and Bearing Capacity Calculations by Generalized Procedure of Slices," Proc. 4th Internat. Conf. on Soil Mech. and Found. Engr., II:207-212, 1957.

Jayne, B. A., Tech. Assoc. Pulp Paper Ind., 42, 1959.

Kallnes, O., and Bernier, G. A., Trans. of the Symposium on the Formation and Structure of Paper, Oxford, 1961, ed. by F. Bolam, Technical Section of the British Paper and Board Makers' Association, Kenley, 1962.

Kavalenko, N. P., "Preparation of Peat Lands for Construction by the Surcharge Method," Soil Mech. and Found. Engr., No. 2, March-April, 1968.

Kelly, A., and Tyson, W. R., Proc. of the Second International Symposium on Fiber Strengthened Materials, University of California, Berkeley, California, June 1964.

Koch, H. C., and Lugar, J. J., "Addition of Nitrate to Papermill Wastes," Proc. of 13th Industrial Waste Conference, Purdue University Engineering Extension Series, Bull. No. 96, 1958.

Lambe, T. William, Soil Testing for Engineers, John Wiley and Sons, Inc., New York, 1951.

Lambe, T. William, and Whitman, Robert V., Soil Mechanics, John Wiley and Sons, Inc., New York, 1969.

Laza, R. W., "Permeability and Shear Strength of Dewatered High Ash Content Pulp and Papermill Sludges," Ph.D. Dissertation, Michigan State University, 1971.

Leonards, G. A., Foundation Engineering, McGraw-Hill Book Co., Inc., New York, 1962.

Leopold, B., and McIntosh, D. C., Tech. Assoc. Pulp Paper Ind., 44, 1961.

Lynch, D. L., and Cotnoir, L. J., Jr., "The Influence of Clay Minerals on the Breakdown of Certain Organic Substrates," Soil Science Soc. Am., Vol. 20, pp. 367-370, 1956.

Lyne, L. M., and Gallay, W., Pulp Paper Mag. of Canada, 55, 1954.

MacFarlane, Ivan C., ed., Muskeg Engineering Handbook, Univ. of Toronto Press, 1969.

Mazzola, C. A., "Soil Index Properties of High Ash Primary Pulp and Paper Sludges," National Council of the Paper Industry for Air and Stream Improvement, Inc., October 1969.

National Council for Stream Improvement, Inc., "Recent Developments in the Disposal of Pulp and Paper Industry Sludges," Tech. Bull. No. 136, 1960.

National Council for Stream Improvement, Inc., "Mechanical Pressing of Primary Dewatered Papermill Sludges," Tech. Bull. No. 174, 1964.

Nemerow, N. L., Liquid Waste of Industry, Addison-Wesley, Reading, Mass., 1971.

Olson, R. E., "Shearing Strengths of Kaolinite, Illite, and Montmorillonite," Journ. of the Geotechnical Engr. Div., Am. Soc. of Civil Engineers, 100:GT11:1215-1229, 1974.

Parry, R. H. G., "Stability Analysis for Low Embankments on Soft Clays," Stress-Strain Behavior of Soils, Proc. of the Roscoe Memorial Symposium, Cambridge University, England, 29-31 March 1971.

Roberston, A. A., Meindersma, E., and Mason, S. G., Pulp Paper Mag. of Canada, 62, 1961.

Salvato, J. A., Wilkie, W. G., and Mead, B. E., "Sanitary Landfill Leaching Prevention and Control," Journ. Water Pollution Control Federation, 43:10:2084, 1971.

Sears, G. W., "Ultimate Strength of Crystals," Journ. of Chem. and Phys., 36, 862, 1968.

Stoll, V. W., "Mechanical Properties of Milled Domestic Trash," Am. Soc. of Civil Engineers National Water Resources Engineering Meeting, Phoenix, Arizona, January 1971.

Terzaghi, Karl, Theoretical Soil Mechanics, John Wiley and Sons, Inc., New York, 1943.

Terzaghi, Karl, and Peck, Ralph B., Soil Mechanics in Engineering Practice, 2nd ed., John Wiley and Sons, Inc., New York, 1967.

Umbreit, W. W., "Soil Microbiology," Modern Microbiology, W. H. Freeman and Company, San Francisco, 1962.

Vallee, R. P., "A Field Consolidation Study of High Ash Papermill Sludge," Ph.D. Dissertation, Michigan State University, 1973.

Vallee, R. P., and Andersland, O. B., "Field Consolidation of High Ash Papermill Sludge," Journ. of the Geotechnical Engr. Div., Am. Soc. of Civil Engineers, 100:GT3:309-327, 1974.

Whitman, R. V., and Bailey, W. A., "Use of Computers for Slope Stability Analysis," Journ. of the Soil Mech. and Found. Div., Am. Soc. of Civil Engineers, 93:SM4:475-498, 1967.

Wohrer, L. C., and Economy, J., "Single Crystal Fiber Reinforcements," Proc. 10th National Symposium on Advanced Fibrous Reinforced Composites, Soc. of Aerospace Material and Process Engineers, San Diego, November 1966.

Zienkiewicz, O. C., The Finite Element Method in Engineering Science, 2nd ed., McGraw-Hill, London, 1971.

APPENDICES

APPENDIX A

TABLE A-1. SURFACE MOVEMENTS

Date	Horizontal distance, ft									Remarks
mo-da-yr	I-WX	I-WY	I-WZ	II-WX	II-WY	II-WZ	III-WX	III-XY	III-WZ	
9-19-72	51.47	71.61	91.39	51.85	70.80	91.17	51.60	71.38	91.29	initial distance
9-25-72	51.46	71.62	91.37	51.88	70.82	91.18	51.63	71.40	91.29	
9-30-72	-	-	-	51.89	70.83	91.21	-	-	-	
10- 2-72	51.45	71.61	91.36	51.87	70.80	91.18	51.63	71.40	91.29	
10- 3-72	-	-	91.36	-	-	91.18	-	-	91.29	
10- 4-72	51.46	71.62	91.37	-	-	91.19	-	71.40	91.31	
10- 7-72	51.46	71.62	91.37	51.87	70.82	91.19	51.63	71.42	91.33	
10-10-72	51.47	71.63	91.38	51.87	70.82	91.21	51.63	71.42	91.34	
10-13-72	51.48	71.65	91.41	51.90	70.85	91.23	51.66	71.44	91.36	3:4 slope completed
10-19-72	51.49	71.66	91.42	51.90	70.86	91.24	51.66	71.44	91.36	
10-23-72	-	-	91.41	-	-	91.23	-	-	91.35	1:8 slope completed
10-25-72	-	71.67	91.52	-	70.87	91.37	-	71.46	91.47	
10-26-72	-	71.67	91.56	-	70.88	91.40	-	71.46	91.50	
10-28-72	51.50	71.67	91.62	51.91	70.88	91.48	51.69	71.48	91.55	
11- 1-72	-	71.67	91.67	-	70.88	lost	-	71.47	91.58	
11- 8-72	-	71.69	91.73	-	-	-	-	71.49	91.73	
11-14-72	-	71.69	91.76	-	-	-	-	71.49	91.80	
11-21-72	-	71.70	91.76	-	-	-	-	71.49	91.80	
4- 7-72	51.55	71.73	91.75	51.95	70.91	-	51.71	71.50	91.88	trench filled with sludge
6-14-72	51.52	71.70	91.68	51.93	70.90	-	51.72	71.50	91.83	

Line -- I West 20 ft
II Centerline of fill
III East 20 ft
$\Bigg\}$ see Figure 4.2

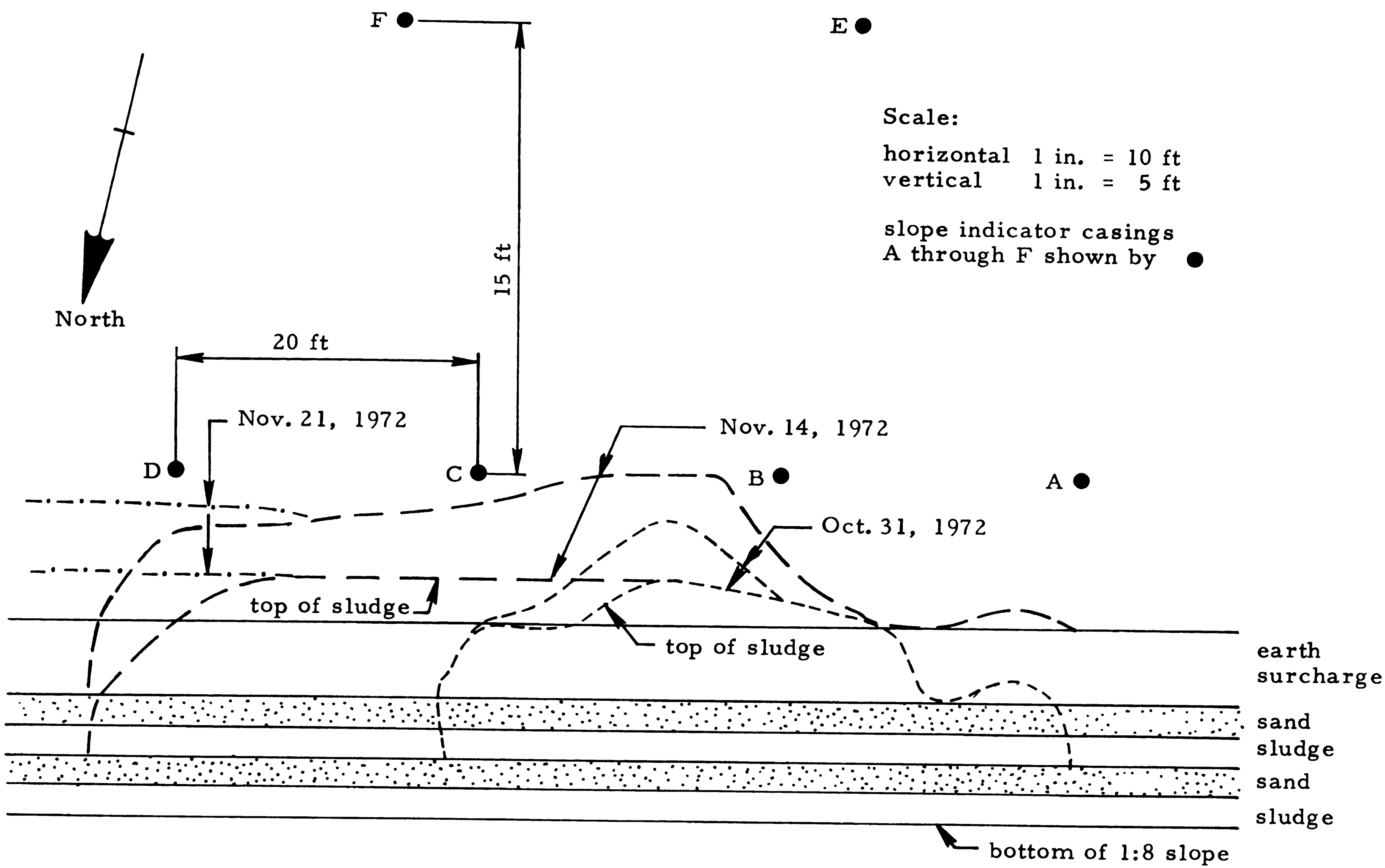

Figure A-1. Slope failure areas, plan view.

APPENDIX B

TABLE B-1. SLOPE INDICATOR DATA, September 25, 1972

Casing movement, north, inches

Casing	A		B		C		D	
Elev., ft.	North	East	North	East	North	East	North	East
94.6	-0.102		0.060		0.084		0.102	
92.6	-0.192		0.036		0.078		0.084	
90.6	-0.246		0.006		0.072		0.066	
88.6	-0.258		-0.012		0.060		0.048	
86.6	-0.252		-0.018		0.054		0.030	
84.6	-0.204		-0.024		0.030		0.012	
82.6	-0.126		-0.024		0.030		0.012	
80.6	-0.072		-0.012		0.006		0.012	
78.6	-0.030		-0.006		0.000		0.012	
76.6	-0.012		0.000		0.000		0.006	
75.6	0.000		0.000		0.000		0.000	

Casing	E		F		G		Remarks
Elev., ft.	North	East	North	East	North	East	
94.6							Two days after trench cut
92.6							
90.6							
88.6							
86.6							
84.6							
82.6							
80.6							
78.6							
76.6							
75.6							

TABLE B-2. SLOPE INDICATOR DATA, October 3, 1972

Casing movement, north or east*, inches

Casing	A		B		C		D	
Elev., ft.	North	East	North	East	North	East	North	East
94.6	-0.006	0.246	0.222	0.246	0.264	-0.042	0.252	-0.108
92.6	-0.158	0.336	0.174	0.204	0.264	-0.006	0.216	-0.132
90.6	-0.258	0.366	0.120	0.174	0.210	0.024	0.186	-0.132
88.6	-0.300	0.336	0.072	0.156	0.162	0.036	0.150	-0.108
86.6	-0.306	0.258	0.036	0.132	0.114	0.042	0.102	-0.078
84.6	-0.258	0.162	0.006	0.096	0.060	0.048	0.060	-0.042
82.6	-0.168	0.114	-0.006	0.060	0.042	0.036	0.042	-0.030
80.6	-0.096	0.072	0.000	0.030	0.012	0.018	0.024	-0.024
78.6	-0.048	0.036	0.006	0.006	0.000	0.012	0.018	-0.024
76.6	-0.018	0.012	0.006	-0.006	-0.006	0.006	0.000	-0.006
75.6	0.000	0.000	0.000	0.000	0.000	0.000	0.000	0.000

Casing	E		F		G		Remarks
Elev., ft.	North	East	North	East	North	East	
94.6	0.072		0.114		0.150		*minus sign indicates movement south or west
92.6	0.072		0.096		0.120		East end of north dike excavated to toe
90.6	0.072		0.066		0.108		
88.6	0.054		0.048		0.096		
86.6	0.042		0.042		0.078		
84.6	0.036		0.036		0.042		
82.6	0.018		0.118		0.042		
80.6	0.006		0.012		0.024		
78.6	0.000		0.006		0.006		
76.6	0.000		0.000		0.000		
75.6	0.000		0.000		0.000		

TABLE B-3. SLOPE INDICATOR DATA, October 4, 1972

Casing movement, north*, inches

Casing	A		B		C		D	
Elev., ft.	North	East	North	East	North	East	North	East
94.6	0.078		0.162		0.510		0.348	
92.6	-0.078		0.126		0.468		0.318	
90.6	-0.180		0.096		0.408		0.294	
88.6	-0.234		0.072		0.324		0.264	
86.6	-0.258		0.042		0.246		0.216	
84.6	-0.222		0.012		0.156		0.150	
82.6	-0.138		0.000		0.108		0.108	
80.6	-0.072		0.000		0.048		0.072	
78.6	-0.036		0.000		0.018		0.036	
76.6	-0.012		0.006		0.000		0.012	
75.6	0.000		0.000		0.000		0.000	

Casing	E		F		G		Remarks
Elev., ft.	North	East	North	East	North	East	
94.6							*minus sign indicates movement south
92.6							
90.6							
88.6							
86.6							
84.6							
82.6							
80.6							
78.6							
76.6							
75.6							

TABLE B-4. SLOPE INDICATOR DATA, October 7, 1972

Casing movement, north*, inches

Casing	A		B		C		D	
Elev., ft.	North	East	North	East	North	East	North	East
94.6	0.138		0.324		0.684		0.558	
92.6	-0.006		0.300		0.660		0.516	
90.6	-0.108		0.264		0.660		0.480	
88.6	-0.162		0.210		0.504		0.432	
86.6	-0.204		0.162		0.396		0.360	
84.6	-0.180		0.114		0.270		0.270	
82.6	-0.102		0.084		0.186		0.198	
80.6	-0.042		0.060		0.096		0.120	
78.6	-0.018		0.030		0.036		0.054	
76.6	-0.006		0.012		0.000		0.012	
75.6	0.000		0.000		0.000		0.000	

Casing	E		F		G		Remarks
Elev., ft.	North	East	North	East	North	East	
94.6	0.132		0.318				*minus sign indicates movement south
92.6	0.126		0.270				Part of west end of north dike remaining to be excavated.
90.6	0.114		0.222				
88.6	0.096		0.180				
86.6	0.072		0.144				
84.6	1.060		0.114				
82.6	0.030		0.084				
80.6	0.012		0.054				
78.6	0.000		0.024				
76.6	-0.006		0.006				
75.6	0.000		0.000				

TABLE B-5. SLOPE INDICATOR DATA, October 11, 1972

Casing movement, north*, inches

Casing	A		B		C		D	
Elev., ft.	North	East	North	East	North	East	North	East
94.6	0.300		0.396		0.792		0.588	
92.6	0.174		0.394		0.780		0.522	
90.6	0.078		0.342		0.726		0.522	
88.6	0.012		0.282		0.630		0.474	
86.6	-0.048		0.216		0.498		0.402	
84.6	-0.066		0.150		0.354		0.306	
82.6	-0.024		0.102		0.240		0.126	
80.6	-0.006		0.060		0.120		0.126	
78.6	0.000		0.030		0.048		0.054	
76.6	0.000		0.012		0.006		0.012	
75.6	0.000		0.000		0.000		0.000	

Casing	E		F		G		Remarks
Elev., ft.	North	East	North	East	North	East	
94.6	0.234		0.342		0.282		*minus sign indicates movement south
92.6	0.222		0.288		0.240		
90.6	0.204		0.234		0.198		
88.6	0.174		0.192		0.162		
86.6	0.138		0.144		0.126		
84.6	0.108		0.108		0.072		
82.6	0.066		0.072		0.066		
78.6	0.006		0.024		0.012		
76.6	0.000		0.006		0.000		
75.6	0.000		0.000		0.000		

TABLE B-6. SLOPE INDICATOR DATA, October 14, 1972

Casing Movement, North or East*, inches

Casing	A		B		C		D	
Elev., ft.	North	East	North	East	North	East	North	East
94.6	0.480	0.252	0.606	0.246	0.870	-0.076	0.666	-0.216
92.6	0.396	0.342	0.624	0.204	0.912	-0.228	0.660	-0.252
90.6	0.318	0.378	0.606	0.174	0.888	-0.180	0.642	-0.252
88.6	0.240	0.348	0.528	0.150	0.786	-0.138	0.600	-0.222
86.6	0.150	0.270	0.432	0.132	0.624	-0.102	0.528	-0.180
84.6	0.096	0.174	0.324	0.096	0.438	-0.078	0.420	-0.132
82.6	0.096	0.126	0.220	0.066	0.300	-0.060	0.306	-0.096
80.6	0.078	0.078	0.144	0.042	0.156	-0.036	0.192	-0.066
78.6	0.042	0.042	0.072	0.012	0.066	-0.024	0.084	-0.042
76.6	0.018	0.018	0.024	0.000	0.006	0.000	0.018	-0.018
75.6	0.000	0.000	0.000	0.000	0.000	0.000	0.000	0.000

Casing	E		F		G		Remarks
Elev., ft.	North	East	North	East	North	East	
94.6	0.330	0.114	0.378	-0.102	0.312	0.096	*Minus sign indicates movement South or West
92.6	0.300	0.156	0.312	-0.126	0.264	0.096	
90.6	0.270	0.168	0.252	-0.114	0.222	0.084	
88.6	0.228	0.150	0.204	-0.108	0.180	0.066	
86.6	0.186	0.120	0.156	-0.078	0.144	0.048	
84.6	0.150	0.078	0.114	-0.060	0.078	0.024	3:4 slope
82.6	0.096	0.054	0.072	-0.054	0.072	0.012	
80.6	0.054	0.018	0.036	-0.030	0.042	0.018	
78.6	0.012	0.006	0.012	-0.018	0.012	0.006	
76.6	0.000	0.000	0.006	-0.006	-0.006	-0.006	

TABLE B-7. SLOPE INDICATOR DATA, October 19, 1972

TABLE B-7. SLOPE INDICATOR DATA, October 19, 1972

Casing Movement, North or East, inches

Casing	A		B		C		D	
Elev., ft.	North	East	North	East	North	East	North	East
94.6	0.558		0.648		0.894		0.720	
92.6	0.492		0.690		0.984		0.732	
90.6	0.420		0.684		0.984		0.726	
88.6	0.336		0.606		0.882		0.684	
86.6	0.228		0.492		0.708		0.594	
84.6	0.156		0.366		0.504		0.468	
82.6	0.140		0.252		0.342		0.354	
80.6	0.108		0.156		0.180		0.210	
78.6	0.066		0.084		0.078		0.030	
76.6	0.024		0.036		0.012		0.018	
75.6	0.000		0.000		0.000		0.000	

Casing	E		F		G		Remarks
Elev., ft.	North	East	North	East	North	East	
94.6	0.420		0.444		0.420		3:4 slope
92.6	0.372		0.366		0.366		
90.6	0.336		0.300		0.312		
88.6	0.270		0.246		0.252		
86.6	0.216		0.192		0.204		
84.6	0.168		0.144		0.132		
82.6	0.108		0.096		0.114		
80.6	0.054		0.066		0.072		
78.6	0.012		0.036		0.030		
76.6	0.000		0.012		0.006		
75.6	0.000		0.000		0.000		

TABLE B-8. SLOPE INDICATOR DATA, October 23, 1972

Casing Movement, North or East, inches

Casing	A		B		C		D	
Elev., ft.	North	East	North	East	North	East	North	East
94.6	0.606		0.684		0.990		0.750	
92.6	0.540		0.744		1.08		0.768	
90.6	0.474		0.750		1.08		0.768	
88.6	0.390		0.672		0.966		0.720	
86.6	0.270		0.546		0.774		0.630	
84.6	0.186		0.408		0.546		0.498	
82.6	0.156		0.282		0.366		0.372	
80.6	0.120		0.174		0.192		0.222	
78.6	0.072		0.090		0.073		0.096	
76.6	0.030		0.036		0.006		0.018	
75.6	0.000		0.000		0.000		0.000	

Casing	E		F		G		Remarks
Elev., ft.	North	East	North	East	North	East	
94.6	0.440		0.516		0.408		
92.6	0.390		0.426		0.354		3:4 slope
90.6	0.348		0.342		0.300		
88.6	0.294		0.282		0.240		
86.6	0.240		0.222		0.186		
84.6	0.186		0.168		0.114		
82.6	0.120		0.114		0.096		
80.6	0.060		0.072		0.054		
78.6	0.018		0.036		0.024		
76.6	0.000		0.012		0.006		
75.6	0.000		0.000		0.000		

TABLE B-9. SLOPE INDICATOR DATA, October 25, 1972

TABLE B-9. SLOPE INDICATOR DATA, October 25, 1972

Casing Movement, North or East, inches

Casing	A		B		C		D	
Elev., ft.	North	East	North	East	North	East	North	East
94.6	1.368		1.854		2.124		1.494	
92.6	1.188		1.722		2.028		1.410	
90.6	1.008		1.506		1.842		1.314	
88.6	0.810		1.224		1.536		1.176	
86.6	0.594		0.924		1.188		0.996	
84.6	0.420		0.642		0.834		0.780	
82.6	0.318		0.426		0.552		0.552	
80.6	0.216		0.252		0.282		0.324	
78.6	0.114		0.120		0.114		0.138	
76.6	0.042		0.048		0.018		0.030	
75.6	0.000		0.000		0.000		0.000	

Casing	E		F		G		Remarks
Elev., ft.	North	East	North	East	North	East	
94.6	0.576		0.666		0.498		
92.6	0.516		0.558		0.438		
90.6	0.456		0.456		0.372		1:8 slope
88.6	0.390		0.378		0.306		
86.6	0.312		0.294		0.240		
84.6	0.240		0.216		0.156		
82.6	0.162		0.144		0.126		
80.6	0.090		0.090		0.078		
78.6	0.030		0.048		0.036		
76.6	0.006		0.018		0.006		
75.6	0.000		0.000		0.000		

TABLE B-10. SLOPE INDICATOR DATA, October 26, 1973

TABLE B-10. SLOPE INDICATOR DATA, October 26, 1973

Casing Movement, North or East*, inches

Casing	A		B		C		D	
Elev., ft.	North	East	North	East	North	East	North	East
94.6	1.602	0.432	2.388	0.372	2.766	-0.438	1.830	-0.444
92.6	1.392	0.462	2.166	0.270	2.562	-0.336	1.710	-0.438
90.6	1.170	0.450	0.842	0.204	2.262	-0.240	1.560	-0.396
88.6	0.836	0.384	1.452	0.162	1.848	-0.162	1.368	-0.330
86.6	0.678	0.282	1.068	0.132	1.398	-0.096	1.134	-0.252
84.6	0.474	0.168	0.708	0.096	0.966	-0.048	0.864	-0.174
82.6	0.348	0.120	0.468	0.054	0.618	-0.030	0.600	-0.114
80.6	0.228	0.072	0.270	0.030	0.330	-0.018	0.348	-0.066
78.6	0.114	0.036	0.126	0.006	0.138	-0.006	0.150	-0.042
76.6	0.042	0.018	0.042	0.000	0.024	0.006	0.036	-0.018
75.6	0.000	0.000	0.000	0.000	0.000	0.000	0.000	0.000

Casing	E		F		G		Remarks
Elev., ft.	North	East	North	East	North	East	
94.6	0.606		0.726		0.498		
92.6	0.540		0.606		0.438		
90.6	0.480		0.504		0.372		1:8 slope
88.6	0.402		0.408		0.300		
86.6	0.324		0.318		0.228		*Minus sign indicates movement South or West
84.6	0.246		0.240		0.144		
82.6	0.168		0.156		0.114		
80.6	0.090		0.090		0.060		
78.6	0.030		0.048		0.030		
76.6	0.006		0.018		0.006		
75.6	0.000		0.000		0.000		

TABLE B-11. SLOPE INDICATOR DATA, October 28, 1972

Casing movement, north, inches

Casing	A		B		C		D	
Elev., ft.	North	East	North	East	North	East	North	East
94.6	1.920		3.090		3.426		2.238	
92.6	1.662		2.736		3.096		2.064	
90.6	1.398		2.274		2.676		1.878	
88.6	1.110		1.746		2.136		1.614	
86.6	0.804		1.236		1.566		1.320	
84.6	0.546		0.774		1.026		0.996	
82.6	0.384		0.516		0.660		0.684	
80.6	0.240		0.300		0.348		0.390	
78.6	0.114		0.138		0.144		0.168	
76.6	0.036		0.048		0.024		0.042	
75.6	0.000		0.000		0.000		0.000	

Casing	E		F		G		Remarks
Elev., ft.	North	East	North	East	North	East	
94.6	0.666		0.762				
92.6	0.594		0.642				
90.6	0.528		0.534				
88.6	0.444		0.438				
86.6	0.360		0.336				
84.6	0.276		0.246				
82.6	0.192		0.156				
80.6	0.108		0.090				
78.6	0.048		0.036				
76.6	0.012		0.012				
75.6	0.000		0.000				

TABLE B-12. SLOPE INDICATOR DATA, November 1, 1972

Casing movement, north, inches

Casing	A		B		C		D	
Elev., ft.	North	East	North	East	North	East	North	East
94.6	2.328		3.678		4.224		2.766	
92.6	2.034		3.174		3.732		2.556	
90.6	1.716		2.592		3.174		2.298	
88.6	1.368		1.980		2.514		1.968	
86.6	0.984		1.392		1.812		1.584	
84.6	0.654		0.834		1.134		1.176	
82.6	0.456		0.588		0.744		0.792	
80.6	0.288		0.366		0.414		0.444	
78.6	0.138		0.186		0.174		0.186	
76.6	0.042		0.072		0.036		0.042	
75.6	0.000		0.000		0.000		0.000	

Casing	E		F		G		Remarks
Elev., ft.	North	East	North	East	North	East	
94.6							
92.6							
90.6							
88.6							
86.6							
84.6							
82.6							
80.6							
78.6							
76.6							
75.6							

TABLE B-13. SLOPE INDICATOR DATA, November 3, 1972

Casing Movement, North or East*, inches

Casing	A		B		C		D	
Elev., ft.	North	East	North	East	North	East	North	East
94.6	2.502	0.672	3.774	0.540	4.530	-0.768	3.186	-0.756
92.6	2.184	0.666	3.276	0.450	3.372	-0.606	2.898	-0.696
90.6	1.848	0.606	2.700	0.360	3.360	-0.444	2.556	-0.600
88.6	1.470	0.486	2.076	0.282	2.640	-0.300	2.154	-0.474
86.6	1.056	0.342	1.464	1.210	1.890	-0.186	1.698	-0.336
84.6	0.696	0.198	0.894	0.156	1.164	-0.096	1.236	-0.216
82.6	0.474	0.138	0.636	0.096	0.756	-0.066	0.828	-0.138
80.6	0.282	0.090	0.402	0.054	0.402	-0.042	0.468	-0.072
78.6	0.138	0.048	0.210	0.012	0.168	-0.012	0.198	-0.036
76.6	0.042	0.018	0.078	0.000	0.030	0.006	0.048	-0.006
75.6	0.000	0.000	0.000	0.000	0.000	0.000	0.000	0.000

Casing	E		F		G		Remarks
Elev., ft.	North	East	North	East	North	East	
94.6	0.828		0,900		0.618		1:8 slope
92.6	0.738		0.762		0.546		
90.6	0.648		0.636		0.468		*Minus sign indicates movement South or West
88.6	0.540		0.510		0.378		
86.6	0.432		0.390		0.282		
84.6	0.336		0.282		0.192		
82.6	0.228		0.180		0.144		
80.6	0.132		0.102		0.084		
78.6	0.054		0.048		0.036		
76.6	0.018		0.018		0.006		
75.6	0.000		0.000		0.000		

TABLE B-14. SLOPE INDICATOR DATA, November 8, 1972

Casing Movement, North or East, inches

Casing	A		B		C		D	
Elev., ft.	North	East	North	East	North	East	North	East
94.6	2.880		3.990		5.442		4.116	
92.6	2.508		3.468		4.614		3.648	
90.6	2.118		2.868		3.786		3.126	
88.6	1.686		2.220		2.922		2.568	
86.6	1.230		0.578		2.064		2.004	
84.6	0.828		0.954		1.254		1.434	
82.6	0.570		0.684		0.816		0.948	
80.6	0.348		0.426		0.438		0.528	
78.6	0.174		0.216		0.180		0.222	
76.6	0.054		0.078		0.030		0.054	
75.6	0.000		0.000		0.000		0.000	

Casing	E		F		G		Remarks
Elev., ft.	North	East	North	East	North	East	
94.6	0.890		0.966		0.642		
92.6	0.798		0.828		0.564		1:8 slope
90.6	0.708		0.696		0.486		
88.6	0.600		0.570		0.390		
86.6	0.486		0.438		0.294		
84.6	0.372		0.312		0.192		
82.6	0.252		0.216		0.144		
80.6	0.138		0.126		0.084		
78.6	0.060		0.060		0.036		
76.6	0.018		0.024		0.006		
75.6	0.000		0.000		0.000		

TABLE B-15. SLOPE INDICATOR DATA, November 14, 1972

Casing Movement, North or East, inches

Casing	A		B		C		D	
Elev., ft.	North	East	North	East	North	East	North	East
94.6	3.054		4.146		5.490		4.800	
92.6	2.670		3.642		4.656		4.158	
90.6	2.262		3.042		3.870		3.504	
88.6	1.812		2.382		3.054		2.826	
86.6	1.332		1.722		2.214		2.154	
84.6	0.906		1.086		1.386		1.500	
82.6	0.624		0.762		0.948		1.020	
80.6	0.378		0.480		0.558		0.588	
78.6	0.186		0.246		0.270		0.264	
76.6	0.060		0.090		0.084		0.072	
75.6	0.000		0.000		0.000		0.000	

Casing	E		F		G		Remarks
Elev., ft.	North	East	North	East	North	East	
94.6	0.954		1.05		0.684		
92.6	0.852		0.900		0.612		
90.6	0.756		0.756		0.528		
88.6	0.648		0.618		0.426		
86.6	0.522		0.486		0.324		1:8 slope
84.6	0.408		0.354		0.216		
82.6	0.276		0.234		0.167		
80.6	0.156		0.144		0.096		
78.6	0.072		0.072		0.042		
76.6	0.024		0.024		0.006		
75.6	0.000		0.000		0.000		

TABLE B-16. SLOPE INDICATOR DATA, November 21, 1972

Casing Movement, North or East*, inches

Casing	A		B		C		D	
Elev., ft.	North	East	North	East	North	East	North	East
94.6	3.108	0.786	4.158	0.594	5.508	-0.708	4.698	-1.236
92.6	2.730	0.756	3.660	0.528	4.698	-0.546	4.104	-1.050
90.6	2.328	0.690	3.072	0.444	3.924	-0.402	3.486	-0.858
88.6	1.872	0.558	2.424	0.360	3.126	-0.288	2.844	-0.660
86.6	1.380	0.402	1.758	0.276	2.292	-0.186	2.844	-0.462
84.6	0.948	0.240	1.116	0.198	1.452	-0.102	1.560	-0.294
82.6	0.654	0.180	0.780	0.114	1.002	-0.084	1.062	-0.192
80.6	0.402	0.114	0.486	0.054	0.594	-0.060	0.612	-0.102
78.6	0.198	0.060	0.246	0.018	0.282	-0.036	0.264	-0.048
76.6	0.066	0.024	0.090	0.000	0.078	-0.006	0.072	-0.012
75.6	0.000	0.000	0.000	0.000	0.000	0.000	0.000	0.000
Casing	E		F		G		Remarks	
Elev., ft.	North	East	North	East	North	East		
94.6	1.002	0.276	1.044	-0.192	0.726	0.054		
92.6	0.900	0.312	0.900	-0.216	0.636	0.066		
90.6	0.798	0.318	0.768	-0.192	0.546	0.060	1:8 slope	
88.6	0.678	0.282	0.642	-0.150	0.444	0.042		
86.6	0.552	0.228	0.504	-0.096	0.342	0.018		
84.6	0.420	0.162	0.366	-0.066	0.228	-0.006		
82.6	0.276	0.114	0.240	-0.042	0.168	0.000	*minus sign indicates movement south or west	
80.6	0.162	0.054	0.144	-0.018	0.096	0.006		
78.6	0.072	0.018	0.072	-0.006	0.036	0.000		
76.6	0.018	0.000	0.030	0.000	0.000	0.000		
75.6	0.000	0.000	0.000	0.000	0.000	0.000		

TABLE B-17. SLOPE INDICATOR DATA, December 12, 1972

Casing movement, north or east*, inches

Casing	A		B		C		D	
Elev., ft.	North	East	North	East	North	East	North	East
94.6	3.384	0.828	4.302		5.616		4.644	-1.206
92.6	2.970	0.792	3.828		4.830		4.122	-1.044
90.6	2.562	0.708	3.270		4.080		3.576	-0.864
88.6	2.094	0.570	2.628		3.294		2.982	-0.672
86.6	1.572	0.408	1.950		2.454		2.352	-0.480
84.6	1.104	0.240	1.266		1.596		1.710	-0.312
82.6	0.768	0.174	0.882		1.110		1.176	-0.204
80.6	0.468	0.108	0.546		0.660		0.684	-0.114
78.6	0.228	0.054	0.276		0.318		0.300	-0.054
76.6	0.272	0.018	0.102		0.096		0.084	-0.012
75.6	0.000	0.000	0.000		0.000		0.000	0.000

Casing	E		F		G		Remarks
Elev., ft.	North	East	North	East	North	East	
94.6	1.134		1.134		0.864		*minus sign indicates movement south or west
92.6	1.014		0.984		0.762		
90.6	0.900		0.840		0.654		
88.6	0.780		0.702		0.534		
86.6	0.642		0.558		0.414		
84.6	0.492		0.408		0.294		
82.6	0.342		0.276		0.204		
80.6	0.198		0.168		0.114		
78.6	0.084		0.084		0.048		
76.6	0.024		0.030		0.012		
75.6	0.000		0.000		0.000		

TABLE B-18. SLOPE INDICATOR DATA, December 29, 1972

Casing Movement, North or East*, inches

Casing	A		B		C		D	
Elev., ft.	North	East	North	East	North	East	North	East
94.6	3.468	0.936	4.422		5.718		4.662	-1.242
92.6	3.090	0.888	3.948		4.914		4.176	-1.086
90.6	2.676	0.798	3.390		4.158		3.642	-0.912
88.6	2.202	0.642	2.748		3.372		3.072	-0.726
86.6	1.668	0.462	2.070		2.532		2.454	-0.528
84.6	1.182	0.204	1.380		1.680		1.812	-0.348
82.6	0.828	0.210	0.972		1.164		1.248	-0.228
80.6	0.510	0.138	0.606		0.690		0.726	-0.132
78.6	0.252	0.072	0.312		0.330		0.324	-0.066
76.6	0.090	0.030	0.114		0.102		0.096	-0.018
75.6	0.000	0.000	0.000		0.000		0.000	0.000

Casing	E		F		G		Remarks
Elev., ft.	North	East	North	East	North	East	
94.6	1.224		1.188		0.912		
92.6	1.092		1.020		0.786		1:8 slope
90.6	0.978		0.870		0.672		
88.6	0.846		0.732		0.552		*Minus sign indicates movement South or West
86.6	0.702		0.588		0.432		
84.6	0.540		0.438		0.312		
82.6	0.372		0.204		0.222		
80.6	0.216		0.180		0.126		
78.6	0.096		0.090		0.054		
76.6	0.030		0.036		0.012		
75.6	0.000		0.000		0.000		

TABLE B-19. SLOPE INDICATOR DATA, February 10, 1973

Casing Movement, North or East, inches

Casing	A		B		C		D	
Elev., ft.	North	East	North	East	North	East	North	East
94.6			4.440		5.934			
92.6			3.996		5.088			
90.6			3.486		4.302			
88.6			2.880		3.504			
86.6			2.214		2.670			
84.6			1.512		1.818			
82.6			1.056		0.284			
80.6			0.660		0.780			
78.6			0.336		0.396			
76.6			0.132		0.132			
75.6			0.000		0.000			

Casing	E		F		G		Remarks
Elev., ft.	North	East	North	East	North	East	
94.6	1.320		1.356		0.126		
92.6	1.170		1.170		0.888		
90.6	1.032		1.002		0.756		1:8 slope
88.6	0.888		0.846		0.624		
86.6	0.726		0.684		0.492		
84.6	0.558		0.522		0.360		
82.6	0.384		0.360		0.246		
80.6	0.216		0.228		0.132		
78.6	0.084		0.120		0.048		
76.6	0.024		0.048		0.000		
75.6	0.000		0.000		0.000		

TABLE B-20. SLOPE INDICATOR DATA, April 7, 1973

Casing Movement, North or East*, inches

Casing	A		B		C		D	
Elev., ft.	North	East	North	East	North	East	North	East
94.6	3.624	1.080	4.572	0.726	6.288	-0.588	4.770	-1.272
92.6	3.324	1.026	4.170	0.642	5.394	-0.480	4.338	-1.104
90.6	2.970	0.924	3.684	0.558	4.542	-0.366	3.852	-0.930
88.6	2.502	0.756	3.078	0.450	3.690	-0.276	3.300	-0.744
86.6	1.956	0.570	2.376	0.354	2.814	-0.198	2.694	-0.546
84.6	1.422	0.390	1.620	0.264	1.920	-0.108	2.064	-0.354
82.6	1.002	0.282	1.152	0.168	1.380	-0.090	1.446	-0.234
80.6	0.630	0.186	0.732	0.102	0.876	-0.066	0.876	-0.126
78.6	0.330	0.108	0.390	0.048	0.480	-0.030	0.426	-0.048
76.6	0.132	0.048	0.156	0.018	0.192	0.000	0.150	-0.006
75.6	0.000	0.000	0.000	0.000	0.000	0.000	0.000	0.000

Casing	E		F		G		Remarks
Elev., ft.	North	East	North	East	North	East	
94.6	1.452	0.282	1.458	-0.192	1.074	0.048	1:8 slope
92.6	1.302	0.324	0.248	-0.228	0.942	0.072	10 ft water in trench
90.6	1.152	0.348	1.062	-0.228	0.804	0.072	*Minus sign indicates movement South or West
88.6	0.984	0.336	0.894	-0.192	0.654	0.060	
86.6	0.810	0.294	0.720	-0.126	0.516	0.030	
84.6	0.630	0.222	0.546	-0.078	0.396	0.006	
82.6	0.450	0.138	0.384	-0.048	0.258	-0.006	
80.6	0.270	0.066	0.246	-0.024	0.138	0.006	
78.6	0.120	0.024	0.132	-0.012	0.054	-0.006	
76.6	0.036	0.006	0.060	-0.006	0.006	-0.012	
75.6	0.000	0.000	0.000	0.000	0.000	0.000	

TABLE B-21. SLOPE INDICATOR DATA, June 14, 1973

Casing Movement, North East, inches

Casing	A		B		C		D	
Elev., ft.	North	East	North	East	North	East	North	East
94.6	3.054		3.876		5.628		4.182	
92.6	2.562		3.258		4.494		3.654	
90.6	2.082		2.652		3.528		3.114	
88.6	1.608		2.052		2.712		2.550	
86.6	1.134		1.452		1.974		1.962	
84.6	0.714		0.840		1.254		1.386	
82.6	0.462		0.582		0.966		1.002	
80.6	0.264		0.378		0.690		0.660	
78.6	0.132		0.222		0.480		0.378	
76.6	0.054		0.108		0.192		0.168	
75.6	0.000		0.000		0.000		0.000	

Casing	E		F		G		Remarks
Elev., ft.	North	East	North	East	North	East	
94.6	1.278		1.260		1.032		
92.6	1.116		1.056		0.894		
90.6	0.960		0.870		0.756		1:8 slope
88.6	0.804		0.720		0.606		
86.6	0.636		0.564		0.462		Readings taken about 2 months after trench filled with fresh sludge.
84.6	0.450		0.402		0.354		
82.6	0.318		0.300		0.216		
80.6	0.180		0.210		0.108		
78.6	0.078		0.126		0.048		
76.6	0.030		0.060		0.012		
75.6	0.000		0.000		0.000		

APPENDIX C

TABLE C-1. SETTLEMENT PLATE ELEVATIONS AT THE BOTTOM SAND BLANKET

Date	Plate Elevation, ft.							
mo-da-yr	G1-1	G2-1	G3-1	G4-1	G5-1	G6-1	G7-1	G8-1
8-1-72	78.27	78.05	77.71	77.43	77.65	77.92	78.26	77.72
9-11-72	78.27	78.04	77.70	77.42	77.65	77.91	78.26	77.71
9-25-72[a]	78.27	78.05	77.71	77.43	77.65	77.91	78.26	77.72
9-30-72[b]	78.25	78.04	77.70	77.41	77.64	77.90	78.25	77.70
10-3-72	78.27	78.04	77.66	77.42	77.65	77.89	78.25	77.71
10-5-72	78.25	78.03	77.66	77.40	77.64	77.89	78.24	77.69
10-7-72	78.25	78.02	77.68	77.41	77.62	77.88	78.22	77.70
10-10-72	78.27	78.03	77.70	77.42	77.65	77.90	78.25	77.71
10-13-72[c]	78.26	78.04	77.71	77.41	77.65	77.90	78.25	77.71
10-19-72	78.25	78.04	77.70	77.41	77.64	77.91	78.25	77.71
10-23-72	78.27	78.04	77.71	77.42	77.65	77.90	78.25	77.71
10-25-72[d]	78.26	78.04	77.70	77.41	77.63	77.88	78.24	77.70
10-26-72	78.26	78.04	77.70	77.40	77.64	77.89	78.24	77.70
11-1-72	78.27	78.05	77.71	77.40	77.65	77.88	78.25	77.71
11-13-72	-	-	-	77.40	77.64	77.87	-	77.70
11-8-72	78.27	78.05	77.70	77.40	77.64	77.87	78.25	77.71
11-14-72	78.26	78.04	77.70	77.40	77.64	77.87	78.25	77.69
11-21-72	78.26	78.05	77.70	77.40	77.64	77.87	78.25	77.71
12-12-72	78.26	78.04	77.70	77.40	77.65	77.87	78.25	77.71
12-29-72	-	-	-	77.38	77.63	77.87	-	77.70
2-10-73	78.25	78.05	77.70	77.38	77.64	77.87	78.25	77.70
4-7-73	78.26	78.05	77.71	77.39	77.64	77.87	78.25	77.70
6-14-73[e]	78.26	78.03	77.70	77.38	77.62	77.88	78.24	77.70

[a]Two days after test trench was dug and middle sand blanket drained.

[b]After six days rain.

[c]3:4 slope completed.

[d]1:8 slope completed.

[e]About two months after trench filled with fresh papermill sludge.

TABLE C-2. SETTLEMENT PLATE ELEVATIONS AT THE MIDDLE SAND BLANKET

Date	Plate Elevation, ft.							
mo-da-yr	G1-3	G2-3	G3-3	G4-3	G5-3	G6-3	G7-3	G8-3
8-1-72	85.61	85.87	85.54	85.69	85.67	85.71	85.69	85.51
9-11-72	85.60	85.85	85.52	85.67	86.65	85.69	85.67	85.48
9-25-72[a]	85.59	85.84	85.48	85.67	85.65	85.68	85.66	85.47
9-30-72[b]	85.58	85.82	85.49	85.63	85.63	85.65	85.63	85.44
10-3-72	85.57	85.82	85.51	85.64	85.60	85.66	85.64	85.45
10-5-72	85.57	85.51	85.48	85.63	85.61	85.64	85.63	85.44
10-7-72	85.56	85.81	85.49	85.62	85.61	85.64	85.63	85.44
10-10-72	85.57	85.82	85.49	85.64	85.62	85.65	85.64	85.46
10-13-72[c]	85.56	85.82	85.50	85.62	85.63	85.64	85.64	85.44
10-19-72	85.56	85.82	85.49	85.62	85.61	85.64	85.63	85.44
10-23-72	85.56	85.81	85.48	85.62	85.62	85.64	85.63	85.43
10-25-72[d]	85.55	85.80	85.47	85.59	85.60	85.61	85.62	85.42
10-26-72	85.55	85.80	85.47	85.58	85.60	85.60	85.61	85.42
11-1-72	85.55	85.80	85.48	85.58	85.60	85.58	85.62	85.42
11-3-72	-	-	-	85.57	85.60	85.57	-	85.39
11-8-72	85.54	85.80	85.47	85.58	85.60	85.57	85.62	85.40
11-14-72	85.53	85.78	85.46	85.58	85.59	85.56	85.61	85.39
11-21-72	85.53	85.79	85.46	85.56	85.59	85.57	95.61	85.39
12-12-72	85.52	85.76	85.45	85.56	85.58	85.54	85.59	85.37
12-29-72	-	-	-	85.56	85.56	85.53	-	85.36
2-10-73	85.48	85.74	85.41	85.54	85.55	85.52	85.57	85.34
4-7-73	85.45	85.74	85.39	85.55	85.54	85.51	85.55	85.33
6-14-73[e]	85.42	85.72	85.38	85.54	85.53	85.52	85.54	85.32

[a] Two days after test trench was dug and middle sand blanket drained.

[b] After six days rain.

[c] 3:4 slope completed.

[d] 1:8 slope completed.

[e] About two months after trench filled with fresh papermill sludge.

TABLE C-3. SETTLEMENT PLATE ELEVATIONS AT THE TOP SAND BLANKET

Date	Plate Elevation, ft.							
mo-da-yr	G1-5	G2-5	G3-5	G4-5	G5-5	G6-5	G7-5	G8-5
8-1-72	95.06	94.94	95.06	94.83	94.94	94.84	94.80	94.73
9-11-72	94.98	94.87	94.99	94.72	94.88	94.75	94.73	94.64
9-25-72[a]	94.95	94.84	94.95	94.68	94.80	94.72	94.70	94.63
9-30-72[b]	94.92	94.81	94.93	94.66	94.81	94.67	94.67	94.59
10-3-72	94.90	94.81	94.92	94.65	94.81	94.68	94.66	94.60
10-5-72	94.89	94.78	94.90	94.64	94.78	94.66	94.64	94.57
10-7-72	94.88	94.79	94.90	94.61	94.78	94.65	94.64	94.58
10-10-72	94.89	94.78	94.90	94.62	94.78	94.65	94.64	94.57
10-13-72[c]	94.87	94.78	94.90	94.59	94.77	94.63	94.63	94.56
10-19-72	94.85	94.75	94.86	94.56	94.75	94.60	94.60	94.53
10-23-72	94.82	94.74	94.85	94.54	94.75	94.58	94.60	94.51
10-25-72[d]	94.81	94.72	94.82	94.48	94.72	94.54	94.57	94.47
10-26-72	94.80	94.72	94.82	94.46	94.71	94.53	94.58	94.47
11-1-72	94.79	94.70	94.80	94.42	94.70	94.50	94.56	94.44
11-3-72	-	-	-	94.41	94.68	94.48	-	94.43
11-8-72	94.77	94.69	94.79	94.41	94.69	94.49	94.54	94.43
11-14-72	94.75	94.68	94.78	94.39	94.66	94.47	94.53	94.41
11-21-72	94.74	94.67	94.77	94.39	94.67	94.46	94.52	94.41
12-12-72	94.71	94.63	94.74	94.38	94.63	94.43	94.49	94.37
12-29-72	-	-	-	94.33	94.60	94.39	-	94.34
2-10-73	94.63	94.57	94.67	94.29	94.56	94.34	94.41	94.29
4-7-73	94.61	94.54	94.64	94.25	94.53	94.31	94.39	94.25
6-14-73[e]	94.58	94.53	94.62	94.24	94.53	94.31	94.38	94.25

[a] Two days after test trench was dug and middle sand blanket drained.

[b] After six days rain.

[c] 3:4 slope completed.

[d] 1:8 slope completed.

[e] About two months after trench filled with fresh papermill sludge.

TABLE C-4. SETTLEMENT PLATE ELEVATIONS AT THE MID-POINTS OF THE LOWER AND UPPER SLUDGE LAYERS

Date	Plate Elevations, ft.						
mo-da-yr	G5-2	G6-2	G7-2	G8-2	G5-4	G6-4	G7-4
8-1-72	81.36	81.53	81.88	80.88	90.30	90.18	89.95
9-11-72	81.35	81.51	81.88	80.86	90.28	90.14	89.91
9-25-72[a]	81.32	81.51	81.86	80.85	90.25	90.12	89.88
9-30-72[b]	81.31	81.48	81.85	80.83	90.22	90.06	89.88
10-3-72	81.32	81.51	81.87	80.82	90.21	90.08	89.87
10-5-72	81.27	81.48	81.86	80.83	90.20	90.07	89.86
10-7-72	81.31	81.48	81.85	80.81	90.19	90.06	89.85
10-10-72	81.33	81.50	81.86	80.83	90.20	90.06	89.85
10-13-72[c]	81.33	81.50	81.86	80.83	90.19	90.05	89.85
10-19-72	81.31	81.50	81.85	80.85	90.18	90.03	89.84
10-23-72	81.33	81.50	81.86	80.85	90.17	90.02	89.83
10-25-72[d]	81.31	81.48	81.85	80.82	90.16	89.99	89.82
10-26-72	81.32	81.46	81.85	80.82	90.14	90.00	89.82
11-1-72	81.32	81.45	81.85	80.83	-	89.98	89.82
11-3-72	81.31	81.42	-	80.81	90.14	89.98	-
11-8-72	81.32	81.46	81.84	80.83	90.14	89.96	89.80
11-14-72	81.32	81.48	81.84	80.82	90.13	89.95	89.79
11-21-72	81.31	81.47	81.85	80.83	90.12	89.84	89.78
12-12-72	81.30	81.45	81.84	80.83	90.11	89.92	89.86
12-29-72	81.30	81.46	-	80.78	90.08	89.89	-
2-10-73	81.28	81.45	81.82	80.81	90.05	89.86	89.70
4-7-73	81.29	81.45	81.81	80.81	90.03	89.84	89.69
6-14-73[e]	81.29	81.47	81.81	80.80	90.03	89.85	89.68

[a] Two days after test trench was dug and middle sand blanket drained.

[b] After six days rain.

[c] 3:4 slope completed.

[d] 1:8 slope completed.

[e] About two months after trench filled with fresh papermill sludge.

APPENDIX D

TABLE D-1. PORE WATER PRESSURES FOR THE LOWER AND UPPER 1/4 POINTS OF THE LOWER AND UPPER SLUDGE LAYERS

Date mo-da-yr	Time	Pore water pressure in psi for piezometer							
		G4-2	G5-2	G4-6	G5-6	G4-4	G5-4	G4-8	G5-8
8-1-72	-	-	1.90	-	2.00	-	3.10	-	0.25
9-11-72	-	3.55	2.00	2.10	1.77	2.25	3.15	0.35	0.05
9-19-72	-	3.60	-	1.30	-	2.30	-	0.40	-
9-25-72	-	2.80	1.75	1.70	1.22	1.95	2.85	-	0.10
9-30-72[a]	-	2.75	1.90	1.75	1.40	2.00	2.85	0.75	0.10
10-2-72	-	2.90	1.90	1.85	1.45	2.00	2.75	0.65	0.20
10-3-72	2 pm	2.85	1.95	1.75	1.50	2.00	2.75	0.40	0.25
10-3-72	6 pm	2.80	-	1.70	-	2.00	-	0.60	-
10-4-72	2 pm	2.85	1.95	1.75	1.50	2.00	2.75	0.75	0.25
10-4-72	6 pm	2.80	-	1.75	-	1.95	-	0.70	-
10-5-72	7 pm	2.75	-	1.80	-	2.00	-	0.45	-
10-7-72	9 am	2.65	1.75	1.80	1.50	1.85	2.75	0.25	0.10
10-7-72	2 pm	2.50	1.80	1.80	1.60	1.85	2.85	0.25	0.20
10-10-72	3 pm	2.40	1.40	1.75	1.10	1.65	2.50	0.20	0.15
10-11-72	7 pm	2.40	1.45	1.80	1.30	1.65	2.55	0.40	0.05
10-13-72[b]	7 pm	2.40	1.20	0.75	1.35	1.45	2.60	0.15	0.15
10-19-72	10 am	2.10	0.50	1.60	1.00	1.15	2.25	0.05	0.00
10-23-72	2 pm	2.05	0.10	1.25	1.30	1.20	2.50	2.00	0.05
10-24-72	10 am	1.70	0.25	1.05	1.20	1.10	2.30	0.00	0.00
10-24-72	5 pm	1.55	0.35	0.95	1.15	1.00	2.30	0.00	0.05
10-25-72[c]	11 am	-	-	-	-	0.90	2.30	0.00	0.00
10-25-72	7 pm	-	-	-	-	0.95	2.30	0.00	0.00
10-26-72	11 pm	1.90	0.20	0.85	1.15	0.95	2.30	0.00	0.05
10-28-72	12 noon	2.05	0.00	1.05	1.00	1.05	2.30	0.00	0.00
11-1-72	3 pm	1.50	0.15	1.30	1.00	1.15	2.35	0.15	0.00
11-2-72	3 pm	1.75	0.35	1.40	1.30	1.30	2.50	0.15	0.10
11-3-72	3 pm	1.85	0.20	1.20	1.15	1.10	2.30	0.30	0.00
11-8-72	2 pm	1.85	0.20	1.70	1.05	0.25	2.30	0.35	0.00
11-14-72	4 pm	1.75	0.40	1.75	1.05	1.40	2.30	0.20	0.05
11-21-72	2 pm	1.50	0.70	1.65	0.95	1.15	2.20	0.30	0.05
12-12-72	12 noon	0.85	0.65	1.20	0.85	1.05	2.10	0.35	0.00
12-29-72	3 pm	0.70	0.80	1.10	0.80	0.95	2.25	0.30	0.00
2-10-73	-	0.60	0.80	1.15	0.55	0.70	1.95	0.40	0.00
4-7-73[d]	-	1.10	1.25	1.05	0.95	0.85	1.95	0.40	0.00
6-14-73[e]	-	0.00	1.90	2.05	2.15	3.00	3.00	0.50	0.05

[a] After six days rain.

[b] 3:4 slope completed.

[c] 1:8 slope completed.

[d] Ten feet water in trench.

[e] Two months after trench filled with fresh papermill sludge.

TABLE D-2. PORE WATER PRESSURES FOR THE CENTER OF THE LOWER AND UPPER SLUDGE LAYERS

Date mo-dy-yr	Time	Pore water pressure in psi for piezometer							
		G4-3	G5-3	G6-3	G7-3	G4-7	G5-7	G6-7	G7-7
8-1-72	-	-	2.25	2.30	2.25	-	1.10	0.90	1.60
9-6-72	-	-	2.25	2.25	2.25	-	1.85[a]	0.90	1.60
9-11-72	-	2.95	2.30	2.45	2.35	1.30	1.25	1.00	1.70
9-19-72	-	2.70	-	-	-	1.35	-	-	-
9-25-72	-	2.00	2.15	2.30	2.10	1.20	-	0.85	1.40
9-30-72[b]	-	2.15	2.35	2.50	2.20	1.45	-	1.05	1.70
10-2-72	-	2.20	2.20	2.35	2.10	1.60	-	1.00	1.50
10-3-72	2 pm	2.15	2.20	2.40	2.20	1.60	-	1.00	1.50
10-3-72	6 pm	2.10	-	-	-	1.55	-	-	-
10-4-72	2 pm	2.10	2.25	2.40	2.20	1.50	-	1.00	1.65
10-4-72	6 pm	2.00	-	-	-	1.45	-	-	-
10-5-72	7 am	2.05	-	-	-	1.50	-	-	-
10-7-72	9 pm	1.75	2.25	2.40	2.25	1.45	-	1.00	1.45
10-7-72	2 pm	1.65	2.30	2.45	2.35	1.50	-	1.15	1.70
10-10-72	3 pm	1.45	2.00	2.10	2.05	1.20	0.75	0.75	1.30
10-11-72	7 pm	1.40	2.05	2.20	2.15	1.35	0.70	0.90	1.50
10-13-72[c]	7 pm	1.15	2.10	2.30	2.15	1.15	0.80	0.95	1.45
10-19-72	10 am	1.15	1.30	1.90	1.75	0.55	-	0.50	0.90
10-23-72	2 pm	1.30	1.75	2.10	2.15	0.45	0.80	0.60	1.30
10-24-72	10 am	1.15	1.55	2.05	2.00	0.55	0.55	0.45	1.20
10-24-72	5 pm	1.05	1.45	2.00	2.00	0.45	0.65	0.45	1.20
10-25-72[d]	11 am	1.00	1.50	2.00	2.00	0.35	0.50	0.45	1.15
10-25-72	7 pm	1.05	1.55	2.00	2.05	0.40	0.60	0.50	1.20
10-28-72	11 am	1.05	1.50	2.00	2.00	0.40	0.70	0.40	1.15
10-28-72	12 noon	1.20	1.55	2.05	1.80	-	0.65	0.30	1.00
11-1-72	3 pm	1.00	1.35	1.80	1.95	1.25	0.95	0.40	0.95
11-2-72	3 pm	1.10	1.70	2.10	2.15	1.35	1.55	0.70	1.35
11-3-72	3 pm	1.00	1.50	2.05	2.05	1.25	1.30	0.60	1.15
11-8-72	2 pm	1.20	1.35	1.80	1.85	1.30	0.65	0.55	1.10
11-14-72	4 pm	1.00	1.40	1.90	1.85	1.15	0.60	0.65	1.10
11-21-72	2 pm	1.15	1.30	1.85	1.80	1.25	0.50	0.45	0.85
12-12-72	12 noon	0.60	1.15	1.80	1.65	1.10	0.55	0.35	0.95
12-29-72	3 pm	0.35	1.30	1.95	1.90	0.90	0.40	0.35	1.00
2-10-73	-	0.15	0.90	1.70	1.60	1.10	0.30	0.20	0.40
4-7-73[e]	-	0.75	1.20	1.90	1.80	1.15	0.55	0.75	0.75
6-14-73[f]	-	2.75	2.15	2.40	2.15	1.65	1.05	1.45	2.00

[a] Drilling rig near G5-7 at time of reading.

[b] After six days rain.

[c] 3:4 slope completed.

[d] 1:8 slope completed.

[e] Ten feet water in trench.

[f] Two months after trench filled with fresh papermill sludge.

TABLE D-3. PORE WATER PRESSURES FOR THE LOWER AND MIDDLE SAND BLANKETS

Date mo-dy-yr	Time	Pore water pressure in psi for piezometer			
		G5-1	G7-1	G5-5	G7-5
8-1-72	-	0.30	0.30	1.50	1.10
9-11-72	-	0.50	0.35	1.90	1.50
9-19-72	-	-	0.35	-	-
9-25-72	-	0.32	-	0.55	0.45
9-30-72[a]	-	0.35	-	0.90	0.65
10-2-72	-	0.45	-	1.00	0.60
10-3-72	2 pm	0.32	-	1.00	0.70
10-3-72	6 pm	-	-	-	-
10-4-72	2 pm	0.10	-	1.05	0.60
10-4-72	6 pm	-	-	-	-
10-5-72	7 pm	-	-	-	-
10-7-72	9 am	0.20	0.15	0.70	0.40
10-7-72	2 pm	0.30	-	0.75	0.45
10-10-72	3 pm	0.35	-	0.55	-
10-11-72	7 pm	0.40	-	0.50	-
10-13-72[b]	7 pm	0.30	-	0.30	-
10-19-72	10 am	0.25	-	0.20	-
10-23-72	2 pm	0.40	-	0.25	-
10-24-72	10 am	0.00	-	0.35	-
10-24-72	5 pm	0.20	-	0.30	-
10-25-72[c]	11 am	0.10	-	0.30	-
10-25-72	7 pm	0.35	-	0.35	-
10-26-72	11 am	0.15	-	0.30	-
10-28-72	12 noon	0.20	-	0.25	-
11-1-72	3 pm	0.60	-	0.30	-
11-2-72	3 pm	0.55	-	0.35	-
11-3-72	3 pm	0.30	0.10	0.35	-
11-8-72	2 pm	0.30	-	0.30	-
11-14-72	4 pm	0.30	-	0.25	-
11-21-72	2 pm	0.20	-	0.35	-
12-12-72	12 noon	0.35	0.25	0.25	-
12-29-72	3 pm	0.40	-	0.15	-
2-6-73	-	0.40	0.00	0.00	
4-7-73[d]	-	0.51	0.00	0.20	-
6-14-73[e]	-	0.50	0.10	2.15	-

[a]After six days rain.

[b]3:4 slope completed.

[c]1:8 slope completed.

[d]Ten feet water in trench.

[e]Two months after trench filled with fresh papermill sludge.

APPENDIX E

TABLE E-1. TEMPERATURE DATA FOR THE PAPERMILL SLUDGE LANDFILL

Thermistor No.	1		2		3		4		5	
Elevation, ft.	95.43		93.43		91.43		89.43		87.43	
Date mo-da-yr	I[a]	T[b]	I	T	I	T	I	T	I	T
9- 6-72	2.16	26.0	malfunction		2.36	23.9	2.72	20.7	2.90	19.3
9-11-72	2.52	23.5			2.50	23.7	2.74	20.6	2.89	19.3
10- 7-72	2.81	20.0			2.53	22.4	2.71	20.8	2.86	19.6
10-19-72	3.33	16.3			2.71	20.8	2.75	20.5	2.82	20.0
11- 3-72	3.70	14.0			3.04	18.2	2.91	19.2	2.87	19.5
11-21-72	4.86	8.3			3.40	15.9	3.08	17.9	2.95	18.9
12-12-72	5.79	4.7			3.93	12.7	3.37	16.1	3.10	17.8
2-10-73	6.02	4.0			4.84	8.4	4.13	11.6	3.60	14.6
4- 7-73	4.76	8.8			4.55	9.6	4.35	10.6	3.97	12.4
6-14-73	2.52	23.5			3.55	15.0	3.95	12.6	3.94	12.7
Thermistor No.	6		7		8		9		0	
Elevation, ft.	85.43		83.43		81.43		69.43		77.43	
Date mo-da-yr	I	T	I	T	I	T	I	T	I	T
9- 6-72	3.10	17.8	3.10	17.8	3.19	17.2	3.28	16.0	3.48	15.4
9-11-72	3.09	17.9	3.12	17.7	3.24	16.8	3.35	16.2	3.50	15.3
10- 7-72	3.04	18.2	3.06	18.1	3.19	17.2	3.13	16.5	3.51	15.2
10-19-72	3.01	18.5	3.06	18.1	3.19	17.2	3.32	16.4	3.51	15.2
11- 3-72	3.02	18.4	3.07	18.0	3.21	17.1	3.34	16.3	3.51	15.2
11-21-72	3.03	18.3	3.06	18.1	3.20	17.2	3.33	16.3	3.53	15.0
12-12-72	3.10	17.8	3.08	17.9	3.19	17.2	3.33	16.3	3.54	15.0
2-10-73	3.39	15.9	3.28	16.6	3.28	16.6	3.35	16.2	3.55	14.9
4- 7-73	3.74	13.8	3.54	15.0	3.49	15.3	3.39	16.0	3.55	14.9
6-14-73	3.94	12.7	3.83	13.3	3.79	13.5	3.76	13.7	3.95	12.6

[a]Instrument reading (K - ohms)

[b]Temperature (degrees Centigrade)

APPENDIX F

TABLE F-1. VANE SHEAR STRENGTH DATA, September 7, 1972

Elevation (ft)	Undisturbed		Remolded	
	Torque (kg-cm)	Shear strength (T/m^2)	Torque (kg-cm)	Shear strength (T/m^2)
93.3	210	6.11	140	4.07
92.5	220	6.40	110	3.20
91.5	230	6.69	200	5.82
90.5	255	7.42	180	5.23
89.5	275	8.00	210	6.12
88.5	305	8.87	240	6.98
87.5	360	10.47	245	7.12
86.5	380	11.05	310	9.01
85.5	455	13.23	220	6.40
84.5	420	12.21	335	9.74
83.5	420	12.21	320	9.31
82.5	480	13.96	340	9.89
81.5	560	16.28	380	11.05
80.5	600	17.45	300	8.72
79.5	680	19.77	320	9.31
78.5	610	17.74	380	11.05

2-in. O.D. Acker vane; hole augered to within 6-in. of test depth using hollow stem augers; vane pushed to test depth and rotated 360-degrees for maximum torque; vane rotated 25-times before reading remolded maximum torque.

TABLE F-2. VANE SHEAR STRENGTH DATA, October 6, 1972

Elev. ft.	Undisturbed				Remolded			
	Vertical		Horizontal		Vertical		Horizontal	
	Torque kg-cm	Shear strength T/m^2	Torque kg-cm	Shear strength T/m^2	Torque kg-cm	Shear strength T/m^2	Torque kg-cm	Shear strength T/m^2
92.0	310	6.20	330	6.60	120	2.40	100	2.00
90.5	310	6.20	320	6.40	170	3.40	140	2.80
89.9	280	5.60	305	6.10				
87.9	330	6.60	350	7.00				
87.5*	350	7.00	395	7.90	160	3.20	180	3.60
83.4	440	8.80	455	9.10				
83.4	440	8.80	475	9.50			255	5.10

60.0-mm diameter Geonor vane; tests conducted within 2-to 3-ft from 3:4 slope surface, 1- to 2-days after completion of slope excavation.

*Adjacent to block sample C.

TABLE F-3. DUTCH CONE PENETRATION RESULTS, September 7, 1972

Elevation (ft)	Average load (kg)	Cone resistance (kg/cm^2)
93.3	83.91	8.39
92.5	59.42	5.94
91.5	59.87	5.99
90.5	60.33	6.03
89.5	60.78	6.08
88.5	61.23	6.12
87.5	93.44	9.34
86.5	80.29	8.03
85.5	105.69	10.57
84.5	101.60	10.16
83.5	95.25	9.53
82.5	107.05	10.70
81.5	121.11	12.11
80.5	166.92	16.69
79.5	167.38	16.74
78.5	113.40	11.34

10-sq cm, 60-degree Dutch cone; hole augered to within 1-ft of test elevation with hollow stem auger; cone and casing pushed to test elevation; cone tip pushed 2-in, independently of casing, with average load recorded.

APPENDIX G

TABLE G-1. TOTAL PRESSURE CELL DATA

Total pressure cell No.	G7-1 Horizontal			G7-2 Vertical			G7-3 Vertical		
Date mo-da-yr	I[a]	W[b]	S[c]	I	W	S	I	W	S
9- 6-72	17.3	12.7	14.3	14.9	10.3	11.6	9.75	5.2	5.9
9-30-72	17.25	12.6	14.2	15.0	10.4	11.7	9.5	5.0	5.6
10- 7-72	17.25	12.6	14.2	15.0	10.4	11.7	8.5	4.0	4.5
10-19-72	17.25	12.6	14.2	15.75	11.1	12.6	8.9	4.4	4.9
11- 3-72	17.25	12.6	14.2	15.0	10.4	11.7	9.0	4.5	5.0
11-21-72	17.25	12.6	14.2	16.0	11.4	12.8	8.75	4.2	4.7
2-10-73	17.60	13.0	14.6	see note			9.40	4.9	5.5
4- 7-73	17.6	13.0	14.6				9.40	4.9	5.5
6-14-73	17.40	12.8	14.4				9.4	4.9	5.5

[a]Instrument reading.

[b]W - total pressure, water calibration, psi.

[c]S - total pressure, sand calibration, psi.

Cell G7-2 gave erratic data beginning about 12-15-71.

Piezometer G7-3 was located adjacent to the total pressure cells.

APPENDIX H

TABLE H-1. AVERAGE DAILY TEMPERATURE AND PRECIPITATION

Date	Average temp. (^{o}F)	Pre-cipitation (in.)	Date	Average temp. (^{o}F)	Pre-cipitation (in.)	Date	Average temp. (^{o}F)	Pre-cipitation (in.)
September 1971			October 1971			November 1971		
1	73	0	1	76	0	1	59	0
2	73	.25	2	74	0	2	59	.16
3	72	1.24	3	75	0	3	49	T
4	76	T	4	69	0	4	40	0
5	77	0	5	63	T	5	49	0
6	75	.80	6	61	T	6	43	.22
7	75	0	7	51	0	7	26	0
8	75	0	8	54	T	8	28	0
9	75	0	9	56	.67	9	34	.06
10	75	0	10	48	.03	10	38	0
11	67	.05	11	57	0	11	41	0
12	66	0	12	53	0	12	47	0
13	63	0	13	62	.32	13	52	0
14	64	0	14	58	0	14	57	0
15	67	.02	15	65	0	15	63	0
16	63	T	16	65	.60	16	52	0
17	63	0	17	65	0	17	57	0
18	63	0	18	66	0	18	61	T
19	65	T	19	64	0	19	51	.41
20	58	.97	20	68	0	20	43	T
21	55	0	21	65	.10	21	36	T
22	60	0	22	66	.14	22	29	0
23	62	0	23	65	.10	23	26	.01
24	57	0	24	64	.21	24	31	.02
25	57	.36	25	64	0	25	34	0
26	68	.09	26	63	0	26	34	.05
27	75	0	27	65	0	27	41	.23
28	78	0	28	63	0	28	35	0
29	79	0	29	65	0	29	41	.36
30	77	0	30	65	0	30	33	.03
			31	62	0			

Source: Local climatological data from Dayton, Ohio, municipal airport
T = trace of precipitation.

TABLE H-1. AVERAGE DAILY TEMPERATURE AND PRECIPITATION (continued)

Date	Average temp. (°F)	Pre-cipitation (in.)	Date	Average temp. (°F)	Pre-cipitation (in.)	Date	Average temp. (°F)	Pre-cipitation (in.)
December 1971			January 1972			February 1972		
1	28	0	1	36	.01	1	27	0
2	28	0	2	35	.19	2	34	.01
3	26	0	3	35	0	3	26	.19
4	33	0	4	31	.38	4	9	.03
5	41	.13	5	17	.05	5	15	0
6	50	.69	6	18	0	6	25	.25
7	47	.39	7	28	0	7	9	T
8	45	0	8	28	0	8	7	T
9	48	T	9	42	.21	9	11	.04
10	59	.05	10	43	T	10	14	0
11	42	0	11	36	0	11	29	T
12	40	0	12	37	0	12	37	.03
13	36	0	13	35	.16	13	35	.08
14	43	.86	14	12	0	14	37	0
15	55	.21	15	- 6	0	15	38	.03
16	43	0	16	- 1	0	16	32	0
17	27	.04	17	27	0	17	37	.01
18	19	T	18	43	.07	18	31	.09
19	31	.18	19	41	.01	19	23	.03
20	38	.05	20	44	.01	20	22	0
21	35	0	21	35	0	21	40	0
22	30	0	22	47	.19	22	27	T
23	37	0	23	39	.07	23	29	.04
24	40	0	24	47	.02	24	34	0
25	41	.01	25	24	0	25	34	.01
26	52	.05	26	21	0	26	31	.01
27	54	.07	27	17	.10	27	33	0
28	35	.03	28	12	T	28	48	0
29	29	.04	29	11	0	29	53	0
30	47	1.00	30	11	0			
31	30	0	31	15	0			

Source: Local climatological data from Dayton, Ohio, municipal airport.
T = trace of precipitation.

TABLE II-1. AVERAGE DAILY TEMPERATURE AND PRECIPITATION (continued)

Date	Average temp. (°F)	Precipitation (in.)	Date	Average temp. (°F)	Precipitation (in.)	Date	Average temp. (°F)	Precipitation (in.)
March 1972			April 1972			May 1972		
1	58	.55	1	36	.01	1	66	.04
2	40	.41	2	35	.02	2	66	0
3	23	T	3	37	.17	3	55	0
4	29	.02	4	41	.08	4	53	T
5	20	T	5	46	0	5	56	0
6	26	0	6	57	.22	6	68	0
7	43	.09	7	33	.87	7	69	.22
8	24	T	8	23	T	8	55	1.05
9	23	0	9	34	0	9	49	.21
10	23	0	10	48	T	10	48	0
11	46	0	11	58	.01	11	55	0
12	56	0	12	60	.30	12	61	0
13	50	.35	13	67	.04	13	60	.85
14	34	T	14	58	0	14	66	.46
15	37	.04	15	67	.03	15	60	.34
16	45	.42	16	60	.80	16	58	.02
17	39	.06	17	56	0	17	62	0
18	32	0	18	60	0	18	65	0
19	35	0	19	64	.26	19	67	0
20	48	0	20	55	.22	20	66	T
21	58	.38	21	49	.43	21	67	0
22	42	.09	22	57	T	22	70	0
23	27	T	23	54	.09	23	71	0
24	27	T	24	47	0	24	70	0
25	29	0	25	41	0	25	71	0
26	33	T	26	47	0	26	66	0
27	41	T	27	50	0	27	65	0
28	39	0	28	53	0	28	66	0
29	39	.05	29	61	.10	29	68	.03
30	38	T	30	62	.12	30	60	1.10
31	40	0				31	48	.02

Source: Local climatological data from Dayton, Ohio, municipal airport.
T = trace of precipitation.

TABLE H-1. AVERAGE DAILY TEMPERATURE AND PRECIPITATION (continued)

Date	Average temp. (°F)	Pre-cipitation (in.)	Date	Average temp. (°F)	Pre-cipitation (in.)	Date	Average temp. (°F)	Pre-cipitation (in.)
June 1972			July 1972			August 1972		
1	57	0	1	76	0	1	72	0
2	70	0	2	75	.01	2	76	.37
3	73	.03	3	68	.41	3	74	.04
4	78	0	4	62	.04	4	67	T
5	71	0	5	61	.02	5	63	0
6	70	.20	6	59	0	6	63	.06
7	67	0	7	63	0	7	66	.04
8	69	0	8	70	.04	8	65	.25
9	74	.23	9	74	0	9	63	0
10	57	0	10	77	T	10	65	0
11	56	0	11	80	.34	11	67	0
12	67	T	12	79	0	12	75	.12
13	71	1.67	13	79	0	13	75	0
14	79	T	14	82	0	14	76	.02
15	71	.43	15	76	.67	15	71	0
16	69	0	16	75	.03	16	72	0
17	64	0	17	76	0	17	82	0
18	69	0	18	82	.36	18	85	0
19	76	0	19	81	0	19	77	.36
20	72	T	20	84	0	20	75	0
21	62	T	21	86	0	21	75	0
22	55	T	22	85	0	22	77	.90
23	52	.17	23	84	T	23	79	.39
24	53	T	24	78	.16	24	77	.21
25	62	0	25	76	0	25	77	0
26	68	0	26	70	0	26	75	.32
27	71	0	27	76	0	27	68	.05
28	71	T	28	72	0	28	72	0
29	69	.31	29	70	0	29	72	0
30	70	T	30	71	0	30	73	0
			31	77	0	31	72	0

Source: Local climatological data from Dayton, Ohio, municipal airport.
T = trace of precipitation.

TABLE H-1. AVERAGE DAILY TEMPERATURE AND PRECIPITATION (continued)

Date	Average temp. (°F)	Pre-cipitation (in.)	Date	Average temp. (°F)	Pre-cipitation (in.)	Date	Average temp. (°F)	Pre-cipitation (in.)
September 1972			October 1972			November 1972		
1	77	T	1	50	0	1	57	.67
2	69	0	2	60	0	2	60	.90
3	60	.88	3	64	0	3	48	0
4	65	0	4	59	.86	4	44	T
5	64	T	5	62	.15	5	45	0
6	65	0	6	60	0	6	49	0
7	70	0	7	53	.02	7	51	1.10
8	69	T	8	57	0	8	41	.01
9	62	0	9	49	0	9	41	0
10	61	0	10	50	0	10	44	.18
11	71	.05	11	56	.09	11	45	.01
12	76	.99	12	59	.15	12	42	0
13	79	0	13	52	0	13	41	1.06
14	67	.26	14	52	0	14	36	.31
15	66	0	15	44	0	15	31	T
16	65	0	16	49	T	16	34	0
17	76	0	17	45	0	17	31	0
18	71	.55	18	35	.08	18	38	0
19	68	0	19	37	0	19	36	.40
20	66	0	20	40	0	20	35	T
21	65	.10	21	47	T	21	32	T
22	57	0	22	59	.06	22	34	.04
23	57	.22	23	58	.15	23	30	T
24	68	.48	24	44	.03	24	32	0
25	71	.22	25	41	0	25	34	.13
26	70	.24	26	46	0	26	34	.07
27	62	.06	27	51	.11	27	38	.10
28	62	T	28	56	.09	28	31	.02
29	57	.34	29	48	.02	29	31	0
30	45	.25	30	45	0	30	34	T
			31	44	.41			

Source: Local climatological data from Dayton, Ohio, municipal airport.
T = trace of precipitation.

TABLE II-1. AVERAGE DAILY TEMPERATURE AND PRECIPITATION (continued)

Date	Average temp. (°F)	Pre-cipitation (in.)	Date	Average temp. (°F)	Pre-cipitation (in.)	Date	Average temp. (°F)	Pre-cipitation (in.)
December 1972			January 1973			February 1973		
1	39	T	1	31	0	1	47	.22
2	44	0	2	29	0	2	46	.09
3	40	T	3	37	.53	3	35	T
4	36	.01	4	34	T	4	43	0
5	48	T	5	23	T	5	46	T
6	40	.51	6	21	T	6	45	0
7	18	T	7	22	0	7	36	.05
8	33	.76	8	19	0	8	25	.20
9	33	.01	9	16	T	9	18	0
10	24	T	10	12	0	10	17	T
11	19	.05	11	14	T	11	19	0
12	44	.22	12	19	0	12	26	0
13	30	.04	13	28	0	13	34	.02
14	27	0	14	35	.18	14	38	.40
15	21	.35	15	34	T	15	28	.13
16	7	.02	16	41	0	16	9	T
17	10	0	17	50	0	17	11	0
18	28	0	18	53	.01	18	23	0
19	39	.31	19	42	.04	19	38	0
20	40	.02	20	29	0	20	35	.02
21	39	0	21	34	.28	21	29	.02
22	36	T	22	45	.10	22	24	T
23	38	0	23	32	T	23	29	T
24	39	0	24	34	0	24	35	0
25	35	0	25	42	0	25	42	T
26	33	.09	26	43	.07	26	35	.13
27	30	0	27	43	.07	27	31	0
28	33	0	28	35	.33	28	35	0
29	42	T	29	21	.02			
30	57	.13	30	25	0			
31	46	.29	31	34	0			

Source: Local climatological data from Dayton, Ohio, municipal airport.
T = trace of precipitation.

TABLE H-1. AVERAGE DAILY TEMPERATURE AND PRECIPITATION (continued)

Date	Average temp. (^oF)	Pre-cipitation (in.)	Date	Average temp. (^oF)	Pre-cipitation (in.)	Date	Average temp. (^oF)	Pre-cipitation (in.)
March 1973			April 1973			May 1973		
1	49	0	1	53	.05	1	66	.03
2	52	.04	2	45	T	2	60	.27
3	53	.02	3	43	T	3	48	.02
4	55	.06	4	38	.70	4	48	T
5	60	.10	5	40	T	5	49	0
6	59	0	6	50	0	6	55	0
7	56	.19	7	49	.20	7	60	.03
8	52	0	8	46	.06	8	67	1.11
9	43	.18	9	44	.30	9	67	.01
10	62	.07	10	34	.06	10	67	T
11	62	.79	11	34	T	11	62	0
12	47	.01	12	38	.16	12	56	.01
13	54	0	13	38	0	13	51	T
14	64	.55	14	42	0	14	50	.05
15	63	0	15	55	0	15	46	0
16	48	.65	16	56	.32	16	55	.02
17	34	.39	17	51	.22	17	46	T
18	33	0	18	62	.23	18	52	T
19	34	0	19	65	.10	19	58	.68
20	33	0	20	71	T	20	59	T
21	33	0	21	72	0	21	61	0
22	33	0	22	67	.01	22	68	.02
23	36	0	23	58	.33	23	69	T
24	47	0	24	59	0	24	62	0
25	51	.80	25	50	T	25	66	.25
26	44	.19	26	52	0	26	63	.24
27	44	0	27	47	.56	27	66	.27
28	48	T	28	47	0	28	67	.02
29	56	.41	29	52	T	29	65	.07
30	53	T	30	63	.15	30	61	T
31	55	.19				31	59	0

Source: Local climatological data from Dayton, Ohio, municipal airport.
T = trace of precipitation.

APPENDIX I

TABLE I-1. TRIAXIAL TEST DATA, SAMPLE U-1-10

Axial consolidation pressure = 0.703 kg/cm^2 with K_o = 1

σ_{1_f} = 3.146 kg/cm^2

σ_{3_f} = 2.109 kg/cm^2

u_f = 2.123 kg/cm^2

A_f = 0.69

Initial water content = 182.9%

Final water content = 116.2%

Initial dry density = 25.91 pcf

c_u = 0.519 kg/cm^2

Load (kg)	Displacement (cm)	Pore pressure (kg/cm^2)	Axial strain	$\bar{\sigma}_1$ (kg/cm^2)	$\bar{\sigma}_3$ (kg/cm^2)
0.0000	0.0000	1.4061	0.0000	0.7031	0.7031
3.4474	0.0737	1.5116	0.0124	1.0211	0.5976
4.3546	0.1473	1.7787	0.0248	0.8586	0.3304
4.5814	0.2256	1.8631	0.0380	0.7943	0.2461
5.2164	0.2972	1.9053	0.0501	0.8203	0.2039
5.4432	0.3734	1.9334	0.0629	0.8102	0.1758
5,8968	0.4470	1.9615	0.0753	0.8259	0.1476
6.3050	0.5207	1.9861	0.0877	0.8385	0.1230
6.3504	0.5944	2.0037	0.1001	0.8163	0.1055
6.8040	0.6706	2.0213	0.1130	0.8386	0.0879
7.2576	0.7442	2.0389	0.1254	0.8599	0.0703
7.6205	0.8179	2.0529	0.1378	0.8735	0.0562
8.1648	0.8941	2.0740	0.1506	0.8978	0.0352
8.7091	0.9677	2.0881	0.1630	0.9278	0.0211
9.1174	1.0414	2.1022	0.1754	0.9421	0.0070
9.8431	1.1176	2.1092	0.1883	0.9938	0.0000
10.4328	1.1913	2.1232	0.2007	1.0232	-0.0141

$\bar{\sigma}_1$ and $\bar{\sigma}_3$ equal the major and minor effective principal stresses, respectively. Failure taken at maximum deviator stress or at 20 percent axial strain.

TABLE I-3. TRIAXIAL TEST DATA, SAMPLE U-1-11

Axial consolidation pressure = 1.406 kg/cm^2 with K_o = 1

σ_{1_f} = 4.479 kg/cm^2	Initial water content = 200.0%
σ_{3_f} = 2.812 kg/cm^2	Final water content = 101.2%
u_f = 2.714 kg/cm^2	Initial dry density = 26.53 pcf
A_f = 0.78	c_u = 0.833 kg/cm^2

Load (kg)	Displacement (cm)	Pore pressure (kg/cm^2)	Axial strain	$\bar{\sigma}_1$ (kg/cm^2)	$\bar{\sigma}_3$ (kg/cm^2)
0.0000	0.0000	1.4061	0.0000	1.4062	1.4062
5.4432	0.0737	1.6241	0.0133	1.8385	1.1882
8.2555	0.1473	1.9264	0.0266	1.8589	0.8859
8.9813	0.2256	2.1092	0.0407	1.7463	0.7031
9.1627	0.2972	2.2146	0.0536	1.6476	0.5976
10.0699	0.3734	2.2920	0.673	1.6575	0.5203
10.8864	0.4470	2.3623	0.0806	1.6619	0.4500
11.5668	0.5207	2.4256	0.0939	1.6558	0.3867
11.9750	0.5944	2.4678	0.1071	1.6391	0.3445
12.7008	0.6706	2.5170	0.1209	1.6472	0.2953
13.5173	0.7442	2.5521	0.1342	1.6773	0.2601
14.0162	0.8179	2.5873	0.1474	1.6719	0.2250
14.6059	0.8941	2.6154	0.1612	1.6803	0.1969
15.4224	0.9677	2.6506	0.1745	1.7033	0.1617
16.3296	1.0414	2.6857	0.1877	1.7326	0.1266
17.2368	1.1176	2.7138	0.2015	1.7650	0.0984

$\bar{\sigma}_1$ and $\bar{\sigma}_3$ equal the major and minor effective principal stresses, respectively.
Failure taken at maximum deviator stress or at 20 percent axial strain.

TABLE I-3. TRIAXIAL TEST DATA, SAMPLE U-1-12

Axial consolidation pressure = 2.109 kg/cm^2 with K_o = 1

σ_{1_f} = 5.919 kg/cm^2	Initial water content = 194.4%
σ_{3_f} = 3.515 kg/cm^2	Final water content = 94.3%
u_f = 3.452 kg/cm^2	Initial dry density = 25.75 pcf
A_f = 0.85	c_u = 1.265 kg/cm^2

Load (kg)	Displacement (cm)	Pore pressure (kg/cm^2)	Axial strain	$\bar{\sigma}_1$ (kg/cm^2)	$\bar{\sigma}_3$ (kg/cm^2)
0.0000	0.0000	1.4061	0.0000	2.1092	2.1092
7.2576	0.0737	1.6170	0.0147	2.7554	1.8983
10.7957	0.1473	1.9404	0.0294	2.8308	1.5749
12.2472	0.2256	2.2428	0.0450	2.6744	1.2726
13.6080	0.2972	2.4678	0.0592	2.5819	1.0476
14.6059	0.3734	2.6506	0.0744	2.4850	0.8648
15.7399	0.4470	2.7982	0.0891	2.4355	0.7171
16.6471	0.5207	2.9177	0.1038	2.3857	0.5976
17.7811	0.5944	3.0232	0.1185	2.3707	0.4922
18.9605	0.6706	3.1076	0.1337	2.3764	0.4078
19.9584	0.7442	3.1990	0.1484	2.3535	0.3164
21.3192	0.8179	3.2693	0.1630	2.3846	0.2461
22.5893	0.8941	3.3396	0.1782	2.4006	0.1758
23.6779	0.9677	3.3958	0.1929	2.4099	0.1195
25.3109	1.0414	3.4521	0.2076	2.4670	0.0633

$\bar{\sigma}_1$ and $\bar{\sigma}_3$ equal the major and minor effective principal stresses, respectively.
Failure taken at maximum deviator stress or at 20 percent axial strain.

TABLE I-4. TRIAXIAL TEST DATA, SAMPLE U-1-13

Axial consolidation pressure = 3.515 kg/cm^2 with K_o = 1

σ_{1_f} = 8.768 kg/cm^2	Initial water content = 180.2%
σ_{3_f} = 4.921 kg/cm^2	Final water content = 84.2%
u_f = 4.668 kg/cm^2	Initial dry density = 27.47 pcf
A_f = 0.85	c_u = 1.923 kg/cm^2

Load (kg)	Displacement (cm)	Pore pressure (kg/cm^2)	Axial strain	$\bar{\sigma}_1$ (kg/cm^2)	$\bar{\sigma}_3$ (kg/cm^2)
0.0000	0.0000	1.4061	0.0000	3.5154	3.5154
15.4224	0.0762	2.0389	0.0157	4.7638	2.8826
18.8244	0.1524	2.6576	0.0314	4.5234	2.2639
20.8656	0.2286	3.0865	0.0471	4.2990	1.8350
22.7707	0.3048	3.4099	0.0628	4.1562	1.5116
24.4944	0.3810	3.6560	0.0785	4.0626	1.2655
26.3088	0.4572	3.8528	0.0943	4.0217	1.0687
27.7603	0.5334	4.0075	0.1100	3.9759	0.9140
29.2572	0.6096	4.1581	0.1257	3.9434	0.7734
30.9355	0.6858	4.2747	0.1414	3.9385	0.6468
31.8881	0.7620	4.3590	0.1571	3.8934	0.5625
34.8365	0.8382	4.4926	0.1728	4.0000	0.4289
36.7416	0.9144	4.5770	0.1885	4.0394	0.3445
39.0096	0.9906	4.6684	0.2042	4.1001	0.2531

$\bar{\sigma}_1$ and $\bar{\sigma}_3$ equal the major and minor effective principal stresses, respectively.
Failure taken at maximum deviator stress or at 20 percent axial strain.

TABLE I-5. TRIAXIAL TEST DATA, SAMPLE U-2-21

Axial consolidation pressure = 3.515 kg/cm^2 with K_o = 1

σ_{1_f} = 9.086 kg/cm^2		Initial water content	= 215.0%
σ_{3_f} = 4.921 kg/cm^2		Final water content	= 94.2%
u_f = 4.711 kg/cm^2		Initial dry density	= 23.86 pcf
A_f = 0.79		c_u = 2.082 kg/cm^2	

Load (kg)	Displacement (cm)	Pore pressure (kg/cm^2)	Axial strain	$\bar{\sigma}_1$ (kg/cm^2)	$\bar{\sigma}_3$ (kg/cm^2)
0.0000	0.0000	1.4061	0.0000	3.5154	3.5154
15.1956	0.0762	1.9826	0.0156	4.9064	2.9389
19.0512	0.1524	2.6295	0.0311	4.7198	2.2920
21.3192	0.2286	3.1005	0.0467	4.4941	1.8210
23.5872	0.3048	3.4380	0.0622	4.3927	1.4835
25.4016	0.3810	3.6911	0.0778	4.3114	1.2304
26.9892	0.4572	3.8739	0.0934	4.2659	1.0476
28.4407	0.5334	4.0427	0.1089	4.2121	0.8789
30.1644	0.6096	4.1833	0.1245	4.2117	0.7382
31.7520	0.6858	4.3028	0.1401	4.2100	0.6187
33.5664	0.7620	4.4153	0.1556	4.2341	0.5062
35.2901	0.8382	4.4997	0.1712	4.2689	0.4218
37.1952	0.9144	4.6051	0.1867	4.2950	0.3164
39.6900	0.9906	4.7106	0.2023	4.3751	0.2109

$\bar{\sigma}_1$ and $\bar{\sigma}_3$ equal the major and minor effective principal stresses, respectively. Failure taken at maximum deviator stress or at 20 percent axial strain.

TABLE I-6. TRIAXIAL TEST DATA, SAMPLE U-3-1

Axial consolidation pressure = 0.703 kg/cm^2 with K_o = 1

σ_{1_f} = 3.017 kg/cm^2	Initial water content = 310.0%
σ_{3_f} = 2.109 kg/cm^2	Final Water content = 150.9%
u_f = 2.109 kg/cm^2	Initial dry density = 18.94 pcf
A_f = 0.77	c_u = 0.454 kg/cm^2

Load (kg)	Displacement (cm)	Pore pressure (kg/cm^2)	Axial strain	$\bar{\sigma}_1$ (kg/cm^2)	$\bar{\sigma}_3$ (kg/cm^2)
0.0000	0.0000	1.4061	0.0000	0.7031	0.7031
2.9484	0.0483	1.5678	0.0106	0.8242	0.5414
4.1278	0.1194	1.7014	0.0262	0.7975	0.4078
4.8989	0.1753	1.8139	0.0385	0.7520	0.2953
5.3525	0.2337	1.8842	0.0514	0.7173	0.2250
5.5339	0.2921	1.9053	0.0642	0.7060	0.2039
6.2143	0.3505	1.9545	0.0770	0.7108	0.1547
6.6679	0.4089	1.9721	0.0899	0.7256	0.1371
7.0308	0.4674	2.0037	0.1027	0.7172	0.1055
7.5298	0.5258	2.0389	0.1156	0.7161	0.0703
7.9380	0.5817	2.0459	0.1278	0.7346	0.0633
8.5277	0.6401	2.0730	0.1407	0.7456	0.0352
9.0720	0.6985	2.0811	0.1535	0.7727	0.0281
9.5256	0.7315	2.0951	0.1608	0.7892	0.0141
10.3421	0.8153	2.0986	0.1792	0.8337	0.0105
11.1132	0.8738	2.1057	0.1921	0.8742	0.0035
11.7029	0.9093	2.1092	0.1999	0.9080	0.0000
12.8369	0.9906	2.1092	0.2177	0.9737	0.0000

$\bar{\sigma}_1$ and $\bar{\sigma}_3$ equal the major and minor effective principal stresses, respectively.
Failure taken at maximum deviator stress or at 20 percent axial strain.

TABLE I-7. TRIAXIAL TEST DATA, SAMPLE U-3-2

Axial consolidation pressure = 0.703 kg/cm^2 with K_o = 1

σ_{1_f} = 3.351 kg/cm^2	Initial water content	=	306.0%
σ_{3_f} = 2.109 kg/cm^2	Final water content	=	147.4%
u_f = 2.151 kg/cm^2	Initial dry density	=	18.39 pcf
A_f = 0.60	c_u = 0.621 kg/cm^2		

Load (kg)	Displacement (cm)	Pore pressure (kg/cm^2)	Axial strain	$\bar{\sigma}_1$ (kg/cm^2)	$\bar{\sigma}_3$ (kg/cm^2)
0.0000	0.0000	1.4061	0.0000	0.7031	0.7031
3.8556	0.0686	1.7506	0.0161	0.7349	0.3586
5.4432	0.1499	1.8701	0.0352	0.7600	0.2390
6.4411	0.2134	1.9475	0.0501	0.7686	0.1617
7.2576	0.2819	2.0037	0.0662	0.7777	0.1055
8.1648	0.3632	2.0459	0.0853	0.8041	0.0633
9.0720	0.4293	2.0775	0.1008	0.8408	0.0316
9.7524	0.4978	2.1057	0.1169	0.8578	0.0035
10.8864	0.5791	2.1232	0.1360	0.9190	-0.0141
11.5668	0.6375	2.1373	0.1497	0.9475	-0.0281
12.7008	0.7087	2.1443	0.1664	1.0150	-0.0352
14.2884	0.7798	2.1479	0.1832	1.1191	-0.0387
15.6492	0.8509	2.1514	0.1999	1.1999	-0.0422

$\bar{\sigma}_1$ and $\bar{\sigma}_3$ equal the major and minor effective principal stresses, respectively.
Failure taken at maximum deviator stress or at 20 percent axial strain.

TABLE I-9. TRIAXIAL TEST DATA, SAMPLE U-3-5

Axial consolidation pressure = 3.515 kg/cm^2 with K_o = 1

σ_{1_f} = 7.966 kg/cm^2		Initial water content	= 255.0%
σ_{3_f} = 4.921 kg/cm^2		Final water content	= 97.5%
u_f = 4.696 kg/cm^2		Initial dry density	= 20.32 pcf
A_f = 1.08		c_u = 1.522 kg/cm^2	

Load (kg)	Displacement (cm)	Pore pressure (kg/cm^2)	Axial strain	$\bar{\sigma}_1$ (kg/cm^2)	$\bar{\sigma}_3$ (kg/cm^2)
0.0000	0.0000	1.4061	0.0000	3.5154	3.5154
7.3483	0.0762	2.0334	0.0163	3.9938	2.9881
10.7957	0.1524	2.4010	0.0327	3.9736	2.5205
12.6101	0.2261	2.8826	0.0485	3.7085	2.0389
14.3791	0.3023	3.2341	0.0648	3.5585	1.6874
15.4224	0.3759	3.5294	0.0806	3.3650	1.3921
16.4203	0.4572	3.7403	0.0980	3.2420	1.1812
18.1440	0.5258	3.9583	0.1127	3.2032	0.9632
19.2780	0.6020	4.1481	0.1291	3.1095	0.7734
21.0924	0.6756	4.2747	0.1449	3.1565	0.6468
22.9068	0.7544	4.4504	0.1617	3.1428	0.4711
23.8140	0.8280	4.5418	0.1775	3.1049	0.3797
26.3088	0.9017	4.6543	0.1933	3.2201	0.2672
27.2160	0.9144	4.6965	0.1961	3.2694	0.2250

$\bar{\sigma}_1$ and $\bar{\sigma}_3$ equal the major and minor effective principal stresses, respectively. Failure taken at maximum deviator stress or at 20 percent axial strain.

TABLE I-3. TRIAXIAL TEST DATA, SAMPLE U-1-12

Axial consolidation pressure = 2.109 kg/cm^2 with K_o = 1

σ_{1_f} = 5.919 kg/cm^2	Initial water content = 194.4%
σ_{3_f} = 3.515 kg/cm^2	Final water content = 94.3%
u_f = 3.452 kg/cm^2	Initial dry density = 25.75 pcf
A_f = 0.85	c_u = 1.265 kg/cm^2

Load (kg)	Displacement (cm)	Pore pressure (kg/cm^2)	Axial strain	$\bar{\sigma}_1$ (kg/cm^2)	$\bar{\sigma}_3$ (kg/cm^2)
0.0000	0.0000	1.4061	0.0000	2.1092	2.1092
7.2576	0.0737	1.6170	0.0147	2.7554	1.8983
10.7957	0.1473	1.9404	0.0294	2.8308	1.5749
12.2472	0.2256	2.2428	0.0450	2.6744	1.2726
13.6080	0.2972	2.4678	0.0592	2.5819	1.0476
14.6059	0.3734	2.6506	0.0744	2.4850	0.8648
15.7399	0.4470	2.7982	0.0891	2.4355	0.7171
16.6471	0.5207	2.9177	0.1038	2.3857	0.5976
17.7811	0.5944	3.0232	0.1185	2.3707	0.4922
18.9605	0.6706	3.1076	0.1337	2.3764	0.4078
19.9584	0.7442	3.1990	0.1484	2.3535	0.3164
21.3192	0.8179	3.2693	0.1630	2.3846	0.2461
22.5893	0.8941	3.3396	0.1782	2.4006	0.1758
23.6779	0.9677	3.3958	0.1929	2.4099	0.1195
25.3109	1.0414	3.4521	0.2076	2.4670	0.0633

$\bar{\sigma}_1$ and $\bar{\sigma}_3$ equal the major and minor effective principal stresses, respectively.
Failure taken at maximum deviator stress or at 20 percent axial strain.

TABLE I-4. TRIAXIAL TEST DATA, SAMPLE U-1-13

Axial consolidation pressure = 3.515 kg/cm^2 with K_o = 1			
σ_{1_f} = 8.768 kg/cm^2		Initial water content	= 180.2%
σ_{3_f} = 4.921 kg/cm^2		Final water content	= 84.2%
u_f = 4.668 kg/cm^2		Initial dry density	= 27.47 pcf
A_f = 0.85		c_u = 1.923 kg/cm^2	

Load (kg)	Displacement (cm)	Pore pressure (kg/cm^2)	Axial strain	$\bar{\sigma}_1$ (kg/cm^2)	$\bar{\sigma}_3$ (kg/cm^2)
0.0000	0.0000	1.4061	0.0000	3.5154	3.5154
15.4224	0.0762	2.0389	0.0157	4.7638	2.8826
18.8244	0.1524	2.6576	0.0314	4.5234	2.2639
20.8656	0.2286	3.0865	0.0471	4.2990	1.8350
22.7707	0.3048	3.4099	0.0628	4.1562	1.5116
24.4944	0.3810	3.6560	0.0785	4.0626	1.2655
26.3088	0.4572	3.8528	0.0943	4.0217	1.0687
27.7603	0.5334	4.0075	0.1100	3.9759	0.9140
29.2572	0.6096	4.1581	0.1257	3.9434	0.7734
30.9355	0.6858	4.2747	0.1414	3.9385	0.6468
31.8881	0.7620	4.3590	0.1571	3.8934	0.5625
34.8365	0.8382	4.4926	0.1728	4.0000	0.4289
36.7416	0.9144	4.5770	0.1885	4.0394	0.3445
39.0096	0.9906	4.6684	0.2042	4.1001	0.2531

$\bar{\sigma}_1$ and $\bar{\sigma}_3$ equal the major and minor effective principal stresses, respectively. Failure taken at maximum deviator stress or at 20 percent axial strain.

TABLE I-5. TRIAXIAL TEST DATA, SAMPLE U-2-21

Axial consolidation pressure = 3.515 kg/cm^2 with K_o = 1

σ_{1_f} = 9.086 kg/cm^2		Initial water content	= 215.0%
σ_{3_f} = 4.921 kg/cm^2		Final water content	= 94.2%
u_f = 4.711 kg/cm^2		Initial dry density	= 23.86 pcf
A_f = 0.79		c_u = 2.082 kg/cm^2	

Load (kg)	Displacement (cm)	Pore pressure (kg/cm^2)	Axial strain	$\bar{\sigma}_1$ (kg/cm^2)	$\bar{\sigma}_3$ (kg/cm^2)
0.0000	0.0000	1.4061	0.0000	3.5154	3.5154
15.1956	0.0762	1.9826	0.0156	4.9064	2.9389
19.0512	0.1524	2.6295	0.0311	4.7198	2.2920
21.3192	0.2286	3.1005	0.0467	4.4941	1.8210
23.5872	0.3048	3.4380	0.0622	4.3927	1.4835
25.4016	0.3810	3.6911	0.0778	4.3114	1.2304
26.9892	0.4572	3.8739	0.0934	4.2659	1.0476
28.4407	0.5334	4.0427	0.1089	4.2121	0.8789
30.1644	0.6096	4.1833	0.1245	4.2117	0.7382
31.7520	0.6858	4.3028	0.1401	4.2100	0.6187
33.5664	0.7620	4.4153	0.1556	4.2341	0.5062
35.2901	0.8382	4.4997	0.1712	4.2689	0.4218
37.1952	0.9144	4.6051	0.1867	4.2950	0.3164
39.6900	0.9906	4.7106	0.2023	4.3751	0.2109

$\bar{\sigma}_1$ and $\bar{\sigma}_3$ equal the major and minor effective principal stresses, respectively. Failure taken at maximum deviator stress or at 20 percent axial strain.

TABLE I-6. TRIAXIAL TEST DATA, SAMPLE U-3-1

Axial consolidation pressure = 0.703 kg/cm^2 with K_o = 1

σ_{1_f} = 3.017 kg/cm^2 Initial water content = 310.0%

σ_{3_f} = 2.109 kg/cm^2 Final Water content = 150.9%

u_f = 2.109 kg/cm^2 Initial dry density = 18.94 pcf

A_f = 0.77 c_u = 0.454 kg/cm^2

Load (kg)	Displacement (cm)	Pore pressure (kg/cm^2)	Axial strain	$\bar{\sigma}_1$ (kg/cm^2)	$\bar{\sigma}_3$ (kg/cm^2)
0.0000	0.0000	1.4061	0.0000	0.7031	0.7031
2.9484	0.0483	1.5678	0.0106	0.8242	0.5414
4.1278	0.1194	1.7014	0.0262	0.7975	0.4078
4.8989	0.1753	1.8139	0.0385	0.7520	0.2953
5.3525	0.2337	1.8842	0.0514	0.7173	0.2250
5.5339	0.2921	1.9053	0.0642	0.7060	0.2039
6.2143	0.3505	1.9545	0.0770	0.7108	0.1547
6.6679	0.4089	1.9721	0.0899	0.7256	0.1371
7.0308	0.4674	2.0037	0.1027	0.7172	0.1055
7.5298	0.5258	2.0389	0.1156	0.7161	0.0703
7.9380	0.5817	2.0459	0.1278	0.7346	0.0633
8.5277	0.6401	2.0730	0.1407	0.7456	0.0352
9.0720	0.6985	2.0811	0.1535	0.7727	0.0281
9.5256	0.7315	2.0951	0.1608	0.7892	0.0141
10.3421	0.8153	2.0986	0.1792	0.8337	0.0105
11.1132	0.8738	2.1057	0.1921	0.8742	0.0035
11.7029	0.9093	2.1092	0.1999	0.9080	0.0000
12.8369	0.9906	2.1092	0.2177	0.9737	0.0000

$\bar{\sigma}_1$ and $\bar{\sigma}_3$ equal the major and minor effective principal stresses, respectively. Failure taken at maximum deviator stress or at 20 percent axial strain.

TABLE I-7. TRIAXIAL TEST DATA, SAMPLE U-3-2

Axial consolidation pressure = 0.703 kg/cm^2 with K_o = 1

σ_{1_f} = 3.351 kg/cm^2	Initial water content = 306.0%
σ_{3_f} = 2.109 kg/cm^2	Final water content = 147.4%
u_f = 2.151 kg/cm^2	Initial dry density = 18.39 pcf
A_f = 0.60	c_u = 0.621 kg/cm^2

Load (kg)	Displacement (cm)	Pore pressure (kg/cm^2)	Axial strain	$\bar{\sigma}_1$ (kg/cm^2)	$\bar{\sigma}_3$ (kg/cm^2)
0.0000	0.0000	1.4061	0.0000	0.7031	0.7031
3.8556	0.0686	1.7506	0.0161	0.7349	0.3586
5.4432	0.1499	1.8701	0.0352	0.7600	0.2390
6.4411	0.2134	1.9475	0.0501	0.7686	0.1617
7.2576	0.2819	2.0037	0.0662	0.7777	0.1055
8.1648	0.3632	2.0459	0.0853	0.8041	0.0633
9.0720	0.4293	2.0775	0.1008	0.8408	0.0316
9.7524	0.4978	2.1057	0.1169	0.8578	0.0035
10.8864	0.5791	2.1232	0.1360	0.9190	-0.0141
11.5668	0.6375	2.1373	0.1497	0.9475	-0.0281
12.7008	0.7087	2.1443	0.1664	1.0150	-0.0352
14.2884	0.7798	2.1479	0.1832	1.1191	-0.0387
15.6492	0.8509	2.1514	0.1999	1.1999	-0.0422

$\bar{\sigma}_1$ and $\bar{\sigma}_3$ equal the major and minor effective principal stresses, respectively. Failure taken at maximum deviator stress or at 20 percent axial strain.

TABLE I-8. TRAIXIAL TEST DATA, SAMPLE U-3-3

Axial consolidation pressure = 1.406 kg/cm^2 with K_o = 1

σ_{1_f} = 5.781 kg/cm^2	Initial water content = 276.2%
σ_{3_f} = 2.81 kg/cm^2	Final water content = 118.8%
u_f = 2.755 kg/cm^2	Initial dry density = 19.23 pcf
A_f = 0.45	c_u = 1.485 kg/cm^2

Load (kg)	Displacement (cm)	Pore pressure (kg/cm^2)	Axial strain	$\bar{\sigma}_1$ (kg/cm^2)	$\bar{\sigma}_3$ (kg/cm^2)
0.0000	0.0000	1.4061	0.0000	1.4062	1.4062
8.6184	0.0584	1.8701	0.0135	1.9213	0.9421
12.2018	0.1168	2.2568	0.0270	1.9227	0.5554
14.5152	0.1753	2.3553	0.0406	2.0609	0.4570
16.2389	0.2337	2.4607	0.0541	2.1206	0.3515
17.6904	0.2921	2.5592	0.0676	2.1528	0.2531
18.9605	0.3480	2.6124	0.0805	2.1976	0.1898
20.4120	0.4064	2.6716	0.0941	2.2703	0.1406
21.7728	0.4648	2.7068	0.1076	2.3433	0.1055
23.5872	0.5232	2.7244	0.1211	2.4754	0.0879
24.9480	0.5817	2.7420	0.1346	2.5568	0.0703
26.3088	0.6401	2.7420	0.1481	2.6514	0.0703
28.1232	0.6960	2.7490	0.1611	2.7805	0.0633
29.4840	0.7569	2.7490	0.1752	2.8641	0.0633
30.8448	0.8153	2.7550	0.1887	2.9383	0.0562
32.2056	0.8611	2.7550	0.1993	3.0262	0.0562

$\bar{\sigma}_1$ and $\bar{\sigma}_3$ equal the major and minor effective principal stresses, respectively.
Failure taken at maximum deviator stress or at 20 percent axial strain.

TABLE I-9. TRIAXIAL TEST DATA, SAMPLE U-3-5

Axial consolidation pressure = 3.515 kg/cm^2 with K_o = 1

σ_{1_f} = 7.966 kg/cm^2		Initial water content	= 255.0%
σ_{3_f} = 4.921 kg/cm^2		Final water content	= 97.5%
u_f = 4.696 kg/cm^2		Initial dry density	= 20.32 pcf
A_f = 1.08		c_u = 1.522 kg/cm^2	

Load (kg)	Displacement (cm)	Pore pressure (kg/cm^2)	Axial strain	$\bar{\sigma}_1$ (kg/cm^2)	$\bar{\sigma}_3$ (kg/cm^2)
0.0000	0.0000	1.4061	0.0000	3.5154	3.5154
7.3483	0.0762	2.0334	0.0163	3.9938	2.9881
10.7957	0.1524	2.4010	0.0327	3.9736	2.5205
12.6101	0.2261	2.8826	0.0485	3.7085	2.0389
14.3791	0.3023	3.2341	0.0648	3.5585	1.6874
15.4224	0.3759	3.5294	0.0806	3.3650	1.3921
16.4203	0.4572	3.7403	0.0980	3.2420	1.1812
18.1440	0.5258	3.9583	0.1127	3.2032	0.9632
19.2780	0.6020	4.1481	0.1291	3.1095	0.7734
21.0924	0.6756	4.2747	0.1449	3.1565	0.6468
22.9068	0.7544	4.4504	0.1617	3.1428	0.4711
23.8140	0.8280	4.5418	0.1775	3.1049	0.3797
26.3088	0.9017	4.6543	0.1933	3.2201	0.2672
27.2160	0.9144	4.6965	0.1961	3.2694	0.2250

$\bar{\sigma}_1$ and $\bar{\sigma}_3$ equal the major and minor effective principal stresses, respectively.
Failure taken at maximum deviator stress or at 20 percent axial strain.

TABLE I-10. TRIAXIAL TEST DATA, SAMPLE U-3-6

Axial consolidation pressure = 2.109 kg/cm^2 with K_o = 1

σ_{1_f} = 4.531 kg/cm^2		Initial water content	= 285.8%
σ_{3_f} = 2.109 kg/cm^2		Final water content	= 122.8%
u_f = 2.189 kg/cm^2		Initial dry density	= 18.63 pcf
A_f = 0.90		c_u = 1.200 kg/cm^2	

Load (kg)	Displacement (cm)	Pore pressure (kg/cm^2)	Axial strain	$\bar{\sigma}_1$ (kg/cm^2)	$\bar{\sigma}_3$ (kg/cm^2)
0.0000	0.0000	1.4061	0.0000	2.1092	2.1092
7.1669	0.0737	1.7928	0.0158	2.6145	1.7225
9.8431	0.1473	2.1936	0.0316	2.5272	1.3218
11.5668	0.2256	2.4748	0.0483	2.4325	1.0406
12.7008	0.2972	2.6857	0.0637	2.3334	0.8296
13.6987	0.3734	2.8474	0.0800	2.2616	0.6679
15.0595	0.4470	2.9870	0.0958	2.2492	0.5273
16.2842	0.5207	3.1146	0.1146	2.2302	0.4008
17.2368	0.5944	3.2201	0.1274	2.1973	0.2953
18.2347	0.6706	3.3044	0.1437	2.1854	0.2109
19.5955	0.7442	3.3958	0.1595	2.2022	0.1195
20.8656	0.8179	3.4732	0.1753	2.2182	0.0422
22.4532	0.8941	3.5294	0.1916	2.2812	-0.0141
23.9501	0.9677	3.5716	0.2074	2.3442	-0.0562

$\bar{\sigma}_1$ and $\bar{\sigma}_3$ equal the major and minor effective principal stresses, respectively. Failure taken at maximum deviator stress or at 20 percent axial strain.

TABLE I-11. TRIAXIAL TEST DATA, SAMPLE U-3-7

Axial consolidation pressure = 1.406 kg/cm^2 with K_o = 1

σ_{1_f} = 4.693 kg/cm^2 Initial water content = 289.6%

σ_{3_f} = 2.812 kg/cm^2 Final water content = 127.0%

u_f = 2.777 kg/cm^2 Initial dry density = 18.30 pcf

A_f = 0.73 c_u = 0.940 kg/cm^2

Load (kg)	Displacement (cm)	Pore pressure (kg/cm^2)	Axial strain	$\bar{\sigma}_1$ (kg/cm^2)	$\bar{\sigma}_3$ (kg/cm^2)
0.0000	0.0000	1.4061	0.0000	1.4062	1.4062
1.8144	0.0152	1.4413	0.0032	1.6028	1.3710
3.6288	0.0305	1.5116	0.0063	1.7627	1.3007
4.5360	0.0432	1.5819	0.0090	1.8064	1.2304
5.4432	0.0584	1.6522	0.0121	1.8491	1.1601
6.1236	0.0737	1.7225	0.0153	1.8624	1.0896
6.4411	0.0889	1.7858	0.0185	1.8366	1.0265
7.1215	0.1041	1.8385	0.0216	1.8666	0.9738
7.6205	0.1245	1.9264	0.0259	1.8371	0.8859
8.1648	0.1473	1.9861	0.0305	1.8403	0.8261
9.2988	0.2256	2.1584	0.0469	1.7895	0.6539
10.2060	0.2972	2.2779	0.0618	1.7613	0.5343
11.1132	0.3734	2.3693	0.0776	1.7564	0.4429
12.0204	0.4479	2.4467	0.0929	1.7627	0.3656
12.7462	0.5207	2.5170	0.1082	1.7518	0.2953
13.6080	0.5944	2.5731	0.1236	1.7673	0.2390
14.5152	0.6706	2.6295	0.1394	1.7835	0.1828
15.4224	0.7442	2.6787	0.1547	1.8041	0.1336
16.3296	0.8179	2.7138	0.1700	1.8351	0.0984
17.2368	0.8941	2.7560	0.1859	1.8544	0.0562
18.3708	0.9677	2.7771	0.2012	1.9156	0.0352

$\bar{\sigma}_1$ and $\bar{\sigma}_3$ equal the major and minor effective principal stresses, respectively.
Failure taken at maximum deviator stress or at 20 percent axial strain.

TABLE I-12. TRIAXIAL TEST DATA, SAMPLE U-3-8

Axial consolidation pressure = 3.515 kg/cm^2 with $K_o = 1$

σ_{1_f} = 9.127 kg/cm^2	Initial water content	=	293.6%
σ_{3_f} = 4.921 kg/cm^2	Final water content	=	111.0%
u_f = 4.844 kg/cm^2	Initial dry density	=	18.22 pcf
A_f = 0.82	c_u = 2.102 kg/cm^2		

Load (kg)	Displacement (cm)	Pore pressure (kg/cm^2)	Axial strain	$\bar{\sigma}_1$ (kg/cm^2)	$\bar{\sigma}_3$ (kg/cm^2)
0.0000	0.0000	1.4061	0.0000	3.5154	3.5154
12.6554	0.0762	2.1443	0.0170	4.4755	2.7772
16.3750	0.1499	2.8474	0.0334	4.2349	2.0741
19.0512	0.2261	3.2622	0.0504	4.1290	1.6593
21.0924	0.2997	3.5716	0.0669	4.0370	1.3499
23.1336	0.3759	3.8317	0.0839	3.9832	1.0898
25.3109	0.4521	4.0637	0.1008	3.9648	0.8578
26.8531	0.5258	4.2325	0.1173	3.9251	0.6890
28.8036	0.6020	4.3942	0.1343	3.9316	0.5273
30.8448	0.6782	4.5629	0.1513	3.9326	0.3586
33.3396	0.7518	4.6965	0.1677	4.0133	0.2250
35.8344	0.8280	4.7668	0.1847	4.1433	0.1547
38.5560	0.9017	4.8442	0.2011	4.2824	0.0773

$\bar{\sigma}_1$ and $\bar{\sigma}_3$ equal the major and minor effective principal stresses, respectively.
Failure taken at maximum deviator stress or at 20 percent axial strain.

TABLE I-13. TRIAXIAL TEST DATA, SAMPLE G-3

Axial consolidation pressure = 1.173 kg/cm^2 with K_o = 0.3

Angle between direction of compression and horizontal = 90 degrees

σ_{1_f} = 4.566 kg/cm^2	Initial water content = 159.1%
σ_{3_f} = 3.164 kg/cm^2	Final water content = 142.0%
u_f = 3.123 kg/cm^2	Initial dry density = 20.45 pcf
A_f = 0.45	c_u = 0.701 kg/cm^2

Load (kg)	Displacement (cm)	Pore pressure (kg/cm^2)	Axial strain	$\bar{\sigma}_1$ (kg/cm^2)	$\bar{\sigma}_3$ (kg/cm^2)
15.4200	0.0000	2.8123	0.0000	1.0641	0.3515
16.3296	0.0102	2.8264	0.0013	1.0913	0.3375
17.4636	0.0178	2.8615	0.0022	1.1077	0.3023
18.1440	0.0279	2.8756	0.0035	1.1240	0.2883
18.5976	0.0305	2.8826	0.0038	1.1375	0.2812
19.0512	0.0381	2.8896	0.0047	1.1506	0.2742
21.4099	0.0787	2.9178	0.0098	1.2260	0.2461
22.9975	0.1295	2.9529	0.0161	1.2568	0.2109
24.4944	0.1778	3.0513	0.0221	1.2196	0.1125
25.4016	0.2388	3.0738	0.0296	1.2292	0.0900
26.3088	0.2997	3.0935	0.0372	1.2411	0.0703
27.2160	0.3581	3.1090	0.0444	1.2568	0.0548
28.8036	0.4521	3.1287	0.0561	1.2917	0.0352
29.4840	0.5461	3.1391	0.0678	1.2950	0.0246
30.3912	0.6401	3.1463	0.0794	1.3107	0.0176
31.2984	0.7366	3.1484	0.0914	1.3298	0.0155
31.8427	0.8331	3.1477	0.1034	1.3358	0.0162
33.5664	1.0287	3.1392	0.1276	1.3780	0.0246
35.3808	1.2217	3.1287	0.1516	1.4225	0.0352
36.2880	1.3208	3.1231	0.1639	1.4431	0.0408

$\bar{\sigma}_1$ and $\bar{\sigma}_3$ equal the major and minor effective principal stresses, respectively. Failure taken at maximum deviator stress or at 20 percent axial strain.

TABLE I-14. TRIAXIAL TEST DATA, SAMPLE G-4

Axial consolidation pressure = 1. 173 kg/cm^2 with K_o = 0. 3
Angle between direction of compression and horizontal = 90 degrees

σ_{1_f} = 4. 983 kg/cm^2 Initial water content = 157. 7%

σ_{3_f} = 3. 164 kg/cm^2 Final water content = 134. 0%

u_f = 3. 155 kg/cm^2 Initial dry density = 24. 58 pcf

A_f = 0. 30 c_u = 0. 910 kg/cm^2

Load (kg)	Displacement (cm)	Pore pressure (kg/cm^2)	Axial strain	$\bar{\sigma}_1$ (kg/cm^2)	$\bar{\sigma}_3$ (kg/cm^2)
15. 6500	0. 0000	2. 8123	0. 0000	1. 0333	0. 3515
15. 6492	0. 0102	2. 8123	0. 0010	1. 0327	0. 3515
17. 6904	0. 0203	2. 8404	0. 0021	1. 0928	0. 3234
19. 9584	0. 0381	2. 8756	0. 0039	1. 1547	0. 2883
21. 5460	0. 0559	2. 8932	0. 0057	1. 2043	0. 2707
22. 4532	0. 0737	2. 9079	0. 0075	1. 2271	0. 2559
25. 8552	0. 1676	2. 9599	0. 0171	1. 3113	0. 2039
27. 6696	0. 2616	2. 9965	0. 0268	1. 3409	0. 1673
29. 1211	0. 3556	3. 0303	0. 0364	1. 3565	0. 1336
30. 7541	0. 4521	3. 0584	0. 0462	1. 3837	0. 1055
31. 7520	0. 5512	3. 0795	0. 0564	1. 3901	0. 0844
32. 8860	0. 6477	3. 0978	0. 0662	1. 4043	0. 0661
34. 3375	0. 7442	3. 1090	0. 0761	1. 4374	0. 0548
35. 3808	0. 8407	3. 1202	0. 0860	1. 4529	0. 0436
36. 5148	0. 9373	3. 1273	0. 0958	1. 4753	0. 0366
37. 6488	1. 0363	3. 1322	0. 1060	1. 4985	0. 0316
38. 9642	1. 1328	3. 1371	0. 1159	1. 5280	0. 0267
41. 6405	1. 4275	3. 1427	0. 1460	1. 5709	0. 0211
44. 4528	1. 5240	3. 1484	0. 1559	1. 6508	0. 0155
47. 6280	1. 7221	3. 1498	0. 1761	1. 7241	0. 0141
50. 8032	1. 9202	3. 1533	0. 1964	1. 7898	0. 0105
52. 6176	2. 0193	3. 1547	0. 2065	1. 8287	0. 0091

$\bar{\sigma}_1$ and $\bar{\sigma}_3$ equal the major and minor effective principal stresses, respectively.
Failure taken at maximum deviator stress or at 20 percent axial strain.

TABLE I-15. TRIAXIAL TEST DATA, SAMPLE G-5

Axial consolidation pressure = 1.173 kg/cm^2 with K_o = 0.3

Angle between direction of compression and horizontal = 90 degrees

σ_{1_f} = 5.073 kg/cm^2 Initial water content = 153.7%

σ_{3_f} = 3.164 kg/cm^2 Final water content = 130.0%

u_f = 3.149 kg/cm^2 Initial dry density = 21.95 pcf

A_f = 0.30 c_u = 0.954 kg/cm^2

Load (kg)	Displacement (cm)	Pore pressure (kg/cm^2)	Axial strain	$\bar{\sigma}_1$ (kg/cm^2)	$\bar{\sigma}_3$ (kg/cm^2)
15.6500	0.0000	2.8123	0.0000	1.1543	0.3515
20.8656	0.0305	2.8791	0.0032	1.3532	0.2847
23.6779	0.0864	2.9389	0.0092	1.4303	0.2250
25.4016	0.1372	2.9726	0.0146	1.4772	0.1912
26.5356	0.1905	2.9965	0.0203	1.5030	0.1673
27.3067	0.2388	3.0162	0.0254	1.5149	0.1476
30.7541	0.4978	3.0809	0.0530	1.5793	0.0830
33.4757	0.7518	3.1153	0.0800	1.6308	0.0485
36.2880	1.0084	3.1322	0.1073	1.6959	0.0316
39.2364	1.2824	3.1406	0.1343	1.7682	0.0232
42.6384	1.5215	3.1442	0.1619	1.8557	0.0197
45.8136	1.7755	3.1491	0.1889	1.9239	0.0148
45.2693	2.0295	3.1385	0.2159	1.8489	0.0253

$\bar{\sigma}_1$ and $\bar{\sigma}_3$ equal the major and minor effective principal stresses, respectively.
Failure taken at maximum deviator stress or at 20 percent axial strain.

TABLE I-16. TRIAXIAL TEST DATA, SAMPLE G-6

Axial consolidation pressure = 2.343 kg/cm^2 with K_o = 0.3

Angle between direction of compression and horizontal = 90 degrees

σ_{1_f} = 7.694 kg/cm^2 | Initial water content = 157.2%

σ_{3_f} = 3.504 kg/cm^2 | Final water content = 115.0%

u_f = 3.469 kg/cm^2 | Initial dry density = 23.53 pcf

A_f = 0.24 | c_u = 2.095 kg/cm^2

Load (kg)	Displacement (cm)	Pore pressure (kg/cm^2)	Axial strain	$\bar{\sigma}_1$ (kg/cm^2)	$\bar{\sigma}_3$ (kg/cm^2)
33.5680	0.0000	2.8123	0.0000	2.1508	0.7030
49.4424	0.0406	3.0303	0.0052	2.6070	0.4851
55.3392	0.0914	3.1709	0.0117	2.7039	0.3445
58.5144	0.1372	3.2412	0.0176	2.7542	0.2742
60.7824	0.1905	3.2904	0.0244	2.7832	0.2250
62.5968	0.2438	3.3291	0.0313	2.8024	0.1863
70.7616	0.5029	3.4155	0.0645	2.9557	0.0998
79.3800	0.7366	3.4451	0.0945	3.1714	0.0703
86.1840	0.9601	3.4556	0.1231	3.3201	0.0598
92.0808	1.1862	3.4605	0.1521	3.4231	0.0548
114.3072	1.4326	3.4662	0.1837	4.0747	0.0492
123.8328	1.6891	3.4732	0.2166	4.2274	0.0422

$\bar{\sigma}_1$ and $\bar{\sigma}_3$ equal the major and minor effective principal stresses, respectively.
Failure taken at maximum deviator stress or at 20 percent axial strain.

TABLE I-17. TRIAXIAL TEST DATA, SAMPLE G-7

Unconfined compression test

Angle between direction of compression and horizontal = 90 degrees

σ_{1_f} = 0.637 kg/cm^2	Initial water content	= 158.6%
σ_{3_f} = 0 kg/cm^2	Final water content	= 158.6%
c_u = 0.318 kg/cm^2	Initial dry density	= 27.52 pcf

Load (kg)	Displacement (cm)	Pore pressure (kg/cm^2)	Axial strain	σ_1 (kg/cm^2)	σ_3 (kg/cm^2)
0.0000	0.0000	--	0.0000	0.0000	0.0000
2.1773	0.0457		0.0036	0.1062	
3.1752	0.0914		0.0073	0.1543	
3.9917	0.1321		0.0105	0.1899	
4.8989	0.1829		0.0145	0.2293	
5.6246	0.2337		0.0185	0.2632	
8.6184	0.4851		0.0385	0.3916	
10.9318	0.7391		0.0587	0.4896	
12.6101	0.9957		0.0790	0.5544	
13.5173	1.2522		0.0994	0.5818	
13.6987	1.5062		0.1196	0.5763	
13.6987	1.7602		0.1397	0.5698	
13.5173	1.9990		0.1587	0.5567	
13.1544	2.2327		0.1772	0.5298	
15.6492	2.4663		0.1958	0.6160	
16.3296	2.5603		0.2032	0.6368	

σ_1 and σ_3 equal the major and minor total principal stresses, respectively.
Failure taken at maximum deviator stress or at 20 percent axial strain.

TABLE I-18. TRIAXIAL TEST DATA, SAMPLE G-8

Unconfined compression test

Angle between direction of compression and horizontal = 90 degrees

σ_{1_f} = 0.644 kg/cm^2	Initial water content = 158.6%
σ_{3_f} = 0 kg/cm^2	Final water content = 158.6%
c_u = 0.322 kg/cm^2	Initial dry density = 24.15 pcf

Load (kg)	Displacement (cm)	Pore pressure (kg/cm^2)	Axial strain	σ_1 (kg/cm^2)	σ_3 (kg/cm^2)
0.0000	0.0000	--	0.0000	0.0000	0.0000
2.1773	0.457		0.0038	0.1128	
2.9484	0.0940		0.0079	0.1520	
3.7422	0.1321		0.0111	0.1923	
4.3546	0.1829		0.0153	0.2228	
5.0803	0.2337		0.0196	0.2568	
8.4823	0.4851		0.0406	0.4229	
10.8864	0.7391		0.0619	0.5307	
12.6554	0.9957		0.0833	0.6028	
13.8348	1.2522		0.1048	0.6435	
13.5173	1.5062		0.1261	0.6138	
9.8885	1.7602		0.1473	0.4381	
10.4328	1.9990		0.1673	0.4514	
9.0720	2.2327		0.1869	0.3833	
9.2988	2.4663		0.2064	0.3834	

σ_1 and σ_3 equal the major and minor total principal stresses, respectively.
Failure taken at maximum deviator stress or at 20 percent axial strain.

TABLE I-19. TRIAXIAL TEST DATA, SAMPLE G-9

Axial consolidation pressure = 0.696 kg/cm^2 with K_o = 0.3

Angle between direction of compression and horizontal = 90 degrees

σ_{1_f} = 3.992 kg/cm^2	Initial water content = 157.2%
σ_{3_f} = 3.023 kg/cm^2	Final water content = 153.0%
u_f = 3.002 kg/cm^2	Initial dry density = 26.92 pcf
A_f = 0.40	c_u = 0.484 kg/cm^2

Load (kg)	Displacement (cm)	Pore pressure (kg/cm^2)	Axial strain	$\bar{\sigma}_1$ (kg/cm^2)	$\bar{\sigma}_3$ (kg/cm^2)
9.9547	0.0000	2.8123	0.0000	0.6943	0.2109
12.9276	0.0508	2.8756	0.0041	0.7986	0.1476
13.8348	0.0965	2.8967	0.0077	0.8206	0.1266
14.5152	0.1321	2.9107	0.0106	0.8386	0.1125
14.9688	0.1905	2.9220	0.0153	0.8465	0.1012
15.2863	0.2388	2.9318	0.0191	0.8494	0.0914
16.7832	0.4928	2.9607	0.0395	0.8776	0.0626
18.0533	0.7442	2.9782	0.0596	0.9033	0.0450
19.0966	1.0058	2.9895	0.0806	0.9214	0.0337
20.4120	1.2649	2.9986	0.1013	0.9520	0.0246
21.3192	1.5240	3.0021	0.1221	0.9673	0.0211
22.2264	1.7831	3.0028	0.1428	0.9836	0.0204
22.9068	2.0422	3.0021	0.1636	0.9897	0.0211
23.4058	2.2911	2.9881	0.1835	1.0013	0.0352
23.6779	2.5425	0.29670	0.2037	1.0095	0.0562

$\bar{\sigma}_1$ and $\bar{\sigma}_3$ equal the major and minor effective principal stresses, respectively.
Failure taken at maximum deviator stress or at 20 percent axial strain.

TABLE I-20. TRIAXIAL TEST DATA, SAMPLE G-10

Axial consolidation pressure = 0.703 kg/cm^2 with K_o = 1.0

Angle between direction of compression and horizontal = 0 degrees

σ_{1_f} = 4.413 kg/cm^2	Initial water content = 157.0%
σ_{3_f} = 3.515 kg/cm^2	Final water content = 145.0%
u_f = 3.325 kg/cm^2	Initial dry density = 22.53 pcf
A_f = 0.57	c_u = 0.449 kg/cm^2

Load (kg)	Displacement (cm)	Pore pressure (kg/cm^2)	Axial strain	$\bar{\sigma}_1$ (kg/cm^2)	$\bar{\sigma}_3$ (kg/cm^2)
0.0000	0.0000	2.8123	0.0000	0.7030	0.7030
4.0824	0.0330	2.9529	0.0030	0.7985	0.5625
6.4411	0.0864	3.0162	0.0079	0.8698	0.4992
7.9380	0.1372	3.0549	0.0125	0.9151	0.4605
8.8452	0.1880	3.0830	0.0171	0.9366	0.4324
9.6163	0.2388	3.1076	0.0218	0.9533	0.4078
12.2472	0.5004	3.1849	0.0456	1.0083	0.3304
13.6080	0.7620	3.2271	0.0695	1.0226	0.2883
14.7420	1.0211	3.2552	0.0931	1.0355	0.2601
15.8760	1.2802	3.2763	0.1167	1.0523	0.2390
16.8739	1.5392	3.2974	0.1404	1.0592	0.2180
17.9172	1.7958	3.3150	0.1637	1.0693	0.2004
19.0512	2.0549	3.3255	0.1874	1.0877	0.1898
19.2780	2.1590	3.3326	0.1969	1.0807	0.1828

$\bar{\sigma}_1$ and $\bar{\sigma}_3$ equal the major and minor effective principal stresses, respectively.
Failure taken at maximum deviator stress or at 20 percent axial strain.

TABLE I-21. TRIAXIAL TEST DATA, SAMPLE G-11

Axial consolidation pressure = 2.109 kg/cm^2 with K_o = 1.0

Angle between direction of compression and horizontal = 0 degrees

σ_{1_f} = 7.151 kg/cm^2	Initial water content = 160.0%
σ_{3_f} = 4.920 kg/cm^2	Final water content = 114.0%
u_f = 4.492 kg/cm^2	Initial dry density = 23.74 pcf
A_f = 0.75	c_u = 1.115 kg/cm^2

Load (kg)	Displacement (cm)	Pore pressure (kg/cm^2)	Axial strain	$\bar{\sigma}_1$ (kg/cm^2)	$\bar{\sigma}_3$ (kg/cm^2)
0.0000	0.0000	2.8123	0.0000	2.1092	2.1092
12.7008	0.0533	3.0935	0.0047	2.6795	1.8280
16.3296	0.0183	3.3045	0.0072	2.7091	1.6171
19.0512	0.1600	3.4802	0.0141	2.7064	1.4413
20.8656	0.2108	3.5857	0.0186	2.7151	1.3359
22.5893	0.2616	3.6912	0.0231	2.7168	1.2304
27.2160	0.5232	3.9794	0.0462	2.6905	0.9421
30.3912	0.7849	4.1411	0.0694	2.6855	0.7804
32.2056	1.0465	4.2325	0.0925	2.6577	0.6890
34.2468	1.3081	4.2888	0.1156	2.6729	0.6328
36.0612	1.5697	4.3591	0.1387	2.6545	0.5625
37.8756	1.8313	4.4153	0.1618	2.6445	0.5062
39.9168	2.0930	4.4645	0.1849	216484	0.4570
42.1848	2.3520	4.5067	0.2078	2.6657	0.4148

$\bar{\sigma}_1$ and $\bar{\sigma}_3$ equal the major and minor effective principal stresses, respectively.
Failure taken at maximum deviator stress or at 20 percent axial strain.

TABLE I-22. TRIAXIAL TEST DATA, SAMPLE G-12

Unconfined compression test

Angle between direction of compression and horizontal = 0 degrees

σ_{1_f} = 0.404 kg/cm^2	Initial water content	=	158.6%
σ_{3_f} = 0 kg/cm^2	Final water content	=	158.6%
c_u = 0.202 kg/cm^2	Initial dry density	=	19.92 pcf

Load (kg)	Displacement (cm)	Pore pressure (kg/cm^2)	Axial strain	σ_1 (kg/cm^2)	σ_3 (kg/cm^2)
0.0000	0.0000	--	0.0000	0.0000	0.0000
1.9958	0.0406		0.0043	0.0973	
3.0391	0.0965		0.0103	0.1473	
3.6742	0.1473		0.0157	0.1771	
4.3092	0.1905		0.0203	0.2067	
4.7628	0.2388		0.0254	0.2272	
6.8040	0.4928		0.0524	0.3156	
8.0741	0.7442		0.0792	0.3639	
8.9359	1.0033		0.1068	0.3907	
9.5256	1.2624		0.1343	0.4036	
9.5256	1.5189		0.1616	0.3909	
8.7091	1.7780		0.1892	0.3456	
7.4844	1.9329		0.2057	0.2910	

σ_1 and σ_3 equal the major and minor total principal stresses, respectively. Failure taken at maximum deviator stress or at 20 percent axial strain.

TABLE I-23. TRIAXIAL TEST DATA, SAMPLE G-20

Axial consolidation pressure = 2.341 kg/cm^2 with K_o = 0.3
Undrained test with σ_1 constant and σ_3 decreasing.

Initial water content = 159.0%
Final water content = 122.0%
Initial dry density = 24.37 pcf

σ_1 (kg/cm^2)	σ_3 (kg/cm^2)	pore pressure (kg/cm^2)	Axial strain	$\bar{\sigma}_1$ (kg/cm^2)	$\bar{\sigma}_3$ (kg/cm^2)
5.135	3.5154	2.8123	0.000	2.3412	0.7031
5.1535	3.4893	2.8123	0.001	2.3412	0.6770
5.1535	3.4429	2.8123	0.001	2.3412	0.6306
5.1535	3.3965	2.7947	0.001	2.3588	0.6018
5.1535	3.3501	2.7772	0.002	2.3763	0.5729
5.1535	3.2580	2.7420	0.003	2.4115	0.5160
5.1535	3.1666	2.7068	0.005	2.4467	0.4598
5.1535	3.0745	2.6506	0.006	2.5029	0.4239
5.1535	2.9986	2.7420	0.035	2.4115	0.2566
5.1535	2.9185	2.7772	0.048	2.3763	0.1413
5.1535	2.8362	2.7772	0.057	2.3763	0.0590
5.1535	2.8158	2.7596	0.085	2.3939	0.0562
5.2027	2.8123	2.8123[a]	0.087	2.3904	0.0000
5.2630[b]	2.8123	2.8123	0.091	2.4507	0
5.3504[b]	2.8123	2.8123	0.094	2.5381	0
5.5051[b]	2.8123	2.8123	0.127	2.6928	0
5.5683[b]	2.8123	2.8123	0.136	2.7560	0

[a]Pore pressure increased to initial backpressure.
[b]Small increases in axial stress.
Deformation rate approximately zero when test was terminated.

TABLE I-24. TRIAXIAL TEST DATA, SAMPLE G-21

Axial consolidation pressure = 0.703 kg/cm^2 with K_o = 0.3

Undrained test with σ_1 constant and σ_3 decreasing.

Initial water content =

Final water content = 135.0%

Initial dry density = 31.26 pcf

σ_1 (kg/cm^2)	σ_3 (kg/cm^2)	pore pressure (kg/cm^2)	axial strain	$\bar{\sigma}_1$ (kg/cm^2)	$\bar{\sigma}_3$ (kg/cm^2)
3.5153	3.0232	2.8123	0.000	0.7030	0.2109
3.5153	2.9628	2,7807	0.003	0.7346	0.1821
3.5153	2.9121	2.7561	0.007	0.7592	0.1560
3.5153	2.8622	2.7279	0.009	0.7874	0.1343
3.5153	2,8158	2.7139	0.024	0.8014	0.1019
3.5153	2.8123	2.8123[a]	0.025	0.7030	0.0000
3.5153	2.8123	2.8123[a]	0.101	0.7030	0.0000

[a]Pore pressure increased to initial backpressure.

Deformation rate approximately zero when test was terminated.

TABLE I-13. TRIAXIAL TEST DATA, SAMPLE G-3

Axial consolidation pressure = 1.173 kg/cm^2 with K_o = 0.3

Angle between direction of compression and horizontal = 90 degrees

σ_{1_f} = 4.566 kg/cm^2	Initial water content = 159.1%
σ_{3_f} = 3.164 kg/cm^2	Final water content = 142.0%
u_f = 3.123 kg/cm^2	Initial dry density = 20.45 pcf
A_f = 0.45	c_u = 0.701 kg/cm^2

Load (kg)	Displacement (cm)	Pore pressure (kg/cm^2)	Axial strain	$\bar{\sigma}_1$ (kg/cm^2)	$\bar{\sigma}_3$ (kg/cm^2)
15.4200	0.0000	2.8123	0.0000	1.0641	0.3515
16.3296	0.0102	2.8264	0.0013	1.0913	0.3375
17.4636	0.0178	2.8615	0.0022	1.1077	0.3023
18.1440	0.0279	2.8756	0.0035	1.1240	0.2883
18.5976	0.0305	2.8826	0.0038	1.1375	0.2812
19.0512	0.0381	2.8896	0.0047	1.1506	0.2742
21.4099	0.0787	2.9178	0.0098	1.2260	0.2461
22.9975	0.1295	2.9529	0.0161	1.2568	0.2109
24.4944	0.1778	3.0513	0.0221	1.2196	0.1125
25.4016	0.2388	3.0738	0.0296	1.2292	0.0900
26.3088	0.2997	3.0935	0.0372	1.2411	0.0703
27.2160	0.3581	3.1090	0.0444	1.2568	0.0548
28.8036	0.4521	3.1287	0.0561	1.2917	0.0352
29.4840	0.5461	3.1391	0.0678	1.2950	0.0246
30.3912	0.6401	3.1463	0.0794	1.3107	0.0176
31.2984	0.7366	3.1484	0.0914	1.3298	0.0155
31.8427	0.8331	3.1477	0.1034	1.3358	0.0162
33.5664	1.0287	3.1392	0.1276	1.3780	0.0246
35.3808	1.2217	3.1287	0.1516	1.4225	0.0352
36.2880	1.3208	3.1231	0.1639	1.4431	0.0408

$\bar{\sigma}_1$ and $\bar{\sigma}_3$ equal the major and minor effective principal stresses, respectively.
Failure taken at maximum deviator stress or at 20 percent axial strain.

TABLE I-14. TRIAXIAL TEST DATA, SAMPLE G-4

Axial consolidation pressure = 1.173 kg/cm^2 with K_o = 0.3

Angle between direction of compression and horizontal = 90 degrees

σ_{1_f} = 4.983 kg/cm^2 Initial water content = 157.7%

σ_{3_f} = 3.164 kg/cm^2 Final water content = 134.0%

u_f = 3.155 kg/cm^2 Initial dry density = 24.58 pcf

A_f = 0.30 c_u = 0.910 kg/cm^2

Load (kg)	Displacement (cm)	Pore pressure (kg/cm^2)	Axial strain	$\bar{\sigma}_1$ (kg/cm^2)	$\bar{\sigma}_3$ (kg/cm^2)
15.6500	0.0000	2.8123	0.0000	1.0333	0.3515
15.6492	0.0102	2.8123	0.0010	1.0327	0.3515
17.6904	0.0203	2.8404	0.0021	1.0928	0.3234
19.9584	0.0381	2.8756	0.0039	1.1547	0.2883
21.5460	0.0559	2.8932	0.0057	1.2043	0.2707
22.4532	0.0737	2.9079	0.0075	1.2271	0.2559
25.8552	0.1676	2.9599	0.0171	1.3113	0.2039
27.6696	0.2616	2.9965	0.0268	1.3409	0.1673
29.1211	0.3556	3.0303	0.0364	1.3565	0.1336
30.7541	0.4521	3.0584	0.0462	1.3837	0.1055
31.7520	0.5512	3.0795	0.0564	1.3901	0.0844
32.8860	0.6477	3.0978	0.0662	1.4043	0.0661
34.3375	0.7442	3.1090	0.0761	1.4374	0.0548
35.3808	0.8407	3.1202	0.0860	1.4529	0.0436
36.5148	0.9373	3.1273	0.0958	1.4753	0.0366
37.6488	1.0363	3.1322	0.1060	1.4985	0.0316
38.9642	1.1328	3.1371	0.1159	1.5280	0.0267
41.6405	1.4275	3.1427	0.1460	1.5709	0.0211
44.4528	1.5240	3.1484	0.1559	1.6508	0.0155
47.6280	1.7221	3.1498	0.1761	1.7241	0.0141
50.8032	1.9202	3.1533	0.1964	1.7898	0.0105
52.6176	2.0193	3.1547	0.2065	1.8287	0.0091

$\bar{\sigma}_1$ and $\bar{\sigma}_3$ equal the major and minor effective principal stresses, respectively.
Failure taken at maximum deviator stress or at 20 percent axial strain.

TABLE I-15. TRIAXIAL TEST DATA, SAMPLE G-5

Axial consolidation pressure = 1.173 kg/cm^2 with K_o = 0.3

Angle between direction of compression and horizontal = 90 degrees

σ_{1_f} = 5.073 kg/cm^2 Initial water content = 153.7%

σ_{3_f} = 3.164 kg/cm^2 Final water content = 130.0%

u_f = 3.149 kg/cm^2 Initial dry density = 21.95 pcf

A_f = 0.30 c_u = 0.954 kg/cm^2

Load (kg)	Displacement (cm)	Pore pressure (kg/cm^2)	Axial strain	$\bar{\sigma}_1$ (kg/cm^2)	$\bar{\sigma}_3$ (kg/cm^2)
15.6500	0.0000	2.8123	0.0000	1.1543	0.3515
20.8656	0.0305	2.8791	0.0032	1.3532	0.2847
23.6779	0.0864	2.9389	0.0092	1.4303	0.2250
25.4016	0.1372	2.9726	0.0146	1.4772	0.1912
26.5356	0.1905	2.9965	0.0203	1.5030	0.1673
27.3067	0.2388	3.0162	0.0254	1.5149	0.1476
30.7541	0.4978	3.0809	0.0530	1.5793	0.0830
33.4757	0.7518	3.1153	0.0800	1.6308	0.0485
36.2880	1.0084	3.1322	0.1073	1.6959	0.0316
39.2364	1.2824	3.1406	0.1343	1.7682	0.0232
42.6384	1.5215	3.1442	0.1619	1.8557	0.0197
45.8136	1.7755	3.1491	0.1889	1.9239	0.0148
45.2693	2.0295	3.1385	0.2159	1.8489	0.0253

$\bar{\sigma}_1$ and $\bar{\sigma}_3$ equal the major and minor effective principal stresses, respectively.
Failure taken at maximum deviator stress or at 20 percent axial strain.

TABLE I-16. TRIAXIAL TEST DATA, SAMPLE G-6

Axial consolidation pressure = 2.343 kg/cm^2 with K_o = 0.3
Angle between direction of compression and horizontal = 90 degrees

σ_{1_f} = 7.694 kg/cm^2 Initial water content = 157.2%

σ_{3_f} = 3.504 kg/cm^2 Final water content = 115.0%

u_f = 3.469 kg/cm^2 Initial dry density = 23.53 pcf

A_f = 0.24 c_u = 2.095 kg/cm^2

Load (kg)	Displacement (cm)	Pore pressure (kg/cm^2)	Axial strain	$\bar{\sigma}_1$ (kg/cm^2)	$\bar{\sigma}_3$ (kg/cm^2)
33.5680	0.0000	2.8123	0.0000	2.1508	0.7030
49.4424	0.0406	3.0303	0.0052	2.6070	0.4851
55.3392	0.0914	3.1709	0.0117	2.7039	0.3445
58.5144	0.1372	3.2412	0.0176	2.7542	0.2742
60.7824	0.1905	3.2904	0.0244	2.7832	0.2250
62.5968	0.2438	3.3291	0.0313	2.8024	0.1863
70.7616	0.5029	3.4155	0.0645	2.9557	0.0998
79.3800	0.7366	3.4451	0.0945	3.1714	0.0703
86.1840	0.9601	3.4556	0.1231	3.3201	0.0598
92.0808	1.1862	3.4605	0.1521	3.4231	0.0548
114.3072	1.4326	3.4662	0.1837	4.0747	0.0492
123.8328	1.6891	3.4732	0.2166	4.2274	0.0422

$\bar{\sigma}_1$ and $\bar{\sigma}_3$ equal the major and minor effective principal stresses, respectively.
Failure taken at maximum deviator stress or at 20 percent axial strain.

TABLE I-17. TRIAXIAL TEST DATA, SAMPLE G-7

Unconfined compression test

Angle between direction of compression and horizontal = 90 degrees

σ_{1_f} = 0.637 kg/cm^2 Initial water content = 158.6%

σ_{3_f} = 0 kg/cm^2 Final water content = 158.6%

c_u = 0.318 kg/cm^2 Initial dry density = 27.52 pcf

Load (kg)	Displacement (cm)	Pore pressure (kg/cm^2)	Axial strain	σ_1 (kg/cm^2)	σ_3 (kg/cm^2)
0.0000	0.0000	--	0.0000	0.0000	0.0000
2.1773	0.0457		0.0036	0.1062	
3.1752	0.0914		0.0073	0.1543	
3.9917	0.1321		0.0105	0.1899	
4.8989	0.1829		0.0145	0.2293	
5.6246	0.2337		0.0185	0.2632	
8.6184	0.4851		0.0385	0.3916	
10.9318	0.7391		0.0587	0.4896	
12.6101	0.9957		0.0790	0.5544	
13.5173	1.2522		0.0994	0.5818	
13.6987	1.5062		0.1196	0.5763	
13.6987	1.7602		0.1397	0.5698	
13.5173	1.9990		0.1587	0.5567	
13.1544	2.2327		0.1772	0.5298	
15.6492	2.4663		0.1958	0.6160	
16.3296	2.5603		0.2032	0.6368	

σ_1 and σ_3 equal the major and minor total principal stresses, respectively. Failure taken at maximum deviator stress or at 20 percent axial strain.

TABLE I-18. TRIAXIAL TEST DATA, SAMPLE G-8

Unconfined compression test

Angle between direction of compression and horizontal = 90 degrees

σ_{1_f} = 0.644 kg/cm^2	Initial water content = 158.6%
σ_{3_f} = 0 kg/cm^2	Final water content = 158.6%
c_u = 0.322 kg/cm^2	Initial dry density = 24.15 pcf

Load (kg)	Displacement (cm)	Pore pressure (kg/cm^2)	Axial strain	σ_1 (kg/cm^2)	σ_3 (kg/cm^2)
0.0000	0.0000	--	0.0000	0.0000	0.0000
2.1773	0.457		0.0038	0.1128	
2.9484	0.0940		0.0079	0.1520	
3.7422	0.1321		0.0111	0.1923	
4.3546	0.1829		0.0153	0.2228	
5.0803	0.2337		0.0196	0.2568	
8.4823	0.4851		0.0406	0.4229	
10.8864	0.7391		0.0619	0.5307	
12.6554	0.9957		0.0833	0.6028	
13.8348	1.2522		0.1048	0.6435	
13.5173	1.5062		0.1261	0.6138	
9.8885	1.7602		0.1473	0.4381	
10.4328	1.9990		0.1673	0.4514	
9.0720	2.2327		0.1869	0.3833	
9.2988	2.4663		0.2064	0.3834	

σ_1 and σ_3 equal the major and minor total principal stresses, respectively.
Failure taken at maximum deviator stress or at 20 percent axial strain.

TABLE I-19. TRIAXIAL TEST DATA, SAMPLE G-9

Axial consolidation pressure = 0.696 kg/cm^2 with K_o = 0.3

Angle between direction of compression and horizontal = 90 degrees

σ_{1_f} = 3.992 kg/cm^2	Initial water content	=	157.2%
σ_{3_f} = 3.023 kg/cm^2	Final water content	=	153.0%
u_f = 3.002 kg/cm^2	Initial dry density	=	26.92 pcf
A_f = 0.40	c_u = 0.484 kg/cm^2		

Load (kg)	Displacement (cm)	Pore pressure (kg/cm^2)	Axial strain	$\bar{\sigma}_1$ (kg/cm^2)	$\bar{\sigma}_3$ (kg/cm^2)
9.9547	0.0000	2.8123	0.0000	0.6943	0.2109
12.9276	0.0508	2.8756	0.0041	0.7986	0.1476
13.8348	0.0965	2.8967	0.0077	0.8206	0.1266
14.5152	0.1321	2.9107	0.0106	0.8386	0.1125
14.9688	0.1905	2.9220	0.0153	0.8465	0.1012
15.2863	0.2388	2.9318	0.0191	0.8494	0.0914
16.7832	0.4928	2.9607	0.0395	0.8776	0.0626
18.0533	0.7442	2.9782	0.0596	0.9033	0.0450
19.0966	1.0058	2.9895	0.0806	0.9214	0.0337
20.4120	1.2649	2.9986	0.1013	0.9520	0.0246
21.3192	1.5240	3.0021	0.1221	0.9673	0.0211
22.2264	1.7831	3.0028	0.1428	0.9836	0.0204
22.9068	2.0422	3.0021	0.1636	0.9897	0.0211
23.4058	2.2911	2.9881	0.1835	1.0013	0.0352
23.6779	2.5425	0.29670	0.2037	1.0095	0.0562

$\bar{\sigma}_1$ and $\bar{\sigma}_3$ equal the major and minor effective principal stresses, respectively.
Failure taken at maximum deviator stress or at 20 percent axial strain.

TABLE I-20. TRIAXIAL TEST DATA, SAMPLE G-10

Axial consolidation pressure = 0.703 kg/cm^2 with K_o = 1.0

Angle between direction of compression and horizontal = 0 degrees

σ_{1_f} = 4.413 kg/cm^2	Initial water content = 157.0%
σ_{3_f} = 3.515 kg/cm^2	Final water content = 145.0%
u_f = 3.325 kg/cm^2	Initial dry density = 22.53 pcf
A_f = 0.57	c_u = 0.449 kg/cm^2

Load (kg)	Displacement (cm)	Pore pressure (kg/cm^2)	Axial strain	$\bar{\sigma}_1$ (kg/cm^2)	$\bar{\sigma}_3$ (kg/cm^2)
0.0000	0.0000	2.8123	0.0000	0.7030	0.7030
4.0824	0.0330	2.9529	0.0030	0.7985	0.5625
6.4411	0.0864	3.0162	0.0079	0.8698	0.4992
7.9380	0.1372	3.0549	0.0125	0.9151	0.4605
8.8452	0.1880	3.0830	0.0171	0.9366	0.4324
9.6163	0.2388	3.1076	0.0218	0.9533	0.4078
12.2472	0.5004	3.1849	0.0456	1.0083	0.3304
13.6080	0.7620	3.2271	0.0695	1.0226	0.2883
14.7420	1.0211	3.2552	0.0931	1.0355	0.2601
15.8760	1.2802	3.2763	0.1167	1.0523	0.2390
16.8739	1.5392	3.2974	0.1404	1.0592	0.2180
17.9172	1.7958	3.3150	0.1637	1.0693	0.2004
19.0512	2.0549	3.3255	0.1874	1.0877	0.1898
19.2780	2.1590	3.3326	0.1969	1.0807	0.1828

$\bar{\sigma}_1$ and $\bar{\sigma}_3$ equal the major and minor effective principal stresses, respectively.
Failure taken at maximum deviator stress or at 20 percent axial strain.

TABLE I-21. TRIAXIAL TEST DATA, SAMPLE G-11

Axial consolidation pressure = 2.109 kg/cm^2 with K_o = 1.0

Angle between direction of compression and horizontal = 0 degrees

σ_{1_f} = 7.151 kg/cm^2	Initial water content = 160.0%
σ_{3_f} = 4.920 kg/cm^2	Final water content = 114.0%
u_f = 4.492 kg/cm^2	Initial dry density = 23.74 pcf
A_f = 0.75	c_u = 1.115 kg/cm^2

Load (kg)	Displacement (cm)	Pore pressure (kg/cm^2)	Axial strain	$\bar{\sigma}_1$ (kg/cm^2)	$\bar{\sigma}_3$ (kg/cm^2)
0.0000	0.0000	2.8123	0.0000	2.1092	2.1092
12.7008	0.0533	3.0935	0.0047	2.6795	1.8280
16.3296	0.0183	3.3045	0.0072	2.7091	1.6171
19.0512	0.1600	3.4802	0.0141	2.7064	1.4413
20.8656	0.2108	3.5857	0.0186	2.7151	1.3359
22.5893	0.2616	3.6912	0.0231	2.7168	1.2304
27.2160	0.5232	3.9794	0.0462	2.6905	0.9421
30.3912	0.7849	4.1411	0.0694	2.6855	0.7804
32.2056	1.0465	4.2325	0.0925	2.6577	0.6890
34.2468	1.3081	4.2888	0.1156	2.6729	0.6328
36.0612	1.5697	4.3591	0.1387	2.6545	0.5625
37.8756	1.8313	4.4153	0.1618	2.6445	0.5062
39.9168	2.0930	4.4645	0.1849	216484	0.4570
42.1848	2.3520	4.5067	0.2078	2.6657	0.4148

$\bar{\sigma}_1$ and $\bar{\sigma}_3$ equal the major and minor effective principal stresses, respectively.
Failure taken at maximum deviator stress or at 20 percent axial strain.

TABLE I-22. TRIAXIAL TEST DATA, SAMPLE G-12

Unconfined compression test

Angle between direction of compression and horizontal = 0 degrees

σ_{1_f} = 0.404 kg/cm^2 Initial water content = 158.6%

σ_{3_f} = 0 kg/cm^2 Final water content = 158.6%

c_u = 0.202 kg/cm^2 Initial dry density = 19.92 pcf

Load (kg)	Displacement (cm)	Pore pressure (kg/cm^2)	Axial strain	σ_1 (kg/cm^2)	σ_3 (kg/cm^2)
0.0000	0.0000	--	0.0000	0.0000	0.0000
1.9958	0.0406		0.0043	0.0973	
3.0391	0.0965		0.0103	0.1473	
3.6742	0.1473		0.0157	0.1771	
4.3092	0.1905		0.0203	0.2067	
4.7628	0.2388		0.0254	0.2272	
6.8040	0.4928		0.0524	0.3156	
8.0741	0.7442		0.0792	0.3639	
8.9359	1.0033		0.1068	0.3907	
9.5256	1.2624		0.1343	0.4036	
9.5256	1.5189		0.1616	0.3909	
8.7091	1.7780		0.1892	0.3456	
7.4844	1.9329		0.2057	0.2910	

σ_1 and σ_3 equal the major and minor total principal stresses, respectively.
Failure taken at maximum deviator stress or at 20 percent axial strain.

TABLE I-23. TRIAXIAL TEST DATA, SAMPLE G-20

Axial consolidation pressure = 2.341 kg/cm^2 with K_o = 0.3

Undrained test with σ_1 constant and σ_3 decreasing.

Initial water content = 159.0%

Final water content = 122.0%

Initial dry density = 24.37 pcf

σ_1 (kg/cm^2)	σ_3 (kg/cm^2)	pore pressure (kg/cm^2)	Axial strain	$\bar{\sigma}_1$ (kg/cm^2)	$\bar{\sigma}_3$ (kg/cm^2)
5.135	3.5154	2.8123	0.000	2.3412	0.7031
5.1535	3.4893	2.8123	0.001	2.3412	0.6770
5.1535	3.4429	2.8123	0.001	2.3412	0.6306
5.1535	3.3965	2.7947	0.001	2.3588	0.6018
5.1535	3.3501	2.7772	0.002	2.3763	0.5729
5.1535	3.2580	2.7420	0.003	2.4115	0.5160
5.1535	3.1666	2.7068	0.005	2.4467	0.4598
5.1535	3.0745	2.6506	0.006	2.5029	0.4239
5.1535	2.9986	2.7420	0.035	2.4115	0.2566
5.1535	2.9185	2.7772	0.048	2.3763	0.1413
5.1535	2.8362	2.7772	0.057	2.3763	0.0590
5.1535	2.8158	2.7596	0.085	2.3939	0.0562
5.2027	2.8123	2.8123[a]	0.087	2.3904	0.0000
5.2630[b]	2.8123	2.8123	0.091	2.4507	0
5.3504[b]	2.8123	2.8123	0.094	2.5381	0
5.5051[b]	2.8123	2.8123	0.127	2.6928	0
5.5683[b]	2.8123	2.8123	0.136	2.7560	0

[a]Pore pressure increased to initial backpressure.

[b]Small increases in axial stress.

Deformation rate approximately zero when test was terminated.

TABLE I-24. TRIAXIAL TEST DATA, SAMPLE G-21

Axial consolidation pressure = 0.703 kg/cm^2 with K_o = 0.3

Undrained test with σ_1 constant and σ_3 decreasing.

Initial water content =

Final water content = 135.0%

Initial dry density = 31.26 pcf

σ_1 (kg/cm^2)	σ_3 (kg/cm^2)	pore pressure (kg/cm^2)	axial strain	$\bar{\sigma}_1$ (kg/cm^2)	$\bar{\sigma}_3$ (kg/cm^2)
3.5153	3.0232	2.8123	0.000	0.7030	0.2109
3.5153	2.9628	2,7807	0.003	0.7346	0.1821
3.5153	2.9121	2.7561	0.007	0.7592	0.1560
3.5153	2.8622	2.7279	0.009	0.7874	0.1343
3.5153	2,8158	2.7139	0.024	0.8014	0.1019
3.5153	2.8123	2.8123[a]	0.025	0.7030	0.0000
3.5153	2.8123	2.8123[a]	0.101	0.7030	0.0000

[a]Pore pressure increased to initial backpressure.

Deformation rate approximately zero when test was terminated.

TABLE I-25. TRIAXIAL TEST DATA, SAMPLE C-2

Unconfined compression test

Angle between direction of compression and horizontal = 90 degrees

σ_{1_f}	= 0.268 kg/cm^2	Initial water content	= 162%
σ_{3_f}	= 0 kg/cm^2	Final water content	= 162%
c_u	= 0.134 kg/cm^2	Initial dry density	= 28.17 pcf

Load (kg)	Displacement (cm)	Pore pressure (kg/cm^2)	Axial strain	σ_1 (kg/cm^2)	σ_3 (kg/cm^2)
0.0000	0.0025	--	0.0000	0.0000	0.0000
1.8144	0.0813		0.0086	0.0800	
2.4494	0.1321		0.0141	0.1074	
2.9484	0.1829		0.0195	0.1286	
3.4474	0.2337		0.0249	0.1495	
3.8556	0.2896		0.0308	0.1662	
5.3525	0.5334		0.0567	0.2246	
6.2143	0.7849		0.0835	0.2534	
6.7586	1.0414		0.1108	0.2673	
6.8494	1.1430		0.1216	0.2676	
6.3504	1.2954		0.1378	0.2436	

σ_1 and σ_3 equal the major and minor total principal stresses, respectively. Failure taken at maximum deviator stress or at 20 percent axial strain.

TABLE I-26. TRIAXIAL TEST DATA, SAMPLE C-3

Unconfined compression test

Angle between direction of compression and horizontal = 90 degrees

σ_{1_f} = 0.311 kg/cm^2 — Initial water content = 157%

σ_{3_f} = 0 kg/cm^2 — Final water content = 157%

c_u = 0.156 kg/cm^2 — Initial dry density = 28.83 pcf

Load (kg)	Displacement (cm)	Pore pressure (kg/cm^2)	Axial strain	σ_1 (kg/cm^2)	σ_3 (kg/cm^2)
0.0000	0.0025	--	0.0000	0.0000	0.0000
1.2701	0.0813		0.0073	0.0709	
1.7464	0.1321		0.0119	0.0970	
2.1773	0.1829		0.0164	0.1203	
2.5402	0.2337		0.0210	0.1397	
2.9030	0.2896		0.0260	0.1589	
4.2638	0.5334		0.0479	0.2281	
5.1710	0.7849		0.0705	0.2701	
5.7154	1.0414		0.0935	0.2911	
6.1690	1.2954		0.1163	0.3064	
6.3504	1.4224		0.1277	0.3113	
6.3958	1.5494		0.1391	0.3094	
6.3050	1.6510		0.1482	0.3018	

σ_1 and σ_3 equal the major and minor total principal stresses, respectively.
Failure taken at maximum deviator stress or at 20 percent axial strain.

TABLE I-27. TRIAXIAL TEST DATA, SAMPLE C-4

Unconfined compression test

Angle between direction of compression and horizontal = 90 degrees

σ_{1_f} = 0.204 kg/cm^2	Initial water content	= 163%
σ_{3_f} = 0 kg/cm^2	Final water content	= 163%
c_u = 0.102 kg/cm^2	Initial dry density	= 27.64 pcf

Load (kg)	Displacement (cm)	Pore pressure (kg/cm^2)	Axial strain	σ_1 (kg/cm^2)	σ_3 (kg/cm^2)
0.0000	0.0025	--	0.0000	0.0000	0.0000
1.2247	0.0813		0.0069	0.0637	
1.6330	0.1321		0.0113	0.0846	
1.9505	0.1829		0.0156	0.1006	
2.1773	0.2337		0.0200	0.1118	
2.4494	0.2896		0.0247	0.1251	
3.4020	0.5334		0.0456	0.1701	
3.9917	0.7849		0.0670	0.1951	
4.2638	1.0414		0.0889	0.2035	
4.2185	0.1684		0.0998	0.1989	
3.9917	1.2954		0.1106	0.1860	

σ_1 and σ_3 equal the major and minor total principal stresses, respectively.
Failure taken at maximum deviator stress or at 20 percent axial strain.

TABLE I-28. TRIAXIAL TEST DATA, SAMPLE C-5

Unconfined compression test

Angle between direction of compression and horizontal = 0 degrees

σ_{1_f} = 0.189 kg/cm^2	Initial water content	= 169%
σ_{3_f} = 0 kg/cm^2	Final water content	= 169%
c_u = 0.094 kg/cm^2	Initial dry density	= 27.73 pcf

Load (kg)	Displacement (cm)	Pore pressure (kg/cm^2)	Axial strain	σ_1 (kg/cm^2)	σ_3 (kg/cm^2)
0.0000	0.0025	--	0.0000	0.0000	0.0000
1.4969	0.0813		0.0079	0.0736	
1.9051	0.1321		0.0129	0.0932	
2.1773	0.1829		0.0178	0.1059	
2.4041	0.2337		0.0228	0.1164	
2.6309	0.2896		0.0282	0.1266	
3.4474	0.5334		0.0519	0.1619	
3.9463	0.7849		0.0764	0.1805	
4.2412	1.0414		0.1014	0.1888	
4.2638	1.1684		0.1138	0.1872	
4.1731	1.2954		0.1261	0.1806	

σ_1 and σ_3 equal the major and minor total principal stresses, respectively.
Failure taken at maximum deviator stress or at 20 percent axial strain.

TABLE I-29. TRIAXIAL TEST DATA, SAMPLE C-6

Unconfined compression test

Angle between direction of compression and horizontal = 0 degrees

σ_{1_f}	= 0.152 kg/cm^2	Initial water content	=	169%
σ_{3_f}	= 0 kg/cm^2	Final water content	=	169%
c_u	= 0.076 kg/cm^2	Initial dry density	=	27.75 pcf

Load (kg)	Displacement (cm)	Pore pressure (kg/cm^2)	Axial strain	σ_1 (kg/cm^2)	σ_3 (kg/cm^2)
0.0000	0.0025	--	0.0000	0.0000	0.0000
0.9072	0.0813		0.0075	0.0483	
1.3608	0.1321		0.0122	0.0722	
1.5876	0.1829		0.0169	0.0838	
1.7690	0.2337		0.0216	0.0929	
1.9505	0.2896		0.0267	0.1019	
2.5402	0.5334		0.0493	0.1297	
2.9030	0.7849		0.0725	0.1446	
3.1298	1.0414		0.0962	0.1519	
3.1298	1.1684		0.1079	0.1499	
2.9030	1.2954		0.1196	0.1372	

σ_1 and σ_3 equal the major and minor total principal stresses, respectively.
Failure taken at maximum deviator stress or at 20 percent axial strain.

TABLE I-30. TRIAXIAL TEST DATA, SAMPLE C-7

Unconfined compression test

Angle between direction of compression and horizontal = 45 degrees

σ_{1_f} = 0.208 kg/cm^2 Initial water content = 170%

σ_{3_f} = 0 kg/cm^2 Final water content = 170%

c_u = 0.104 kg/cm^2 Initial dry density = 28.35 pcf

Load (kg)	Displacement (cm)	Pore pressure (kg/cm^2)	Axial strain	σ_1 (kg/cm^2)	σ_3 (kg/cm^2)
0.0000	0.0025	--	0.0000	0.0000	0.0000
1.2701	0.0813		0.0069	0.0648	
1.6330	0.1321		0.0113	0.0829	
1.8824	0.1829		0.0156	0.0951	
2.1092	0.2337		0.0199	0.1061	
2.3360	0.2896		0.0247	0.1170	
3.0845	0.5334		0.0455	0.1512	
3.6515	0.7849		0.0669	0.1749	
3.9917	1.0414		0.0888	0.1867	
4.3546	1.2954		0.1104	0.1989	
4.6721	1.5494		0.1321	0.2082	
4.6948	1.6510		0.1408	0.2071	
4.4453	1.8034		0.1537	0.1931	

σ_1 and σ_3 equal the major and minor total principal stresses, respectively. Failure taken at maximum deviator stress or at 20 percent axial strain.

TABLE I-31. TRIAXIAL TEST DATA, SAMPLE C-8

Unconfined compression test

Angle between direction of compression and horizontal = 45 degrees

σ_{1_f}	= 0.249 kg/cm^2	Initial water content	= 169%
σ_{3_f}	= 0 kg/cm^2	Final water content	= 169%
c_u	= 0.124 kg/cm^2	Initial dry density	= 27.75 pcf

Load (kg)	Displacement (cm)	Pore pressure (kg/cm^2)	Axial strain	σ_1 (kg/cm^2)	σ_3 (kg/cm^2)
0.0000	0.0025	--	0.0000	0.0000	0.0000
0.7258	0.0813		0.0074	0.0374	
1.3608	0.1321		0.0120	0.0699	
1.8144	0.1829		0.0166	0.0927	
2.2000	0.2337		0.0212	0.1119	
2.5402	0.2896		0.0263	0.1285	
3.9917	0.5334		0.0485	0.1974	
4.8082	0.7849		0.0714	0.2320	
5.2618	1.0414		0.0947	0.2475	
5.3525	1.1684		0.1062	0.2486	
5.2618	1.2954		0.1178	0.2412	

σ_1 and σ_3 equal the major and minor total principal stresses, respectively.
Failure taken at maximum deviator stress or at 20 percent axial strain.

TABLE I-32. TRIAXIAL TEST DATA, SAMPLE C-9

Unconfined compression test

Angle between direction of compression and horizontal = 90 degrees

σ_{1_f} = 0.265 kg/cm^2 Initial water content = 178%

σ_{3_f} = 0 kg/cm^2 Final water content = 178%

c_u = 0.132 kg/cm^2 Initial dry density = 25.72 pcf

Load (kg)	Displacement (cm)	Pore pressure (kg/cm^2)	Axial strain	σ_1 (kg/cm^2)	σ_3 (kg/cm^2)
0.0000	0.0025	--	0.0000	0.0000	0.0000
0.9072	0.0559		0.0056	0.0445	
1.5196	0.1118		0.0113	0.0741	
1.9732	0.1626		0.0164	0.0958	
2.3587	0.2134		0.0216	0.1139	
2.8123	0.2667		0.0269	0.1350	
3.6742	0.3988		0.0403	0.1740	
4.2638	0.5334		0.0539	0.1990	
4.8082	0.6604		0.0667	0.2214	
5.2618	0.7849		0.0793	0.2390	
5.8968	1.0363		0.1047	0.2605	
6.0782	1.1633		0.1175	0.2646	
6.1690	1.2903		0.1303	0.2647	
6.1690	1.3411		0.1355	0.2631	
5.5793	1.5519		0.1568	0.2321	
5.3525	1.6002		0.1616	0.2214	

σ_1 and σ_3 equal the major and minor total principal stresses, respectively.
Failure taken at maximum deviator stress or at 20 percent axial strain.

TABLE I-33. TRIAXIAL TEST DATA, SAMPLE C-10

Axial consolidation pressure = 0.7030 kg/cm^2 with K_o = 0.3

Undrained test with σ_1 constant and σ_3 decreasing.

Initial water content = 177.0%

Final water content = 150.0%

Initial dry density = 26.94 pcf

σ_1 (kg/cm^2)	σ_3 (kg/cm^2)	pore pressure (kg/cm^2)	axial strain	$\bar{\sigma}_1$ (kg/cm^2)	$\bar{\sigma}_3$ (kg/cm^2)
3.5153	3.0232	2.8123	0.0000	0.703	0.2109
3.5153	2.9881	2.7982	0.0005	0.7171	0.1899
3.5153	2.9620	2.7912	0.0019	0.7241	0.1708
3.5153	2.9360	2.7877	0.0045	0.7276	0.1483
3.5153	2.9107	2.7912	0.0059	0.7241	0.1195
3.5153	2.8854	2.7912	0.0091	0.7241	0.0942
3.5153	2.8594	2.7912	0.0147	0.7241	0.0682
3.5153	2.8341	2.7771	0.0249	0.7382	0.0570
3.5153	2.8123	2.7560	0.0340	0.7593	0.0563
3.5153	2.8123	2.8123[a]	0.2591	0.7030	0.0000

[a]Pore pressure increased to initial backpressure.

Deformation rate approximately zero when test was terminated.

TABLE I-34. TRIAXIAL TEST DATA, SAMPLE C-11

Axial consolidation pressure = 0.9350 kg/cm^2 with K_o = 0.3
Undrained test with σ_1 constant and σ_3 decreasing.

Initial water content = 174.5%
Final water content = 133.5%
Initial dry density = 27.30 pcf

σ_1 (kg/cm^2)	σ_3 (kg/cm^2)	pore pressure (kg/cm^2)	axial strain	$\bar{\sigma}_1$ (kg/cm^2)	$\bar{\sigma}_3$ (kg/cm^2)
3.7474	3.0935	2.8123	0.0000	0.9351	0.2812
3.7474	3.0626	2.7982	0.0003	0.9490	0.2644
3.7474	3.0373	2.7912	0.0011	0.9561	0.2461
3.7474	3.0113	2.7631	0.0023	0.9631	0.2482
3.7474	2.9859	2.7560	0.0043	0.9701	0.2299
3.7474	2.9606	2.7490	0.0057	0.9772	0.2116
3.7474	2.9353	2.7476	0.0094	0.9997	0.1877
3.7474	2.9107	2.7279	0.0114	1.0193	0.1715
3.7474	2.8854	2.7139	0.0143	1.0334	0.1715
3.7474	2.8608	2.6998	0.0174	1.0475	0.1610
3.7474	2.8376	2.6963	0.0209	1.0509	0.1413
3.7474	2.8123	2.7174[a]	0.0437	1.0298	0.0949
3.7474	2.8123	2.8123[b]	0.0509	0.9351	0.000

[a]Small leak permitted dissipation of reduced pore pressure.

[b]Pore pressure increased to initial backpressure.

Deformation rate approximately zero when test was terminated.

TABLE I-35. TRIAXIAL TEST DATA, SAMPLE C-14

Axial consolidation pressure = 2.3430 kg/cm^2 with K_o = 0.3
Undrained test with σ_1 constant and σ_3 decreasing.

Initial water content = 174.3%
Final water content = 104.3%
Initial dry density = 27.26 pcf

σ_1 (kg/cm^2)	σ_3 (kg/cm^2)	pore pressure (kg/cm^2)	axial strain	$\bar{\sigma}_1$ (kg/cm^2)	$\bar{\sigma}_3$ (kg/cm^2)
5.1553	3.5153	2.8123	0.0000	2.343	0.703
5.1553	3.4873	2.8113	0.0004	2.344	0.676
5.1553	3.4313	2.7983	0.0007	2.357	0.633
5.1553	3.3743	2.7843	0.0012	2.371	0.590
5.1553	3.3253	2.7633	0.0014	2.392	0.562
5.1553	3.2763	2.7353	0.0018	2.420	0.541
5.1553	3.2203	2.7173	0.0025	2.438	0.503
5.1553	3.1633	2.6793	0.0032	2.476	0.484
5.1553	3.1143	2.6643	0.0035	2.491	0.450
5.1553	3.0583	2.6433	0.0046	2.512	0.415
5.1553	3.0093	2.6123	0.0053	2.543	0.397
5.1553	2.9603	2.6013	0.0065	2.554	0.359
5.1553	2.9033	2.5733	0.0081	2.582	0.330
5.1553	2.8543	2.5483	0.0098	2.607	0.306
5.1553	2.8123	2.5313	0.0109	2.624	0.281
5.1553	2.8123	2.8123[a]	0.1193	2.343	0.0000

[a]Pore pressure increased to initial backpressure.
Deformation rate approximately zero when test was terminated.

TABLE I-36. PLANE STRAIN TEST DATA, SAMPLE E-1.

Axial consolidation pressure 0.703 kg/cm^2 with K_o = 0.33

σ_{1_f} = 4.662 kg/cm^2 Initial water content = 174.1%

σ_{3_f} = 3.046 kg/cm^2 Final water content = 153.1%

u_f = 3.046 kg/cm^2 Initial dry density = 26.3 pcf

A_f = 0.20 c_u = 0.808 kg/cm^2

Load (kg)	Displacement (cm)	Pore pressure (kg/cm^2)	Axial strain	$\bar{\sigma}_1$ (kg/cm^2)	$\bar{\sigma}_3$ (kg/cm^2)
9.3169	0.0000	2.8123	0.0000	.7030	.2341
14.0616	.0330	2.8925	.0050	.8582	.1540
17.4182	.1168	2.9775	.0176	.9302	.0689
18.7337	.2159	2.9951	.0325	.9636	.0513
20.0945	.3150	3.0120	.0473	.9979	.0345
21.6821	.4089	3.0268	.0615	1.0439	.0197
24.0862	.5334	3.0324	.0802	1.1291	.0141
26.3088	.6731	3.0352	.1012	1.2014	.0112
28.8943	.7874	3.0802	.1184	1.2906	.0084
31.5252	.8890	3.0408	.1336	1.3803	.0056
34.7911	1.0033	3.0465	.1508	1.4870	.0000
38.5560	1.1125	3.0465	.1672	1.6160	.0000

$\bar{\sigma}_1$ and $\bar{\sigma}_3$ equal the major and minor effective principal stresses, respectively. Failure taken at maximum deviator stress or at 20 percent axial strain.

TABLE I-37. PLANE STRAIN TEST DATA, SAMPLE E-2.

Axial consolidation pressure 1.407 kg/cm^2 with K_o = 0.33

σ_{1_f} = 6.370 kg/cm^2

σ_{3_f} = 3.281 kg/cm^2

u_f = 3.178 kg/cm^2

A_f = 0.17

Initial water content = 170.3%

Final water content = 131.6%

Initial dry density = 26.2 pcf

c_u = 1.545 kg/cm^2

Load (kg)	Displacement (cm)	Pore pressure (kg/cm^2)	Axial strain	$\bar{\sigma}_1$ (kg/cm^2)	$\bar{\sigma}_3$ (kg/cm^2)
18.6384	0.0000	2.8123	0.0000	1.4067	.4690
27.2160	.0254	2.9951	.0043	1.6495	.2862
34.0200	.1143	3.1357	.0194	1.8239	.1455
35.3808	.1778	3.1639	.0302	1.8437	.1174
37.1952	.2286	3.1744	.0388	1.9055	.1069
39.0096	.2921	3.1955	.0496	1.9510	.0858
51.2776	.3632	3.2061	.0617	2.0238	.0752
44.4528	.4369	3.2166	.0742	2.1352	.0647
46.7208	.5080	3.2201	.0863	2.2089	.0612
49.4424	.5842	3.2271	.0993	2.2948	.0541
52.1640	.6604	3.2271	.1122	2.3841	.0541
54.8856	.7264	3.2342	.1234	2.4677	.0471
61.6896	.8763	3.2342	.1489	2.6887	.0471
70.7616	1.0160	3.2061	.1746	3.0208	.0752
76.2048	1.1430	3.1779	.1942	3.1928	.1034

$\bar{\sigma}_1$ and $\bar{\sigma}_3$ equal the major and minor effective principal stresses, respectively. Failure taken at maximum deviator stress or at 20 percent axial strain.

TABLE I-38. PLANE STRAIN TEST DATA, SAMPLE E-3.

Axial consolidation pressure 2.109 kg/cm^2 with K_o = 0.33

σ_{1_f} = 8.816 kg/cm^2	Initial water content = 170.0%
σ_{3_f} = 3.515 kg/cm^2	Final water content = 122. %
u_f = 3.515 kg/cm^2	Initial dry density = 26.5 pcf
A_f = 0.18	c_u = 2.650 kg/cm^2

Load (kg)	Displacement (cm)	Pore pressure (kg/cm^2)	Axial strain	$\bar{\sigma}_1$ (kg/cm^2)	$\bar{\sigma}_3$ (kg/cm^2)
27.9418	0.0000	2.8123	0.0000	2.1091	.7031
34.0200	.0127	2.9529	.0025	2.2701	.5625
44.4528	.0254	3.1498	.0049	2.5914	.3656
53.5248	.0762	3.3467	.0147	2.8224	.1687
58.5144	.1270	3.4381	.0245	2.9495	.0773
62.5968	.1905	3.4943	.0368	3.0550	.0211
66.6792	.2540	3.5154	.0491	3.1906	0.0000
70.7616	.3302	3.5154	.0638	3.3335	0.0000
76.2048	.4064	3.5154	.0785	3.5335	0.0000
81.6480	.4826	3.5154	.0932	3.7255	0.0000
86.1840	.5563	3.5154	.1074	3.8707	0.0000
92.9880	.6274	3.5154	.1212	4.1120	0.0000
104.3280	.7747	3.5154	.1496	4.4641	0.0000
117.9360	.9169	3.5154	.1771	4.8833	0.0000
131.5440	1.0312	3.5154	.1992	5.3007	0.0000

$\bar{\sigma}_1$ and $\bar{\sigma}_3$ equal the major and minor effective principal stresses, respectively. Failure taken at maximum deviator stress or at 20 percent axial strain.

TABLE I-39. PLANE STRAIN TEST DATA, SAMPLE E-4.

Axial consolidation pressure 2.109 kg/cm^2 with K_o = 0.33

σ_{1_f} = 7.588 kg/cm^2 Initial water content = 167.4%

σ_{3_f} = 3.515 kg/cm^2 Final water content = 119.6%

u_f = 3.501 kg/cm^2 Initial dry density = 27.5 pcf

A_f = 0.25 c_u = 2.037 kg/cm^2

Load (kg)	Displacement (cm)	Pore pressure (kg/cm^2)	Axial strain	$\bar{\sigma}_1$ (kg/cm^2)	$\bar{\sigma}_3$ (kg/cm^2)
27.9418	0.0000	2.8123	0.0000	2.1089	.7031
33.1128	.0127	2.9881	.0024	2.1894	.5273
39.9168	.0254	3.1498	.0047	2.3645	.3656
45.3600	.0762	3.2975	.0142	2.4679	.2180
48.0816	.1270	3.3748	.0236	2.5027	.1406
49.8960	.1905	3.4170	.0354	2.5200	.0984
53.0712	.2540	3.4451	.0472	2.6145	.0703
57.1536	.3302	3.4662	.0613	2.7484	.0492
60.7824	.4064	3.4803	.0755	2.8624	.0352
64.4112	.4826	3.4873	.0897	2.9783	.0281
68.9472	.5563	3.4943	.1033	3.1316	.0211
73.4832	.6274	3.5013	.1166	3.2804	.0141
83.4624	.7747	3.5084	.1439	3.6020	.0070
90.7200	.9169	3.5013	.1703	3.8010	.0141
99.7920	1.0160	3.5013	.1887	4.0873	.0141

$\bar{\sigma}_1$ and $\bar{\sigma}_3$ equal the major and minor effective principal stresses, respectively. Failure taken at maximum deviator stress or at 20 percent axial strain.

TABLE I-40. PLANE STRAIN TEST DATA, SAMPLE E-5.

Axial consolidation pressure 1.408 kg/cm^2 with K_o = 0.33

σ_{1_f} = 6.421 kg/cm^2 Initial water content = 161.9%

σ_{3_f} = 3.281 kg/cm^2 Final water content = 132.4%

u_f = 3.258 kg/cm^2 Initial dry density = 27.0 pcf

A_f = 0.20 c_u = 1.57 kg/cm^2

Load (kg)	Displacement (cm)	Pore pressure (kg/cm^2)	Axial strain	$\bar{\sigma}_1$ (kg/cm^2)	$\bar{\sigma}_3$ (kg/cm^2)
18.6430	0.0000	2.8123	0.0000	1.4075	.4690
22.6800	.0508	2.9108	.0099	1.5010	.3705
25.8552	.1143	2.9529	.0222	1.6011	.3283
32.6592	.1778	3.1006	.0345	1.7681	.1807
36.2880	.2286	3.1498	.0444	1.8772	.1315
39.4632	.2921	3.1814	.0567	1.9739	.0998
42.6384	.3607	3.2061	.0700	2.0715	.0752
45.3600	.4318	3.2201	.0838	2.1534	.0612
48.0816	.5080	3.2271	.0986	2.2361	.0541
51.7104	.5842	3.2342	.1133	2.3552	.0471
55.3392	.6604	3.2412	.1281	2.4690	.0401
58.9680	.7239	3.2412	.1404	2.5917	.0401
68.0400	.8763	3.2588	.1700	2.8654	.0225
77.1120	1.0160	3.2588	.1971	3.1392	.0225
86.1840	1.1684	3.2588	.2267	3.3776	.0225
90.7200	1.2243	3.2623	.2375	3.5012	.0190

$\bar{\sigma}_1$ and $\bar{\sigma}_3$ equal the major and minor effective principal stresses, respectively. Failure taken at maximum deviator stress or at 20 percent axial strain.

TABLE I-41. TRIAXIAL TEST DATA, SAMPLE E-10.

Axial consolidation pressure 2.291 kg/cm^2 with K_o = 0.33

σ_{1_f} = 7.895 kg/cm^2	Initial water content = 174.8%
σ_{3_f} = 3.515 kg/cm^2	Final water content = 117.1%
u_f = 3.487 kg/cm^2	Initial dry density = 26.6 pcf
A_f = 0.24	c_u = 2.190 kg/cm^2

Load (kg)	Displacement (cm)	Pore pressure (kg/cm^2)	Axial strain	$\bar{\sigma}_1$ (kg/cm^2)	$\bar{\sigma}_3$ (kg/cm^2)
27.9418	0.0000	2.8123	0.0000	2.2910	.7031
40.8240	.0508	3.1217	.0067	2.6982	.3937
47.1744	.1143	3.2623	.0150	2.8938	.2531
49.8960	.1778	3.2061	.0233	3.0788	.3094
52.6176	.2286	3.3889	.0300	3.0271	.1266
54.4320	.2921	3.4170	.0383	3.0733	.0984
57.6072	.3607	3.4881	.0473	3.1963	.0773
59.8752	.4318	3.4521	.0566	3.2733	.0633
62.5968	.5080	3.4592	.0666	3.3767	.0562
65.3184	.5842	3.4662	.0766	3.4770	.0492
68.9472	.6604	3.4732	.0866	3.6212	.0422
72.5760	.7239	3.4732	.0949	3.7753	.0422
79.8336	.8763	3.4732	.1148	4.0580	.0422
88.9056	1.0160	3.4873	.1332	4.4077	.0281
90.7200	1.1938	3.4943	.1565	4.3699	.0211

$\bar{\sigma}_1$ and $\bar{\sigma}_3$ equal the major and minor effective principal stresses, respectively. Failure taken at maximum deviator stress or at 20 percent axial strain.

TABLE I-42. TRAIXIAL TEST DATA, SAMPLE E-11.

Axial consolidation pressure 1.366 kg/cm^2 with K_o = 0.33

σ_{1_f} = 5.548 kg/cm^2

σ_{3_f} = 3.281 kg/cm^2

u_f = 3.276 kg/cm^2

A_f = 0.34

Initial water content = 172.1%

Final water content = 130 %

Initial dry density = 27.5 pcf

c_u = 1.134 kg/cm^2

Load (kg)	Displacement (cm)	Pore pressure (kg/cm^2)	Axial strain	$\bar{\sigma}_1$ (kg/cm^2)	$\bar{\sigma}_3$ (kg/cm^2)
18.6430	0.0000	2.8123	0.0000	1.3657	.4690
24.4944	.0508	2.9318	.0067	1.5198	.3494
27.2160	.1143	3.0162	.0150	1.5545	.2651
29.0304	.1778	3.0795	.0234	1.5655	.2018
29.9376	.2286	3.1287	.0301	1.5493	.1526
30.8448	.2921	3.1639	.0385	1.5441	.1174
32.2056	.3607	3.1850	.0475	1.5719	.0963
33.3396	.4318	3.2061	.0569	1.5878	.0752
34.4736	.5080	3.2201	.0669	1.6085	.0612
35.8344	.5842	3.2342	.0769	1.6382	.0471
38.5560	.7239	3.2482	.0953	1.7109	.0330
41.2776	.8763	3.2553	.1154	1.7825	.0260
44.9064	1.0160	3.2623	.1338	1.8901	.0190
48.9888	1.1684	3.2623	.1538	2.0130	.0190
52.6176	1.3208	3.2693	.1739	2.1028	.0120
58.9680	1.5240	3.2764	.2007	2.2723	.0049

$\bar{\sigma}_1$ and $\bar{\sigma}_3$ equal the major and minor effective principal stresses, respectively. Failure taken at maximum deviator stress or at 20 percent axial strain.

TABLE I-43. TRIAXIAL TEST DATA, SAMPLE E-12.

Axial consolidation pressure 0.670 kg/cm^2 with K_o = 0.33

σ_{1_f} = 4.222 kg/cm^2 Initial water content = 173.4%

σ_{3_f} = 3.046 kg/cm^2 Final water content = 154.4%

u_f = 3.044 kg/cm^2 Initial dry density = 26.9 pcf

A_f = 0.31 c_u = 0.588 kg/cm^2

Load (kg)	Displacement (cm)	Pore pressure (kg/cm^2)	Axial strain	$\bar{\sigma}_1$ (kg/cm^2)	$\bar{\sigma}_3$ (kg/cm^2)
9.2988	0.0000	2.8123	0.0000	.6701	.2341
13.1544	.0508	2.8967	.0058	.7629	.1498
14.5152	.1143	2.9318	.0129	.7863	.1146
15.4224	.1778	2.9529	.0201	.8019	.0935
16.3296	.2286	2.9670	.0259	.8251	.0794
16.7832	.2921	2.9881	.0331	.8191	.0584
17.6904	.4318	3.0092	.0489	.8260	.0373
19.0512	.5740	3.0233	.0650	.8582	.0232
20.1852	.7239	3.0303	.0820	.8848	.0162
21.7728	.8763	3.0373	.0993	.9285	.0091
22.9068	1.0160	3.0443	.1151	.9524	.0021
24.4944	1.1684	3.0443	.1324	.9984	.0021
25.8552	1.3208	3.0443	.1496	1.0328	.0021
28.1232	1.5265	3.0443	.1729	1.0925	.0021
29.4840	1.6510	3.0443	.1870	1.1258	.0021
31.7520	1.8542	3.0443	.2100	1.1780	.0021

$\bar{\sigma}_1$ and $\bar{\sigma}_3$ equal the major and minor effective principal stresses, respectively. Failure taken at maximum deviator stress or at 20 percent axial strain.